Second Series *June 1, 1932* *Vol. 40, No. 5*

THE

PHYSICAL REVIEW

X-ray Studies of the Thermal Expansion of Bismuth Single Crystals

By ALEXANDER GOETZ *and* RUDOLF C. HERGENROTHER
California Institute of Technology

(Received March 25, 1932)

Previous observations of several authors have shown certain anomalies of bismuth at higher temperatures of which the thermal expansion is very prominent. In order to decide whether those effects are to be ascribed to changes in the crystal lattice or in the mosaic structure, the *temperature shift of Bragg reflections* has been studied quantitatively between liquid air temperature and the melting point of the metal. A modified Siegbahn method, previously described by Hergenrother, has been used and an arrangement is herewith described which allows the crystal to be maintained during the observation at liquid air temperature, or at any temperatures between 20° and 265°C. The shift of Mo $K\alpha$ radiation reflected from the (111) plane of a Bi crystal has been measured for the first to the fifth order at twelve different temperatures and from it $\alpha_{\parallel}$—the thermal expansion of the crystal along (111)—was calculated. These results have been compared with the values of the true specific heat of Bi and a surprisingly high degree of constancy of α/c_p has been found up to a few degrees below the melting point. Between room temperature and melting point the thermal expansion coefficient is given by:

$$\alpha_{\parallel} = 14.4 \times 10^{-6}[1 + 1.76 \times 10^{-3}(T_{\text{abs}} - 298°)]$$

whereas:

$$c_p = 2.84 \times 10^{-2}[1 + 1.76 \times 10^{-3}(T_{\text{abs}} - 323°)].$$

The values of the thermal lattice expansion thus obtained are compared with measurements of $\alpha_{\parallel}$ obtained in the usual macroscopic way by several authors and also with values observed on the same crystals in our laboratories. *The macroscopic values are found to differ from the x-ray values many times more than could possibly be explained by experimental errors*, the principal discrepancies being first a much larger value of $d\alpha/dT$ for the lattice expansion, second the absence of a gradual reversible decline of $d\alpha/dT$ at higher temperatures, which decline is typical for the macroscopic crystal. Accordingly it is considered that Grüneisen's relation of the constancy of the ratio of the expansion coefficient and the specific heat does not hold for the macroscopic crystal. The question is raised whether or not one should expect the same values from an x-ray determination of the thermal displacement of lattice points and from a direct measurement of the crystal, when consideration is given to cubic and fourth order terms of the potential. It is to be remembered that Waller's theory predicts such an agreement. Next the conditions for the validity of $\alpha_{\parallel}/c_p$=const. are discussed. This relation comes out to be true only in a first approximation. An interpretation of the non-parallelism of the macroscopic and the lattice-expansion is attempted, on the assumption of the coexistence of a regular lattice component in the crystal together with an amorphous component, the latter of which increases relative

to the former with increasing temperatures. This however is not assumed to correspond to a statistical disintegration in view of the existence of a sharp melting point, but an effect being closey related to the mosaic structure. Certain conclusions derived from this idea are verified by experiments.

The "allotropy" of bismuth. The x-ray shift does not show any indication of a discontinuity in the expansion within the temperature range observed. Hence the allotropic transformations at 75°C (Cohen, Wurschmidt, Goetz and Hasler) and close to the melting point (Kapitza) do not exist in the sense of a change of the lattice spacing. A definite discontinuity has been found however in the macroscopic expansion at 75°C. This must be ascribed to a very small but sudden change in a periodicity of a larger parameter than the x-ray wave-lengths.

Introduction

THE physical properties of a crystalline metal in the neighborhood of its melting point are known to show certain anomalies which are not easily explained by the theories of an ideal crystal lattice. One of these qualities is the thermal expansion which has been studied by Roberts[1] for Bi single crystals from room temperature up to the point of fusion. Robert's results show that the expansion coefficient begins to decline at from 30°–40° before the melting point is reached. Similar results have been found with other metals though they were not studied in the single-crystalline state. Since there is no parallel in the behavior of the true specific heats, Grüneisen's rule as to the proportionality between the expansion coefficient and the specific heat apparently ceases to hold before fusion occurs, although the validity of this semi-empirical relation seemed to be established for ordinary temperatures in the case of a large number of metals.

There is no satisfactory explanation of these effects that does not meet serious objections, which will be discussed later. It seemed necessary therefore to investigate first whether or not this anomalous change of the expansion coefficient is actually a property of the lattice. To do this the linear expansion coefficients of a single crystal must be determined by x-rays and then compared with the true specific heats. This procedure should show whether Grüneisen's rule does actually hold for the lattice expansion near the melting point.

Apparently no specific attempt has ever been made to compare systematically the macroscopic expansion with the lattice expansion. It was thought that if an actual difference were found between these two magnitudes it would throw light on the problem of the mosaic structure of the crystals, especially since the authors could show in a previous paper[2] that the lattice of Bi crystals grown within and outside of a magnetic field could not be distinguished by x-ray analysis in spite the fact of certain considerable differences in their physical properties.[3,4] It was suggested that these effects might be due to the change in periodicities within the crystal, the parameter of which must be large relative to the x-ray wave-length, i.e., to the interplanar spacing of

[1] J. K. Roberts, Proc. Roy. Soc. **A105,** 385 (1924).
[2] A. Goetz and R. C. Hergenrother, Phys. Rev. **40,** 137 (1932).
[3] A. Goetz and M. F. Hasler, Phys. Rev. **36,** 1752 (1930).
[4] A. Goetz and A. B. Focke, Phys. Rev. **37,** 1044 (1931).

the crystal. It is natural to attempt the identification of this periodicity either with the more general concept of the mosaic structure (of a more or less accidental character) or of the secondary structure proposed by Zwicky[5,6] and verified to some extent by one of the authors[7] by observations upon the size of etching figures.

A comparison of the lattice and the macroscopic expansion should also enable a decision to be made about the much discussed "allotropy" of bismuth which occurs around 75°C where Goetz and Hasler[8] found a Peltier effect[3] such as would indicate under normal circumstances a change in phase. The x-ray analysis should reveal a sudden change of the lattice expansion at this temperature (not indicated in Robert's macroscopic observations) in case the allotropy is "true."

In addition one should expect evidence of Kapitza's hypothetical cubic modification of Bi near the point of fusion.[9]

Experimental Procedure

The x-ray spectrometer used to measure the change of reflected intensities from Bi crystals as well as the angular shift of the reflections with temperature within the range of $-182°$ to $+270°$ has been described recently by one of us.[10] The method of measurement was the same as previously reported and also there was used the same crystal has been used which served for the determination of the lattice parameter.[2] Hence it only remains to describe the arrangements for the heating and the cooling of the crystal.

Fig. 1 shows the crystal mounting used for measurements either above or below room temperature. The crystal c is cemented in the brass cup B which

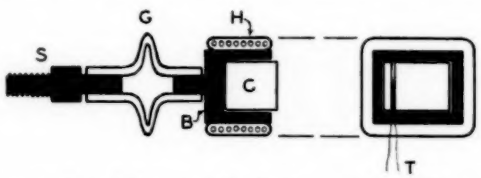

Fig. 1. Heat-insulated mounting of the crystal c in the metal cup B surrounded by the heating coil H. T is a thermocouple imbedded within the crystal.

is in turn attached to the heat insulating glass bushing G. The brass screw S serves to fasten the ensemble to the goniometer. An electrical heating coil H surrounds the cup B. The temperature of the crystal is measured by means of the fine wire thermocouple T, cemented into a narrow groove at one side of the crystal. The cold junction is placed into a constant temperature bath, the potential is measured with a potentiometer. In order to protect the crystal surface of the crystal from air currents it was surrounded by a shield con-

[5] F. Zwicky, Proc. Nat. Acad. **15,** 253; 816 (1929).
[6] F. Zwicky, Hel. Phys. Acta **3,** 269 (1930).
[7] A. Goetz, Proc. Nat. Acad. **16,** 99 (1930).
[8] A. Goetz and M. F. Hasler, reference 3, footnote page 1777.
[9] P. Kapitza, Proc. Roy. Soc. **A119,** 358 (1930).
[10] R. C. Hergenrother, Physics **2,** 63 (1932).

sisting of a metal frame which was covered on both sides with cellophane. With this air tight cover protecting the crystal it was possible to maintain the crystal surface at a temperature constant to 0.1° at any predetermined point. Fig. 2a presents a schematical view of the arrangement.

The method used for maintaining the crystal at liquid air temperature is illustrated in Fig. 2b. From a Dewar container the liquid air is forced through the heat insulated glass tube T upon the crystal surface by means of adjust-

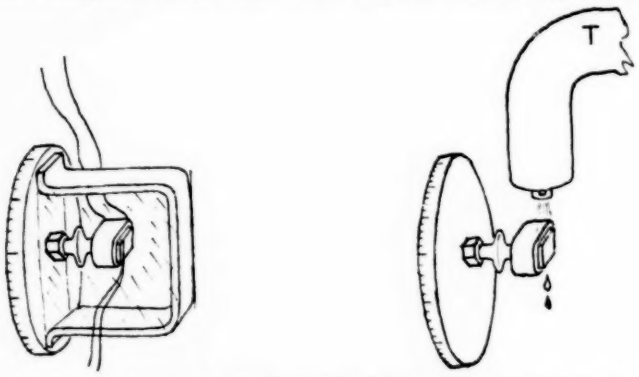

Fig. 2a and b. 2a shows scheme of cellophane hood around the heated crystal. 2b shows arrangement of cooling the crystal with liquid air.

able air pressure. This pressure being properly adjusted the liquid air leaves the nozzle in a fine spray which wets the surface of the crystal with a thin uniform film and keeps the surface free from water and CO_2 crystals.

Experimental Results

The results obtained in the range of temperature used are presented in Figs. 3 to 7. Each diagram represents the intensities reflected from the (111) plane for one order for different temperatures.

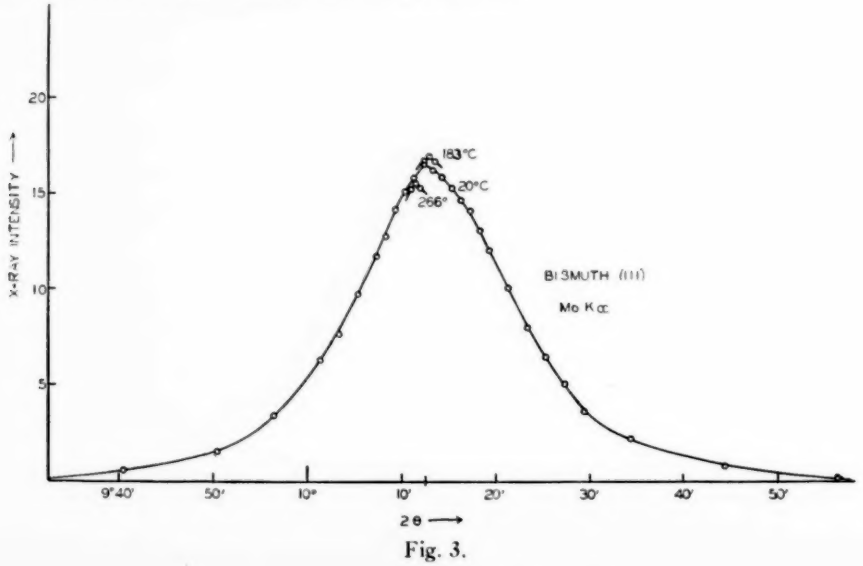

Fig. 3.

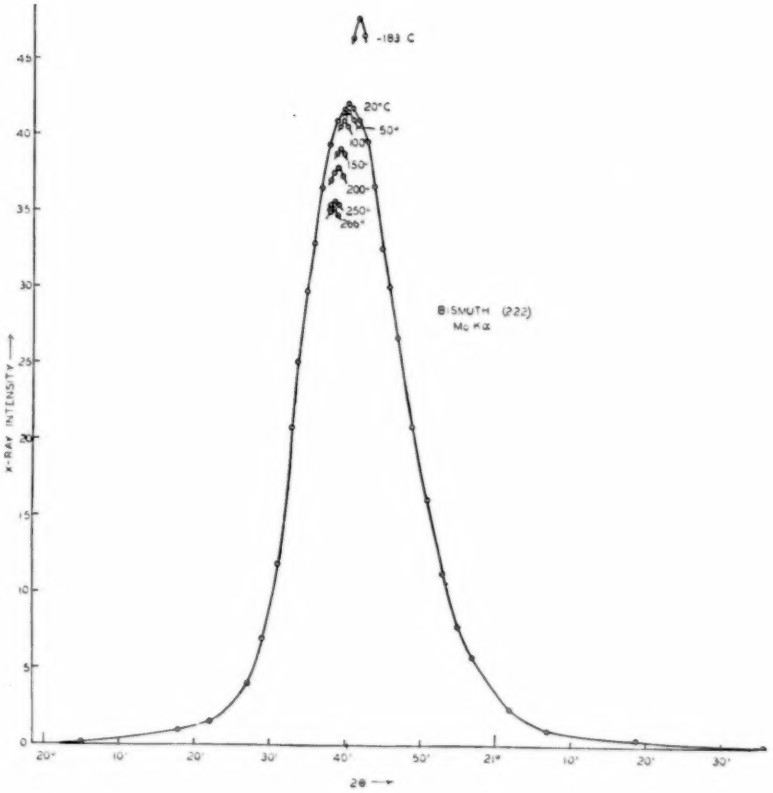
-183 C
20°C
50°
100°
150°
200°
250°
266°
BISMUTH (222)
Mo Kα
X-RAY INTENSITY
2θ

Fig. 4.

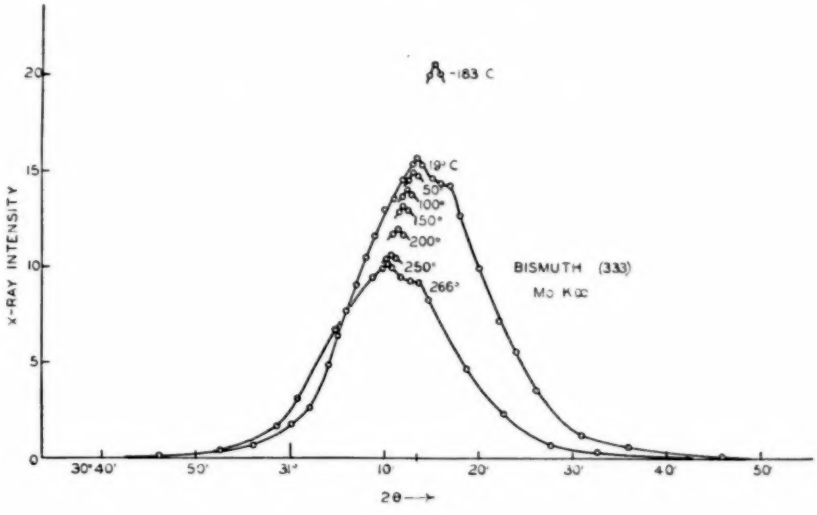
-183 C
19°C
50°
100°
150°
200°
250°
266°
BISMUTH (333)
Mo Kα
X-RAY INTENSITY
2θ

Fig. 5.

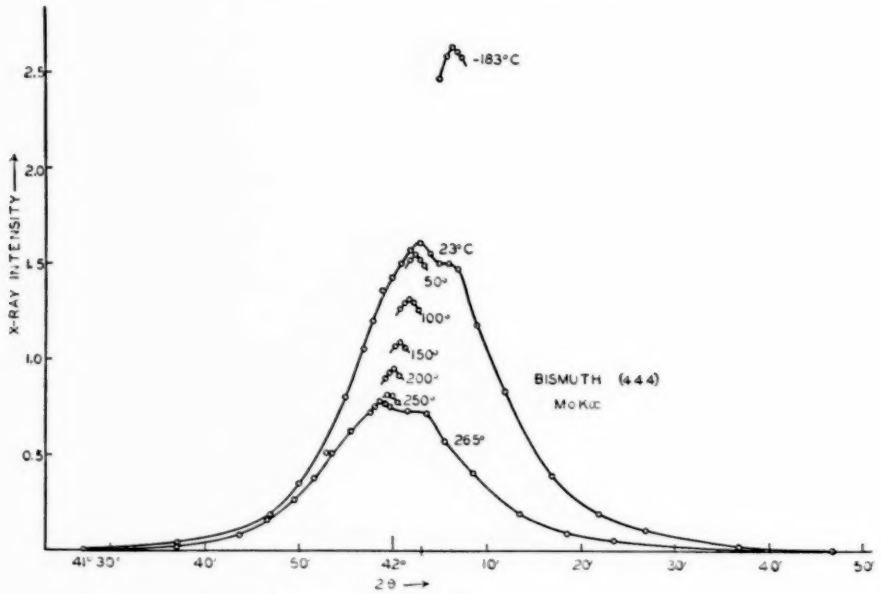

Fig. 6.

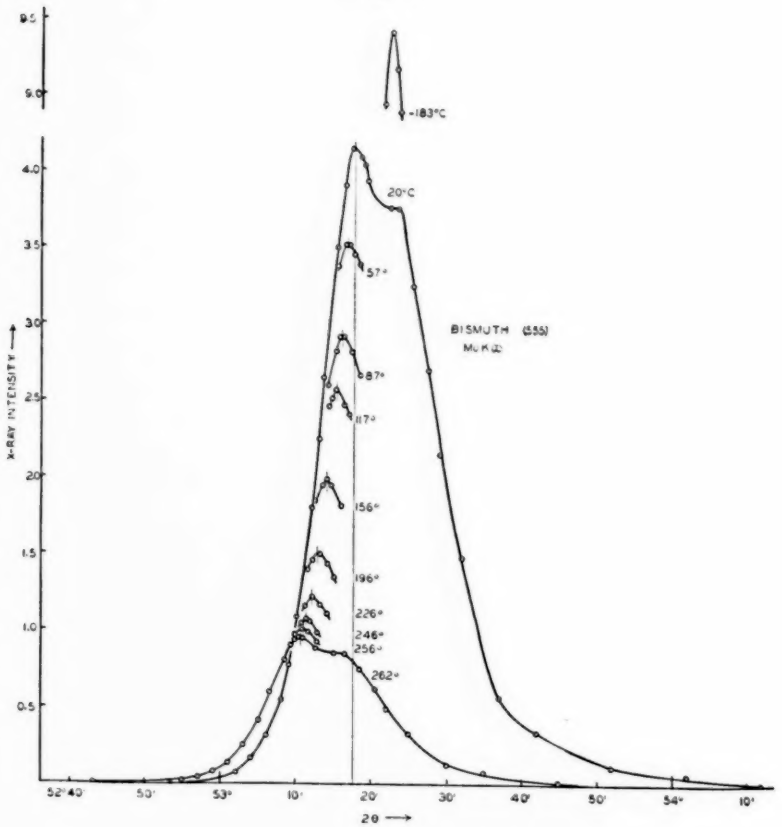

Fig. 7.

Figs. 3–7. Intensity curves of Mo $K\alpha$ radiation for (111) to (555) at different temperatures. A complete curve is drawn for only one temperature for the first two orders, in order to simplify the diagrams.

The area of each curve was determined with a planimeter and the comparison with the maximum intensities showed in each case that the ratio between the integrated intensities and the maximum intensity remained constant. Hence it was considered sufficient for the final measurements to determine only the shape of the curve in the neighborhood of the maximum as shown in the diagrams. This had the advantage of shortening the time necessary for keeping the crystal at constant temperature.

Only the first five orders were used, since the intensity of the seventh order was too weak to measure accurately at high temperatures. The fifth order is best suited for the exact location of the maximum intensity and accordingly the angular values of this order were taken with special care* and they were used exclusively for the determination of the thermal expansion, whereas the values of other orders served for the determination of the Debye factor.

The Thermal Lattice-expansion Along (111)[11]

The thermal expansion of the Bi lattice parallel to the principal axis (111) can be determined from the shift of the maximum intensities towards smaller angles with increasing temperature. From Fig. 7 this shift can be seen to be rather large and the subsequent calculations proved that the accuracy of this type of measurement approaches that of the usual "macroscopic" expansion measurement.

Table I.

1	2	3	4	5	6	7	8	9	10
T(°C)	ΔT	$\frac{1}{2}(T_1+T_2)$	$\Delta\Theta$ observed	D(A) observed	$c_p \cdot 10^5$	α_T	$1+\alpha\,(T_1-T_2)$	D^*(A) calculated	$D-D^*$ $\times 10^4$(A)
21°			0′ 0″	3.9453	270			3.9452	−1
	35°	38°			279	14.72	1.00052		
56°			0′ 46″	3.9475	298			3.9473	−2
	31°	71°			301	15.68	1.00048		
87°			1′ 20″	3.9492	302			3.9492	±0
	30°	102°			309	16.32	1.00049		
117°			1′ 48″	3.9506	314			3.9510	+4
	39°	137°			323	17.22	1.00067		
156°			2′ 47″	3.9534	332			3.9535	+1
	40°	176°			343	18.20	1.00073		
196°			3′ 49″	3.9564	353			3.9561	−3
	30°	211°			363	19.10	1.00057		
226°			4′ 30″	3.9584	372			3.9584	±0
	20°	236°			377	19.72	1.00039		
246°			4′ 57″	3.9598	382			3.9599	+1
	10°	251°			385	20.10	1.00020		
256°			5′ 20″	3.9608	388			3.9607	−1
	6°	259°			390	20.30	1.00012		
262°			5′ 35″	3.9616	391			3.9612	−4

* This means that the temperature of the crystal was changed slowly and that the points near the peaks of the curves were checked from 4 to 8 times. It seems furthermore to be of importance that the complete set of readings was taken without interruption. The position of the maximum was found the same at the beginning and at the end of the run for room temperature. The lower orders however were not measured over an uninterrupted interval and it was found that the angle scale reading would change slightly from day to day. Although those spurious shifts were corrected as well as possible for the smaller orders, the values of the lattice expansion derived from them are not sufficiently reliable.

[11] A brief abstract of this paragraph has been published in a letter to the Editor: A. Goetz and R. C. Hergenrother, Phys. Rev. **38**, 2075 (1931).

Table I shows in column 1 the temperatures T at which the Bragg angle θ has been observed.** The shift $\Delta\theta$ is given in column 4 and from it the absolute value D_T at T of the interplanar spacing along (111) is calculated, based on the previous determination of D for $T=20°$ by the authors.[2] (Column 5.)

Fig. 8 represents these values as functions of T and it is evident that the deviation of the points observed (0) from the smooth curve is much smaller than the previously estimated errors would allow.

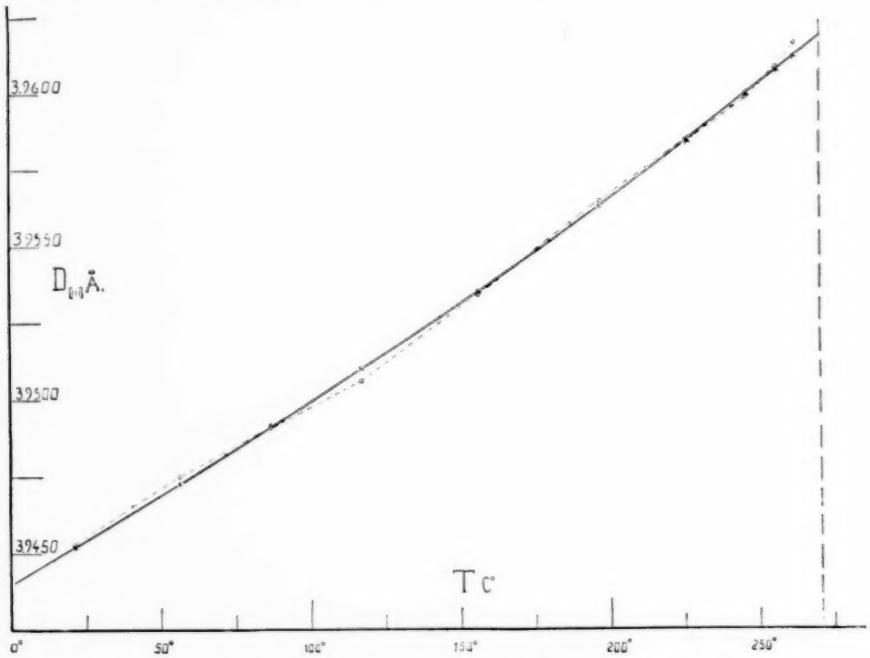

Fig. 8. Diagram of the interplanar spacings D along (111) against temperature T. The observed points are indicated by circles; the points obtained from the β-value of the true specific heats are indicated by crosses.

In order to determine the coefficient of expansion α_{11} and its change with temperature, $d\alpha/dT$, use was made of the following consideration:

If T_1 and T_2 are two neighboring temperatures at which the corresponding spacings D_1 and D_2 have been measured, the expansion coefficient is defined as:

$$\alpha_\tau = \frac{1}{D_\tau}\left(\frac{D_1 - D_2}{T_1 - T_2}\right) = \frac{1}{D_\tau}\cdot\left(\frac{\Delta D}{\Delta T}\right)_\tau \tag{1}$$

where $\tau = \frac{1}{2}(T_1 + T_2)$.

In case $d\alpha/dT = \text{const} \neq 0$, the spacing at the temperature τ is:

$$D_\tau = D_0(1 + T\alpha_\tau) \tag{2}$$

** The measurement at liquid air temperature is omitted because of a possible thermal distortion of the crystal holder due to the asymmetrical application of the liquid air.

If:

$$\alpha_\tau = \alpha_0 + b \cdot \tau \tag{3}$$

Eq. (1) changes to:

$$\alpha_\tau = \frac{D_1 - D_2}{(T_1 - T_2) D_0 \cdot (1 + \alpha_0 \tau + b\tau^2)} \tag{1a}$$

D_0 is a known spacing for which the previous precision determination[2] gave $D_{20} = 3.9453$A.

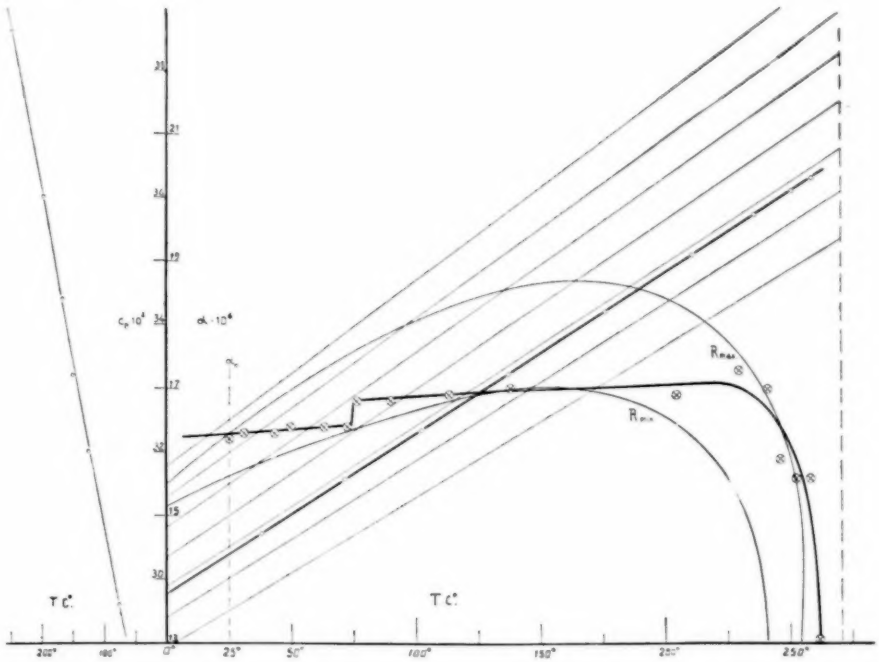

Fig. 9. Diagram of the linear expansion coefficient $\alpha_\parallel$ (right) and the specific heat (left) against temperature. The family of straight lines (right) represent the locus for $\alpha_\parallel = \alpha_0 (1+\beta\tau)$ varying from $13.5 \cdot 10^{-6}$ to $16.5 \cdot 10^{-6}$ in intervals of $5 \cdot 10^{-7}$. The heavy drawn line represents the accepted value of $\alpha_0 = 14.4 \cdot 10^{-6}$. The curved lines show the limiting values of the macroscopic expansion measured by Roberts (R_{max}, R_{min}). The crossed circles indicate the macroscopic expansion coefficients (not averaged) by Ho on crystals of the same stock as the crystal used for the x-ray analysis. The latter curve shows distinct indication of the pseudo-allotropic transformation at 75°C.

In addition to D_0 the coefficients α_0 and b have to be known. Although previous authors have claimed α to be invariant with temperature over the region considered, the curvature of the $D = f(T)$ in Fig. 8 relation disproves this statement and consequently a linear relation was assumed.

This suppositon was also based on the linear relationship of c_p—the true specific heat—with temperature, as shown by Umino[12] for a range from 50° to 250°C. The values for c_p—interpolated, where necessary—are given in column 6 of Table I and Umino's original values are shown in the left part of the diagram Fig. 9.

Since the physical reason of the parallelism of α and c_p will be discussed below it will only be stated here that the determination of α_0 and b is obviously correct only if the relation is valid; the observed values of D however permit an accurate check for each temperature due to their small deviations, in other words: *as soon as the values of D calculated from* α_0 *and* b (i.e., from the temperature variation of c_p) *coincide with the observed values of D,* α *and* $d\alpha/dT$ *are determined as well as the validity of the above assumption is proved.*

If c_{p1}, c_{p2}, $c_{p\tau}$, α_1, α_2, α_τ are the true specific heats and the expansion coefficients at T_1 and T_2 and τ, b is determined by:

$$\frac{c_{p1}-c_{p2}}{c_{p0}(T_1-T_2)}=\frac{\alpha_1-\alpha_2}{\alpha_0(T-T_2)}=\frac{b}{\alpha_0}=\beta. \tag{4}$$

From the values of Table I β is determined to be $1.76\cdot10^{-3}$ deg.$^{-1}$, and the quantitative equation of c_p is calculated as:

$$c_{pT}=2.84\cdot10^{-2}(1+1.76.10^{-3}(T_{\text{abs}}-323°)^{13}$$

Thus the expansion coefficient should follow:

$$\alpha_\tau=\alpha_0(1+\beta\tau). \tag{5}$$

The evaluation of the best fitting value of α_0 was done graphically as shown in Fig. 9, where α is plotted against T. The straight lines show the locus of α_τ for $\beta=1.76\cdot10^{-3}$ and different values of α_0, (α_0 being taken as $\alpha_{25°}$) varying from $13.5\cdot10^{-6}$ to $16.5\cdot10^{-6}$ in intervals of $0.5\cdot10^{-6}$.

The observed D values in Fig. 8 were then joined in an approximately fitting smooth curve and small corrections for D were made. These values were then used for a rough determination of α_τ using Eq. (1) and taking for simplicity $D_\tau=$const. Those values were plotted in the diagram (Fig. 9) and the best fitting of the β lines was interpolated. Thus α_0 came out to be $=14.4\cdot10^{-6}$. This locus is indicated by the heavy drawn line in Fig. 9.*†

With α_0, β and b known, the values for D_T could be calculated from Eq. (1a). Since however the α_τ values could be read directly from the graph (column 7 in Table I) the simpler relation was used namely:

$$D_{T1}=D_{T2}(1+\alpha_\tau(T_1-T_2)) \tag{6}$$

which had the advantage of giving D_T instead of D_τ. This renders a direct comparison with the observed values possible. The values thus calculated of (D_T*) are given in column 9 of Table I and are shown as crosses in the diagram in Fig. 8.

The differences between the observed (D) and calculated (D*) values are given in column 10 of Table I showing that in no case the deviation reaches

* The preliminary corrected D values are not shown in Figs. 8 and 9.

† The values for the temperature relation of c_p in older papers vary considerably for the value of β. Umino's measurement was chosen as being the most recent work with the largest number of observations in the temperature range under consideration.

[12] S. Umino, Sc. Rep. Tohoku University **15**, 604 (1926).

[13] Gmelin's Handb. d. anorg. Chem. Nr. **19**, 46 (1927).

more than 0.01 percent. This however is the case only twice: once at 117°, where the measurement was obviously not perfect and again just before the melting point. The deviation of the latter observation is probably real, as will be discussed later. Excluding the last value for this reason the mean total deviation regarding size and direction is only -1.10^{-5} A or 0.00025 percent of D. Taking the average value of $\alpha_\parallel$ for this temperature range to be $18 \cdot 10^{-6}$ deg.$^{-1}$ and the average ΔT to be 30°, $\alpha_\parallel$ has been determined within 1.9 percent.

The quantitative equation for $\alpha_\parallel$ is:

$$\alpha_T = 14.4 \cdot 10^{-6}(1 + 1.76 \cdot 10^{-3}(T_{\text{abs}} - 298°) \tag{7}$$

or:

$$\alpha_T = 14.4 \cdot 10^{-6} + 2.54 \cdot 10^{-8}(T_{\text{abs}} - 298°). \tag{8}$$

The quantitative agreement between the temperature function of the true specific heat and the lattice expansion was taken as evidence for the validity of the original assumption for the whole range of temperature investigated excepting for the last 10°–15° below the melting point. With regard to this the following suggestions may be made.

It has been found by many authors, for example,[14] that the specific heat ceases to be constant before the fusion sets in and shows an increase, an effect which is in general ascribed to impurities. Dickinson and Osborne[15] found a gradual disappearance of this effect for ice with increasing purity. In the case of metals however a large part of this change seems to be independent of admixtures, since Carpenter and Stoodley[16] in very carefully conducted experiments have found the existence of the increase of c_p even for the purest Hg. Unfortunately the values of c_p in this temperature region are not known since Umino's values which reach from 50°–800°C are taken in intervals of 25°–50° and hence our values are obtained by linear extrapolation. If Bi shows such an increase in c_p, as is most probable, the last point would show less or no deviation from the straight line relation.

Comparison with the Macroscopic Expansion

It is of interest to compare the lattice expansion as determined above with the macroscopic expansion obtained in the usual way by the direct measurement of the change of length of the crystal as a whole with temperature.

The anisotropy of Bi crystals was very early considered to be an interesting subject. In 1869 Fizeau[17] measured $\alpha_\parallel$ and $\alpha_\perp$; $\alpha_\parallel$ was determined to be $16.4 \cdot 10^{-6}$ between 20° and 80°C. Within the last few years the coefficients have been redetermined by Roberts[1] and Bridgman.[18] The latter author obtained $\alpha_\parallel = 13.96 \cdot 10^{-6}$ at 20°C, whereas Roberts made a study of $\alpha_\parallel$ and $\alpha_\perp$

[14] R. Ladenburg and E. Minkowsky, Zeits. f. Physik **8,** 137 (1922).
[15] H. C. Dickinson and N. S. Osborne, Bull. Bur of Stand. **12,** 49 (1915).
[16] L. G. Carpenter and L. G. Stoodley, Phil. Mag. **10,** 249 (1930).
[17] H. Fizeau, C. R. **68,** 1125 (1869).
[18] P. W. Bridgman, Proc. Nat. Acad. **10,** 411 (1924).

for the whole range between room temperature and melting point, and taking special care of determining $d\alpha/dT$. He concluded from a large number of observations that $\alpha_\parallel$ as well as $\alpha_\perp$ are *constant* to approximately 35° below the melting point. Within the region of constancy $\alpha_\parallel$ was computed to be $16.2 \cdot 10^{-6}$. Roberts drew furthermore the conclusion as to the constancy of $\alpha_\parallel/c_p$, by extrapolating the approximately constant values of c_p by Richards and Jackson[19] taken between $-188°$ and $+20°$, for higher temperatures, (Umino's paper had not yet been published and the author apparently did not rely on the older determinations). It is obvious now that the statement was erroneous.

The most astonishing fact is the decline of $\alpha_\parallel$ as well as $\alpha_\perp$ beyond *ca.* 240°C to such an extent that $\alpha_\parallel$ reaches one half of its original value at *ca.* 255°C. The possibility of a plastic deformation of the crystal so close to the melting point must be excluded because of the reversibility of the process and thus the decrease of $\alpha_\parallel$ must be taken as a natural property of the crystal.

Although Robert's mean values show a satisfactory constancy for the lower temperatures ($16.2 \pm 1 \cdot 10^{-6}$) the single observations, though taken with all precautions, are scattered over a large range. His maximum and minimum values are approximately indicated by the two curves (R_{max}, R_{min}) crossing the β lines in Fig. 9. It is obvious that the deviation between the macroscopic and lattice expansion is such that it cannot be explained by experimental errors.

In order to be certain that neither the small imperfection of the crystals used by Roberts nor the different kinds and amounts of impurities caused the difference, Mr. T. L. Ho of this Institute performed macroscopic expansion experiments with a method similar to Roberts'. As a specimen, Bi of the same stock as the metal used in the x-ray experiments was taken, and the crystals were grown by the same method described previously.[20] Hence one should expect them to be commensurable. Since the technique as well as the results of this work will be published separately, further details are omitted and only the $\alpha_\parallel$-values of one typical crystal are shown in Fig. 9 in crosses in circles points. Since no averaging was done the data are rather scattered, though less so than are Roberts'. An approximately best fitting line is drawn through the points and it is evident that except for the highest temperatures these values lie within the limits of Roberts' values. The reversible decline of $\alpha_\parallel$ is also present, though the beginning of it is at slightly higher temperatures. The value of $\alpha_\parallel$ up to 75° is *ca.* $16.3 \cdot 10^{-6}$, which is in good agreement with Roberts' and Fizeau's values. We should consider it premature however to place much importance upon the absolute values of $\alpha_\parallel$ at the present state of this experiment. Nevertheless the qualitative values of $d\alpha/dT$ could be reproduced on a number of different crystals as well as the discontinuity at $75° \pm 2°$, i.e., at the temperature of the pseudo-allotropic transformation, which will be discussed below.

[19] Th. W. Richards and F. G. Jackson, Zeits. f. physik. Chem. **70,** 414 (1910).
[20] A. Goetz, Phys. Rev. **35,** 193 (1930).

The results of the last paragraphs can therefore be summarized in the following statement:

The actual thermal expansion at higher temperatures of a Bi crystal is entirely different from the lattice expansion. Whereas $d\alpha/dT = dc_p/dT = const.$ *from room temperature to the immediate neighborhood of the melting point, the macroscopic (actual) expansion varies much less (if at all) with T and begins to decline 30°–40° before the melting point; accordingly* $d\alpha/dc_p$ *is not constant in this case.*

Fig. 10 shows this difference schematically, $\alpha_\parallel/c_p$ being plotted in arbitrary units against T. The full line represents the values of the lattice expansion, the dashed line represents the macroscopic expansion.

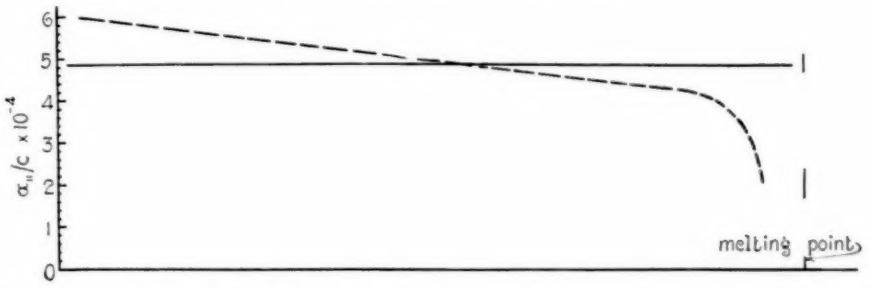

Fig. 10. Diagram of $\alpha_\parallel/c_p$ in arbitrary units plotted against temperature. The full drawn line represents the lattice coefficient, the dashed one the macroscopic expansion.

The "Allotropy" of Bi

In addition to the determination of thermal expansions our observations in combination with the macroscopic measurements give some information about the much discussed allotropy of Bi.

From the x-ray investigation it is evident that no sudden change takes place either at 75° or in the neighborhood of the melting point within the limits of our experimental uncertainty. It seems to prove definitely that there is no allotropic i.e., lattice transformation in Bi in the range of temperature between 20° and 269°.* In view of this Kapitza's hypothesis[9] of the existence of a cubic modification near to the melting point does not seem to be supportable, as has already been pointed out previously from a different line of argument.[21] This agrees also with the results of Webster[22] who recently performed very careful measurements on the change of the diamagnetic susceptibilities of Bi immediately below and above the melting point with special regard to its coincidence with the heat of fusion and the change of rigidity. Since Kapitza ascribed the large crystal diamagnetism to the rhombohedral modification one should expect a decrease at a change into a cubical modification.

* Although the shift of the Bragg angle was only observed to 262°C for the fifth order (Fig. 7), the third (Fig. 5) was taken up to 269°C and though not considered accurate enough for the determination of the lattice expansion, shows no deviation which should account for a sudden change of spacing.

[21] A. Goetz and A. B. Focke, reference 4, footnote page 1054.

[22] W. L. Webster, Proc. Roy. Soc. **A133,** 162 (1931).

Hence the change of the susceptibility should not coincide with the process of fusion; whereas Webster could prove a coincidence to 0.3°C, thus rendering the existence of such an allotropy highly improbable.

The nature of the other allotropic transition at 75°C is much more puzzling, because of an almost equal amount of experimental evidence against and in favor of it. The literature on this subject as given previously[8] was augmented recently by a careful investigation of Schulze[23] concerning the temperature coefficient of the electric resistivity and of the volume expansion in this range of temperature which did not show a discontinuity at any point. His expansion measurements were taken however at intervals of *ca.* 10°, i.e., in the critical region at 70.0°C and 79.8°C, hence a very small discontinuity may have been left unobserved.

The shift of the x-ray reflections with temperature (Fig. 8) shows definitely that *there is no such discontinuous change in the lattice spacing along* (111) as one should expect in case of an allotropic modification.

A careful study of the macroscopic expansion however shows that a small actual change takes place (Fig. 9) which is of the same order of magnitude as Cohen's observations. This proves definitely *that a rearrangement occurs within the crystal at 75°C which is not characterized by a change in the lattice.*

It may be anticipated from a detailed report about the studies of macroscopic expansion that this change can be reproduced in all crystals of different degrees of purity and that it is independent of the thermal history, i.e., its occurrence and size depends neither on the number of times, nor the length of time the crystal was heated above this temperature. Hence the effect can seemingly not be ascribed to recrystallization or to reaction with impurities which latter effect could be conjectured from the transformation point of the ternary system of Bi-Sn-Pb at 76°C which has been recently discovered by Isihara.[24]

Interpretation of Results

The purpose of this paragraph is to discuss the nature of the validity of the α/c_p relation together with the discrepancy between the macroscopic and lattice expansion and to present a tentative hypothesis from which these phenomena may be explained.

First the question may be discussed, whether or not one is entitled to compare the temperature shift of the Bragg reflection with the macroscopic measurement of the thermal expansion; in other words: Is the average of the atomic displacements, effective for the x-ray interference, equivalent to the mean sum of the displacements, effective in the length-determination of the crystal?

Waller[25] has shown in a calculation regarding the cubic terms of the potential energy of atomic displacements in a lattice, that classical as well as quantum-statistics result in an agreement of both types of summation, i.e., the

[23] A. Schulze, Zeits. f. tech. Physik **11,** 16 (1930).
[24] T. Isihara, Sc. Rep. Tohoku Univ. **18,** 715 (1929).
[25] I. Waller, Ann. d. Physik **83,** 153 (1927).

difference between the shift of x-ray reflection with temperature and the corresponding macroscopic thermal expansion of a three-dimensional crystal is negligible. In addition to this the same author also introduces a fourth order term for the potential of a one-dimensional lattice:

$$\Phi = \sum_{L=2}^{L} u_T \text{ for } u_T = A\tfrac{1}{2}\xi_L{}^2 + B\tfrac{1}{3}\xi_L{}^3 + C\tfrac{1}{4}\xi_L{}^4. \tag{9}$$

The second-order approximation for the cubic term together with the first-order approximation of the fourth order term results in an expression for the spacing D_T' effective for x-rays:

$$D_T' = D_0'\left[1 + \alpha T - \frac{kT^2\pi^2\alpha}{3A}\,\frac{(\theta - \theta_0)^2}{\lambda^2}\right] \tag{10}$$

where λ is the wave-length of the radiation and θ, θ_0 the cosines of the reflected and incident radiation respectively. Since:

$$\frac{(\theta - \theta_0)^2}{\lambda^2} \sim n^2 \text{ (order)}$$

one should expect, that D_T' measured by x-rays would be smaller than the macroscopic

$$D_T = D_0(1 + \alpha T)$$

furthermore $D_T - D_T'$ should increase with higher orders as well as with temperature. Waller states that these effects are small and probably negligible for the three-dimensional case, and since our experiments have shown exactly the opposite deviation ($D_T' > D_T$) it seems impossible to ascribe the observed deviation to effects inherent in the difference of the two methods of observation.

The theoretical reasons for the existence of an approximate proportionality between α and c_p were discussed for monatomic crystals by Grüneisen,[26] Born,[27] Debye and implicitly in Waller's paper.[25] The conclusion at which the authors arrive is that the constancy of α/c_p is only an approximate one, the validity of its relation for temperature beyond the T^3-region is only to be expected for monatomic crystals.[27] It is interesting to note that in Waller's treatment of the one dimensional lattice (Eq. (9)) the expression for the mean potential energy contains the term:

$$\frac{5B^2}{6A^3} - \frac{3C}{4A^2}, \text{ whereas } \alpha = -\frac{Bk}{A^2D}.$$

The constancy of α/c_p can only hold if:

$$\frac{5B^2}{6A^3} - \frac{3C}{4A^2} \sim \frac{Bk}{A^2D}, \text{ or if } C = B\left[\frac{B}{A} - 1\right].$$

[26] E. Grüneisen, Ann. d. Physik **39**, 257 (1912).
[27] M. Born, Enz. d. Math. Wiss. **3**, 663, ff. (1925).

Since B has to be negative in order to have $dD/dT>0$, the condition $dc/dT>0$ prescribes:

$$\frac{3B^2}{4A^3}\cdot\left[1+\frac{A}{B}\right]<\frac{5B^2}{6A^3} \text{ or } \left|\frac{A}{B}\right|<0.1111.$$

If C is neglected completely one obtains $(B/A^3)\sim(B/A^2)$ which is obviously not true, though it has to be remembered that these expressions are only valid for one-dimensional lattices.

Grüneisen and Goens[28,29] proved the validity of the α/c_p relation in their classical experiments on Zn and Cd crystals for a range of temperature from $-160°$ to $+100°$ and Borelius and Johannson[30] did the same for polycrystalline Cu between $-182°$ and $+20°$. The experiments prove however the validity of the relation only for α_V, the volume expansion coefficient; they indicate also definite deviations of the relation below *ca.* $-160°$C. α_V [being synonymous with the linear expansion coefficient for the cubic Cu] is defined for hexagonal crystals (Zn, Cd, Bi, etc.) as:

$$\alpha_v=\frac{1}{V}\frac{dV}{dT}=\alpha_\parallel+2\alpha_\perp. \tag{11}$$

The experiments on Zn and Cd showed $\alpha_\parallel/c_p$ to be distinctly different from $\alpha_\perp/c_p$, especially for low temperatures. The first author to test the relation at high temperatures—i.e., $+20°$ to $+270°$C—was Roberts,[1] as has already been seen. The discrepancy between his results and Grüneisen's relation cannot be understood from the difference between the Zn and the Bi lattice, since both metals belong to the same fundamental type of symmetry. In view of the reported observations it seems evident that the linear expansions of Bi also do not show a simple relation to the specific heats as far as macroscopic measurements go, which is also obviously true for the macroscopic α_v.

In any case the most important point seems to be the proof that $\alpha_\parallel$ of the lattice satisfies the relation up to the melting point and we hope to prove this soon for $\alpha_\perp$ also, in which case the same is established for α_v.

This new effect can seemingly only be explained by the existence of *two* components of the macroscopic expansion coefficient: α and α', of which α is the expansion coefficient of the ideal lattice and α' the expansion of a disintegrated portion of the crystal. Of these the first and *only* the first component is accessible to the x-ray measurement, whereas the macroscopic method integrates over both components, thus the expansion of the ideal lattice follows Grüneisen's relation whereas the disintegrated part does not do so.

The question arises as to the cause of such gradual disintegration which disagrees completely with our usual concept of the sharp melting point of a crystalline substance, accompanied by a sudden change of the physical quali-

[28] E. Grüneisen and E. Goens, Phys. Zeits. **24,** 507 (1923).
[29] E. Grüneisen and E. Goens, Zeits. f. Physik **29,** 141 (1924).
[30] G. Borelius and C. H. Johannson, Ann. d. Physik **75,** 23 (1924).

ties typical for a solid body. The explanation which several authors have advanced to explain phenomena similar to the decrease of the macroscopic α, is the assumption of a gradual dissociation of the crystal into a semi-liquid; near the melting point a crystal would therefore be considered as a solid solution of the liquid substance in the remains of the lattice. However any theory assuming a statistical distribution of dissociation atoms over the crystal is untenable in view of the existence of a sharp melting point, as Roberts[1] has already indicated.

However, if one accepts the picture of a mosaic crystal, consisting of units of rather definite size, one does not encounter the above objection. In an ideally pure crystal the boundaries of the mosaic units consist of atoms the spacing of which is slightly different from the interior as has been pointed out by Zwicky.[6] If enantiomorphous impurities are present, the probability of their deposition in those boundaries is more probable than inside the unit[4]; they cause however an additional distortion within these boundaries. At higher temperatures one must assume a farther reaching distorting influence of the boundary upon the intact lattice of the unit, with the effect that a "decrystallization" starts with increasing temperature. The total volume of the crystal existing in a "decrystallized" state increases therefore with the approach to the melting point at the expense of the truly crystalline volume; hence the macroscopic qualities will be increasingly influenced by the qualities of the amorphous substance. It may be emphasized that such a system can very well be in a perfect thermodynamic equilibrium and have a sharp melting point due to the fact that sufficiently large complexes of atoms in an undisturbed spacing exist to grant the interaction necessary for a sharp melting point. In a recent paper Zwicky[31] has pointed out the necessity that cooperative phenomena of such kind are necessary to understand a sharp melting point which after all is the most characteristic quality of a crystal. One has to assume apparently that the cooperation of a definite number of atoms is necessary in order to cause fusion; in other words *a definite minimum number of atoms able to cooperate since coexisting within an ideal lattice configuration*. Since however the number able to stay in such configuration at high temperatures depends on the degree of decrystallization, which itself depends to a certain extent on the number of foreign atoms, the lowering of the melting point by comparatively small admixtures may be understandable.

This suggestion seems to gain probability in view of the expansion phenomena. If N_c is the number of atoms per unit volume of a large crystal existing in a perfect lattice configuration, N_d the corresponding number of decrystallized atoms, the macroscopic expansion coefficient is given by:

$$\alpha_m = \frac{N_c\alpha + N_d\alpha'}{N_c + N_d} \tag{12}$$

where α and α' have the same meaning as before. Furthermore:

$$\frac{N_d}{N_c + N_d} = f(T). \tag{13}$$

[31] F. Zwicky, Proc. Nat. Acad. **17**, 524 (1931).

Combining Eq. (12) and (13) one obtains for the degree of decrystallization

$$\frac{N_d}{N_c + N_d} = \frac{\alpha_m - \alpha}{\alpha' - \alpha} = f(T) \tag{14}$$

which can easily be determined from Fig. 9, showing $f(T)$ to be an exponential function as expected.*

To account for the large difference between α and α' one has to remember the well-known fact that the expansion coefficient of solids in the amorphous state is generally much smaller than in the crystalline, [as for instance, SiO_2 shows only one thirtieth of the linear crystal expansion in the amorphous state]. A plausible physical explanation of this fact can be found in a balancing effect of the irregular spacing of the atoms on the dislocating action of the anharmonic oscillations.

Three of the numerous consequences accessible to experiment to be drawn from the above suggestions may be mentioned, though their detailed discussion shall be left to later publications:

(1). If the impurities in a crystal assist the process of decrystallization without being entirely responsible for it, one should expect: (a) that the purest obtainable metal would show the effect as well as metals with impurities; (b) that for slightly impure crystals the decline of α_m would begin at lower temperatures compared with the pure crystal.

The experiments of Mr. Ho and the senior of the authors on the macroscopic expansion have actually proved these postulates.

(2). If the macroscopic crystal at higher temperatures actually consists of an ideally crystalline and of an amorphous component, the intensities of reflected x-rays should decline faster with increasing temperatures than is predicted by the theory of Debye and Waller which accounts only for the the increased undirected scattering caused by the thermal agitation of lattice atom. The presence of an amorphous component should increase the scattered radiation by an additional amount proportional to $N_d/(N_c+N_d)$.

In fact our intensity measurements at different temperatures (Figs. 3–7) show a large deviation from Debye's law at higher temperatures, such that the measured intensities grow increasingly smaller than the theoretical values. A similar effect has been found previously for NaCl and Al crystals.

(3). Grüneisen's relation can be expected to hold only for the lattice expansion and not for the macroscopic one, as long as $\int_0^T u\alpha T$, the atomic heat contents for the decrystallized and the ideal part of the crystal, do not differ greatly.

Although the suggested hypothesis seems to describe the observed effects satisfactorily without assuming too much *ad hoc*, our experiments cannot be considered as definite proof of it. Whereas there already exists certain direct

* The quantitative evaluation of this function needs more systematic observations of the macroscopic expansion, which however will be published soon; an estimate shows however that more than 30 percent of the crystal is decrystallized in the neighborhood of the melting point.

experimental evidence of the periodic absorption of impurities in a metal crystal[32,33] it will be exceedingly difficult to decide by experiment whether or not the strict periodicity of the mosaic structure assumed by Zwicky is present *a priori* or is due to impurities, since so far no crystal containing an insufficient number of foreign atoms (including gases) to fill the internal surface has been available.

Further experiments on this subject, soon to be published, are expected to bring additional information to the problem of the effects of foreign atoms in a homopolar lattice.

In conclusion the authors wish to express their thankfulness to Dr. W. V. Houston for theoretical discussions and to Messr. A. B. Focke, T. L. Ho and R. B. Jacobs for general assistance.

[32] M. Straumanis, Zeits. f. anorg. Chem. **180,** 1 (1929).
[33] M. Straumanis, Zeits. f. physik. Chem. **148,** 112 (1930).

A Precision Comparison of Calculated and Observed Grating Constants of Crystals

By YUCHING TU
Ryerson Physical Laboratory, University of Chicago, Chicago, Ill.

(Received April 18, 1932)

A precision comparison of the calculated and observed grating constants of calcite, rocksalt, artificial KCl, and diamond crystals is made with calcite as standard. The calculated valûes are determined from density measurements, while the observed values are calculated from the angles of reflection for the Mo $K\alpha_1$ line obtained by means of a precision double-crystal spectrometer. The value of λ obtained from the calculated grating constant of calcite is used to determine the observed grating constants of the other crystals. The density of rocksalt and KCl is measured by immersion in Russian mineral oil whose density and change of density with temperature was found to be 0.88011 at 24°C. and 0.000064 per 0.1° respectively .The density of diamond is determined by weighing a solution of thallous formate and thallous malonate, in which the diamond just floats, in a calibrated specific gravity bottle of approximately 50 cc capacity. Two methods are used in the x-ray measurements, namely, the calcite method, described by A. H. Compton and S. K. Allison and J. H. Williams, and the rocksalt method. The latter consists of measuring the peak position of the beam reflected from crystal *B* by swinging the ionization chamber past the beam, with two narrow slits between it and the crystal, ranging in width from 0.04 to 0.08 mm and separated by a distance of 18 cm. Calculated and observed values of the grating constants of these crystals are found to agree within experimental error, ranging from 0.004 to 0.011 percent, showing no evidence of Zwicky's "secondary structure," which he offered as a possible explanation of the discrepancy between x-ray wave-lengths obtained by the crystal method and those by the ruled grating method. Measurements on two quartz crystals showed a decided variation in the internal structure of the crystal, and indicate that quartz is unsuitable for precise wave-length measurements.

INTRODUCTION

IT HAS been known that x-ray wave-lengths measured by crystals are less than those measured by ruled gratings by about 0.2 percent. Zwicky[1] offered as a possible explanation of the difference, the existence in crystals, of a "secondary structure" consisting of perfect crystal blocks, surrounded by planes whose density is larger than that of the crystal proper, thereby making the calculated grating constants smaller than those observed by means of x-rays. In other words, when calculated values of grating constants are used without taking into account this secondary structure, the wave-lengths obtained should be too small. By assuming a difference of 10 percent in the density of the secondary planes and the reflecting planes, and the existence of one secondary plane for every 30 reflecting planes, Zwicky calculated that there should be a relative correction for density of approximately 0.01, thereby giving a relative correction for grating constant of 0.003. This investigation is undertaken to compare the calculated and observed grating constants of various crystals with the purpose of discovering any difference which might explain the discrepancy between the two methods of measuring x-ray

[1] F. Zwicky, Proc. Nat. Acad. Sci. **16**, 211 (1930).

wave-lengths. Since the absolute value of the wave-length used must be assumed to be unknown, only relative values can be obtained from this investigation. Consequently, some crystal has to be chosen as a standard. Calcite is chosen to serve as such a standard.

General Procedure

The grating constant of calcite is calculated from its density by assuming a value for Avogadro's number. Since only relative results are sought for in this case, it is immaterial which value is chosen. Both 6.064×10^{23}, as given by Birge,[2] and 6.0594×10^{23} are used in the calculations. The value of D thus obtained is used to determine the wave-length of the Mo $K\alpha_1$ line, which is the wave-length used in this experiment, from the angle of reflection obtained from the x-ray measurements. This value of λ is then used to determine the observed grating constants of all other crystals. It should be noted here that no importance whatsoever is attached to the value of λ thus obtained as an absolute value.

Methods of Observation

A. X-ray measurements

The x-ray measurements are made by means of a precision double-crystal spectrometer of the type described by Compton.[3] Two methods are used

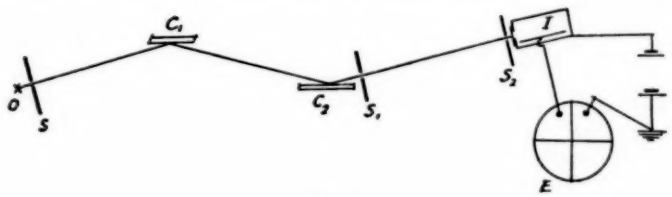

Fig. 1.

(1) the calcite method, the details of which are described by Compton, Allison and Williams,[4] (2) the rocksalt method. The calcite method is characterised by the narrow width of the rocking curve, which serves as a criterion of the accuracy of adjustment. Rocksalt, being an imperfect crystal, has a large angular range of reflection. No narrow rocking curve can be obtained from it. To obtain the desired accuracy in this case, a different method has to be used, which for convenience, is labelled the "rocksalt method." Fig. 1 is a diagrammatic sketch showing the general arrangement.

The principle of the method is based on the assumption that however imperfect the crystal may be, the peak of the beam reflected from it must make an angle with the incident beam equal to twice the angle required by Bragg's law, subject only to correction due to divergence of the incident beam and index of refraction. Naturally, a system of narrow slits is necessary in order to determine the angle accurately. By setting the crystal near the range of

[2] R. T. Birge, Phy. Rev. Supplement **1**, 1 (1929).
[3] A. H. Compton, Rev. Sci. Inst. **2**, 365 (1931).
[4] S. K. Allison and J. H. Williams, Phy. Rev. **35**, 1476 (1930).

maximum reflection, and observing the peak of the beam with an ionization chamber for both the parallel and anti-parallel positions, 4θ is obtained.

O is the x-ray source furnished by a Coolidge water-cooled Mo tube run at 50 k.v. peak voltage and 25 m.a. C_1 is a calcite crystal (referred to later as crystal A); C_2 is rock-salt crystal (referred to later as crystal B). Both crystals are mounted on holders which permit micrometer adjustments in the horizontal plane in two directions, one perpendicular to the crystal face, and one parallel to it. The former adjustment can be made to a fraction of 0.01 mm. The holders are mounted on tables with levelling screws to adjust the vertical tilt of the crystals. S_1 and S_2 are two narrow slits, generally from 0.04 mm to 0.08 mm width, depending upon the intensity of the beam. I is an ionization chamber of a type described by Compton, filled with krypton gas at atmospheric pressure. E is a Compton electrometer set at a sensitivity of 8000 scale divisions per volt.

Adjustments

1. To set crystal A parallel to the axis of rotation of crystal B. A calcite crystal is mounted on the crystal B holder and set parallel to its axis of rotation and over the center of rotation by a method described below. The vertical tilt of crystal A is adjusted until the smallest width of the rocking curve of crystal B is obtained in the parallel position.

2. To set crystal B parallel to the axis of rotation and directly over the center of rotation. An optical parallel plate glass is set over the center of the crystal table. A telescope with a Gauss eyepiece is used to observe the image of the cross-hairs reflected from the glass. Both the crystal table and the telescope are levelled until the image of the horizontal cross-hair coincides with the hair itself as seen in the eyepiece both before and after the crystal table is turned through 180°. This makes the axis of the telescope perpendicular to the axis of rotation of the crystal table. As the rocksalt cleavage face is not perfect enough to obtain a clear image of the cross-hair, the optical plane glass is set flat against the crystal face by tying it to the crystal holder with a rubber band. The crystal table is then levelled to make the two images coincide. To set the crystal face over the center of rotation, a sharp point is placed over the table and adjusted until it does not change its position when the table is rotated around, as seen in a microscope. The crystal face is then brought close to the point until the point and its image in the crystal just come into contact as seen in the microscope. An accuracy of 0.01 mm can easily be obtained.

3. To set the slits S_1 and S_2 parallel to the axis of rotation of crystal B. An optical plane glass is set parallel to the axis as before. A thin plane mirror is set between the jaws of the slit S_1. S_1 is near enough to the crystal table so that the reflections of a scale in the glass and the mirror can be viewed side by side in the same field of a telescope placed about 2 meter distant from either. The slit is then rotated until the same reading is obtained as from the glass. The error of adjustment is not more than 10 seconds of arc. By using an

auxiliary mirror which is long enough to stretch over the distance between the two slits and the same method, S_2 is set parallel to S_1.

4. To make the beam reflected from crystal A pass through the axis of rotation of crystal B. An approximate adjustment is made by moving crystal A in a horizontal plane until the same deflection of the electrometer is observed before and after crystal B is turned around 180°, with one of the slits, S_1, opened wider than S_2. To make the final adjustment, the slit at the x-ray tube is made very narrow, 0.02 mm. An optical plane glass is tied to crystal B, and separated from the latter at the top and bottom by a strip of aluminum

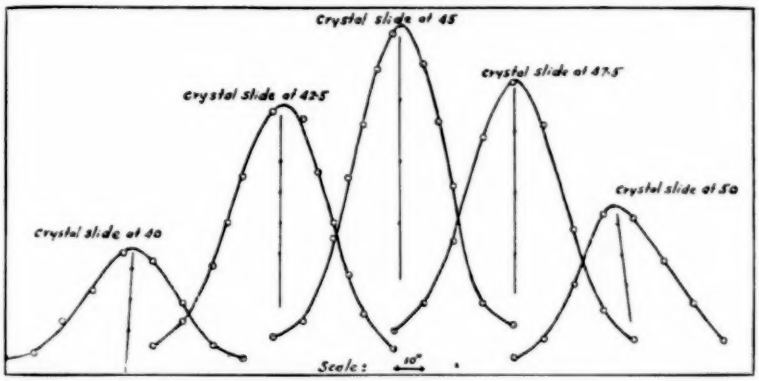

Fig. 2. Effect of changing position of crystal A.

0.02 mm thick. This makes a slit at the center of the table $16 \times 20 \times 0.02$ mm. The slit S_2 is also made 0.02 mm wide, and the x-ray beam made to pass through these two slits and give the same deflection before and after the crystal is turned through 180°. This test also checks whether or not crystal B is set accurately over the center. S_1, also made 0.02 mm wide, is then shifted laterally until the same deflection is observed as when it is opened wide. This then makes the line joining the slits S_1 and S_2, and the x-ray beam pass through

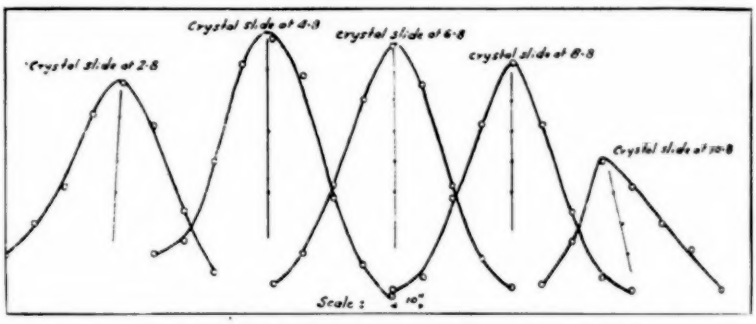

Fig. 3. Effect of changing position of crystal B.

the axis of rotation of crystal B. Provided all the adjustments are correct, the curves taken by swinging the ionization chamber pass the beam ought to be symmetrical. A series of curves are taken to test the effect of alignment on the shape of the curves. (Figs. 2 and 3)

A difference of 1 in the crystal slide reading means a shift of the crystal of 0.01 mm parallel to itself. From the curves it can be easily seen that a displacement of either one of the crystals of 0.1 mm or 0.08 mm produces a decided difference in the symmetry of the curves. As the beam sweeps across the face of the crystal, the curve first leans to one side, becomes symmetrical, and then leans to the other side. The curves with good symmetry invariably give much larger peak intensities. The width at half-maximum of these curves is about 40″, which is nothing but the angle subtended by the two slits, the slits being 0.04 mm wide, and 18 cm apart.

From these adjustments and tests, it is concluded that the criterion of accuracy of adjustment for the "rocksalt method" is the symmetry of the curve. This method has been used for rocksalt, artificial KCl, and quartz crystals. However, wherever it is possible, the calcite method is used as a check.

With diamond crystal, an additional factor needs to be considered. Diamond is known to be a perfect crystal, but the faces are polished without regard to their parallelism to the natural reflecting planes. Rotation photographs are taken to ascertain the planes nearest to the polished faces. In both of the diamonds, the 100 plane is found. But in the one case, the angle of tilt is about 2°, while in the other it is about 8°. To eliminate any error which may arise due to this tilt, measurements are taken with various orientations of the crystal with respect to the x-ray beam. Since the diamonds are cut square, the orientations are changed either by 90° or 180°. For both diamonds, the calcite method is used.

B. Density measurements

All density measurements are made on the same crystal or crystal block as the x-ray measurements. The density of calcite and quartz is determined by the immersion method, with distilled water as the liquid. A wire loop is used to hold the crystal in the liquid. The weight of the loop in the liquid is obtained by removing the crystal from the loop, the crystal still remaining in the liquid. The difference between the two weighings gives directly the weight of the crystal in the liquid without any corrections.

The density of rocksalt and KCl is determined by immersion in Russian mineral oil. It is not only necessary to determine the density of the oil, but also its change with temperature. To determine the latter, two quartz crystals, a rocksalt and a KCl crystal are used and the temperature noted at each weighing. The weighings of the two quartz crystals, after reduction to the same temperature are used to calculate the density of the oil at that particular temperature. In calculating the change of density with temperature, the thermal expansion of the crystals has been taken into account. Table I gives the results in a condensed form. The temperature difference observed ranges from 0.2 to 0.6 degree.

For the density of diamond, resort has to be made to an entirely different method, as the crystals are far too small to use the immersion method to obtain any reasonable degree of accuracy. A solution[6] of thallous formate and

thallous malonate can be made to have a density of 4 or more, so that the diamond can float in it. At first, it was attempted to determine the density of the liquid by the ordinary method of immersion, after it has been made to the desired concentration. But it was found that successive weighings in the same solution did not agree very well with each other. It was either due to the change of density with evaporation, although the container was covered, change of density with temperature, or due to the existence of a density gradient in the liquid. The first two factors can be eliminated by weighing the liquid in a specific gravity bottle with a vacuum jacket to maintain constant temperature. Due to the probable existence of a density gradient in the

TABLE I. *Change of density of Russian mineral oil with temperature. Densities of crystals used*

Crystal	cub. exp.[5] coef. $\times 10^{-4}$	approx. vol. cc	decrease in wt. per 0.1° due to expansion of crystal	obs. increase per $0.1° \times 10^{-4}$ gm	true change $\times 10^{-4}$ gm	change in density per 0.1°
$quartz_1$	0.384	57.32	1.93	36.6	38.5	6.7×10^{-5}
$quartz_2$	0.384	41.90	1.42	20.8	22.2	5.3×10^{-5}
rocksalt	1.212	5.68	.6	3.48	4.08	7.2×10^{-5}
KCl	1.094	14.24	1.37	7.44	8.81	6.2×10^{-5}

The average change of density of oil per $0.1° = 6.4 \times 10^{-5} \pm 0.5 \times 10^{-5}$. *From this value of change of density, the first quartz crystal gives 0.88010 for the density at 24°C and the second gives 0.88012 giving an average value of 0.88011 at 24°C.*

liquid, there is no clear demarcation between the solution in which the diamond floats and that in which it sinks. The only way to overcome this difficulty is to narrow down the range of uncertainty by gradually diluting a solution in which the diamond unquestionably floats and making more concentrated a solution in which it undoubtedly sinks. Near and within the range there will be times when the diamond will float somewhere in the middle of the liquid. The range thus found represents 0.036 percent of the total weight of the liquid for the smaller diamond, and 0.019 percent for the larger one.

CORRECTIONS

1. Vertical divergence

In the x-ray measurements, correction must be applied to the angle of reflection due to the vertical divergence of the incident beam according to the formula.[3]

$$\delta\theta = \tfrac{1}{2}\alpha^2 \tan\theta$$

where α is the angle of vertical divergence, and θ the observed angle of reflection. By integrating over the two slits

$$\delta\theta = \frac{1}{24}\frac{a^2 + b^2}{L^2}\tan\theta$$

where a and b are the slit heights and L the distance between them.

[5] Smithsonian Tables, p. 220, 1923.

[6] R. G. O'Meara and J. B. Clemmer, Chem. Abstracts **23,** 1589 (1929).

For the rocksalt method, the same correction should be applied. In order to find out whether the same formula applies to this case or not, the angle of reflection for calcite has been measured by both methods, the rocksalt method giving a value larger by 1.1″. The correction as calculated from the formula, from the slit heights used, comes out to be 1.3″, showing the formula can be applied to the rocksalt method. However, in order to increase the intensity in the case of rocksalt, KCl and quartz, higher slits are used (both a and b are 1.7 cm) and L 58 cm), giving a larger correction.

2. Index of refraction

To correct for the index of refraction the ordinary formula is used, namely,

$$n\lambda = 2D \sin\theta(1 - \delta/\sin^2\theta)$$

where δ is calculated from the equation

$$\delta = ne^2/2\pi mv^2.$$

3. Calibration of the circle

The crystal circle has been calibrated.[3] It has been found that the circle can be relied on to 1″ of arc without correction. It has also been found that the largest errors in the calibration came in the microscope readings of the circle graduations. The ionization chamber circle has not been calibrated, but can be assumed to have the same degree of accuracy. Corrections for the ionization chamber observations are made by assuming the same curve for calibration.

4. Temperature effect on angle measurements

The correction for angle measurements due to temperature is calculated from the equation $d\theta = -\alpha(t-18)\tan\theta$, where α is the expansion coefficient of the crystal. This gives the corrections per degree of temperature shown in Table. II.

TABLE II. *Angle corrections per degree temperature.*

Crystal	Linear expansion coef.	Angle correction per degree of temp.
Calcite	$1.04.10^{-5}$	0.25″
Rocksalt	$4.04.10^{-5}$	1.07″
KCl	$3.65.10^{-5}$	0.86″
Quartz	$1.28.10^{-5}$	0.22″ for the A face 0.28″ for the 101 face
Diamond*	$0.118.10^{-5}$	0.11″ for the 400 face

* Int. Critical Tables: Vol. III, p. 21.

RESULTS

A. Angle measurements

All the angles given in Tables III–IX are corrected for circle calibration and reduced to 18°C. The results for calcite in the first order for both cleavage and polished faces are given in Tables III and IV.

TABLE III. *Angle measurements. Calcite—natural cleavage face, first order.*

Slit height, 6.5 mm		Slit height,† 3 mm		Slit height,† 0.8 mm	
Angle	Width at ½ max.	Angle	Width at ½ max.	Angle	Width at ½ max.
6°–42′–35.6″	4.5″	6°–42′–36.4″	5.7″	6°–42′–35.2″	6.6″
35.6″	4.8″	35.0″	5.4″	35.1″	6.8″
36.9″	4.8″	35.8″	5.8″	35.6″	6.8″
36.2″	4.1″	35.2″	5.5″	35.2″	6.4″
35.5″	4.7″				
36.2″	4.3″				
36.2″	4.9″				
36.5″	4.6″				
36.2″	4.9″				
Aver.	6°–42′–36.1″	6°–42′–35.6″		6°–42′–35.3″	
Corrected for vertical divergence	6°–42′–35.6″	6°–42′–35.5″		6°–42′–35.3″	

Resulting average 6°–42′–35.5″ ±0.1″

† These were taken after a complete new alignment.

TABLE IV. *Angle measurements. Calcite—polished face, first order.*

Slit height, 3 mm		Slit height 0.8 mm	
Angle	Width at ½ max.	Angle	Width at ½ max.
6°–42′–35.8″	12.0″	6°–42′–35.8″	12.6″
36.6″	11.8″	35.9″	11.0″
36.7″	11.4″	36.0″	12.0″
36.5″	11.5″	35.7″	11.6″
35.3″	11.6″	36.2″	11.2″
35.9″	12.7″		
36.0″	11.6″		
35.9″	11.8″		
35.5″	11.9″		
Aver. 6°–42′–36.2″		6°–42′–35.9″	

When corrected for divergence these give an average of 6°–42′–36.0″ ±0.1″, which is 0.5″ larger than that found for the cleavage face. The difference is probably due to the fact the polished face is not quite parallel to the original cleavage face.

Table V gives the results for calcite of the angle β between the axes. A piece is cleft from the same block as the crystals used above. Two good adjacent faces are used for this measurement. The line of intersection between the faces is set parallel and over the axis of rotation by the method previously described. The accuracy of the adjustment is borne out by the fact that the

TABLE V. *Angle measurements. Calcite—angle β between axes.*

Width of rocking curve				
Face 1	Face 2	Slit height	Angle α	Corrected angle
6.4″	6.2″	0.8 mm	105°–3′–23.9″	105°–3′–23.6″
7.4″	7.2″	2.0 mm	105°–3′–24.9″	105°–3′–23.4
6.6″	6.7″	0.8 mm	105°–3′–24.5″	105°–3′–24.2″
			Aver.	105°–3′–23.7 ±0.3″

widths of the rocking curves in the (1, −1) position are practically the same for both faces. The angle the crystal is rotated through between the two (1, −1) peaks gives the horizontal projection of the dihedral angle between the faces, from which the angle β can be calculated. Three different settings give the following values shown in Table V.

The angle β can be calculated from the equation

$$\cos \tfrac{1}{2}\beta = \frac{1}{2 \sin \tfrac{1}{2}\alpha},$$

giving

$$\beta = 101°\text{–}54' - 0.4'' \pm 0.3''$$

The unit volume of the crystal is then found from

$$\phi(\beta) = \frac{(1 + \cos \beta)^2}{(1 + 2 \cos \beta) \sin \beta} .$$

$$= 1.09592 \text{ at } 23°.5\text{C or } 1.09602 \text{ at } 18°\text{C}^7$$

Measurements by the optical method with a telescope with a Gauss eye-piece give 105°–3′–11.9″ as an average of five readings, which is some 12″ smaller than that obtained from the x-ray measurements. This incidentally

TABLE VI. *Angle measurements. Rocksalt—cleavage face, first order.*

	1st setting	2nd setting	Polished face
	7°–13′–36.0″	7°–13′–35.2″	7°–13′–37.0″
	7°–13′–36.4″	7°–13′–34.3″	7°–13′–37.4″
	7°–13′–35.5″	7°–13′–35.2″	7°–13′–38.1″
	7°–13′–36.7″	7°–13′–34.9″	7°–13′–35.9″
	7°–13′–36.7″	7°–13′–35.4″	7°–13′–36.1″
	7°–13′–36.7″	7°–13′–35.4″	7°–13′–36.4″
	7°–13′–36.1″	7°–13′–36.0″	7°–13′–38.6″
	7°–13′–35.9″	7°–13′–36.7″	
Aver.	7°–13′–36.3″	7°–13′–35.4″	7°–13′–37.1″

TABLE VII. *Angular measurements. KCl—natural cleavage face, first order.*

	1st setting	2nd setting	3rd setting
	6°–28′–28.8″	6°–28′–28.7″	6°–28′–27.9″
	6°–28′–28.8″	6°–28′–31.1″	6°–28′–28.8″
	6°–28′–29.2″	6°–28′–29.4″	6°–28′–28.4″
	6°–28′–28.7″	6°–28′–303.″	6°–28′–28.3″
			6°–28′–29.1″
			6°–28′–29.8″
			6°–28′–31.1″
			6°–28′–28.5″
Aver.	6°–28′–28.9″	6°–28′–29.9″	6°–28′–29.0″

[7] H. N. Beets, Phy. Rev. **25,** 621 (1925). $\phi(\beta)$ increases by 0.000018 per degree of decrease in temp.

gives an idea of the accuracy attainable in adjusting the second crystal parallel to its axis of rotation.

The results for rock salt are given in Table VI. The average of the two sets there given, after correcting for vertical divergence, gives 7°–13′–34.0″ ±0.3″. The measurements on KCl are presented in Table VII.

The average of three settings is 6°–28′–29.3″ and when corrected for divergence this becomes 6°–28′–27.6±0.3″. Measurements were made on two diamond crystals. They are summarized in Tables VIII and IX.

TABLE VIII. *Angular measurements. 0.89 karat diamond—polished, 400 plane.*

	Position 1	Width at ½ max.	Position 2 (Position 1 turned 180°)	Width at ½ max.
	23°–26′–5.6″	50″	23°–26′–6.3″	45″
	23°–26′–5.9″	50″	23°–26′–6.9″	45″
	23°–26′–5.5″	48″	23°–26′–7.0″	43″
	23°–26′–5.0″	48″	23°–26′–7.7″	47″
Aver.	23°–26′–5.5″		23°–26′–7.0″	
		Average:	23°–26′–6.3″	
		Corrected for div.:	23°–26′–3.6″ ±0.5″	

TABLE IX. *Angular measurements. 1.78 karat diamond—polished, 400 plane.*

	Position 1	Position 2 (Position 1 turned through 180°)	Position 3 (Position 1 turned through 90°)	Position 4 (Position 3 turned through 180°)
	23°–26′–5.7″	23°–26′–11.8″	23°–26′– 8.6″	23°–26′–6.3″
	23°–26′–6.5″	23°–26′–12.3″	23°–26′–10.9″	23°–26′–6.5″
	23°–26′–6.4″	23°–26′–11.4″	23°–26′– 9.9″	23°–26′–6.8″
	23°–26′–5.8″	23°–26′–12.9″	23°–26′–10.3″	23°–26′–6.0″
	23°–26′–6.8″	23°–26′–11.8″	23°–26′–10.2″	23°–26′–6.2″
	23°–26′–6.7″	23°–26′–11.1″	23°–26′–11.5″	
	23°–26′–6.0″			
	23°–26′–6.6″			
Aver.	23°–26′–6.3″	23°–26′–11.9″	23°–26′–10.2″	23°–26′–6.4″
	Average:	23°–26′–9.1″		23°–26′–8.3″
		Grand average:	23°–26′–8.7″ ±0.4″	
		Corrected for div.:	23°–26′–6.0″ ±0.4″	

B. Density measurements

The density measurements are summarized in Tables X, XI and XII.

TABLE X. *Density measurements.*

Calcite			Rocksalt		
Density	Temp. deg. C	Density at 18°C	Density	Temp. deg. C	Density at 18°C
2.70976	27.1	2.71009	2.16282	24.4	2.16450
2.70970	26.6	2.71002	2.16234	24.5	2.16404
2.70975	26.5	2.71007	2.16219	24.7	2.16395
2.70973	27.5	2.71009	2.16231	25.1	2.16417
2.70960	22.9	2.70990	2.16239	25.0	2.16422
	Average	2.71003 ±.00005			2.16418 ±.00014

TABLE XI. *Density measurements. KCl.*

Density	Temp.	Density at 18°C
1.98797	24.5	1.98933
1.98743	24.8	1.98885
1.98792	24.8	1.98934
1.98798	24.8	1.98940
1.98792	24.9	1.98936
1.98786	25.0	1.98932
1.98757	25.1	1.98905
1.98797	25.3	1.98949
1.98796	25.4	1.98951
1.98781	25.5	1.98938
		Average: 1.98930 ±0.00014

TABLE XII. *Density measurements. Diamond.*

0.89 karat diamond			1.78 karat diamond		
Weight of bottle and liquid			Weight of bottle and liquid		
Just floating	Just sinking	Floating in middle	Just floating	Just sinking	Floating in middle
235.629	235.560	235.611	235.623	235.586	235.595
235.621	235.575	235.611	235.623	235.591	235.603
235.630	235.569	235.618	235.625	235.595	235.608
235.627	235.557				235.619
	235.555				235.614
Aver. 235.6268	235.5632	235.6133	235.6243	235.5907	235.6064
Aver.: 235.5950		235.6133	235.6075		235.6064
Aver.: 235.6042			235.6070		
Calculated density at 18°C 3.5141 ±0.0001			3.5142 ±0.0001		

C. Calculation of grating constants

From the values of density and angles obtained, the values of calculated and observed grating constants are calculated and set forth in Tables XIII. The observed values are given in Table XIV.

TABLE XIII. *Calculated grating constants.*

Crystal	No. Mol. per unit cell	*M*	Unit vol.	Density at 18°C	Grating constant	
					$N=6.0594 \times 10^{23}$	$N=6.064 \times 10^{23}$
Calcite	½	100.075[2]	1.09602	2.71003	3.02940	3.03863
		±0.005	±0.00001	±0.00005	±0.00005	±0.00005
Rocksalt	4	58.454*	1	2.1642	2.81418	2.81347
				±0.0001	±0.00005	±0.00005
KCl	4	74.557	1	1.9893	3.13889	3.13810
				±0.0001	±0.00005	±0.00005
Diamond	8	12.003[2]	1	3.5141	3.55942	3.55852
(0.89 k)		±0.001		±0.0001	±0.00009	±0.00009
Diamond		12.003	1	3.5142	3.55938	3.55848
(1.78 k)		±0.001		±0.0001	±0.00009	±0.00009

* Mol. wt. of NaCl.

TABLE XIV. *Observed grating constants.*

Crystal	Face	Angle	$1-\mu\times10^{-6}$	Grating constant $N=6.0594\times10^{23}$	Grating constant $N=6.064\times10^{23}$
Calcite	Cleavage	6–42′–35.5″ ±0.1″	1.85		
Rocksalt	100	7–13′–34.0″ ±0.3″	1.41	2.81387 ±0.00005	2.81316 ±0.00005
KCl	100	6–28′–27.6″ ±0.3″	1.31	3.13900 ±0.00005	3.13822 ±0.00005
Diamond (0.89 k)	400	23–26′– 3.6″ ±0.5″	2.39	3.55966 ±0.00005	3.55875 ±0.00005
Diamond (1.78 k)	400	23–26′– 6.0″ ±0.5″	2.39	3.55956 ±0.00005	3.55866 ±0.00005

The differences between the calculated and observed grating constants are given in Table XV.

TABLE XV. *Difference between the calculated and observed grating constants.*

Crystal	Calculated value	Observed value	$\frac{D_{cal.}-D_{obs.}}{D_{cal.}}$
Calcite	3.02940		
Rocksalt	2.81418	2.81387	0.011%
KCl	3.13889	3.13990	−0.004%
Diamond (0.89 k)	3.55942	3.55966	−0.007%
Diamond (1.78 k)	3.55938	3.55956	−0.005%

For the sake of comparison the results of some of the other investigators are included in Table XVI. Since no accurate results are recorded for the

TABLE XVI. *Comparison with results of others.*

Angle cleavage face	Author	Density	Author	Unit volume	Author
6°–42′–34.3″	Leide[8]				
6°–42′–35.4″	Larsson[9]				
6°–42′–33.3″	Allison and Armstrong[10]	2.7102	Defoe and Compton[13]	1.09634	Beets[14]
6°–42′–36.0″	Compton[11]				
6°–42′–35.3″ to 35.6″	Bearden[12]	2.71026	Bearden[12]	1.09598	Bearden[12]
6°–42′–35.5″	Present	2.71003*	Present	1.09602	Present

Note: All values given above are reduced to 18°C.

* The author also made a density determination on a calcite crystal which is polished all around, giving a value of 2.71010.

[8] A. Leide, Comptes Rendus **180,** 1203 (1925).

[9] A. Larsson, Phil. Mag. **3,** 1136 (1927).

[10] S. K. Allison and A. H. Armstrong, Phy. Rev. **26,** 701 (1925).

[11] A. H. Compton, corrected by J. H. Williams, Letter to the Editor, Phy. Rev. May 15, 1932.

[12] J. A. Bearden, Phy. Rev. **38,** 1389 (1931).

[13] O. K. Defoe and A. H. Compton, Phy. Rev. **25,** 618 (1925).

[14] H. N. Beets, Phy. Rev. **25,** 621 (1925).

crystals used in this investigation with the exception of calcite, only those for calcite are listed below.

For rocksalt, using Siegbahn's[15] precise comparisons between the grating constants of rocksalt and calcite, and the value of D for calcite, adopted as a standard here, it is found that the D for rocksalt would be 2.81421 as compared with 2.81387 obtained above.

Defoe and Compton's measurement of the density of rocksalt gave 2.1637 ± 0.0004 as compared with 2.1642 obtained by the author.

Data for Quartz Crystals

Angle measurements on quartz crystals are presented in Table XVII, XVIII and XIX.

Table XVII. *Angle measurements. Quartz (1)–(100) face.*

Face 1 (polished) Position 1	Face 1 (polished) Position 2	Face 2 Natural	Face 2 Polished	Face 3 natural
4°–46′–55.2″	4°–46′–54.0″	4°–46′–37.9″	4°–46′–36.5″	4°–46′–37.2″
4°–46′–54.8″	4°–46′–53.2″	4°–46′–37.9″	4°–46′–36.9″	4°–46′–37.4″
4°–46′–55.4″	4°–46′–54.1″	4°–46′–37.3″	4°–46′–36.7″	4°–46′–37.5″
4°–46′–52.6″	4°–46′–53.1″	4°–46′–38.4″	4°–46′–36.6″	4°–46′–37.3″
4°–46′–54.6″				
4°–46′–53.9″				
4°–46′–54.7″				
Av. 4°–46′–54.3″	4°–46′–53.6″	4°–46′–37.9″	4°–46′–36.6″	4°–46′–37.4″
Corr. 4°–46′–53.1″	4°–46′–52.4″	4°–46′–36.7″	4°–46′–35.4″	4°–46′–36.2″
±0.6″	±0.4″	±0.3″	±0.2″	±0.1″

Table XVIII. *Angle measurements. Quartz (1)–(101) face.*

Face 3 Rocksalt method natural	Face 3 Calcite method	Face 4 Polished	Face 5 natural
6°–5′–26.5″	6°–5′–25.9	6°–5′–27.2″	6°–5′–31.7″
6°–5′–27.8″	6°–5′–25.1″	6°–5′–28.1″	6°–5′–31.5″
6°–5′–28.0″	6°–5′–26.2″	6°–5′–27.9″	
6°–5′–28.5″		6°–5′–27.3″	
Av. 6°–5′–27.7″	6°–5′–25.7″	6°–5′–27.6″	6°–5′–31.6″
Corr. 6°–5′–26.1″	6°–5′–25.4″	6°–5′–26.0″	6°–5′–30.0″
±0.7″	±0.4″	±0.3″	

Discussion of Results

Bearden,[16] using the value he obtained for the Cu $K\alpha$ line from a ruled grating and the value of $\sin\theta$ obtained by Siegbahn and Dolejsek from crystal measurements, and Larsson's value for the correction for index of refraction, obtained 3.0359 ± 0.0003 for the grating constant of calcite. This value is 0.217 percent larger than the value obtained here, using $6.0594.10^{23}$ for Avogadro's number, and 0.243 percent larger if $6.064.10^{23}$ is used. From the results of this experiment, it can be seen that the calculated and observed grating

[15] M. Siegbahn, Phil. Mag. **37**, 601 (1919).

[16] J. A. Bearden: Phy. Rev. **37**, 1210 (1931).

constants agree within experimental error for calcite, KCl and diamond. The probable errors are due mainly to the probable errors in molecular weight. The results for rocksalt are not as good, the significant fact being that the deviation is in the opposite direction. As far as the four crystals used in this experiment are concerned, there is found no definite proof for the existence of the mosaic effect suggested by Zwicky, or if it does exist, it can not affect the x-ray wave-length measurements by more than 0.01 percent . It can be concluded, therefore, that the crystal method of measuring x-ray wave-lengths can be relied on to within 0.01 percent when a perfect crystal is used, provided, of course, Avogadro's number is known to the same degree of accuracy.

TABLE XIX. *Angle measurements. Quartz (2).*

Face 1 Natural 100 face	Face 2 Natural 101 face		Face 3 Polished 100	Face 4 101 Polished
	Rocksalt method	Calcite method		
4°–46′–31.9″	6°–5′–19.4″	6°–5′–16.9″	4°–46′–48.5″	6°–5′–26.8″
4°–46′–32.6″	6°–5′–18.7″	6°–5′–17.0″	4°–46′–48.2″	6°–5′–26.0″
4°–46′–31.8″	6°–5′–19.9″	6°–5′–18.1″	4°–46′–48.2″	6°–5′–25.4″
4°–46′–30.7″	6°–5′–19.7″	6°–5′–17.8″	4°–46′–47.3″	6°–5′–25.4″
4°–46′–31.1″		6°–5′–18.2″	4°–46′–47.9″	
		6°–5′–17.6″		
Av. 4°–46′–31.9″	6°–5′–19.4″	6°–5′–17.6″	4°–46′–48.0″	6°–5′–25.9″
Corr. 4°–46′–30.3″	6°–5′–17.8″	6°–5′–17.3″	4°–46′–46.4″	6°–5′–24.3″
±0.5″	±0.4″	±0.4″	±0.3″	±0.4″

The density measurements are as follows:
Quartz (1) 2.64848 at 18°C ±0.00002. Quartz (2) 2.64864 at 18°C ±0.00002.

As to the data on quartz crystals, it may be said at the outset that the crystals are not as good as one would desire from the appearance of the faces. It can be easily seen from the angle measurements that quite different values of the grating constant will be obtained, depending on which set of planes is used. The differences are far beyond any experimental error, in the light of measurements on the other crystals. The differences can not be very well ascribed to surface conditions of the faces, because measurements on the same face, both natural and polished, gave practically the same value. They are certainly not due to the method used, because both the calcite and rocksalt method, when applied to the same face, gave practically the same value, which incidentally shows the validity of the rocksalt method. The differences, therefore, must be due to some variation in the structure of the crystal. However, in order to ascertain this variation definitely, a large number of observations must be made on different faces of the same crystal, and also on different crystals. It can be concluded, however, that quartz crystals are not suitable for precise wave-length measurements.

In conclusion, the writer wishes to extend his deep gratitude to Professor A. H. Compton who suggested this problem, for his valuable help and advice throughout the investigation, and to Professors W. H. Zachariasen and S. K. Allison for their helpful suggestions. Finally, I am indebted to Mr. J. Milhening of Chicago for loaning the diamonds used in this experiment.

Two-Crystal Analysis of *L*-Absorption Limits of Mercury

By H. L. HULL
Columbia University

(Received April 18, 1932)

An investigation of the shape and width of the *L* II and *L* III absorption limits of mercury has been made with the two-crystal x-ray spectrometer. Mercury was used in the liquid and vapor states and in chemical combination. The absorption limits are found to be asymmetrical. Approaching the limit from the long wave-length side, the intensity of the transmitted beam falls off rather sharply at first. This is followed by a more gradual decrease to the minimum value. The observed curves appear to bear out the suggestion by Kossel that the ejected electron may sometimes not be removed completely from the atom by the absorbed quantum, but only to an unoccupied upper level. The curves for the vapor have an over-all width of 45–50 volts. The curves for the liquid state are practically identical with the vapor curves at the long wave-length side, but fall off in intensity more slowly as the wave-length is decreased. The curves for the compounds are wider than those for the liquid and vapor and some exhibit fine structure.

INTRODUCTION

MOST investigations of x-ray absorption spectra have been concerned with the position and magnitude of the principal absorption edges and with the nature of the associated fine structure and secondary absorption. The single crystal spectrograph has been used in most of these researches. The high resolving power of the two-crystal spectrometer suggests its use in the study of the width and structure of absorption limits. The suitability of this instrument for such investigations was demonstrated by Bergen Davis and Harris Purks.[1]

The present investigation was undertaken to determine the effect of (1) physical state, and (2) chemical combination, upon the structure and width of an absorption edge.

A study was made of mercury in the vapor and liquid states and in compounds. It was observed that the edges were not symmetrical. This lead to a careful study of the shapes of the absorption curves.

The term *fine structure* is used to describe the discontinuities occurring at energy distances from the main edge of less than the ionization potential of the atom in question. The terms *secondary absorption* and *secondary structure* are used to describe discontinuities occurring at distances from the main edge, greater than the ionization potential.

Various investigations have shown that in many cases the main edge was marked by an absorption line followed by one or more regions of weaker and stronger absorption before the continuous absorption region is reached. The work of Kievit and Lindsay[2] in which was reported secondary structure for the *K* absorption spectra of elements calcium to gallium is typical of many researches in this field.

[1] Bergen Davis and Harris Purks, Phys. Rev. **32**, 336 (1928).
[2] Ben Kievit and George A. Lindsay, Phys. Rev. **36**, 648 (1930).

Secondary absorption edges have been accounted for by Coster,[3] Lindsay and Voorhees,[4] Ray,[5] and others by the assumption of simultaneous transitions of two or more electrons due to the absorption of a single quantum.

More recently Kronig[6] has proposed the following explanation for the existence of secondary structure. The energy spectrum of an electron moving in a determined direction through a periodic potential field consists of permitted and forbidden zones of finite width. The energy of the electron at the end of the absorption process therefore lies within these permitted zones. Kronig also shows why such secondary structure occurs not only in crystals consisting of a large number of atoms, but also in polyatomic molecules, while it is absent in isolated atoms.

Kossel[7] predicted that a fine structure near the main edge should be found corresponding to the removal of the electron to the various permissible unoccupied optical orbits. While Kossel's interpretation is generally accepted, there is a lack of accurate correlation between it and the fine structure actually observed.

E. C. Stoner[8] considers the shape of an absorption edge on the basis of Kossel's suggestion. By analogy with optical spectra, the probability of absorption of the first line should be much greater than that of the higher members. The width of the fine structure range and the resolving power of the spectrometer would determine in the particular case whether the observed edge would be smooth or exhibit discontinuities. As Stoner points out, the fine structure range would be much increased in the case of ionized atoms.

A complete account of the work in this field up to 1930 is given by A. E. Lindh.[9]

The effect of chemical combination and physical state on the L absorption limits of mercury has recently been investigated by Hanawalt[10] with the single crystal spectrograph. His data show that secondary absorption exists for the compounds but not for the liquid or vapor mercury. It was found that the edges of Hg are simple with no indication of a white line. Hanawalt points out that his resolution may not have been great enough to observe possible fine structure. A shift of -2.5 volts in the position of the liquid edge with respect to the vapor edge was found. In the case of $HgCl_2$ and HgO in the solid forms, shifts of $+1.2$ and -7.4 volts respectively were reported.

Pauling[11] has recently attacked the problem of the shifts of the x-ray absorption limits due to chemical combination. He gives the following relation

$$h\nu_{\text{abs}} = h\nu_0 + e\Phi - E_{\text{crystal}}$$

[3] D. Coster, Zeits. f. Physik **25,** 83 (1924).
[4] G. A. Lindsay and H. R. Voorhees, Phil. Mag. **6,** 910 (1928).
[5] B. B. Ray, Nature **122,** 771 (1928).
[6] R. de L. Kronig, Zeits. f. Physik **70,** 317 (1931).
[7] W. Kossel, Zeits. f. Physik **1,** 119 (1920).
[8] E. C. Stoner, Phil. Mag. **2,** 97 (1926).
[9] Handbuch der Experimental Physik **XXIV 2,** Teil (1930).
[10] J. D. Hanawalt, Phys. Rev. **37,** 715 (1931).
[11] Linus Pauling, Phys. Rev. **34,** 954 (1929).

in which ν_{abs} is the frequency of an absorption edge for an ion in a crystal and ν_0 that for a free ion. Φ is the potential at the center of an ion in a crystal due to all other ions. $E_{crystal}$ is the electron affinity which may be calculated in terms of the magnetic susceptibility. Φ is positive for anions and negative for cations. $E_{crystal}$ has the same effect for both. The agreement between theory and observed values in the case of the chlorine K edge in chlorides and the potassium K edge in various halides is very good. The shift of the potassium K edge is in the direction of longer wave-length and that of the chlorine K in the direction of shorter wave-length.

Apparatus

The double x-ray spectrometer was of the type described by Davis and Purks.[12] The ionization current was amplified by an F. P. 54 pliotron and read on a Leeds and Northrup type R galvanometer. Methyl bromide was used in the ionization chamber. The Pyrex vapor cell V, with thin windows W, was 22 cm long. It was provided with a side tube for holding the liquid Hg. The arrangement was such that the vapor could be superheated in the

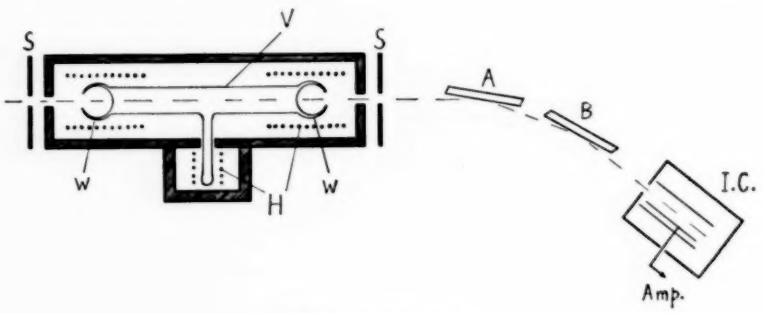

Fig. 1. Apparatus.

main part of the tube. The heat was supplied by the coils H. These coils were wound on cylindrical forms which were placed over the ends of the vapor cell. This arrangement prevented condensation on the windows. In actual operation a temperature of about 310°C was maintained in the side furnace. The main furnace was held about 25°C higher. The temperature could be maintained to ± 1°C. The absorption under these conditions afforded the maximum contrast consistent with a reasonable amount of transmitted energy. The slits S were 8 mm wide and 10 mm high. X-ray tubes with molybdenum and tungsten targets were used. The observed curves were always corrected for the variations in the intensity of the spectrum obtained without the absorber. The correction was made in the following manner. A reference point was chosen on the energy-wave-length curve (without absorber). The energies at all other wavelengths were compared with that at the reference point. This correction in percent was then made in the observed curves. The x-ray tube was usually operated at 40 k.v. and 50 m.a.

[12] Bergen Davis and Harris Purks, Proc. Nat. Acad. Sci. **13**, 419 (1927).

Preparation of Materials

To observe the absorption edges of liquid Hg in about the same contrast as in the case of the vapor requires a film about 0.003 cm thick. Many methods were tried in an attempt to obtain a uniform film of this thickness without success. Finally a suitable suspension of Hg was found. Its composition is as follows:

Mercury	500 gm	Prepared suet	230 gm
Oleate of mercury	20 gm	Benzoinated lard	250 gm

A very satisfactory absorbing sample may be made from this preparation by mixing it with additional lard. This allows the use of a sample of sufficient thickness to insure uniformity in absorption over the exposed area. Upon dissolving out the fat it was possible to recapture the mercury in the metallic form.

Attention should be called to the fact that with the double x-ray spectrometer used in this investigation, the point at which the beam of x-rays of

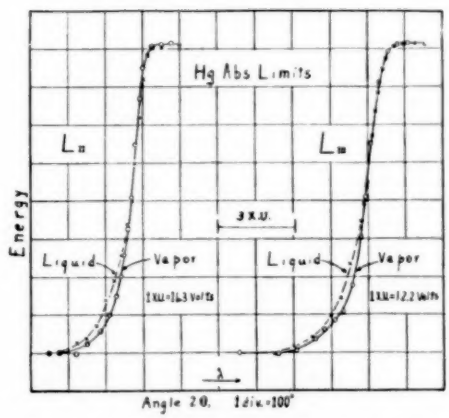

Fig. 2. Hg *L* II and *L* III absorption limits for the vapor and liquid states.

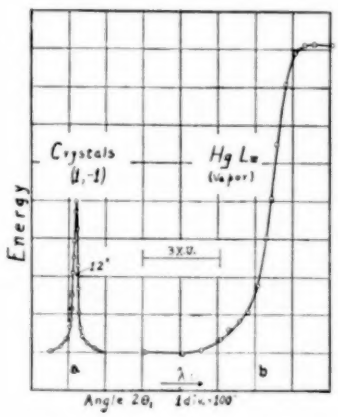

Fig. 3. (*a*). Rocking curve for crystals in the parallel position (1, −1). (*b*), Hg vapor *L* III absorption limit.

given λ strikes crystal *A*, moves as crystal *B* is rotated. This means that the beam will shift across the absorbing sample slightly as crystal *B* is rotated. By placing the sample near the x-ray tube this effect may be minimized.

Samples of $Hg(NO_3)_2$ and $HgCl_2$ were obtained by dipping cigarette papers in the solutions of these salts. Several of these sheets were superposed in making up the samples. HgO and HgI_2, which were in powder form, were rubbed on cigarette papers, many sheets being used to obtain uniformity in the thickness of compounds in the sample. To test the uniformity, absorption curves were taken with the samples in many different positions.

Experimental Results

Liquid and vapor curves

Fig. 2 shows the absorption curves for Hg L II and Hg L III in the liquid and vapor states. The intensity of the transmitted radiation is seen to fall off sharply at the long wave-length side of the curves. The decrease is more gradual at the short wave-length side. In the upper part, the liquid curve is practically identical with the vapor curve but a departure is observed in the lower part. The intensity falls off more slowly in the case of the liquid as the wave-length is decreased.

In Fig. 3 a rocking curve taken with the crystals in the parallel (1, −1) position is shown together with that of the vapor Hg L III (1, 1). The resolving power of the instrument depends upon the half maximum width of the curve in Fig. 3 (a). This is observed to be 12″ and is equivalent to 2.1 volts. In taking this curve, the slits were of the same width as in the absorption measurements. The same part of the surface of crystal A was used in

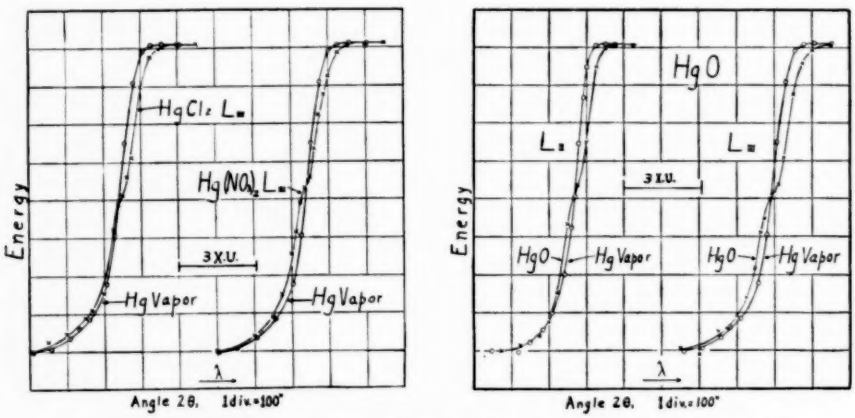

Fig. 4. *a*. HgO L II and L III limits. *b*, $HgCl_2$ and $Hg(NO_3)_2$ L III limits.

both cases, since crystal A remains fixed in position. Although crystal B must be reversed in changing from the (1, 1) position to the (1, −1) position, the portions of its surface used in each case can be made very nearly the same.

The absorption curves for HgO (yellow), $HgCl_2$ and $Hg(NO_3)_2$ are shown in Fig. 4. The Hg vapor curves are plotted for comparison. HgO (see Fig. 4a) shows a definite break in L II and L III. $HgCl_2$ L III and $Hg(NO_3)_2$ L III (see Fig. 4b) exhibit this structure also. In each case the main edge comes at a longer wave-length than that for the vapor with the additional break displaced to the short wave-length side of the vapor edge. No evidence of fine structure was found in $HgCl_2$ L II and $Hg(NO_3)_2$ L II. However these curves were none too reliable. The decrease in intensity from the long wave-length side to the short wave-length side was usually only 25 to 30 percent in the case of L II. In the case of L III the decrease in transmitted energy was about 50 percent.

There is no evidence of fine structure in the L II and L III curves of HgI_2 (red), (see Fig. 5).

The L II and L III curves were plotted to the same scale for purposes of comparison. The absorption curves for the compounds show the gradual sloping off at the high energy (short wave-length) side in common with the liquid and vapor curves.

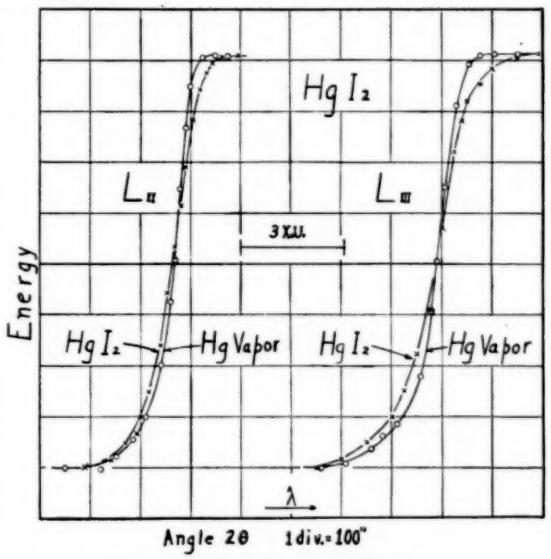

Fig. 5. HgI_2 L II and L III limits.

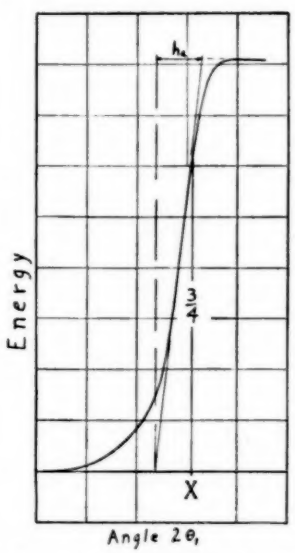

Fig. 6. Absorption limit showing method of estimating angular position and h_a width.

Discussion of Experimental Results

To determine whether or not a shift in the position of the limit occurs between the liquid and vapor states, all of the observed curves were examined in the following manner. A point whose ordinate (see Fig. 6) is 3/4 of the value

of the maximum ordinate is chosen. The abscissa of this point (x) which gives the angular setting on crystal $B(2\theta_1)$ is then read off. These angles were tabulated for all of the liquid and vapor curves. In the case of L III the mean for the liquid curves lies 4 seconds to the long wave-length side of the mean for the vapor curves. In the case of L II the mean for the liquid curves falls within one second of that for the vapor curves. Consideration of the data does not justify specifying these means to better than 5 seconds. It must be concluded that within the limits of the accuracy of the present measurements, the L II and L III absorption edges have the same energy value for both the liquid and vapor states. In the L III position, 5 seconds is equivalent to 0.88 volts. Hanawalt reported a shift of -2.5 volts but did not estimate the precision of his measurements. He states that his dispersion was 70 to 90 volts per mm (on photographic plate) in this wave-length region. A shift of 2.5 volts is equivalent to 14 seconds on crystal B.

Schwarzschild[13] has calculated the correction for the observed breadth of an absorption edge in terms of the width of the curve with the crystals in the (1, -1) position (see Fig. 3). The calculation is for a symmetrical absorption limit. The quantity h_a (see Fig. 6) is taken as a measure of the diffuseness of the absorption edge. If H_c is the half maximum width of the (1, -1) curve it is shown that

$$h = (h_a^2 - 1.13H_c^2)^{1/2}.$$

The quantity h is the corrected width of the absorption edge. All values are expressed in seconds of arc for convenience.

In the present case where the absorption discontinuities are not found to be symmetrical, this correction would not be expected to apply rigorously. If h_a is estimated for the L III curves it is found that the mean is 86″. H_c is 12″. Upon substitution in Schwarzschild's formula it is found that h is 85″. It is thus seen that the correction is negligible.

It is of interest to note that h_a for the L III edge when expressed in volts is nearly the same as h_a for L II expressed in volts.

h_a for L III vapor = 86″ ≐ 15.2 volts
h_a for L II vapor = 67″ ≐ 15.8 volts

The over all width of the L II and L III discontinuities is about 45–50 volts.

When an electron is removed from one of the L shells of mercury (80), the resulting configuration resembles a thallium atom. Thus the possible optical levels will be those of Tl and not those of Hg. The International Critical Tables give for the resonance potentials of thallium 0.96, 3.27, and 4.47 volts. The first ionization potential is given as 6.08 volts. The resolving power of the spectrometer as used was about 2 volts. This might explain why the observed vapor curves are smooth. However there seems to be no ready explanation of the width (45–50 volts) on this simple basis.

[13] Myron Schwarzschild, Phys. Rev. **32**, 162 (1928).

In the compound curves it is found that the main edges for HgO, $Hg(NO_3)_2$ and $HgCl_2$ are shifted -4.8 v, -2.8 v and -3.5 v respectively. They are all shifted in the direction of longer wave-length. Hanawalt found a shift of -7.4 v for HgO and a shift of $+1.2$ v for $HgCl_2$.

In conclusion the writer wishes to thank Professor Bergen Davis for suggesting this problem and for the many privileges enjoyed in his laboratory.

Diffraction of Low-Speed Electrons by Single Crystals of Copper and Silver

By H. E. FARNSWORTH
Brown University, Providence, Rhode Island
(Received March 28, 1932)

Diffraction beams for normal incidence on the (100) faces of copper and silver crystals.—Previous results for a *copper crystal* are checked and extended, by using another crystal of exceptionally pure copper. All of the expected diffraction beams which are x-ray analogues in the two principal azimuths and in the range below 325 volts are found. These beams require values of refractive index greater than unity, but the associated values of inner potential are *not constant*. Another class of weak beams is found characteristic of the copper lattice, but which require a refractive index of approximately unity for the first order beams of the two principal azimuths. These weak beams accompany the main beams on the high voltage side as satellites. Conditions for orders higher than the 1st are more complicated and indicate that the above method of classification is not sufficient. For a *silver crystal* the number of experimental maxima is considerably greater than the number of theoretical beams in the low-voltage range. These maxima cannot be classified as main beams requiring a refractive index greater than unity, and weak satellites requiring unit refractive index as in case of a copper crystal, but whenever two or more experimental maxima are to be associated with a given theoretical beam, they are, in general, grouped as components of fine structure of a single diffraction beam.

Intensity measurements on diffraction beams as a function of angle of incidence.—*For copper*, as the angle of incidence is changed by only a few degrees from normal, large intensity changes of the various diffraction beams are observed. Some beams increase while others decrease in intensity for a given change in angle of incidence. Primary voltage and collector angle are adjusted for each observation. For *silver*, as the angle of incidence is changed from normal the relative intensities of the components associated with a particular beam change rapidly. Some components may disappear and others appear at different voltages, as the incident angle is changed a few degrees. The plane grating formula is approximately satisfied over considerable ranges in the angle of incidence, but there are other ranges for which it is not satisfied. The above variations for various beams do not correspond; neither do those for the beams associated with different orders of reflection from the same set of Bragg planes. Intensity measurements are given for most of the beams in the two principal azimuths below 350 volts for ranges in the angle of incidence, including normal incidence, through which the beams are observable.

Regular reflection of electrons from the (100) set of planes.—For copper, with angle of incidence equal to angle of reflection, curves obtained by measuring collector current as a function of primary voltage show many irregularities. For silver, the curves contain many irregularities which do not correspond to those for a copper crystal under similar conditions. For the same angle of incidence and the same set of reflecting planes, the results are not the same for the plane of reflection in the (100) and the (111) azimuths, respectively.

Diffraction beams due to a surface gas lattice on the (100) faces of copper and silver crystals.—For copper, "additional" beams which were formerly reported have since been found to decrease in intensity after prolonged heat treatment of the copper crystal at temperatures near its melting point. These beams indicate a *simple-cubic, single-spaced* lattice with the same constant as that for the copper lattice. They require values of refractive index greater than unity. When the surface gas lattice becomes thin it changes in structure from a *simple-cubic, single-spaced* lattice to a *face-centered*,

double-spaced lattice. The beams characteristic of the latter structure require *unit* refractive index. Hydrogen also forms in either of the above two lattices on a copper crystal, depending on the pressure of the hydrogen while the lattice is formed. The lattice which is characteristic of the thicker layer is very unstable and soon changes to that of the thinner layer after the pressure is removed. For *silver*, only a few very weak beams due to a surface gas lattice are found below 50 volts after heating the crystal a short time at red heat. They indicate a double-spaced, face-centered structure.

Inner potential. The measured value of the inner potential is neither constant nor a continuous function of the voltage. It is found to change discontinuously, by several volts in some cases, as the angle of incidence is varied. Results for the crystals of copper and silver which have the same lattice structure are found to differ widely. Hence they appear to be a function of the type of atom.

Surface action. Experimental methods of distinguishing between effects due to surface action and those due to a space lattice are discussed.

Introduction

EXPERIMENTS on electron diffraction by solids may be divided, according to their correlation with simple theory, into two classes. (1) Those with high-speed electrons having energies of several thousand equivalent volts have been performed by various observers[1] with polycrystalline targets. The results are all in accord with those to be expected on the basis of de Broglie's original equation $\lambda = h/mv$. Recently Rupp[2] has extended previous measurements to electron energies as high as 220 k.v. and finds the results in accord with theory when relativity is included. Although Kikuchi[3] obtained unusual results when using mica crystals, they are explained when proper account is taken of the particular conditions which obtain in the mica crystal. G. P. Thomson[4] has recently extended measurements with high-speed electrons to single crystals of copper, silver, and rocksalt. Although the results are much more complicated than one should anticipate, they appear to be accounted for by assuming that the etched surface of the crystal is composed of lumps of dimensions about 10^{-6} cm through which electrons can pass when striking the surface at glancing angles of incidence.* (2) Experiments with low-speed electrons having energies less than a few hundred volts show many deviations from the predictions of simple theory. In the original experiments of Davisson and Germer,[5] using normal incidence on the (111) face of a single nickel crystal, several expected beams were missing while a few unexpected beams were found. When using an arrangement corresponding to Bragg reflection, i.e., angle of incidence other than normal and equal to angle of reflection, many anomalous beams were present.[6] Rupp,[7] with an

[1] See references in "Wave Mechanics of Free Electrons" by G. P. Thomson.

[2] E. Rupp, Ann. d. Physik **10**, 927 (1931).

[3] S. Kikuchi, Proc. Imp. Jap. Acad. **4**, 271, 275, 354, 471 (1928); Jap. Jour. Physics **5**, 83 (1928).

[4] G. P Thomson, Proc. Roy. Soc. **133 A**, 1 (1931).

* Recent experiments of Davisson and Germer (paper at Cambridge meeting of Am. Physical Society, Feb. 1931) with high-speed electrons and single crystals of nickel and tungsten do not show such characteristics.

[5] C. Davisson and L. H. Germer, Phys. Rev. **30**, 705 (1927).

[6] C. Davisson and L. H. Germer, Proc. Nat. Acad. **14**, 619 (1928).

[7] E. Rupp, Ann. d. Physik **5**, 453 (1930); see also H. E. Farnsworth, Phys. Rev. **36**, 1799 (1930).

arrangement similar to the latter, appears to find fewer anomalies but reports several half-order beams. Early experiments by the writer,[8] using normal incidence on a (100) face of a single copper crystal, showed the presence of several "additional" beams which were later[9] greatly reduced in intensity by prolonged heating of the crystal at temperatures near the melting point of copper, and hence are attributed to gas. In these later experiments another weak class of beams (referred to as satellites) was found whose intensity did not decrease with prolonged heating of the crystal. Most of them occur at such voltages as to require a unit refractive index while the intense beams require values of refractive index greater than unity. Boas and Rupp[10] have more recently reported similar beams for tungsten. Previously unpublished results obtained by the writer for a copper crystal using an arrangement corresponding to Bragg reflection also show the presence of many unexpected beams.

It thus seems clear, as has already been emphasized by G. P. Thomson,[4] that high-speed electrons are much more suitable for investigations of crystal structure similar to those made with x-rays.

On the other hand, the very fact that unexpected results are obtained with low-speed electrons shows that certain conditions within the crystal reveal themselves to this method of experiment, but entirely escape detection by high-speed electrons or x-rays. Since low-speed electrons, when impinging on a crystal surface, are affected by fields which have little or no influence on high-speed electrons or x-rays, possibilities at once suggest themselves of obtaining, by the use of low-speed electrons, valuable information which is inaccessible to other methods of investigation. Questions of inner potential and the associated refractive index are immediately involved. The regions in the outermost parts of the atoms that play no part in the scattering of x-rays may here be expected to make significant contributions. Although estimates of the inner potential of ionic crystals have been made from observations with high-speed electrons,[11] it seems reasonable to expect that information regarding possible variations from its mean value can be obtained only with the use of low-speed electrons. A wide range of experimental observations combined with a satisfactory method of interpretation are required to make this information available.

The theory of electron diffraction by a space-lattice has been discussed by Bethe[12] and by Morse.[13] The latter has accounted for the anomalous results of Davisson and Germer for a nickel crystal. v. Laue[14] has estimated the influence of the gradual transition of the field across the boundary of a crystal and found that the surface action may be neglected for electrons of 200 or more volts energy, but that for lower energies the theories of Bethe and

[8] H. E. Farnsworth, Phys. Rev. **34**, 679 (1929).
[9] H. E. Farnsworth, Phys. Rev. **35**, 1131 (1930).
[10] W. Boas and E. Rupp, Ann. d. Physik **7**, 983 (1930).
[11] A. G. Emslie, Nature **123**, 977 (1929). G. P. Thomson, Proc. Roy. Soc. **133A**, 1 (1931).
[12] H. Bethe, Ann. d. Physik **87**, 55 (1928).
[13] P. M. Morse, Phys. Rev. **35**, 1310 (1930).
[14] M. v. Laue, Phys. Rev. **37**, 53 (1931).

Morse require extension. Contributions have also been made by Kronig and Penny,[15] and by Hill.[16] There is, however, nothing in these treatments which would lead one to expect that the results might vary greatly among different substances having identical crystal lattices. The results contained in the present paper show that this is actually the case.

It appears that further progress can only be made by first obtaining experimental data for various crystals under similar conditions. These data should include an accurate measure of the intensities of the various diffraction beams over a considerable range of the variables upon which the values of the intensities depend. That the angle of incidence of the primary beam is one of the most significant of these variables was observed a few years ago by the writer during some of the first experiments with a copper crystal. At that time, while searching for a possible polarization effect due to weak magnetic fields, it was found that large changes of intensities of some of the diffraction beams were produced by a transverse magnetic field of a fraction of a gauss. The primary voltage was adjusted to best value for each field. The observed changes of intensities appeared much larger than those which one might reasonably expect as a result of the small change in the angle of incidence produced by the magnetic field. In order to determine the cause, the apparatus was modified so that the angle of incidence could be varied. It was then found that the large intensity changes were due entirely to the small changes in the angle of incidence. These intensity changes have now been investigated in some detail.

The present paper contains results for a copper crystal which supplement those previously reported.[8,9] Some of the results reported here have been briefly described in a letter to the Editor of the Physical Review[9] some time ago. A more detailed account has been postponed since it appeared that an interpretation of some of them might depend on corresponding results for a crystal of some other metal. That this is the case is shown by unexpected results which have now been obtained for a silver crystal.

Apparatus

The experimental arrangement in use at present is a modification of that which has already been described in detail.[8] Hence it will be sufficient to refer to the original description and to indicate what changes have been made. These changes have been incorporated at different times during the last two and one-half years, so that all of the results reported here have not been obtained with the apparatus in its present form.

The electron gun has been altered to the form shown by AB, Fig. 1. The diaphragmed tube which limits the primary electron beam has been greatly increased in length. This results in a more sharply defined electron beam, and makes possible a more accurate alignment of its direction. In order to keep the total distance between filament and target the same as previously, an alteration in the geometry of the parts near the filament was required. Al-

[15] R. de L. Kronig and W. G. Penny, Proc. Roy. Soc. **130**, 499 (1931).
[16] E. L. Hill, Phys. Rev. **37**, 785 (1931).

though this modified form does not produce as large electron currents as the former one at very low primary energies of the order of a few equivalent volts, its other advantages make it preferable for the present experiments.

The former mounting of the crystal has been replaced by one which permits a rotation of the crystal about an axis lying in the crystal face and perpendicular to one of the principal azimuths, thus permitting a range in the angle of incidence of the primary electron beam from $-15°$ to $+50°$, measured from the normal. The arrangement is shown in Fig. 1. The crystal is first cut in the approximate form of a rectangular parallelepiped of dimensions about $6\times6\times12$ mm, one of the ends being accurately parallel to a (100) set of planes of the crystal. The sides are cut either parallel to (100) or (110) planes, depending on whether the crystal is to be rotated about an axis parallel to the (100) or (110) azimuths, respectively. The method of prepar-

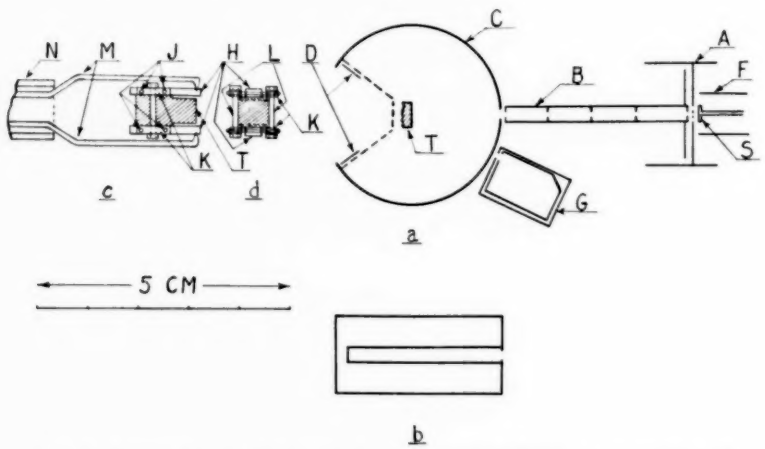

Fig. 1. Apparatus. *a*—top view, *b*—side view of drum, *c*—mounting of crystal, side view, *d*—mounting of crystal, front view.

ing the surfaces has already been described.[8] The etching process varies with the metal of which the crystal is composed. After cutting the crystal to the approximate dimensions given above, one of the cross-sectional dimensions is reduced on the front half of the crystal in order to form a clearance between this half of the crystal and the mounting, as shown in Fig. 1. The mounting consists of two beams of rectangular cross-section *H* made from molybdenum sheet and clamped rigidly to the back half of the crystal. Four tungsten rods *J* pass through holes in these beams and also through holes in four other molybdenum beams *K* arranged as shown. Two other tungsten rods *L*, threaded on the ends, pass through holes in the beams *K*. Thin steel nuts on the ends of the threaded tungsten rods hold the mounting in place. The amount of metal contained in the nuts is so small that their magnetic effect at the face of the target is negligible. A tungsten strip (not shown) is held against one side of the crystal near the rear. To outgas the crystal, this strip is bombarded and the crystal thus heated by conduction. This form of mounting was adopted after trying another less satisfactory one. It must ful-

fill the rigid requirement of keeping the crystal in its original adjustment when heated at red-heat temperatures. This mounting makes it unnecessary to drill holes in the crystal, an important consideration for metals which recrystallize rather easily. Small holes (No. 80 drill) near the ends of the beams H admit the points of the tungsten rods M which serve as pivots. These rods pass through a Pyrex glass tube N (parallel to the axis) of 24 cm diameter and 1.2 cm length. At the end nearest the crystal the rods pass through close fitting holes in a molybdenum frame (not shown) fitting inside the tube. At the other end of the tube the rods pass through holes in a steel frame which fits the end of the tube. Set screws prevent the rods from slipping parallel to the tube. The arrangement is such that one of the rods may be moved a small distance parallel to the tube by turning a screw which presses against the end of the rod. This permits a fine adjustment at the time of mounting the crystal. A bar of soft iron which is attached to the steel frame at right angles to the tube axis, serves as a magnetic control by means of which the tube may be rotated about its axis or displaced parallel to it. A molybdenum rod passes along the axis of the tube and may be displaced parallel to it. At the end near the crystal, this rod attaches by means of a tungsten pivot to one end of a movable arm. The other end of the arm is attached by another tungsten pivot to an arm (now shown) fixed to the crystal mounting. At the other end of the tube, the molybdenum rod is connected by suitable coupling to a steel screw which may be turned by another magnetic control. Turning this screw thus rotates the crystal. Loose play is eliminated by a flexible tungsten coiled spring. The Pyrex glass tube is ground accurately round at two points which serve as bearings when an adjustment of azimuth is made. This Pyrex tube slides and rotates in another frame which fits snugly into a part of the main experimental tube.* This frame is the same as that which formerly supported the Faraday cylinder E, Fig. 1 of previous article.[8] The Faraday cylinder E has been removed in the present arrangement. This arrangement makes it possible to withdraw the crystal into a side tube where it may be outgassed by electron bombardment from the rear. An automatic trap door prevents evaporated metal from entering the main part of the tube. All motions are effected by magnetic controls sufficiently removed from the crystal to have no disturbing magnetic effect.

The accuracy of the adjustments depends to a great extent on the accuracy of the mounting of the crystal. The front face of the crystal can be made parallel to a desired plane to within 0.5° by methods previously described.[8] After cutting and etching the crystal to the desired size and shape it is placed in the mounting, care being taken not to scratch the forward half of the crystal by touching with any hard surface. The front half is protected with moist filter paper during the adjustment, care being taken that nothing touches the front face. After clamping the mounting on the crystal as nearly as possible in adjustment, it is placed on a goniometer and viewed with a telescope at several feet distant rather than with one attached to the instru-

* I am indebted to Mr. Newton Underwood for the design of certain parts of this arrangement.

ment. The telescope is mounted with its axis perpendicular to the axis of the goniometer, and a small beam of light nearly coincident with the telescope axis is directed toward the crystal. If the crystal has been properly etched, reflections may be observed from the sides as well as from the front. These make it possible to test the adjustment with the desired accuracy. With silver good reflections were obtained from both (100) and (110) planes on the sides of the crystal. The crystal is so oriented with respect to the goniometer and telescope that it may be rotated about the proper axis to test the alignment of the mounting with respect to the crystal. The straight line connecting the centers of the small holes in the mounting should lie in a desired azimuth and pass through the center of the front face parallel to a particular plane. If the front face were cut and etched exactly parallel to the desired plane then, of course, the line in question should lie in the plane of the face. Also, if this adjustment were exact, the line connecting the centers of the small holes would be parallel to the line of sight when the visible halves of the holes appear lined up in the telescope. (Only one-half of each hole is visible by transmitted light, the other half being shielded by the crystal.) If the front plane is not exactly parallel to the desired plane, the line connecting the visible parts of the holes will not be parallel to the atomic plane in question. To eliminate this possible error, indicator marks were placed in the mounting at the same distance, to within 0.01 mm, from each hole. The line connecting these could be adjusted to the desired position to within 0.5°. The crystal and mounting were cleaned before adjusting and were not subsequently touched with the hands. After placing the crystal with its mounting in position between the two tungsten pivots, one of these is adjusted so that the desired crystal plane is perpendicular to the axis of the Pyrex glass tube which supports the crystal. To check the alignment in the experimental tube, the parts are first assembled with the filament, which acts as the electron source, removed. The alignment is then adjusted until a narrow beam of light, which is sent down the electron gun, is reflected by the crystal face back through the gun into a telescope placed 10 feet from the tube.

Further Experiments with a Copper Crystal

Preparation of crystal

The crystal used for the present experiments was cut from one made of exceptionally pure copper* by slowly lowering the melt through a constant (in time) temperature gradient in a vertical-type, molybdenum-wound, hydrogen furnace. A lowering speed of 1/8 in. per hour was used. From 90 to 100 hours were required for the run including time of bringing the furnace up to temperature. The mold was made from graphite rod of highest purity obtainable from the Acheson Graphite Corporation. A coating of nickel electroplated on the outside of the crucible helped to preserve it. The original crystal was 3/4 in. in diameter and 7 in. long with the lower end tapering to

* I am indebted to Dr. S. Skowronski of the Rantan Copper Works, Perth Amboy, N. J., for the copper which was of greater purity than the standard melting point copper used by the Bureau of Standards.

TABLE I. *Main diffraction beams for the copper lattice; approximately normal incidence.*

Beam and order numbers*	Plane of reflection	Experimental colatitude angle	Experimental voltage	Theoretical voltage	Voltage difference	Corrected intensity: Background intensity	Corrected relative intensity
			(100) Azimuth				
1–1	(210)	63.0°	60.3	72.2	11.9	20.4	100
2–1	(310)	43.0°	115.5	128.4	12.9	3.3	62
3–1	(410)	31.5°	191.5	208.5	17.2	2.3	76
4–1	(510)	25.0°	296.5	312.4	15.9	1.2	54
1–2	(320)	74.0°	200.5	217.0	16.5	2.4	10
2–2	2(210)	56.5°	260.5	288.9	28.4	1.9	11
			(111) Azimuth				
1–1	(311)	67.5°	26.5	38.8	12.3	49.0	84
2–1	(511)	35.8°	69.7	84.2	14.5	6.9	88
3–1	(711)	25.8°	127.5	153.3	24.8	2.5	70
4–1	(911)	17.5°	220.0	245.7	25.7	1.2	61
1–2	(211)	74.0°	99.0	104.0	5.0	5.5	11
2–2	2(311)	54.0°	138.0	155.3	17.3	4.7	45
3–2	(411)	41.2°	203.0	234.0	31.0	1.8	22
4–2	2(511)	31.0°	320.0	337.0	17.0	4.6	69
2–3	(733)	63.5°	242.5	264.5	22.1	3.9	7

* The notation 2–1, e.g., refers to the second beam in the first order. The notation of orders is the same as that originally used by Davisson and Germer. It should be noted that the second-order beams in this notation are not all second-order beams in the Bragg notation. This is seen by comparing with the corresponding values in the second column. The 2–2 beam in the (100) azimuth is, however, a second order reflection from the (210) set of planes. The lowest index numbers are used for the Miller indices in the second column. The corresponding reflections are respectively (420), (620), (820), (10,2,0), (640), (840), (311), (511), (711), (911), (422), (622), (822), (10,2,2), (733).

TABLE Ia. *Corresponding satellites.*

Experimental colatitude angle	Theoretical colatitude angle	Experimental voltage	Theoretical voltage	Voltage difference
	(100) Azimuth			
55.3°	53.1°	72.5	72.2	−0.3
37.5°	36.9°	128.5	128.4	−0.1
30.5°	28.1°	210.5	208.7	−1.8
24.7°	22.7°	310.5	312.4	1.9
	67.4°		217.0	
57.8°	53.1°	277.0	288.9	11.9
	(111) Azimuth			
53.7°	50.5°	37.3	38.8	1.5
29.5°	31.6°	87.0	84.2	−2.8
24.5°	22.3°	146.0	153.3	7.3
17.5°	17.9°	243.0	245.7	2.7
64.5°	70.3°	111.0	104.0	−7.0
50.5°	50.5°	154.5	155.3	0.8
39.0°	38.0°	215.0	234.0	19.0
62.0°	64.4°	260.0	264.6	4.6

a point. Orientation of the crystal was determined by the method previously described.[8] Etching was done sometimes with ammonium persulphate and sometimes electrolytically with the crystal as anode. In the latter case it was found that for low current densities etching occurs only parallel to (111) planes. For higher current densities etching occurs predominantly parallel to (100) planes if the conditions are right.

Number and relative intensities of main diffraction beams for approximately normal incidence

The results obtained with the first copper crystal of unknown purity which was obtained from the General Electric Company are in satisfactory agreement with those obtained with this crystal under the same conditions when one considers a slight difference in the angles of incidence due to error, and the corresponding voltage changes which have been found to result from small changes in the angle of incidence. *All* of the expected diffraction beams in the two principal azimuths and in the range below 325 volts were observed for the second crystal. As before, only full-speed electrons were admitted to the Faraday collector. After further heating of this crystal at temperatures considerably higher than those previously used, a class of "additional" beams occupying the positions required by a *simple cubic* structure had decreased in intensity to a small fraction of their former values and hence are due to a gas lattice on the surface. (This crystal has been heated at various red-heat temperatures, some near the melting point, for 43 hours. During this time recrystallization occurred only to a slight extent in the region where the mounting and crystal came in contact).

Table I contains the relative intensities of the main diffraction beams for approximately normal incidence. These are the maximum deflections obtained for the various beams with optimum values of primary voltage and colatitude angle, and with a constant primary electron current. It might appear advisable to obtain the relative intensity of an electron diffraction beam by the method of integrated reflection used for x-rays. This has not been done because of the experimental difficulties which would be involved. Also, in view of the irregularities which are found, the type of measurements made here appear just as significant. Because the adjustment for normal incidence was in error by approximately 1° (the accurate method of adjustment described above was not used for this crystal), and since the intensities of the beams vary with the angle of incidence, the values of intensity in Table I probably differ somewhat from the correct values for normal incidence.

Beams requiring unit refractive index

In addition to the beams described above there is another class of weak beams a few of which were observed during the investigation with the first copper crystal.[8] Most of the observations on these beams were obtained after the gas beams had been greatly reduced in intensity. The first beams of this class which were observed occur at such primary voltages as to require a unit refractive index, while the "main" beams require a refractive index greater

than unity. A search for other weak beams of this nature revealed a whole series of such beams which accompany the main intense diffraction beams as satellites on the high voltage side. Most of these satellites are so close to the main beams and have such a small relative intensity that they are not completely resolved, and hence were not observed by the usual method of taking colatitude curves for various primary voltages. In these cases their presence was detected by varying the primary voltage in small steps, and measuring the current to the Faraday collector, whose angular position was adjusted for the maximum of the beam at *each* reading, while the total primary current

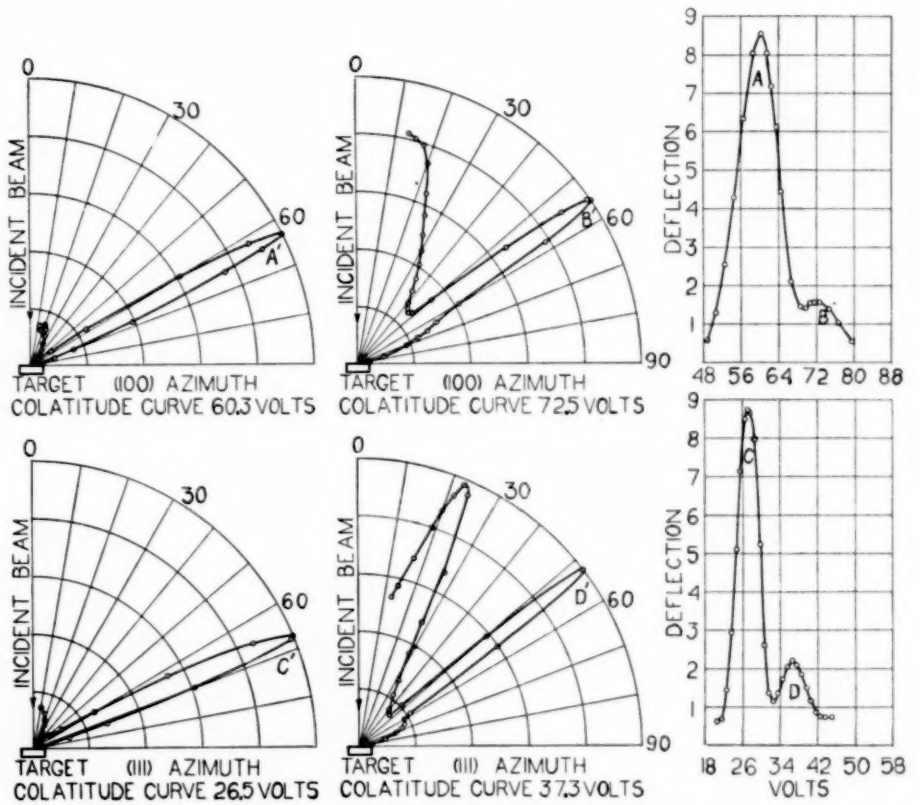

Fig. 2. Curves showing satellites for a copper crystal. The maxima B and D are the satellites of the main beams A and C, respectively. The colatitude curves A', B', C', and D' correspond to the maxima A, B, C, and D, respectively.

was held *constant* for the entire set of observations. The operating conditions of the experimental tube must be kept very constant for such a set of observations. A fine adjustment in the filament circuit controlled the primary current. The results of these observations may be plotted as in Figs. 2 and 3. Curves at the right in Fig. 2 show the deflections corresponding to the beam maximum for various primary voltages. These curves show the growth and decay of particular diffraction beams with weaker beams accompanying them on the high voltage side. The colatitude curves are shown for the voltages

corresponding to the peaks of these curves. The satellite D is seen to be very well resolved and was originally detected as a beam distinct from C. The curve in the upper left of Fig. 3 shows two main beams A and C with the accompanying satellites B and D. A slight indication of another beam at G is due to a weak gas beam. At higher voltages the satellites are very weak and appear as bulges in the curve of the main beam, as shown in the curves at the right of Fig. 3.

The positions of the various beams are given in Table Ia. It is to be noted that in the (100) azimuth the satellites which accompany the 4 first-order beams below 325 volts all occur within 2 volts of the theoretical values for unit refractive index; that of one second-order beam occurs within 11.9 volts;

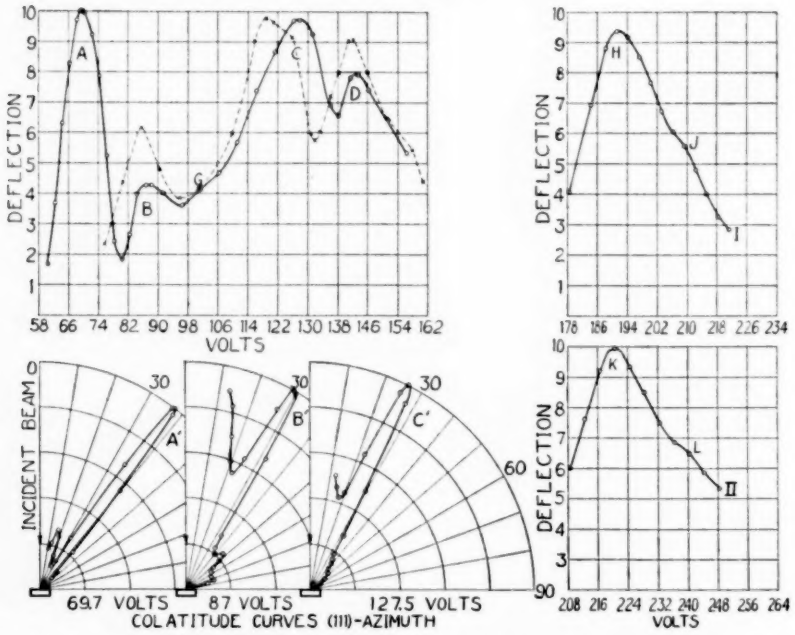

Fig. 3. Curves showing satellites for a copper crystal. The maxima B and D are the satellites of the main beams A and C, respectively. J and L are satellites of H and K, respectively. The colatitude curves A', B', and C' correspond to the maxima A, B, and C, respectively. The dotted curve is for angle of incidence $-2.5°$. Curve I is for the 3rd beam, 1st order, (100) azimuth; curve II for the 4th beam, 1st order, (111) azimuth.

that of the other second-order beam is missing. In the (111) azimuth, the satellites of 3 first-order beams are within 2.8 volts of theoretical values; that of the other first-order beam below 325 volts is within 7.0 volts; those of 2 second-order beams are within 4.6 volts; that of the other second-order beam is within 19.0 volts; that of 1 third-order beam is within 5 volts. The intensities of the satellites of first-order beams are between 10 and 20 percent of those of the main diffraction beams at the lowest voltages, and decrease to an unmeasurable amount at about 325 volts. The satellites are as sharp in voltage and colatitude angle as the main diffraction beams, and are not confined to large colatitude angles. Hence, they are not due to a two-dimensional sur-

face grating effect. At the time these observations were taken it was thought that all of the above beams were to be associated with a unit value for the refractive index. Although the values for several of the beams are off by more than the experimental error, it seemed significant that with only one exception all of the first-order beams fall well within observational error of the required value for unit refractive index. However, since several of the beams classified as satellites of higher order beams for the copper lattice require values of refractive index which differ from unity by more than the experimental error, it appears that this method of classification is not sufficient for these results. It is also entirely inadequate for classification of the results to be described for a silver crystal.

Beams due to a surface gas lattice

There are, however, certain significant facts pertaining to diffraction from a gas lattice which are in accord with the above classification. Some of the stronger gas beams characteristic of the simple cubic lattice were found to have satellites requiring a refractive index of unity. Also, as the stronger gas beams become less intense on outgassing the crystal, their voltage shifts so as to make the corresponding value of the refractive index closer to unity. Furthermore, gas beams characteristic of a *double-spaced, face-centered* lattice appear only when the gas layer is very thin and these require a refractive index close to *unity*.

G. P. Thomson[4] has recently suggested that the "additional" beams which the writer first listed for copper may be due to a layer of compound on the surface which might be formed by moderate heating if the vacuum is not high, and that heating strongly enough to vaporize the copper would probably remove the layer. This does not appear probable to the writer because even the first heating, after which the beams in question were still strong, was sufficient to evaporate considerable copper from the surface. It appears more probable that these particular beams are due to a surface layer of gas of simple-cubic, single-spaced structure having the same lattice constant as copper; that when the gas layer becomes thin after sufficient outgassing, it changes over to a double-spaced, face-centered structure; and that this gas layer is much more difficult to remove by heat treatment than are similar gas layers on nickel or silver.

G. P. Thomson[4] also states that Rupp's half-order beams are undoubtedly to be explained as a penetration of the metal lattice by hydrogen atoms in such a manner as to make alternate planes different without appreciably altering the spacing. My own results for a hydrogen lattice[9] indicate, however, that the gas lattice is on the surface rather than interpenetrating with the metal lattice. As previously pointed out by the writer,[9] hydrogen was found to form in two different lattices depending on the pressure of the hydrogen while the lattice is formed. At small pressures (less than 0.5 mm Hg) a relatively thin, double-spaced, face-centered structure is formed; at higher pressures (2 mm Hg) a thicker, single-spaced, simple-cubic structure takes its place. The beams for the first structure require a refractive index of approxi-

mately *unity* while those of the second structure require one *greater than unity*. The fact that this second structure is extremely unstable and reverts to the first structure during a few minutes seems to confirm the idea of the surface lattice.

From observations on certain diffraction beams from a surface layer of gas atoms assumed to be one atom deep, Germer[17] concluded that the spacing between the layer of gas atoms and the surface layer of nickel atoms is not a whole number multiple of the spacing between the adjacent layers of nickel atoms. He was led to this idea from the marked differences in the intensities of the various beams from the surface gas layer, but his computations on the spacing in question were based only on the positions and wave-lengths of these beams, without taking into account a refractive index. It is clear that

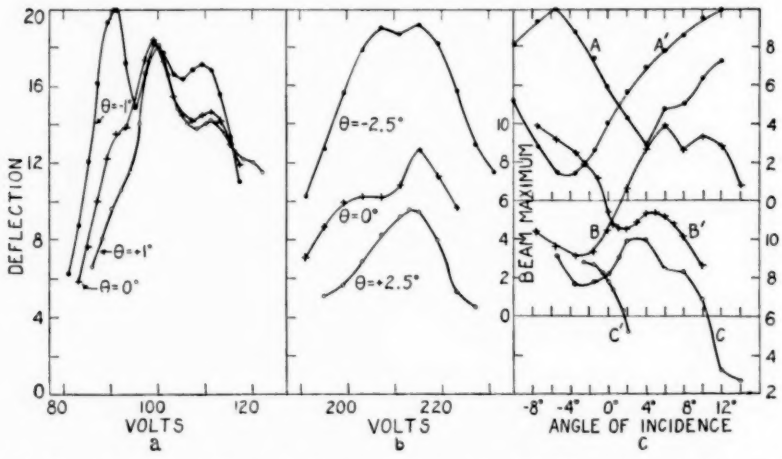

Fig. 4. Curves showing effects of changes in the angle of incidence. *a.*—1st beam including associated components, 2nd order, (111) azimuth for three different angles of incidence. *b.*—3rd beam including associated components, 2nd order, (111) azimuth for three different angles of incidence. *c.*—intensity change with angle of incidence for the following: *A.*—1st beam, 1st order, (111) azimuth; *A'.*—satellite of this beam; *B.*—2nd beam, 1st order, (111) azimuth; *B'.*—satellite of this beam; *C.*—3rd beam, 1st order, (111) azimuth; *C'.*—satellite of this beam.

with a value of the refractive index other than unity, a different spacing would result. The observations described below on the variations in intensities of the main beams due to a metal lattice, and in the associated values of refractive index make Germer's interpretation appear very doubtful.

Intensity measurements as a function of angle of incidence

Only a relatively small number of this type of observations has been obtained for copper, but before getting more it seemed desirable to obtain corresponding observations for another metal such as silver. The curves in Fig. 4c show the variations of intensities of some of the diffraction beams with changes in the angle of incidence. For various angles of incidence (measured from the normal) the primary voltage and Faraday collector angle were ad-

[17] L. H. Germer, Zeits. f. Physik **54,** 408 (1929); Bell Tech. Jour. **8,** 591 (1929).

justed for maximum deflection while the total primary current was held constant. These curves have not been corrected for background scattering. Negative angles indicate that the normal is on the opposite side of the primary electron beam from the Faraday collector. The ordinates are arbitrary units, and those of one curve are not to be compared with those of another. Curves for three main diffraction beams in the first order of the (111) azimuth are shown with those of the corresponding satellites. There appears to be no similarity between the curves for the different beams; neither is there a correspondence between the behavior of a particular beam and its satellite.* Some beams increase in intensity for a given change in angle of incidence while others decrease. It is also to be noted that in some cases the magnitude of the intensity changes by a hundred percent when the angle of incidence is changed by a few degrees.

The curves in Fig. 4a and b, show the growth and decay of the first and third beams of the second order in the (111) azimuth for slightly different angles of incidence. These observations were taken by the same method as that described above for the curves which have similar coordinates in Figs. 2 and 3. In the curve for normal incidence ($\theta = 0$) shown at the left in Fig. 4 there are two peaks or components with an indication of a third at the left. The small peak at 111 volts is tabulated in Table Ia as the satellite of the stronger beam at 99 volts. It is seen, however, that for an angle of incidence $\theta = -1°$, a component at 91 volts is stronger than either of the other two, while at $\theta = +1°$, this component has practically disappeared. Hence, it is clear that the classification of satellites described above is not sufficient for the present case. It may be emphasized that all of these three components occur within a primary voltage range which should contain only one maximum according to simple theory, so that the different components cannot be ascribed to reflection from different sets of atomic planes in the crystal or to half-order reflections from a double spaced gas lattice. The dotted curve in Fig. 3 shows the corresponding curve for the 2nd beam of the 1st order in the (111) azimuth for angle of incidence $-2.5°$. It is to be noted that a new component has appeared at 119 volts although it is so close to the original one that they are not completely resolved.

Regular reflection from the (100) set of planes

By setting the angle of incidence at some value other than normal and adjusting the position of the Faraday collector so that the angle of incidence equals the angle of reflection, we obtain curves corresponding to the Bragg reflection for x-rays. Three such curves are shown in Fig. 5 for the (100) face of the copper crystal with the plane of reflection containing the (111) azimuth. They are obtained by observing the current to the Faraday collector as the primary voltage is changed in small steps, while the primary electron current is held constant for the entire set of observations. The apparatus per-

* These observations were taken previous to those of the type shown in Fig. 4a. Hence it is possible that additional components exist for the beams in Fig. 4c for certain angles of incidence, but were not detected by this method of measurement.

mitted observations for only small angles of incidence when these observations were obtained. However, a comparison of the three curves shows that very striking changes occur in the range of angle of incidence from 8° to 12°. The arrows along the $V^{1/2}$ axis indicate the positions of theoretical beams for different orders computed from simple theory, assuming unit refractive index It is seen that the small changes in the angle of incidence produce only very slight changes in the positions of these arrows. It may be noted in the curve for $\theta = 10°$ that several of the maxima have double peaks and that the left one is relatively much more intense for $\theta = 8°$ while the right one is more intense for $\theta = 12°$; in other cases the changes are more complicated. The num-

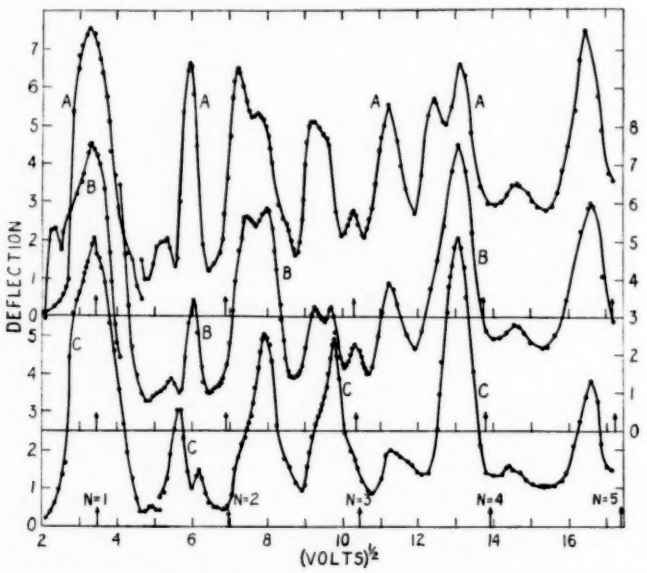

Fig. 5. Regular reflection from the (100) set of planes with the plane of reflection in the (111) azimuth. Curves *A*, *B*, and *C*, are for angles of incidence 8°, 10°, and 12°, respectively. Arrows indicate positions of theoretical beams for different orders, assuming unit refractive index. Discontinuities in the curves indicate changes in the scale of plotting. Vertical scales which overlap are same for all curves. Zero lines are indicated.

ber of experimental maxima is greater than the theoretical number. The irregularities obtained with this type of measurement are undoubtedly to be associated with those obtained by the other type of measurement near normal incidence.

Experiments with Silver Crystals

Preparation of crystal

The crystal was made from pure silver obtained from the U. S. Mint. The original crystal was 3/4 in. in diameter and 7 in. long with the lower end tapering to a point. It was made by the same method as that used for the copper crystal. The crystalline structure is face-centered cubic, the same as copper, with a lattice constant of 4.079A. The dimensions and mounting of the single crystal pieces used in the experimental tube are the same as for the

experiments with copper. Three different pieces of single crystal have been cut and prepared for the experimental investigation. The surface to be studied was in every case cut parallel to a (100) set of planes, but one of the crystals was mounted so that it could be rotated about an axis perpendicular to the (100) azimuth while the other two rotated about an axis perpendicular to the (111) azimuth. Two crystals of the latter type were tested as a check to eliminate the possibility of a faulty crystal and to make sure that the results obtained are really characteristic of silver. Complete observations were taken with only two of them. I am indebted to Dr. B. E. Warren of the Massachusetts Institute of Technology for making an x-ray examination of one of the silver crystals. The crystal was found to have a mosaic dispersion of not more than 1°, and the geometric boundary was found to be parallel to the (100) set of planes to within less than 0.5°. Dilute nitric acid develops the various facets of the crystal which are easily detected by reflected light. In addition to (100) and (111) facets (which are the only strong ones found for copper), (110) facets are almost equally brilliant in reflected light. Etching in strong nitric acid was found to be most suitable for the final preparation of the (100) surface. By using about 55 percent by volume of acid in distilled water, a very smooth mirror-like (100) surface was obtained with no visible reflection from any other planes. Under these conditions the etching is very rapid and only a very short time (a few minutes or less) is required to produce the desired result. The conditions are also very critical. If the solution is slightly too strong, the surface is left very rough and irregular; if it is too weak etching occurs parallel to other planes as well as the plane in question. This method of etching can apparently be applied to planes other than the (100); the necessary condition is that the geometric boundary must be very nearly parallel to the plane in question. Smooth (110) faces were obtained in this way on the sides of one of the crystals.

Silver recrystallizes much more readily than copper under red-heat treatment and consequently it is essential to clamp and bombard the crystal at some distance from the face to be used. In the first trial a silver crystal was mounted at the rear as described above, placed in a preliminary tube, and heated at a dull red heat for eight hours. At the end of this time recrystallization had occurred throughout the whole crystal with the exception of the front end for a distance of about 2 mm. On the other hand it is much easier to outgas silver than copper sufficiently for the present experiments. After giving one of the silver crystals a red-heat treatment of only 10 min. (subsequent to the usual baking of the whole tube), the diffraction beams from the surface gas layer were extremely weak, and the beams characteristic of silver were more intense and sharp than those obtained from a copper crystal after 43 hours of outgassing. The sharpness of the diffraction beams appears to be determined to a greater extent by the etching of the surface than by complete freedom from gas. For example, the diffraction beams from the crystal which had received 8 hours of red-heat treatment were both weaker and broader in colatitude angle than those of another crystal which had received only 10 min. of red-heat treatment. The first crystal had been etched in dilute nitric

acid so that the smooth mirror-like surface was *not* obtained as in the case of the second crystal.

Number of diffraction beams

The curves in the upper part of Fig. 6 show the various beams in the 1st order of the (111) azimuth below 160 volts for normal incidence. These were obtained by the same method as that used for the curves at the right in Fig. 2. The arrows along the voltage axis indicate the positions of theoretical beams. The number of experimental peaks is seen to be much greater than the three theoretical beams in this voltage range. Further, the beams cannot be classi-

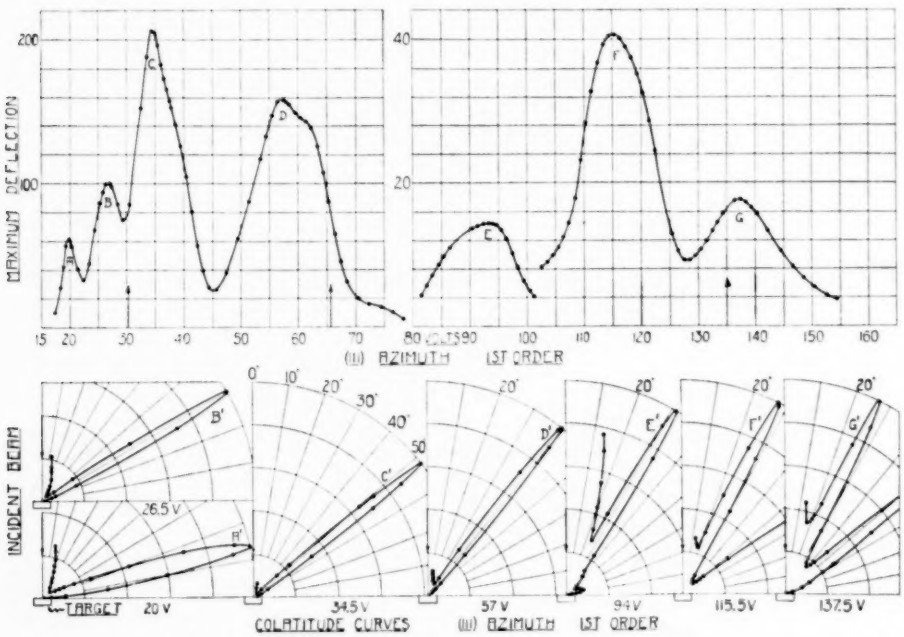

Fig. 6. Curves showing diffraction beams for silver in the 1st order, (111) azimuth below 160 volts for approximately normal incidence. Colatitude curves correspond to maxima in the upper curves which have the same letters.

fied as main diffraction beams requiring a refractive index greater than unity accompanied by weak satellites requiring a refractive index of unity, as was the case for many of the beams for copper. There are three well defined components, with indication of a fourth at 40 volts, in the region of the first theoretical beam at 30 volts; two components in the region of the second theoretical beam; and three components in the region of the third. The colatitude curves at the lower part of Fig. 6 indicate the sharpness of the beams in colatitude and the small amount of background scattering. None of these beams is due to a gas lattice since the half-order gas beams were very weak compared to any of the first order beams shown above.

Table II shows the positions and relative intensities of the diffraction beams for normal incidence. When several experimental components correspond to a single theoretical beam, only the most intense experimental com-

ponent is given in the table. The other components may be obtained from curves to be described below. The *uncorrected* values of intensity are given so that comparison may be made with the curves in Figs. 9 and 10 below. Values of background intensity for normal incidence were not obtained for all of the beams. In general, the ratio of beam intensity to background intensity is much greater for silver than for copper.

TABLE II. *Main* diffraction beams for the silver lattice; normal incidence.*

Beam and order numbers	Plane of reflection	Experimental voltage	Theoretical voltage $V=150/\lambda^2$	Voltage difference	Corrected intensity / Background intensity	Uncorrected approximate relative intensity
			(100) Azimuth			
1–1	(210)	46.1	56.3	10.2	300	100
2–1	(310)	93.5	100.2	6.7	1.7	5
3–1	(410)	141.0	162.8	21.8	7.8	21
4–1	(510)	229.5	243.8	14.3	3.3	7
5–1	(610)	335.5	343.0	7.5		6
1–2	(320)	152.5	169.3	16.8		4
2–2	2(210)	206.5	225.4	18.9		19
3–2	(520)	280.5	303.3	22.8		7
			(111) Azimuth			
1–1	(311)	34.0	30.3	−3.7	150	70
2–1	(511)	56.0	65.7	9.7	75	78
3–1	(711)	115.0	119.6	4.6	8	16
4–1	(911)	168.3	191.7	23.4		4
1–2	(211)	77.5	81.1	3.6	36	9
2–2	2(311)	112.5	121.2	8.7	36	16
3–2	(411)	158.5	182.6	24.1	36	9
4–2	2(511)	250.5	262.9	12.4		9
2–3	(733)	192.5	206.5	14.0	30	6
3–3	3(311)	252.5	272.7	20.2		7

* Only the values for the most intense component of each beam are given. See note below Table I for notation.

Gas beams for silver

Only a few very weak beams due to a surface gas lattice were found below 50 volts. They fall on the one-half order lines in both the (100) and (111) azimuths so as to indicate a double-spaced, face-centered, structure. Because of their extreme weakness compared to the other beams (less than 2 percent of the most intense beam), their influence must be negligible.

Intensity measurements as a function of angle of incidence

Because of the many irregularities in the diffraction beams, no curves of the type of those at the right in Fig. 4 were obtained. A more complete record is obtained by curves similar to those at the left in Fig. 4 or those in Fig. 6 for various angles of incidence. The curves in Figs. 7 and 8 show some of the changes which occur for beams in the (100) azimuth with changes in angle of incidence. These curves all illustrate the fact that any particular diffraction beam consists of several components whose relative intensities change rapidly with change in angle of incidence. The curves in Fig. 8 show the changes which occur in a single diffraction beam over a considerable range in

angle of incidence. Starting at the upper left and proceeding from top to bottom in each successive column we trace the changes which occur as the angle

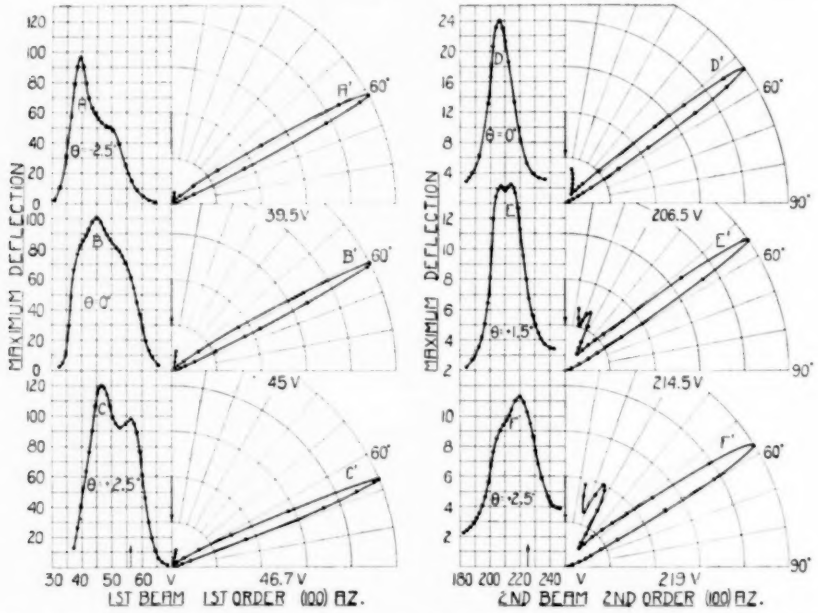

Fig. 7. Curves showing effects of changes in the angle of incidence. (The values of θ for the curves of the 1st beam—1st order should be corrected by subtracting 0.5° from each of the values given.)

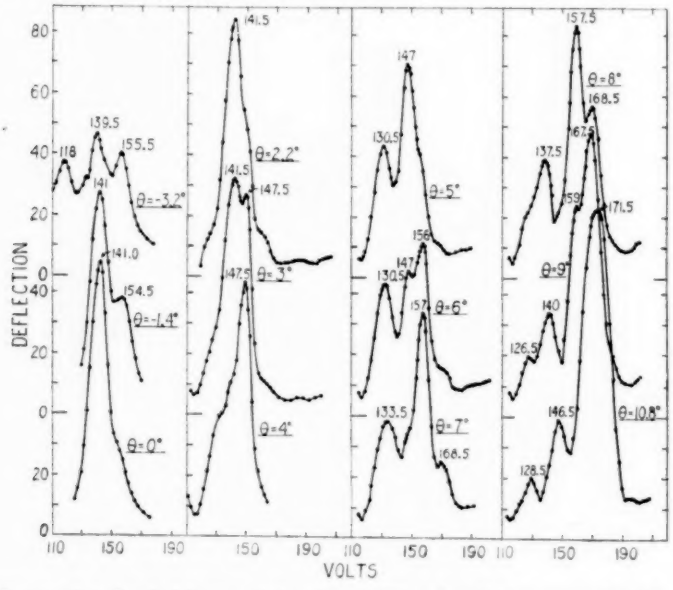

Fig. 8. Curves for the 3rd beam, 1st order, (100) azimuth for several angles of incidence. Corrected voltages for the various maxima are given on the curves.

of incidence is varied from negative values to positive values. In some cases components appear on the high voltage side and increase in intensity while

those on the low voltage side disappear. This, however, is not a general rule. It is a striking feature that for many of the components the voltage corresponding to the peak deflection remains practically constant over the whole range of angles θ at which the component is observable. This means, of course, that for each of these components the associated wave-length is independent of the angle of incidence within certain limits. Since, however, the *plane* grating formula *is satisfied* over a considerable range in the angle of incidence, (see also next section) it is evident that for this case the colatitude angle of the beam does not change by twice the change in the angle of incidence, but by an amount such as to keep the wave-length of the maximum constant. This is clearly not in accord with the simple theory according to which one

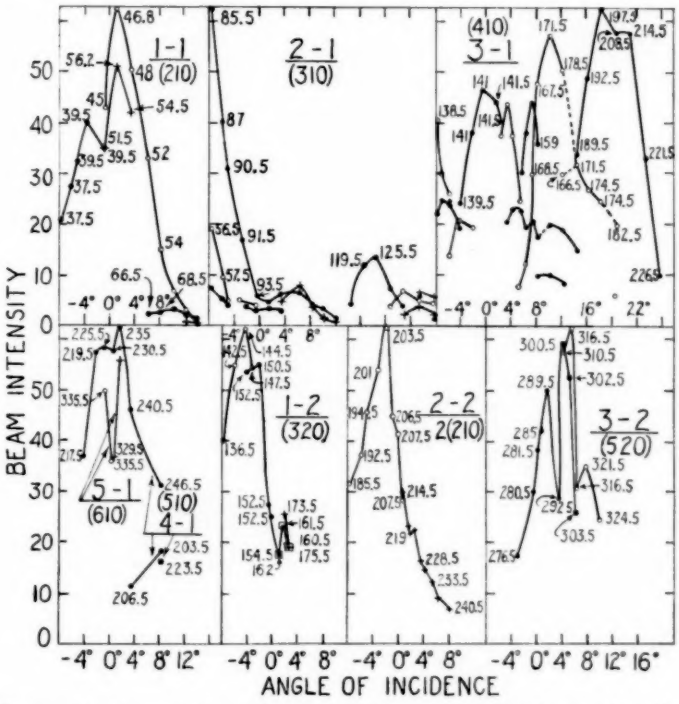

Fig. 9. Curves showing relative intensities of beam components as a function of angle of incidence for the (100) azimuth (uncorrected for background scattering). Plane of reflection is in the (100) azimuth. Designation of beam 3–2 signifies third beam in the second order as per notation in Table I. Values of corrected voltages are given for several of the points.

should expect only one component for each angle of incidence, with the maximum shifting in voltage, as θ is changed, so as to satisfy the Bragg reflection formula; and also the condition that the change in the colatitude angle of the beam shall be twice the change in the angle of incidence.

Observations similar to those of Fig. 8 have been obtained for most of the diffraction beams in the (100) and (111) azimuths in the voltage range below 350 volts and for angles of incidence in the range from $-10°$ to $+25°$ at which the beams have a measurable intensity. In order to indicate the variations in intensity of the large number of beams, each having several com-

ponents, the results have been plotted as in Figs. 9 and 10. Each of the plotted points of these curves represents a peak in the type of curves shown in Fig. 8, that is, any one of the curves in Figs. 9 and 10 shows the variation of intensity of a particular component of a diffraction beam as a function of the angle of incidence of the primary beam. Corresponding to each plotted point there is a particular colatitude angle and primary voltage, the values of which are given in Figs. 9 and 10 for some of the points. In case two components of the same beam have equal intensities at the same angle of incidence, even though their optimum voltages are different, their points on the plots of Figs. 9 and 10 will coincide. Referring, for example, to the first beam in the first order of

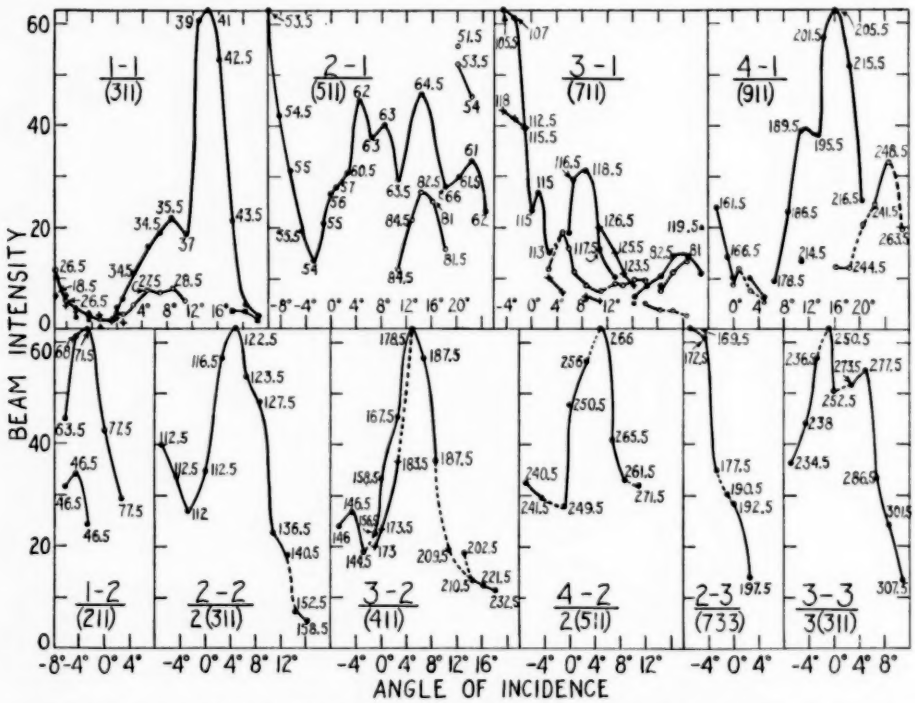

Fig. 10. Curves showing relative intensities of beam components as a function of angle of incidence for the (111) azimuth (uncorrected for background scattering). Plane of reflection is in the (111) azimuth. Notation is the same as in Fig. 9.

the (100) azimuth, Fig. 9, we see that for $\theta = -8°$ there is only one component of this beam. As θ becomes more nearly zero, the intensity of this component increases and then decreases and is not observed for positive angles of incidence. At $\theta = -0.5°$ there are two components of equal intensity and one of greater intensity, all of which appear at different voltages (see curve B of Fig. 7). As θ is increased, two of these components increase in intensity and then decrease, one of them continuing to $\theta = 14°$. Two weaker components also appear at the larger angles of incidence.

The curves in Figs. 9 and 10 have not been corrected for background scattering or for the overlapping of different components in the voltage range. The latter condition probably introduces considerable change in the rela-

tive intensities but corrections are uncertain and since the changes of intensities of the various components are so great, the general features of the curves in Figs. 9 and 10 are not seriously affected by the above uncertainties. Although great accuracy is not claimed for the exact shape of the curves for the weaker components of any one beam, their number indicates the complexity of the phenomenon. In some cases there is uncertainty as to the course of a curve between plotted points. In these cases the most probable course is indicated by a dotted line. This uncertainty is due partly to the fact that more experimental observations are needed in these regions and partly to the lack of resolution of the components in question. In some cases two components appear to merge into one.

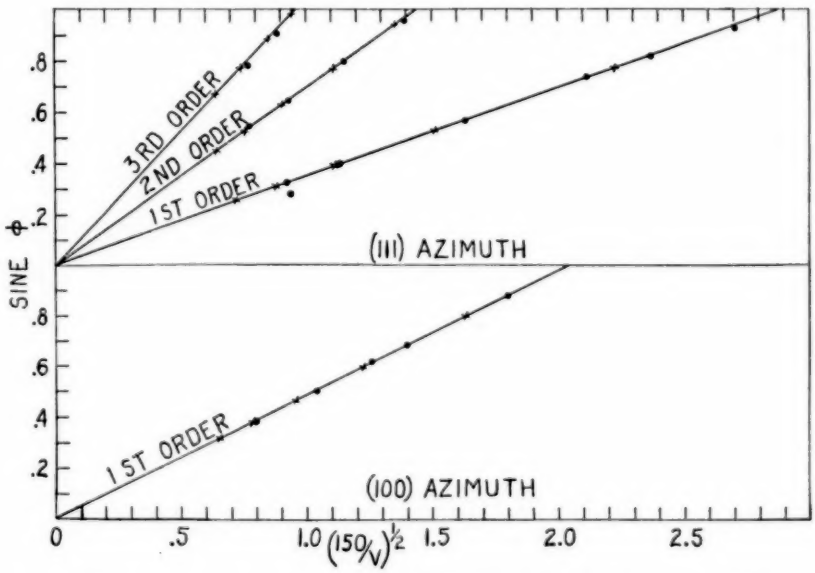

Fig. 11. Plot of sin ϕ against $\lambda = (150/V)^{\frac{1}{2}}$, ϕ = colatitude angle for normal incidence. Solid circles denote experimental maxima. Crosses denote theoretical beams.

The intensities of the components of one beam are not to be compared with those of another beam directly from the plots in Figs. 9 and 10 since the maximum points of the various beams have obviously been made the same. However, a comparison may be made with the use of Table II which gives the approximate relative intensities of the *most intense* components of the various diffraction beams for normal incidence of the primary beam. The relative intensities change somewhat with the vacuum conditions so that they must be considered as approximate. Although each beam is characterized by very great and unique intensity changes with change in angle of incidence, special comment may be made about the 2nd beam of the 1st order in the (100) azimuth. At normal incidence the intensities of the components of this beam are so weak as to be scarcely observable, while for $\theta = -8°$ the intensity of one component is at least one-half of the maximum value which the 1st beam ever attains.

Test of plane grating formula

Fig. 11 shows a plot of sin ϕ against $\lambda = (150/V)^{1/2}$ for normal incidence. The solid lines were plotted from the plane-grating formula using a grating spacing a = 4.079A taken from International Critical Tables. The solid circles were obtained from the experimental values corresponding to the different components of the electron diffraction beams. The crosses represent positions of theoretical beams. The fact that the points lie so closely on the lines furnishes an excellent check of the plane-grating formula and at the same time shows that the angle of incidence is zero within the error of measurement.* The 3rd order beams are slightly displaced due to the fact that they emerge from the crystal at large colatitude angles. These observations were obtained for the third silver crystal after improvements in apparatus had been made. For angles of incidence other than zero the plane grating formula $\lambda = D/n$ (sin θ_2-sin θ_1) is found to apply approximately to the various beam components over certain ranges of the incident angle, but for other ranges the formula fails to hold. In general, it appears that the formula does not hold for incident angles which differ from zero by more than several degrees or for beams whose intensities are very weak for the incident angle in question, although there are exceptions to this statement. Table III shows values for two typical beams selected at random. The calculated values of θ_2 were obtained by solving the above plane grating formula for θ_2, in which $\lambda = (150/V)^{1/2}$. It is seen that the observed and calculated values of θ_2 are in fair agreement except in the case of the 2nd beam for angles of incidence greater than about 5°, where the two values differ by as much as 5 or 6 degrees. Referring to Fig. 10, we see that this beam is most intense for $\theta = 5°$.

TABLE III. *Test of plane grating formula.*

V in volts observed	θ_1 observed	θ_2 observed	θ_2 calculated	V in volts observed	θ_1 observed	θ_2 observed	θ_2 calculated
	1st beam, 1st order, (100) Azimuth				*2nd beam, 2nd order, (111) Azimuth*		
37.5	−7.7°	58.7°	57.8°	112.5	− 6.2°	43.2°	43.8°
37.5	−5.8°	60.8°	61.6°	112.5	− 4.4°	45.4°	46.3°
39.5	−5.0°	61.0°	60.3°	112.0	− 2.6°	48.1°	49.2°
39.5	−3.0°	64.5°	64.6°	112.5	0°	53.0°	53.1°
45.0	−0.5°	62.0°	62.4°	116.5	+ 2.8°	55.7°	56.7°
46.8	+1.7°	65.7°	65.4°	122.5	+ 5.0°	56.5°	58.9°
56.2	+1.7°	57.1°	56.2°	123.5	+ 6.8°	59.7°	62.1°
48.0	+3.5°	69.3°	68.1°	127.5	+ 8.8°	61.7°	65.0°
54.5	+3.5°	62.0°	61.0°	136.5	+10.9°	62.6°	66.5°
52	+6.4°	69.7°	70.8°	140.5	+13.0°	64.5°	70.2°
66.5	+6.4°	59.4°	57.9°	152.5	+14.6°	66.9°	70.5°
54.0	+8.3°	73.6°	73.9°	158.5	+16.4°	68.6°	73.3°
68.5	+8.3°	61.7°	60.4°				

* It may be noted that there are 2 experimental components to be associated with the 4th beam in the 1st order of the (111) azimuth. One of these components falls exactly on the line but the other does not. For an angle of incidence $\theta = -1°$, only the component which *does not* fall on the line is present, while for $\theta = +1°$, only the component which *does* fall on the line is present. (See Fig. 10).

Regular reflection from the (100) set of planes

Figs. 12 and 13 show curves for silver which were obtained by the same method as that used to obtain similar curves for copper. The two curves in Fig. 12 were both obtained for the same angle of incidence of 8.5° but for the upper one the plane of reflection contains the (100) azimuth while for the lower one the plane of reflection contains the (111) azimuth. In Fig. 13 are shown two corresponding curves each for 20° angle of incidence and a third for 40° angle of incidence in the (100) azimuth. Many other curves were obtained for other angles of incidence between 7° and 40°. From an inspection of the curves it appears that for the same angle of incidence the results for the (100) and (111) azimuths are quite different, but the difference appears to be greater for the larger angles of incidence than for the smaller ones. The

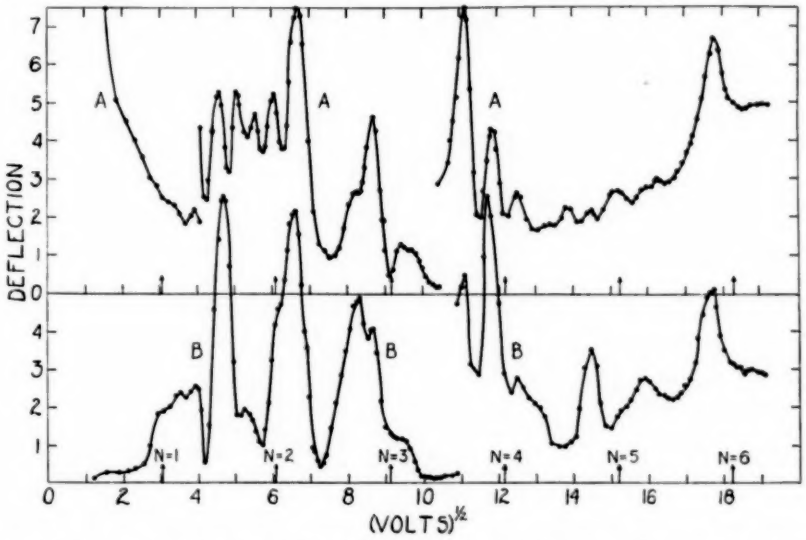

Fig. 12. Regular reflection from the (100) set of planes. Both curves are for angle of incidence 8.5°. For curve *A* the plane of reflection is in the (100) azimuth. For curve *B* the plane of reflection is in the (111) azimuth. Arrows indicate positions of theoretical beams for different orders, assuming unit refractive index. Discontinuities in the curves indicate changes in the scale of plotting.

results in a particular azimuth also appear to be more complicated for the larger angles of incidence than for the smaller ones. Several of the curves have been checked to establish the reality of the numerous maxima and minima. For example, the upper curve in Fig. 13 was obtained at two times differing by about one month and after different previous heat treatments of the crystal. The two curves were, however, exactly alike in all details except for very slight changes in relative intensities of some of the peaks. Although the angles of reflection at which the beams attain maximum intensity are, in general, equal to the corresponding angles of incidence, within experimental error, several cases have been noted for which the deviations from the expected values (3° in some cases) for certain beams are too large to be attributed to experimental error. These deviations have not been investigated in detail, but

they are probably to be associated with the deviations from the plane grating formula mentioned in the previous section.

Discussion of the Results

A comparison of the results for copper with those for silver

For normal incidence the deviations from the predictions of simple theory are more noticeable in the results for a silver crystal than in those for a copper crystal. Referring to the relative intensities of the corresponding beams in Tables I and II, we see that those for silver vary through wider ranges and appear more unsystematic than those for copper. The number of experimental components to be associated with a single theoretical beam is in general also greater for silver than for copper.

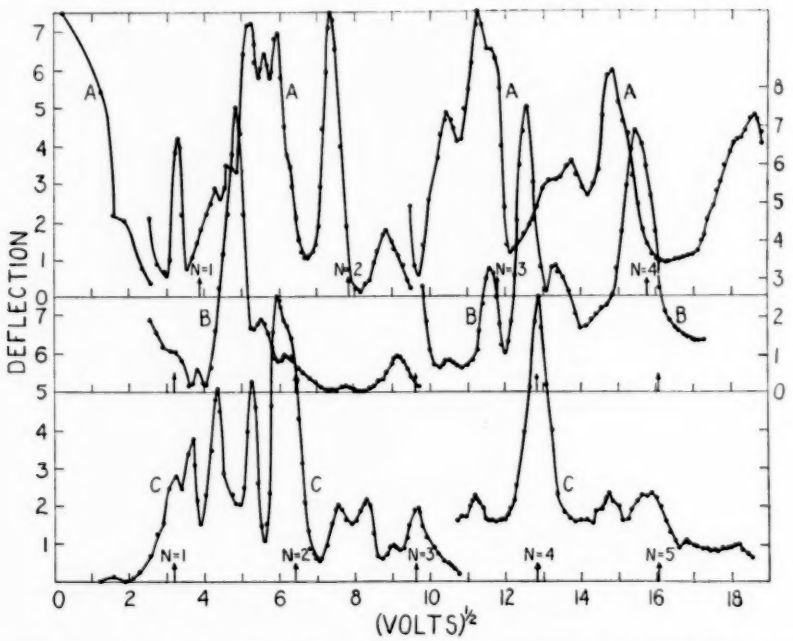

Fig. 13. Regular reflection from the (100) set of planes. Curves *A* and *B* are for angles of incidence of 40° and 20°, respectively, with the plane of reflection in the (100) azimuth. Curve *C* is for angle of incidence 20° with the plane of reflection in the (111) azimuth. Other notation is the same as for Fig. 12.

Although a detailed comparison of the variations of intensities of the main diffraction beams due to changes in angle of incidence for silver with those for copper cannot be made at present because of insufficient observations for the copper crystal, a qualitative comparison for certain corresponding beams is possible. Referring to Fig. 4c we note the variations of the 1st, 2nd, and 3rd main beams in the 1st order (111) azimuth for copper as given by the curves *A*, *B*, and *C*, respectively. Comparing these with the corresponding curves, 1–1, 2–1, 3–1 in Fig. 10 for the strongest components of the same beams for silver, we observe no particular correspondence. For regular reflec-

tion from the (100) face at angles of incidence other than normal under similar conditions the results for the two crystals do not correspond.

It is thus clear that although there are deviations from the simple theory in the case of both crystals, these deviations are widely different for the two crystals. Since both crystals have the same lattice structure and since the surface of the crystal was in each case parallel to the (100) face, it would seem that the difference must be due to differences in conditions brought about by the two different kinds of atoms.*

Inner potential and refractive index

From my first experiments with a copper crystal,[8] it appeared that the inner potential could be represented by a smooth curve which approaches a constant value for the higher primary voltages, but which decreases with decreasing primary voltage below about 150 volts. Although some of the experimental points deviated considerably from this line, the differences were attributed to experimental error. The results for copper and silver reported here show that the concept of a constant inner potential or even of one that varies smoothly in the manner indicated above is not in accord with the results obtained by such experiments on electron diffraction. One need only consider curves such as shown in Figs. 7 and 8. If the voltage corresponding to the maximum of a diffraction beam is obtained for normal incidence, the inner potential is given at once by the difference between this voltage and that of the corresponding theoretical beam. If now the angle of incidence is changed only a small amount, the beam maximum may occur at a voltage differing by several volts from the first value, while the change in angle is too small to appreciably change the corresponding theoretical voltage. As a result, the inner potential as determined from the second observation will differ widely from that of the first. Hence a small change in the angle of incidence results in a greatly different measured value of the inner potential.

The fact that the results for the case of regular reflection depend on the azimuth of the crystal which lies in the plane of reflection, as shown in Fig. 12, clearly indicates that the usual concept of a refractive index does not apply in this case, for the distance between adjacent reflecting planes is the same in the two cases.

Intensities of diffraction beams

The extraordinary dependence of the intensities of the diffraction beams on the angle of incidence of the primary beam leads one to make a comparison with x-ray measurements. It is well known that the intensities of x-ray reflections are interpreted in terms of the electron distribution in the atoms. Measurements with x-rays indicate spherical symmetry of the individual atoms in the crystal lattice, but, as recently emphasized by James and Brind-

* The only other difference is that of the lattice constant. This, of course, causes the diffraction beams to appear at different electron speeds or equivalent wave-lengths, the influence of which on the present results is not exactly known. This uncertainty can be eliminated by comparing observations on silver and gold, which have practically the same lattice constant.

ley,[18] the scattering of x-rays "at any appreciable angle is due mainly to the inner electrons of the atoms, for which the departure from spherical symmetry due to the packing of the atoms in the crystal is small, and the scattering powers of atoms in simple crystals in general depend only on the angle through which the radiation has been scattered, and not on the direction in which it has passed through the crystal." They further emphasize that "in any real crystal structure, the arrangement of the outer electrons of the atoms must be to some extent distorted from spherical symmetry, and this procedure of assigning a definite scattering power to each atom, and assuming it to remain the same for a given type of atom from crystal to crystal, can only be an approximation."

In the results reported here one might expect a similarity to exist between the characteristics of the diffraction beams corresponding to different orders of reflection from the *same set* of atomic planes.* An examination of the results given above shows four such cases for consideration. The curves 1–1 and 2–2 in Fig. 9 correspond to 1st and 2nd order reflection from the (210) set of planes. Similarly the curves 2–2, 4–2, and 3–3 in Fig. 10 correspond to 2nd order reflections from (311) and (511) planes and 3rd order reflection from (311) planes, respectively. It cannot be said that the curves for different order reflections from the same set of planes correspond in any of these cases. However, it should be emphasized that these different order reflections correspond to considerably different primary voltages so that if the effect in question is a function of the associated wave-length of the incident electrons as well as the direction, we are here unable to separate the two.

Mark and Wierl[19] have already determined the atom form factors for Al, Ag, and Au in the polycrystalline state with the use of high-speed electrons, and have shown that the atom form factor F^* as determined with high-speed electrons is related to the F determined with x-rays by the relation $F^* = (Z - F)/\sin^2\theta$ (Z = atomic number, 2θ = the scattering angle) as is to be expected from a consideration of the different conditions which govern the scattering of x-rays and electrons. Comparison is made with the x-ray F curve for aluminum obtained by James, Bridley and Wood[20] which is in good accord with the theoretical one obtained from the charge distribution determined by the method of Hartree. The above method cannot be used with very low-speed electrons, and uncertainties would arise in attempting to use single crystals since values of extinction and absorption coefficients are required for the crystal in question, and these would be difficult to determine for low-speed electrons.

During discussions of these experiments with various physicists the following questions have been raised. (1) Can the components of fine structure be accounted for by a mosaic structure of the crystal? If one considers two or more sets of lattices making small angles with one another, then, of course,

[18] R. W. James and G. W. Brindley, Phil. Mag. **12**, 81 (1931).

* I am indebted to Dr. J. C. Slater for this suggestion.

[19] H. Mark and R. Wierl, Die Naturwiss **18**, 778 (1930); Zeits. f. Physik **60**, 741 (1930).

[20] R. W. James, G. W. Brindley and R. G. Wood, Proc. Roy. Soc. **125 A**, 401 (1929).

the conditions for constructive interference for the different lattices would require different wave lengths for a given primary beam which would result in an apparent fine structure. However, an examination of observations over the ranges of variables used shows that such an hypothesis is insufficient. Furthermore this possibility is excluded by the fact that the results have been checked for more than one specimen of a particular crystal. (2) Can the components be a type of secondary maxima such as are observed in the optical case with a grating having a small number of rulings? Although there appears to be a similarity in the two cases, an examination shows that there is no close correspondence. It is difficult to see how the relative intensity changes may be accounted for on this view. Also, the secondary maxima are decreased in intensity as the number of lines in the grating is increased. A consideration of the sharpness in colatitude angle for the beams from copper and silver crystals indicates that the number of rows of atoms in the elementary crystal gratings is greater in the case of silver, while the components of fine structure are also more pronounced for silver.

Surface action

Before considering further a possible interpretation of these results on diffraction of low-speed electrons it is essential to determine the influence of the surface action due to the gradual transition of the field across the boundary of the crystal as considered by v. Laue.[14] Is it possible, for example, that the observations in question are due entirely to this surface action, or are they fundamentally characteristic of a space-lattice with perhaps a minor alteration resulting from the surface action? As already mentioned, v. Laue's own deductions lead to the conclusion that this surface influence may be neglected for electrons having energies greater than 200 volts. The desirability of obtaining experimental evidence on this point is immediately apparent. Fortunately there appear to be several methods of approach to this problem. (1) A comparison of the results for primary electron energies above and below 200 volts. This shows that although the results in the lower voltage region are in general more complicated in regard to the number of components of a particular beam, the general characteristics of this fine structure together with the great dependence of intensity on angle of incidence is certainly present at the highest energies studied at 325 volts. An extension to still higher energies is desirable. (2) A comparison of the results obtained when different thicknesses of the surface gas lattice are present. It has been shown that for a (100) surface of a copper crystal, the gas forms in either a single-spaced, simple-cubic or a doubled-spaced, face-centered structure, depending on the thickness of the gas layer. We have here a transition, not from a copper lattice to vacuum, but from a copper lattice to a gas lattice. The characteristic beams for the copper lattice can then be influenced only by *inter-surface* action which may arise from the transition from a copper to a gas lattice, and only the beams due to the gas lattice can be affected by a pure surface action. The first of these should certainly be expected to change when the gas layer becomes thinner and shifts from one to the other of its characteristic structures.

No evidence of a change in the characteristics of the beams for a copper lattice have been observed when the above change occurs. This point must, however, be investigated in more detail. From intensity measurements it appears that the thicker gas lattice on a copper crystal must in some cases be at least several atoms deep, even when a strong diffraction beam for the copper lattice at 26.5 volts can be observed. Hence, these low-speed electrons must pass through *several layers* of gas atoms without excessive absorption. (3) Comparison of results obtained when atoms of one metal are deposited by evaporation on a single crystal of another metal. From our information about surface gas lattices it would appear that a surface metal lattice could be formed. The characteristics of the underlying metal could then be influenced by only an *inter-surface* action arising from the transition from one metal to another. This presumably should be less than that due to a metal-gas junction. (4) Investigation of a silver crystal with the surface parallel to a (110) set of planes. With this arrangement diffraction beams can be obtained which correspond to Bragg reflection from one set of planes that is the same as for the case where the crystal surface is parallel to a (100) set of planes, the difference being that the incident and emergent beams of electrons pass through a (110) boundary plane in one case and a (100) boundary plane in the other. Any difference must then be due to the influence of the boundary plane. A silver crystal is suitable since (110) etched planes can be obtained.

The available evidence at the present time thus indicates that the results are characteristic of a space lattice and that the surface action is at most a relatively minor consideration.

In addition to the experiments suggested above it appears desirable to obtain results for a gold crystal since the lattice constants of gold and silver are so nearly the same. Hence the positions of the theoretical beams are almost identical so that possible differences due to different electron energies of corresponding beams are eliminated, and any differences must result from the different types of atoms.

Experiments with a gold crystal are now well under way, and the suggested experiments on surface action are to be carried out in the immediate future.

The recent tendency in the field of electron diffraction seems to be to avoid experiments with low-speed electrons because of undesirable surface effects and other characteristics not easily accounted for. However, it would seem that a more thorough investigation of these phenomena should lead to significant contributions to our understanding of the metallic state.

I am indebted to friends of the University for continued support of these experiments. Messrs. Newton Underwood, F. E. White, and K. R. Page have greatly aided at different times during the course of the work, and Mr. Morgan Williams assumed responsibility in the production of the single metal crystals.

The Analysis of Cosmic-Ray Observations

By LEROY D. WELD
Department of Physics, Coe College
(Received March 28, 1932)

A method of rendering non-linear observation equations susceptible to least-square adjustment is adapted to observations on the absorption of cosmic rays in bodies of water, data on which have appeared from time to time; the object being to obtain the most probable values of the constants of the assumed discrete components of the radiation. Applied to the most consistent data so far published, viz., those reported by Millikan and Cameron in 1931, the adjustment shows that the quantitative conclusions deduced from them by the observers are not derivable from the data by the method of least squares.

I. THEORY OF THE ADJUSTMENT

THE receipt of several requests for details of the least-square adjustment of cosmic-ray observations reported in a recent letter to the Editor,[1] together with the increasing attention which the cosmic-ray problem is attracting, leads the writer to set forth the method at greater length.

When measurements on the absorption of cosmic rays in water were first interpreted as indicating the existence of discrete components of definite intensity and hardness, the question naturally arose as to whether, with the accumulation of precise data, it might not be possible to apply the well-known methods of least-square adjustment to the determination of the several sets of constants.

If, as has apparently been established, the radiation reaches the earth with the same intensity from all directions, if absorption in any one direction proceeds with a constant absorption coefficient, and if the rays are not refracted, it is easy to deduce an exponential law of attenuation with depth in a material substance. To wit: the initial intensity and absorption coefficient of any one component being respectively I_0 and μ, then the intensity at any depth H in a horizontal layer of homogeneous material, which the rays reach only through the upper hemisphere, is

$$I = I_0 \int_1^\infty x^{-2} e^{-H\mu x} dx. \tag{1}$$

x represents the cosecant of the angle of incidence upon the horizontal surface.[2]

The definite integral in this expression is a function only of the argument $H\mu$. We shall call it the "Gold integral" and designate it by $G(H\mu)$; because a table of its values has been published by Gold.[3] If the radiation is composed

[1] Weld, Phys. Rev. **37**, 1368 (1931).

[2] The equation given by Millikan and Cameron, Phys. Rev. **28**, 860 (1926), inadvertently contains a factor 2π. Their computations were, however, apparently based on the correct formula (1) above.

[3] Gold, Proc. Roy. Soc. **A82**, 62 (1909); Millikan and Cameron, Phys. Rev. **31**, 926 (1928). See also part 2 of this paper.

of several distinct monochromatic components with initial intensities I_{01}, I_{02}, $\cdots$ and absorption coefficients μ_1, μ_2, $\cdots$, then at any depth H the sum of their intensities should be

$$I_{01}G(H\mu_1) + I_{02}G(H\mu_2) + \cdots = \Sigma I. \tag{2}$$

This may be taken as a form of observation equation, in which the unknown quantities are the constants I_{01}, μ_1, I_{02}, μ_2, $\cdots$, and in which ΣI is observed by means of the ionization measurements. I believe that the depth H may be justifiably regarded as a known coefficient, since its measurement is presumably subject to a comparatively small percentage of uncertainty.

But (2) is a *non-linear* function of the μ's. Before such observations can be subjected to practicable least-square adjustment, the observation equations must be replaced by equivalent equations of linear form. There is an approximation method of accomplishing this, somewhat analogous to Horner's method of solving non-linear algebraic equations. Its use is contingent upon our having first obtained, by some means, fairly approximate values of the unknown quantities; and it is then the required *small corrections* to these values that are computed in the adjustment.[4]

In this case, let the approximate values assumed for I_{01}, I_{02}, $\cdots$ be designated by α_1, α_2 $\cdots$, and the corresponding corrections by c_1, c_2, $\cdots$; likewise let the approximate values and corrections for μ_1, μ_2, $\cdots$ be β_1, β_2, $\cdots$ and k_1, k_2, $\cdots$, respectively. Then the *true* values of the unknowns are represented by

$$\left.\begin{aligned} I_{01} &= \alpha_1 + c_1 \\ I_{02} &= \alpha_2 + c_2 \\ \cdots &\quad \cdots \\ \mu_1 &= \beta_1 + k_1 \\ \mu_2 &= \beta_2 + k_2 \\ \cdots &\quad \cdots \end{aligned}\right\}. \tag{3}$$

Substitution of these in the typical observation Eq. (2) gives

$$(\alpha_1 + c_1)G[H(\beta_1 + k_1)] + (\alpha_2 + c_2)G[H(\beta_2 + k_2)] + \cdots = \Sigma I; \tag{4}$$

which is still non-linear, but in which the unknowns to be adjusted are now the presumably *small* corrections c_1, c_2, $\cdots$, k_1, k_2, $\cdots$.

Each term of (4), when expanded by Taylor's theorem as in the method cited, assumes the form (dropping subscripts):[5]

[4] See Weld, *Theory of Errors and Least Squares*, p. 178; or Merriman, *Method of Least Squares*, p. 175.

[5] In this process we encounter the following:

$$\frac{\partial}{\partial\beta}G(H\beta) = \frac{\partial}{\partial\beta}\int_1^\infty x^{-2}e^{-H\beta X}dx = -H\int_1^\infty x^{-1}e^{-H\beta x}dx \text{ (integrate by parts)}$$

$$= \frac{1}{\beta}\left[\int_1^\infty x^{-2}e^{-H\beta x}dx - e^{-H\beta}\right] = \frac{1}{\beta}[G(H\beta) - e^{-H\beta}];$$

$$\frac{\partial^2}{\partial\beta^2}G(H\beta) = \frac{G(H\beta) - e^{-H\beta} + H\beta e^{-H\beta} - G(H\beta) + e^{-H\beta}}{\beta^2} = \frac{H}{\beta}e^{-H\beta}.$$

$$(\alpha + c)G[H(\beta + k)] = \alpha G(H\beta) + G(H\beta)\cdot c + \frac{\alpha}{\beta}[G(H\beta) - e^{-H\beta}]k$$

$$+ \frac{H\alpha}{2\beta}e^{-H\beta}k^2 + \frac{1}{\beta}[G(H\beta) - e^{-H\beta}]ck + \cdots . \qquad (5)$$

This is strictly linear in c. If k is very small, the higher terms can be dropped. Whether k is small enough to justify this must be investigated. The steps necessary to insure the negligibility of the non-linear terms in k will appear in the second part of the paper. Let us assume that they are negligible, and that therefore only the first three terms of (5) need be employed.

Besides the terms included in the first member of (2), one for each cosmic-ray component, there may be added a term R representing such observed effects as are not so included: the *Restgang*, the small residual source of ionization, the leakage of the electroscope, or whatever it is that the ionization appears to approach as an irreducible minimum limit. If R is the true value of this, and ρ its assumed approximate value, then to preserve the symmetry of the method we may let $R=\rho+r$, where r is, again, a small correction.

Using now the linear part of the expansion (5) and adding the residual ionization just mentioned, the observation equation takes the form, linear in the c's, the k's, and r:

$$\Sigma G(H\beta)c + \Sigma\frac{\alpha}{\beta}[G(H\beta) - e^{-H\beta}]k + \Sigma\alpha G(H\beta) + (\rho + r) = \Sigma I; \qquad (6)$$

in which the summations carry over whatever number of discrete cosmic-ray components is assumed to exist. Or if we designate the coefficients of the respective c's by A's, those of the k's by B's, and the third terms by P's, and transpose, (6) may be more intelligibly written

$$A_1c_1 + A_2c_2 + \cdots + B_1k_1 + B_2k_2 + \cdots + r$$
$$= \Sigma I - (P_1 + P_2 + \cdots + \rho); \qquad (7)$$

the key to which is

$$\left.\begin{aligned} A_1 &= G(H\beta_1), \text{ etc.} \\ B_1 &= \frac{\alpha_1}{\beta_1}[G(H\beta_1) - e^{-H\beta_1}], \text{ etc.} \\ P_1 &= \alpha_1 G(H\beta_1), \text{ etc.} \end{aligned}\right\} \qquad (8)$$

The observation equations actually used in this adjustment were all of the form (7), differing from each other only in the values given to H and in the corresponding observed values of the apparent total ionization ΣI. The rest of the process follows the well-known procedure of the method of least squares for observations assumed to be of equal weight.

II. Application to Actual Cosmic-Ray Data

The first step is a survey of the available experimental data. Millikan and Cameron have taken most elaborate pains to obtain accurate readings on the

ionization at various depths in water, and their most recent published results[6] have been used as the basis of this analysis. There are tabulated forty-four observations on the total ionization ΣI at depths varying from about 8 to 80 meters. From their study of the results, Millikan and Cameron conclude that there are four principal components, whose constants they estimate as follows (using the above notation):

Initial intensity	Absorption coefficient
$33 = \alpha_1$	$0.03 = \beta_1$
$80 = \alpha_2$	$0.10 = \beta_2$
$130 = \alpha_3$	$0.20 = \beta_3$
$141{,}000 = \alpha_4$	$0.80 = \beta_4$

(9)

Also their preliminary estimate of R, the residual minimum ionization, is 1.2, which is therefore the value of our ρ. This makes *nine* unknowns, viz., the corrections c_1, c_2, c_3, c_4, k_1, k_2, k_3, k_4, and r.

Now α_4 is so large that there is grave question whether the k^2 term in (5), viz.,

$$\frac{H\alpha_4}{2\beta_4} e^{-H\beta_4} k_4^2, \tag{10}$$

can be ignored; even if k_4 were small, which is doubtful. At the greater depths, however, the exponential factor of (10) becomes sensibly zero, as does the coefficient of ck in (5). Moreover, Millikan and Cameron express their belief that the presence of secondary radiation due to the Compton effect may render the absorption coefficients actually variable during the earlier stages of the absorption, that is, at the lesser depths. For both reasons it has been thought best to confine the analysis at first to the greater three-fourths of the depth range. Beyond $H = 16$ meters, the k_4^2 term (10), and at the same time the coefficients of c_4, k_4, and $c_4 k_4$, become vanishingly small, so that these two unknowns are eliminated entirely, leaving only to the *seven* unknown corrections c_1, c_2, c_3, k_1, k_2, k_3, r to be adjusted.

To test the validity of the linear approximation (6), an arbitrary correction of one percent was assumed for each unknown ($C_1 = 0.01\ \alpha_1$, etc.), and (6) was applied at the most unfavorable point of the range (16 meters). The discrepancy due to the approximation was found to be only one part in 10,000.

Proceeding therefore along this line, the twenty-two observation equations corresponding to the last twenty-two depth-ionization measurements were set up in accordance with (7) and adjusted in the usual manner, giving seven normal equations corresponding to the seven required corrections.

Before this adjustment could be undertaken, it was found necessary to compute values of the Gold integral intermediate between those given in Gold's published table[3] and to extend the table to include somewhat larger values of the argument $H\mu$;—a laborious computation in itself.[7] A calculating

[6] Millikan and Cameron, Phys. Rev. **37**, 235 (1931).

[7] Copies of the enlarged table are available to anyone interested.

machine was used throughout, all work was carefully checked, and the final results were found to satisfy the normal equations exactly.

The adjusted values of the seven unknowns are as follows:

$$\left.\begin{aligned} c_1 &= -\ 0.7078 & k_1 &= -\ 0.001269 \\ c_2 &= -\ 513.63 & k_2 &= -\ 0.09225 \\ c_3 &= -\ 3958.4 & k_3 &= -\ 2.5138 \\ & r = +\ 0.0008 & & \end{aligned}\right\} \tag{11}$$

If these corrections were applied to the tentative values given by Millikan and Cameron the results would be:

$$\left.\begin{aligned} I_{01} &= \ 32.2922 & \mu_1 &= \ 0.028731 \\ I_{02} &= -\ 433.63 & \mu_2 &= \ 0.00775 \\ I_{03} &= -\ 3828.4 & \mu_3 &= -\ 2.3138 \\ & R = 1.2008 & & \end{aligned}\right\} \tag{12}$$

The values of I_{01}, μ_1, and R are reasonable enough; but in the other cases the results are entirely devoid of meaning. Most of the corrections are larger than the tenative values. We computed the residuals from the adjusted values (11) by substitution in (7) and found the sum of the squares to be 0.3572, while the algebraic sum of the residuals is exactly zero. If the tenative values were correct, that is, if the seven corrections were all zero, the same substitution would give the sum of the squared residuals as 0.5573, and that of the residuals themselves as -0.06. All this indicates that the utterly impossible results (11) are, nevertheless, more probable than the consequences of assuming the tentative values to be correct.

This is the disconcerting report that has to be made on the matter. We were looking for a refinement of Millikan and Cameron's estimates, and there is no question that, if their assumptions as to the makeup of the radiation were true and if (9) were fair approximations of the involved constants, this adjustment would have yielded a reasonable set of small corrections for the three more penetrating components. The writer can arrive at only one alternative conclusion, namely, that however closely the values fixed upon by Millikan and Cameron may fit their observational curve, those values are not, reciprocally, deducible from the observations by the method of least squares.

It should be remarked, in passing, that half of the observations are crowded into the upper one-fourth of the depth range; and that there is a tendency to "bunch" the observations, that is, to take several at nearly the same depth. While the reasons for this are obvious, it would better serve the purposes of analysis if the same number of readings could have been taken at approximately uniform intervals of, say, two meters.

In conclusion the writer wishes to acknowledge the great assistance afforded by a grant from the Iowa Academy of Science which made possible the employment of a skilled computer, and also his appreciation of the services of that computer, Miss Edna Kerchmar, whose painstaking work and intelligent grasp of the problem made its solution possible.

A New Determination of the Disintegration Constant of Uranium by the Method of Counting α-Particles

By Alois F. Kovarik and Norman I. Adams, Jr.
Sloane Physics Laboratory, Yale University

(Received April 18, 1932)

Alpha-particles emitted by a known amount of pure U_3O_8 in the form of thin films were restricted in their passage into an ionization vessel by cylindrical channels of a grid placed over the material. The method of counting α-particles alone was that of Greinacher. All α-particles entering the ionization chamber automatically registered on a mechanical counter, for which an elaborate electrical and mechanical arrangement of apparatus was used. Over 100,000 counts were made from two specimens differing in surface density in the ratio of nearly 5 to 1. The $\lambda_{U\,I}$ obtained is $1.53_2(10)^{-10}$ yr^{-1} or $T=4.52_4(10)^9$ yr, a value consistent with Gleditsch's $\lambda_{Ra}=4.11(10)^{-4}$ yr^{-1}, Boltwood's radium to uranium ratio of $7.40(10)^{-7}$ and branching ratio between 0.96 and 0.97.

Introduction

IN THE determination of the age of radioactive minerals two disintegration constants, in particular, are needed, namely those of uranium and thorium. For minerals containing mainly the uranium series, the disintegration constant of uranium is of prime importance while on the other hand for thorites and thorianites containing predominantly thorium, an accurate value of the thorium disintegration constant is demanded.

In the case of thorium there is a discrepancy of thirty percent in the two values usually accepted and in the case of uranium the discrepancy is from three to ten percent. Because of these rather widely differing values, the National Research Council's committee on the measurement of geological time by atomic disintegration has urged for some time the advisability of obtaining by direct laboratory methods more accurate values for these constants.

We have undertaken this work and the present paper deals with the uranium alone. The work on thorium is well under way but certain difficulties in connection with the thoron have arisen which have not yet been successfully solved.

Method, Material and Procedure

There are two ways in which the disintegration constant of uranium may be determined accurately. The first method was used by Geiger and Rutherford[1] when they counted the scintillations produced by the α-rays from a thin film of uranium oxide of known weight. This method is direct and involves fundamentally counting and weighing in the experimental procedure. The second method can be just as accurate as the first but it is more

[1] H. Geiger, and E. Rutherford, Phil. Mag. [6] **20**, 691–698 (1910).

involved. The value is given in terms of the radium disintegration constant, the radium to uranium ratio when these two members of the same radioactive series are in equilibrium—as they are in old unaltered uranium bearing minerals—and the so-called branching ratio of the actinium series to the uranium series. Since the values for the radium disintegration constant have extremes differing by ten percent, a determination by this method cannot have a greater percent accuracy than that which may be given to the radium constant. When counting scintillations was the only known way of counting α-particles the numbers counted were not always as large as the laws of probability demanded for great accuracy for various obvious reasons. Geiger and Rutherford counted only 900 scintillations from the oxide films and 2000 from the mineral films for their determination of the uranium disintegration constant. Since the first electrical automatic registration of the various kinds of rays was reported by one of us[2] using then the Geiger point counter, several new methods of attack have been developed and among these is the method of Greinacher[3] in which the ions produced by the α-particle charge up a small capacity electrode. This effect is then amplified by means of a suitable arrangement of vacuum tubes and the momentary current from the last tube is utilized in an Eindhoven galvanometer, an oscillograph, or some other indicating device. The ionization effect of the α-particle is so great for a short path in comparison to that of the β-particle or the electrons liberated by γ-rays, x-rays or cosmic rays that it is possible to adjust the sensitivity so that only the α-particles are effective. For these reasons we have adopted this method and by using a power tube as the last unit, a sensitive relay is caused to be operated by an α-ray and not by a β-ray or a γ-ray. This is important since all three types of radiations are emitted by a uranium oxide film. A second relay was made to close a local circuit containing a mechanical counter, known as the Cenco impulse counter, which automatically registered the α-rays individually as they appeared in the electric field of the ionization chamber. The number so counted can be made as large as is desirable without encountering the physical fatigue which accompanies counting scintillations.

The source was a thin film of pure U_3O_8 on an aluminum plate about 7.8 cm in diameter and 0.12 mm thick. The uranium oxide was prepared by the late B. B. Boltwood. It was a purified and many times recrystallized uranium nitrate prepared from an uraninite[4] and was labelled by him "very pure U_3O_8." The film was prepared by grinding the oxide moistened with chloroform in an agate mortar, and afterwards washing it with chloroform into a test tube making the volume of the chloroform about 20 cm.[3] The material was violently shaken up and quickly poured into another test tube. Particles too big to be held readily in suspension remained in the first test tube. The second test tube containing the impalpable particles was shaken

[2] Alois F. Kovarik, Phys. Rev. [2] **13,** 272–280 (1919).

[3] H. Greinacher, Zeits. f. Physik **36,** 364–373 (1926); **44,** 319–325 (1927).

[4] The uraninite bears letters F.M.C. which no doubt refer to the exact source of the mineral. So far, we have not found in his notebooks the key to this.

and the liquid was poured over the aluminum plate placed in a brass dish in which a recess was made equivalent to the thickness of the plate. The liquid extended more than a centimeter beyond the circumference of the aluminum plate. The plate was held down by a weight on three needle points which came in contact with the plate near the circumference. On account of the quantity of chloroform used the time required for the evaporation was about one hour and the particles settled down gradually and uniformly over the plate. The time can be advantageously increased by covering the dish: thus impeding the evaporation. Under such conditions excellent films were obtained. The aluminum plate was weighed with great care before and after the deposition of the film on it, being warmed for some time previous to the weighing in each case.

The film of oxide was protected by a thin aluminum foil attached to a ring of aluminum of the same thickness as the plate. On top of this source was placed a grid through the channels of which α-particles emerged into the ionization chamber. The grid was made by drilling a machined brass plate of uniform thickness so as to produce identical cylindrical channels according to a carefully selected pattern such that if the grid was placed in successive angular positions differing by about 20° every part of the source came under some channel at some time of observation. If a strong source was used it was not desirable to have the counts per minute exceed a safe number (found by experiment) above which the mechanical device did not register accurately. In such a case a simple expedient was resorted to, some of the holes being closed by means of screw heads of appropriate size. The depth of the channel was $h = 5.184$ mm and the radius was 1.962 mm. A thin aluminum foil held on a narrow brass ring was placed over the grid. This prevented ions formed in the channels from being drawn out by the electric field and thus prevented counting some α-particles which did not pass through the top opening of the channel.

The collecting electrode was 8 cm in diameter and was placed 2.5 cm from the top of the grid and approximately the same distance from the roof and the sides of the enclosing case. The case with the electrode attached could be removed readily to get at the specimen placed on an insulated table which was connected through the electromagnetic filter to the source of potential. The capacity of the electrode in this relative position to its surroundings was considerably higher than that used by other experimenters using this method of counting. We found that our amplification system and the allowance of nearly 1.5 cm as the effective range of the α-particles in the electric field made it possible to record the particles. In fact, when a polonium source was used in some of the test experiments, the collecting electrode had a diameter of 11 cm and its capacity was about 25 e.s.u. The polonium α-particles have a range considerably greater than those of U I, and the latter gave about 1.5 cm effective range in the ionization chamber. While it was possible to count the U I α-particles in this case also, it was observed that we were working near the limit of sensitivity and for this reason the capacity was reduced by making the collecting electrode smaller (8 cm). All α-particles,

even those from the extreme channels used, had their total effective range entirely in the field between the collecting electrode and the aluminum foil placed over the grid.

The details of the amplifying system are indicated in Fig. 1. In order to obtain as large a signal as possible the collecting electrode of the ionization chamber was connected to the grid of a vacuum tube with small input capacity. This tube was followed by three tubes giving high voltage amplification. Following these was a power tube which actuated a sensitive relay. A less sensitive relay and finally the Cenco impulse counter followed in turn.

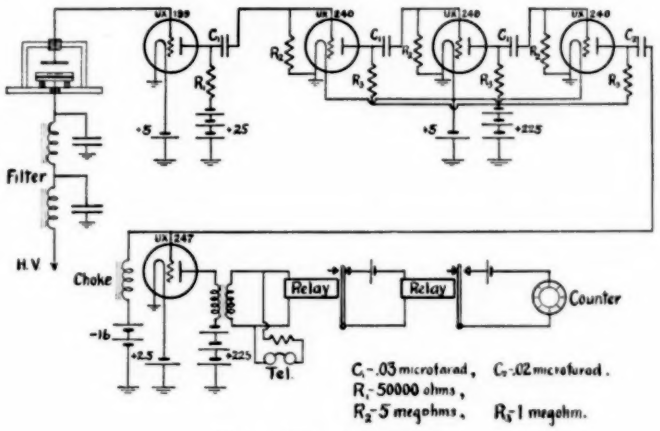

Fig. 1. Circuit diagram.

The values of the circuit constants are shown in the legend of the figure. The calculated value of the voltage amplification to the grid of the power tube is about 40,000. Hence, as the signal produced by an α-particle in the ionization chamber was of the order of $2.5 \cdot (10)^{-4}$ volt the grid swing of the power tube was of the order of 10 volts. This was ample for the operation of the relay-counter assembly.

In order to be able to determine whether the adjustment of the relays and counter were correct so that no "counts" were missed, a telephone head set with a high resistance in series was shunted across the secondary of the output transformer coupling the power tube and the first relay. This monitoring device proved a great convenience.

The counter with its relay and operating battery and the telephone head set were the only parts of the apparatus which were not housed in earthed metal boxes. Two large metal boxes, each with four compartments, were used for the apparatus. All the batteries used in the three-tube voltage amplification unit were on the floor of the compartment below that housing the vacuum tube arrangement and similarly in the case of the power tube and its sensitive relay. The large capacity condensers and choke coils, used for filtering, were on the floor of the compartment below the ionization chamber. The small dry cells used with the first stage of amplification were built compactly with the tube and placed with it.

The ionization chamber, the first stage amplification unit, the three-stage unit and the power tube unit were each separately suspended by a damping device. The damping arrangement in each case consisted of two fairly heavy boards, the upper being suspended from the roof of the box by three short elastics of good rubber tubing (sometimes several fold) and the lower board, carrying the instruments in question, being suspended from the upper board by longer rubber tubings (same material). Some experimentation was necessary before the proper lengths were found to produce the proper mechanical damping.

The boxes were covered with thick heavy sheets of hair felt. At first, vibrations produced by slamming of doors and very loud sounds of some particular vibration frequency caused disturbances but these were ultimately almost completely eliminated. The first stage of amplification was particularly susceptible to such vibrations. To insure certainty of minimum possible trouble, periods of time were chosen for experimentation—generally at night—when everything was quiet.

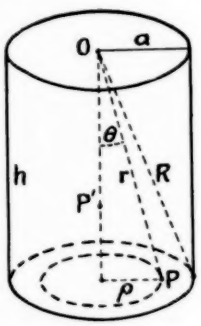

Fig. 1.

The Cenco impulse counter had to be checked for accuracy in recording α-particles. Using a uniform source, counts were obtained for the α-particles coming through various numbers of channels. The count in a unit time was found to be strictly proportional to the number of channels until the total count exceeded the mean value of about two per second. It was obvious, therefore, that in no case should the counts be a very large number per minute. Various tests indicated that it was safe to count up to 100 per minute and we arranged to use such a number of channels for a given source that about 75 per minute or less were counted.

The field in the ionization chamber was obtained from a storage battery of 4000 volts located in another room. It was found that from 800 to 1200 volts was sufficient potential difference to be used for satisfactory performance of the counting devices. Since the battery line to our apparatus acted occasionally as an antenna and since other uses were made of adjacent cells of the battery resulting sometimes in electromagnetic disturbances, we allowed the large capacity condensers to charge up and then carried on the counting for a period of ten or fifteen minutes during which the voltage of the condensers did not change appreciably. Proceeding in this manner we

found we were quite free of *accidental counts* due to these extraneous causes. There were, however, possible accidental counts due to internal discharges in the condensers. These are included in the *naturals* given below.

Calculation of the Number of α-Rays Emerging Through a Channel

Since the grid is placed directly on top of the thin aluminum foil protecting the source, the source may be considered for each channel as covering the base of it. In order to calculate the proportion of the emitted rays which emerge through the circular top of the channel, we must know the solid angle subtended by the top opening at any point P of the base.

For a point P' (Fig. 2) on the axis of the cylinder at a distance x from the top,

$$\Omega_{P'} = 2\pi \cdot \left\{1 - \left[1 + \left(\frac{a}{x}\right)^2\right]^{-1/2}\right\}.$$

For P at r from O, where $x = h$, $\cos\theta = h/r$,

$$\begin{aligned}\Omega_P = 2\pi\Big\{&\frac{1}{2}\cdot\frac{a^2}{r^2}\cdot P_1(\cos\theta) - \frac{3}{8}\cdot\frac{a^4}{r^4}\cdot P_3(\cos\theta)\\ &+ \frac{5}{16}\cdot\frac{a^6}{r^6}\cdot P_5(\cos\theta) - \frac{35}{128}\cdot\frac{a^9}{r^9}\cdot P_7(\cos\theta)\\ &+ \frac{63}{256}\cdot\frac{a^{10}}{r^{10}}\cdot P_6(\cos\theta) - \text{etc.}\Big\}\end{aligned}$$

where $P_n(\cos\theta)$ is the zonal harmonic.

Now, if N_0 is the number of α-particles emitted from a square millimeter of the source; N, the number of α-particles emerging through the top opening of the channel; and $R = (a^2 + h^2)^{1/2}$, then

$$\begin{aligned}N &= \int_0^a \frac{\Omega}{4\pi}\cdot N_0 \cdot 2\pi\rho d\rho\\ &= \frac{N_0}{2}\int_h^R \Omega \cdot r\, dr\\ &= \pi a^2 \cdot N_0 \cdot \left(\frac{h}{a}\right)\cdot\Big\{\frac{1}{2}\left(\frac{a}{h} - \frac{a}{R}\right) + \frac{3}{16}\left(\frac{a}{R}\right)^3\cdot\left[\left(\frac{h}{R}\right)^2 - 1\right]\\ &\quad - \frac{5}{128}\cdot\left(\frac{a}{R}\right)^5\cdot\left[7\cdot\left(\frac{h}{R}\right)^4 - 10\left(\frac{h}{R}\right)^2 + 3\right]\\ &\quad + \frac{35}{2048}\cdot\left(\frac{a}{R}\right)^7\cdot\left[33\cdot\left(\frac{h}{R}\right)^6 - 63\left(\frac{h}{R}\right)^4 + 35\left(\frac{h}{R}\right)^2 - 5\right]\\ &\quad - \frac{63}{32768}\cdot\left(\frac{a}{R}\right)^9\cdot\left[715\left(\frac{h}{R}\right)^8 - 1716\left(\frac{h}{R}\right)^6 + 1386\left(\frac{h}{R}\right)^4\right.\\ &\quad \left. - 420\left(\frac{h}{R}\right)^2 + 35\right] + \text{etc.}\Big\}\end{aligned}$$

and for the experimental dimensions:

$$a = 1.962 \text{ mm} \qquad h = 5.184 \text{ mm} \qquad R = 5.5424 \text{ mm}$$

we have

$$N = \pi a^2 \cdot N_0 \cdot [0.029824] = N_0 \cdot (0.36067).$$

Experimental Results

Two sources were used, one having a total weight of 77.18 mg U_3O_8 with a surface density of 1.615$_3$ mg U_3O_8 per cm^2 and the other 17.88 mg with a surface density of 0.3759 mg U_3O_8 per cm.^{2} Counts were obtained for a time so long as to approximate to 5000 for each position of the grid. In order to show the probability variations with time, a complete record for one position of the stronger source is given in Table I.

Table I. *Sample record.*

Grid 0° Source: 77.18 mg U_3O_8 $\sigma = 1.615_3$ mg U_3O_8/cm^2

Count	Time	α/min.	Count	Time	α/min.
			2773	45 min.	
345	5 min.	69.0	310	5 "	62.0
283	"	56.6	320	"	64.0
309	"	61.8	319	"	63.8
300	"	60.0	334	"	66.8
333	"	66.6	306	"	61.2
302	"	60.4	325	"	65.0
307	"	61.4	317	"	63.4
302	"	60.4	297	"	59.4
292	"	58.4	325	"	65.4
2773	45 min.		5624 ÷ 90 = 62.5$_3$/min.		

By placing the grid in the various positions any lack of uniformity in the film is corrected, but it will be seen from Table II that the lack of uniformity could not have been appreciable. The final results for the two sources are given in Table II.

Table II.

77.18 mg U_3O_8 $\sigma = 1.615_3$ mg U_3O_8/cm^2; 10 channels				17.88 mg U_3O_8 $\sigma = 0.3759$ mg U_3O_8/cm^2; 34 channels			
Grid	Count	Time (min.)	Count/min.	Grid	Count	Time (min.)	Count/min.
0°	5451	70	77.87	0°	5628	90	62.53
20°	5602	75	74.69	20°	5518	"	61.31
40°	5496	70	78.51	40°	5621	"	62.46
60°	5375	"	76.79	60°	5460	"	60.67
80°	5419	"	77.41	80°	5552	"	61.69
90°	5427	"	77.54	100°	5520	"	61.33
110°	5619	"	80.27	120°	5609	"	62.33
130°	5866	75	78.21	140°	5515	"	61.28
150°	5356	70	76.51	160°	5586	"	62.07
170°	5217	"	74.53				
	54828 ÷ 710 min. = 77.22/min.				50009 ÷ 810 min. = 61.74/min.		
	Naturals = 3.71/min.				Naturals = 3.71/min.		
	Net = 73.51/min.				Net = 58.03/min.		

The number 3.71 per minute, labelled naturals, is a correction. It was obtained either by removing the source or by covering the grid with a thick aluminum plate which stopped all α-rays. A count of this sort was taken for about 30 minutes after each position count and sometimes also preceding it. It varied only little in value and the mean over the total time of 671 minutes was 3.71 per minute. It is due partly to contamination from the polonium source used in the original test experiments (which contamination was reduced but could not be completely removed) and partly it is due to sudden changes of charge in the condensers sufficiently great to actuate the relay.

It will be noticed that more than 50,000 counts were obtained for each specimen, i.e., over 100,000 in all. In order to average the results it is necessary to reduce the net results for each specimen to the net count per channel per minute and to a common value of surface density, e.g., $\sigma = 1$ mg U_3O_8 per cm^2 which reduction is shown in Table III. Since we desire to know the

TABLE III.

Source mg U_3O_8	Net count / minute	Channels	σ	Net count per channel per minute for $\sigma = 1$ mg U_3O_8/cm^2
77.18	73.51	10	1.615_3	4.5509
17.88	58.03	34	0.3759	4.5411
				Mean = 4.5460

number of α-particles emitted by 1 gram of uranium per second it is necessary to perform the reduction of units.

$$\frac{4.5460}{1 \text{ min.} \cdot 1 \text{ mg } U_3O_8/\text{cm}^2} \times \left[\frac{1 \text{ min.}}{60 \text{ sec.}} \cdot \frac{1 \text{ mg } U_3O_8}{0.84807 \text{ mg U}} \cdot \frac{10^3 \text{ mg}}{1 \text{ gm}} \cdot \frac{100 \text{ mm}^2}{1 \text{ cm}^2}\right]$$

$$= 8.934 \times (10)^3 \frac{\alpha}{\text{sec.}} \text{ per gram U(I + II)}.$$

Since U I and U II are isotopes in radioactive equilibrium, the number of α-particles from each in a unit of time is the same. Therefore, if N and N_0 refer to the number of α-particles from U I alone,

$$N = 8.934(10)^3/2 = N_0(0.36067)$$

from which,

$N_0 = 12.385_2(10)^3$, the number of α-particles emitted by U I per second from 1 gram of U(I+II).

Using the current values of the disintegration constants of U I and of U II and values of Loschmidt's number and the atomic weight of U(I+II) we get that 1 gm U(I+II) contains

$$\frac{0.9999_3 \times 6.06_4(10)^{23}}{238.17} \text{ U I atoms} = 2.546_1 \text{ U I atoms}.$$

Therefore

$$\lambda_{UI} = \frac{12.385_2(10)^3}{2.546_1(10)^{21}} \text{ sec.}^{-1} = 4.865(10)^{-18} \text{ sec.}^{-1} = 1.53_2(10)^{-10} \text{ year}^{-1}$$

corresponding to a half-value period of $T = 4.52_4(10)^9$ years.

It is interesting to see what check this gives on the value of the disintegration constant of radium. Professor Ellen Gleditsch's[5] value for λ_{Ra} is $4.11(10)^{-4}$ yr^{-1}; B. B. Boltwood's ratio of radium to uranium in unaltered primary uraninites is $3.40(10)^{-7}$.

If we take the branching ratio to be

$$0.97 \text{ (Hahn-Meitner)}, \lambda_{UI} = 1.52(10)^{-10} \text{ yr}^{-1};$$

and if we take the value

$$0.96 \text{ (v. Grosse)}, \lambda_{UI} = 1.53_5(10)^{-10} \text{ yr}^{-1}.$$

Whichever ratio is taken, our value seems to be in excellent agreement with Gleditsch's value for the disintegration constant of radium. Since the $\lambda_{Ra} = 4.11(10)^{-4}$ yr^{-1} gives for the number of α-particles emitted per second from a gram of radium $Z = 3.49_3(10)^{10}$ it would appear that this value, rather than the high value[6] $Z = 3.70(10)^{10}$, is checked by our experiments.

In conclusion we desire to express our thanks to the Bell Telephone Laboratories for a gift of one of the relays used which was made specially for us. The other relay used is also their product.

[5] See Radioactivity, N. R. C. bulletin No. 51 (1925), and Age of the Earth, N. R. C. bulletin No. 80 (1931).

[6] Jour. de Physique [7] **2**, 273–289 (1931).

Gamma-Radiation and its Relation to Nuclear Structure

By P. GERALD KRUGER
Department of Physics, University of Illinois

(Received April 6, 1932)

A formula has been obtained which enables the calculation of the wave-lengths of γ-radiation from the nucleus. Such calculations have been made for fourteen different radio-active elements and the observed and calculated λ's compared. The largest discrepancy is about twelve percent. γ-ray series which check the observed γ-ray wave-lengths to less than five percent have been calculated for AcX and RaB. The intensities of the lines in these series are peculiar. With the same formula the shortest possible radiation from U has been calculated and found to be of the order of magnitude of cosmic radiation.

BRYDEN[1] and White[2] have shown that the protons in the nucleus may be arranged in equivalent proton groups, which are similar to the electron configurations of the outer electrons, and that such an arrangement explains the observed nuclear moments of the first ten elements of the periodic system of elements rather well. This leads one to wonder where the electrons in the nucelus might be and what kind of equation might be obtained to express the observed γ radiations from the nucleus.

In order to study the problem the following assumptions were made. (1) Assume that the electrons in the nucleus collect to form a negatively charged center in the nucleus. (2) Assume that this center does not move. (3) Assume that the protons rotate about this center. (4) Assume that the effective charge on the center is $eZP^{\frac{1}{2}}/(t'+1)$; where P is the total number of protons present, t', with Bryden's notation, means the total quantum number of the proton which is being excited, Z takes on values of 1, 2, $\cdots$ 146 for the 1st, 2nd, $\cdots$ 146th spectrum, and e is the charge on the electron.

The fourth assumption describes the nuclear field and prescribes a screening effect of such a nature the 146 electrons may bind 238 protons in the nucleus. This assumption was stated in its present form because it leads to a formula which fits the γ-ray data to be discussed below.

By applying the simple Bohr theory to the system the total energy

$$E = -\frac{2\pi^2 e^4 Z^2 M}{h^2}\cdot\frac{P}{(t'+1)^2}\cdot\frac{1}{t^2}, \tag{1}$$

where M is the mass of proton, and t the total quantum number similar to n in the atomic case.

The frequency, expressed in cm^{-1}, radiated when a proton transition occurs thus becomes

$$\bar{\nu} = R'Z^2\frac{P}{(t'+1)^2}\left(\frac{1}{t_1^2}-\frac{1}{t_2^2}\right), \tag{2}$$

[1] Bryden, Phy. Rev. **38**, 1989 (1931).
[2] White, Phy. Rev. **38**, 2073 (1931).

where

$$R' = \frac{2\pi^2 e^4 M}{h^3} = R\frac{M}{m}, \tag{3}$$

and R is the Rydberg constant. Thus R' is easily computed. It becomes

$$R' = 1.097 \times 10^5 \times 1836 = 2.017 \times 10^8 \text{ cm}^{-1}.$$

It also follows that the radius of an orbit is expressed by

$$A' = \frac{t^2h^2(t'+1)}{4\pi^2e^2ZMP^{1/2}} = \frac{A}{1836}\frac{(t'+1)}{P^{1/2}} \tag{4}$$

where $A = t^2h^2/4\pi^2e^2Zm$, and m is the mass of the electron for the atomic case. Thus A' for gold becomes

$$A'(\text{Au}) = \frac{0.5284 \times 10^{-8}}{1836}\frac{(9+1)}{197^{1/2}} = 2.05 \times 10^{-12} \text{ cm}$$

where t' takes the value 9, since, according to Bryden's table, the outermost orbit in this case would be the one having 9 s^2 protons.

The only check available from experimental data on this value is one from scattering experiments. They give 3×10^{-12} cm as the distance which is the upper limit of the radius of the gold nucleus, so that the above value is a reasonable one.

A similar calculation for U gives

$$A'(\text{U}) = 2.055 \times 10^{-12} \text{ cm}.$$

A calculation of the radiated frequency (cm^{-1}) for a proton transition from the second to the first total quantum state in the U nucleus (radiation which corresponds to the $K\alpha_1\alpha_2$ x-rays of U in the atomic case) gives,

$$\bar{\nu} = 2.017 \times 10^8(2/2^2)146^{2\cdot\frac{3}{4}}$$
$$= 16.14 \times 10^{11} \text{ cm}^{-1}.$$

Here P is 2 since $1s^2$ protons are present before ionization and one of these $1s^2$ protons are removed from the nucleus; t' is one, since $1s^2$ protons are concerned; Z is 146.

This radiation would correspond to about 2×10^8 volts energy and would have a wave-length of 0.0618X.U. Millikan and Cameron[3] report their shortest cosmic ray to be 0.08 X.U. So it might be possible that cosmic radiation has its origin in the nucleus and is emitted by a similar process, in the nucleus, to that which produces x-ray in an atom. Moreover, it is not untenable to think that excited or ionized nuclei exist in stars. On the other hand, according to the calculations of L. H. Gray,[4] and assuming that an extrapolation of the Klein-Nishina formula is valid, observed absorption coefficients point to the existence of cosmic radiation of the order of 90 to 2,000 million volts. Such radiation could not be explained by the above formula.

[3] Millikan and Cameron, Phy. Rev. **31**, 929 (1928).
[4] L. H. Gray, Proc. Roy. Soc. **A122**, 647 (1929).

The radioactive elements fall into three groups as shown in tables on page 24 of Rutherford, Chadwick and Ellis.[5] Data from these tables have been used in substituting the proper values in formula (2) to calculate the wave-length of γ-radiation, when $t_1 = 1$ and $t_2 = 2$. The results of these calculations are given in Tables I, II and III. The observed λ's with which the calculated λ's are compared, are the longest wave-lengths for each element as given by Rutherford, Chadwick and Ellis.

TABLE I. *Comparison of observed and computed γ-ray wave-lengths for radioactive elements of group I.*

$$\bar{\nu} = R'Z^2 \frac{P}{(t'+1)^2}\left(\frac{1}{t_1^2} - \frac{1}{t_2^2}\right), \qquad t_1 = 1,\ t_2 = 2$$

Element	Type of disintegration	Total No. protons	Z	P	t'	Proton configuration	Cal. $\bar{\nu}\times 10^{-5}$ cm^{-1}	Cal. λ	Obs. λ
UX_1	β	234	1	234	6	$8d^{10}9p^6 10s^2 6h^{11}$	7.22	138.5 X.U.	134.2X.U.
RaB	β	214	1	214	8	$7f^{14}8d^{10}9p^2$	4.00	250.	230.3
RaC	$\alpha\beta$	214	1	214	7*	$7f^{14}8d^{10}9p^2$	5.06	197.6	209.5
RaD	β	210	1	210	8	$7f^{14}8d^8$	3.92	255	261
Pa	—	231	1	231	6	$8d^{10}9p^6 10s^2 6h^{11}$	7.13	140	130.
Ra	α	226	2	225	8*	$8d^{10}9p^6 10s^2 6h^5$	16.81	59.5	65.2

TABLE II. *Comparison of observed and computed γ-ray wave-lengths for radioactive elements of group II.*

Element	Type of disintegration	Total No. protons	Z	P	t'	Proton configuration	Cal $\times 10^{-5}$ cm^{-1}	Cal. λ	Obs. λ
AcX	α	223	2	222	10	$8d^{10}9p^6 10s^2 6h^3$	11.1	90.1X.U.	86.0X.U.
RdAc	α	227	1	227	10	$8d^{10}9p^6 10s^2 6h^7$	2.84	352.	392.
AcC	$\alpha\beta$	211	3	208	9*	$7f^{14}8d^9$	29.3	35.3	34.9

TABLE III. *Comparison of observed and computed γ-ray wave-lengths of radioactive elements of group III.*

Element	Type of disintegration	Total No. protons	Z	P	t'	Proton configuration	Cal. $\bar{\nu}\times 10^{-5}$ cm^{-1}	Cal. λ	Obs. λ
M_sTh^2	β	228	1	228	7*	$8d^{10}9p^6 10s^2 6h^8$	5.39	186.X.U.	212.X.U.
ThD	Stable	208	1	208	9*	$6g^{18}7f^{14}8d^6$	3.15	317.	305.
RdTh	α	228	1	228	6	$8d^{10}9p^6 10s^2 6h^8$	7.04	142.	145.
ThB	β	212	2	211	8	$7f^{14}8d^{10}$	15.76	63.5	64.6
ThC''	β	208	1	208	9*	$6g^{18}7f^{14}8d^6$	3.15	317.	303.

The largest variation between observed and calculated values occurs for MsTh2 and RdAc where the difference is about 12 percent. All other cases fit reasonably well and some differences are of the order of one percent.

In column seven the proton configurations for the element in question are given. These were taken from Bryden's[1] table.

In most cases t' has the value of the total quantum number of the last sub-shell to be filled and since in general one would expect such protons to be the first to be excited, it was stated above that t' was the total quantum number of the proton being excited. In Table I, RaC and Ra are exceptions

[5] Rutherford, Chadwick and Ellis, *Radiations from Radioactive Substances.*

to this rule and the t' values have been given an asterisk for that reason. Both of these elements emit α particles, whereas the other elements in the table emit β particles, and this may be a reason why protons of a different total quantum number, than that expected, are excited.

RaB may also seem to be an exception to the rule, but since t' is involved only in $P/(t'+1)^2$, which is a screening function, it means that the $9p^2$ protons have very little screening effect and that t' therefore has the value 8.

With this in mind Table II contains only one exception, AcC, which emits both α and β particles. Table III has three exceptions. Here t' equals the total quantum number of the last filling-shell plus one. There is no apparent reason for the discrepancy.

For the two elements AcX and RaB, it has been possible to calculate a series of wave-lengths which fit the observed wave-lengths rather well. Formula 2 has been used to make the calculations when $Z=2$, and t_1 takes on the values 3/4, 7/8, 15/16 $\cdots$ 1 successively. The calculated wave-lengths check the observed wave-lengths to less than 5 percent error.

The intensities of the γ-rays listed in Tables IV and V were obtained from β ray lines, and therefore may be in error. The limit of the AcX series is

TABLE IV. *γ-ray spark spectrum of AcX.*

$$\dot{\nu}=R'Z^2\frac{P}{(t'+1)^2}\left(\frac{1}{t_1^2}-\frac{1}{t_2^2}\right) \qquad \begin{matrix} t_2=2 \\ t_1=3/4,\ 7/8,\ 15/16,\ 31/32,\ \cdots\ 1 \end{matrix}$$

App. Int.	t_1	Calculated $\dot{\nu}$	Calculated λ	Observed λ_1
130	3.4	22.6×10^8 cm^{-1}	44.2 X.U.	45.9 X.U.
25	7/8	15.63	64.0	61.7
80	15/16	13.1	76.3	78.6
180	31/32	12.0	83.0	80.6
155	1	11.10	90.1	86.0

TABLE V. *γ-ray spark spectrum of RaB.*
$Z=2$, $P=213$, $t_1=3/4,\ 7/8,\ 15/16,\ 31/32\ \cdots\ 1$, $t_2=2$, $t'=7$

Int.	t_1	Calculated $\dot{\nu}$	Calculated λ	Observed λ_1
?	3/4	41.0×10^8 cm^{-1}	24.4 X.U.	26.2 X.U.
125	7/8	28.36	35.26	34.9
100	15/16	23.8	42.02	41.6
4	31/32	21.86	45.8	47.5
90	1	20.14	49.65	50.8

11.10×10^8 cm^{-1}, and is the smallest frequency of the series. The intensities, however, are degraded in the opposite direction. This presents a difficulty which can not be explained at the present time.

In Table IV the intensities decrease as the series limit is approached , except for the intensity of λ26.2 X.U. which is questionable. λ50.8 X.U. is the head of the series and may contain several lines which are not resolved. This would account for its large intensity.

Thus, although there are numerous points still to be explained, it seems more than a coincidence, that the computed and observed wave-lengths should check as well as they do. The result is that the idea of equivalent proton states in the nucleus has been supported.

The Angular Distribution of Electrons Scattered Elastically and Inelastically in Mercury Vapor

By JOHN T. TATE* AND R. RONALD PALMER
University of Minnesota

(Received March 7, 1932)

A long electron gun was mounted to rotate about a well-shielded scattering region from which electrons scattered by gas molecules through a definite angle from a beam of small cross-section were collected, and their velocities determined, by a stationary collector containing an efficient Faraday cage, 6.0 cm in length. Angular distribution curves for electrons scattered elastically, for electrons scattered due to excitation of the atom (mainly 6.7 volt energy loss), and for electrons resulting from ionizing impacts are presented for 80, 120, 230, 490, and 700-volt electrons. In general, for a particular group, the curves are steeper the higher the velocity of the incident electron. The elastic group shows a diffraction pattern at large angles and the positions of the peaks agree well with those found by Arnot. The curves for the excitation group are much steeper than are those for the elastic group, and fall to very small values at large angles. The curves for the ionization group are also steeper but not so steep as the excitation group; at large angles the scattering is due mainly to slow electrons of this group. The ionization group is divided into sections and further characteristics are observed. Numerical integration of these curves gives the cross-sectional area for collision, the efficiency of ionization, and the efficiency of excitation.

INTRODUCTION

OF THE many methods devised to study the structure of the molecule and its accompanying field of force, those involving the measurement of the scattering of electrons in gases are yielding information of much value. Early experiments contented themselves with measuring the total number of electrons scattered from an electron beam due to interaction with gas molecules resulting in a deflection or energy loss sufficient to remove the electron from the beam. Among the important results of such experiments to determine the cross-section for interception of electrons have been those of Ramsauer who found that the inert gases show a special transparency to electrons of a few volts velocity, a result which Townsend simultaneously and independently discovered by an indirect method. Other investigators have studied the energy losses suffered by electrons which continue nearly undeviated after impact, and have identified these losses with certain critical potentials for excitation of the molecule. These experiments yielded early significant verifications of the quantum theory.

In the last few years a new type of experiment has developed, that of studying the angle of deflection of electrons which have interacted with gas molecules. Such experiments were inspired partially by the hope that diffraction phenomena would be observed. The now classical experiments of Davisson and Germer, which exhibited the wave nature of the electron, had

* The senior author wishes to acknowledge a grant made by the Graduate School to assist in this work.

just been performed. Also there was the hope that the new wave mechanics would be able to make calculations on such problems and checks could be made with theory. The fulfillment of the first hope was denied to those who first worked in this field[1-4]—they observed merely that the number of electrons scattered decreased rapidly with increase in angle of deflection—and it has been but recently that such diffraction phenomena have been observed. Mark and Wierl[5] first obtained diffraction rings by using high speed electrons in complex molecular gases, and others[6-10] have subsequently observed similar effects with lower velocities in various gases. As for the second hope, wave mechanics has probably lent itself more satisfactorily to the calculation of collision problems than any previous theory. A general summary of the methods used in the application of wave mechnaics has been given by Condon.[11] Mott,[12] using Born's approximation method, has succeeded in calculating the angular distribution of electrons scattered elastically by the atoms of a gas. He has neglected such factors as polarization of the atom due to the incident electron, possibility of exchange between the incident electron and an orbital electron, and distortion of the incident electron wave due to the atomic field. Supposedly these factors would be of small importance for high velocity electrons, and indeed Mott found fair agreement with the results of Dymond and Watson for 210-volt electrons in helium. Other observers[6,7,9] have also found fair agreement with experiment in the region of small angle scattering of moderately fast electrons in a few other gases. Attempts to incorporate the neglected factors into theory have resulted in further, qualitative at least, agreement with experiment.[6,7,13,14] However, it seems that the factor to be taken into consideration in a particular case, depends on which one gives the best agreement with experiment. There remains much to be done along this line.

The experimental work on angular scattering has also been often open to criticism. In general the scattering region has not been as free from stray

[1] E. G. Dymond and E. E. Watson, Proc. Roy. Soc. **A122,** 571 (1929). Dymond had earlier reported maxima and minima in scattering curves but he later found these effects were spurious.

[2] G. P. Harnwell, Phys. Rev. **33,** 559 (1929); **34,** 661 (1929).

[3] F. L. Arnot, Proc. Roy. Soc. **A125,** 660 (1929).

[4] J. H. McMillen, Phys. Rev. **36,** 1034 (1930).

[5] H. Mark and R. Wierl, Naturwiss. **18,** 205 (1930).

[6] F. L. Arnot, Proc. Roy. Soc. **A130,** 655 (1931); **A133,** 615 (1931).

[7] E. C. Bullard and H. S. W. Massey, Proc. Roy. Soc. **A130,** 579 (1931); **A133,** 637(1931).

[8] J. M. Pearson and W. N. Arnquist, Phys. Rev. **37,** 970 (1931).

[9] A. L. Hughes and J. H. McMillen, Phys. Rev. **39,** 585 (1932).

[10] C. Ramsauer and R. Kollath, Phys. Zeits. **32,** 867 (1931).

[11] E. U. Condon, Rev. Mod. Phys. **3,** 43 (1931).

[12] N. F. Mott, Proc. Camb. Phil. Soc. **25,** 304 (1928).

[13] H. Faxen and J. Holtzmark, Zeits. f. Physik **45,** 307 (1927), take into account the distortion of the incident electron wave due to the atomic field. Using this method Holtzmark, Zeits. f. Physik **55,** 437 (1929); **66,** 49 (1930), has calculated the total cross-sectional area of argon and krypton for slow electrons and has obtained good agreement with the Ramsauer-Townsend effect.

[14] H. S. W. Massey and C. B. O. Mohr, Proc. Roy. Soc. **A132,** 605 (1931) by further refine ments have calculated the probabilities of a number of collision problems.

electric fields and secondary electrons as it should have been; also the means of collecting the scattered electrons has not always been satisfactory. It was partially for these reasons that the present research was undertaken. The immediate cause was the disagreement between the results of Arnot[3] for the scattering of 82-volt electrons in mercury vapor and those of one of us.[15] Indirect evidence bearing on the angular distribution of scattered electrons indicated that the scattering curves should not be so steep as those obtained by Arnot.

Apparatus

The apparatus used for this work is sketched in Fig. 1a. It was constructed entirely of copper. The electron gun, G, was mounted in such a way that it could be rotated about axis $a-a$, and electrons scattered by gas molecules through a definite angle, θ(Fig. 1 (b)), were collected in the Faraday cage, FC. The electron gun was made sufficiently long and the defining slits of

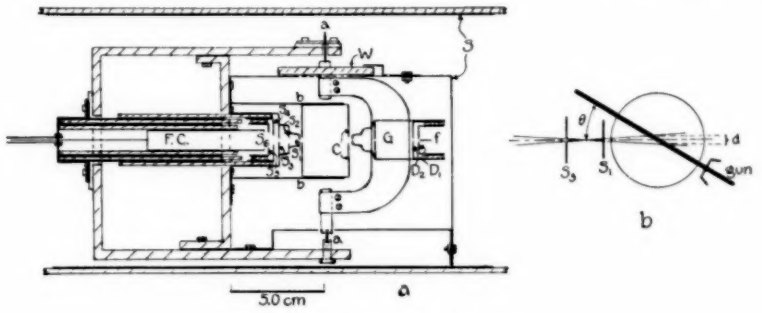

Fig. 1. Diagram of apparatus.

such a size (about 0.7 mm in diameter) that the electron beam was of small cross-section in the scattering region. The filament was mounted on a small cylinder which could be clamped in position behind the first diaphragm, D_1. A difference of potential between diaphragms D_1 and D_2 defined the velocity of the electrons. Flexible filament leads were brought out through the shield near the lower pivot. Two coaxial cylinders, C, separated by about 3 mm, were mounted as indicated, and the electron beam passed between them, being absorbed by the outer cylindrical shield and end-plates, S. These cylinders served the double purpose of shielding the scattering region from both stray electric fields and secondary electrons. The slits S_1, S_2, and S_3, spaced 5.0 mm apart, were about 0.35 mm in width and 1.4, 10, and 3.0 mm in height, respectively. S_4, S_5 and S_6 increased in size to 6.2×10.5 mm for S_6, and were spaced about 3.0 mm apart. The length of the beam from which scattered electrons could be collected is $d/\sin\theta$ (where $d=1.3$ mm) as defined by slits S_1 and S_3. As these slits are at the same potential this length is independent of the velocity of the electrons. Different potentials could be

[15] R. R. Palmer, Phys. Rev. **37**, 70 (1931) measured the absorption coefficient (cross-section for interception) of electrons with a Mayer type of apparatus, with a diaphragm of variable aperture mounted at the end of the scattering chamber.

applied to the diaphragms S_4, S_5 and S_6, for the purpose of analyzing the velocities of the scattered electrons. To insure its being a good collector of electrons the Faraday cage was over 6.0 cm in length. The metal parts for the gun and collector were spun cylinders and were all separated with Pyrex tubing excepting for the quartz tubing used as insulation between the Faraday cage and its shield. The ends of the gun and collector were tapered, the slits were bevelled, and important surfaces were sooted to reduce further errors due to secondary electrons. The gun could be rotated by means of the grooved wheel, W. A cable of fine copper wires making one turn about this wheel was connected to a long rod mounted to slide on the main frame of the apparatus. This rod extended into a side tube and could be moved by means of a special magnetic device so constructed that all magnetic material could be removed at each reading. The angular setting could be read from a scale on the wheel, W.

The apparatus was housed in a large Pyrex tube one end of which was closed by means of a copper plate sealed to the tube with low vapor pressure wax. The tube was long enough that it was possible to heat the apparatus up to about 300°C without softening the wax. The metal parts had previously been outgassed in a quartz furnace at about 600°C. Vacuum conditions were such that a pressure of less than 10^{-5} mm would build up in the system in 24 hours. A pair of Helmholtz coils was used to neutralize the earth's magnetic field.

Tests on the Apparatus

An electrometer was used to measure the current to the Faraday cage and a galvanometer connected to the outer cylinder measured the main beam current. For a particular angular setting, electron velocity and gas pressure, it is of course necessary that the ratio of these two should remain constant as one varies the filament emission. This was found to be the case, but not until the Pyrex tubing which was first used as insulation between the Faraday cage and its shield was finally replaced by a quartz tube. The intensity of the electron beam was varied by as much as a factor of 60, and no sensible change in this ratio was observed. This, of course, signifies that the electrometer system is well insulated and well shielded. It also indicates that neither the filament current nor the electron beam influence appreciably the electron scattering.[16]

[16] F. L. Arnot, Proc. Roy. Soc. **A129,** 361 (1930), has studied the effect of the passage of an electron beam through an otherwise field-free enclosure. He used beam currents of from 5 to 25 microamperes intensity passing through mercury vapor at a pressure of about 0.001 mm, and observed that a difference of potential of as much as 2.0 volts was set up between the interior of the beam and the outer electrodes. This is due to the relative slowness with which the positive ions diffuse out of the beam in comparison with the scattered electrons. Since the work we are reporting has been done with lower beam currents (in all cases less than 0.3 microampere) and since the electron velocities (excepting for those electrons scattered with loss in energy) were greater than 80 volts, it would seem unnecessary to take this into account. Indeed the linear relationship observed between the beam current and the scattered current indicates that this is the case.

In Fig. 2a are plotted three typical velocity distribution curves for the scattered electrons. The scattered current to the Faraday cage is plotted as a function of the retarding potential between slits S_4 and S_5. Curve A is for 80-volt incident electrons at an angular setting of 7°; curves B and C are for 120-volt electrons at angular settings of 10° and 43° respectively. Since the difference between the ordinates for two values of the retarding potential, V_1 and V_2, is a measure of the number of electrons with energies between V_1 and V_2, one can obtain from such curves the number of electrons scattered in any particular energy range. For instance, for curve A the value of the

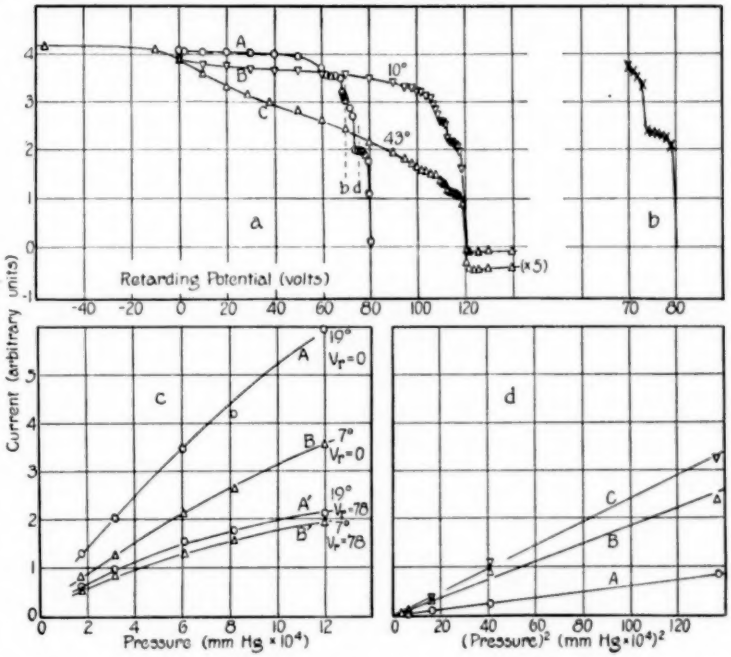

Fig. 2*a*, Typical velocity distribution curves. Curve A, 80-volt electrons ($\theta = 7°$). Curves B and C, 120-volt electrons. *b*. To show penetration of fields through slits. *c*, Scattered current as a function of gas pressure. *d*, Positive ion current as a function of the square of the pressure. (80-volt electrons, 86 volts retarding potential).

ordinate at d indicates the number of electrons scattered with their original velocity (elastically scattered electrons). The difference between this and the value of the ordinate at b (for a retarding potential of 80 − 10.4 volts— the velocity of the incident electrons less the ionization potential of mercury) represents the number of electrons which have excited the mercury atom to various energy levels. The abrupt rise at about 73 volts indicates that most of these electrons have excited the 6.7 volt energy level. The difference between the value of the ordinate at b and that for zero retarding potential is a measure of those electrons which have resulted from collisions in which the energy loss is greater than the ionization potential. Such collisions may result in direct ionization with the removal of one or more electrons from the atom or in the excitation of the atom to an energy state greater than the ionization

potential. In the latter case the atom may return to the normal state either by radiation alone or by radiation accompanied by the emission of one or more electrons. The curves for 120-volt electrons show these same features. It is to be noted that relatively more of the electrons scattered through large angles are slow electrons than is the case for small angles. Most curves show a more or less flat section in the region from 12 to 18 volts less than the incident electron velocity—this shows up distinctly in curve A. This must mean that when an electron loses more than the ionizing energy to a mercury atom the process is such that it is not likely to lose from 2 to 8 volts in addition to the energy of ionization. This point has not been studied systematically, but it has been observed in most velocity distribution curves which have been taken. It may be linked with the so-called "ultra-ionization" potentials which have been observed in mercury.

When the retarding potential is greater than that necessary to stop all of the scattered electrons a negative current is obtained. This is shown for curve C. When the potential is further increased this current goes through a maximum and then slowly decreases. This effect might be due to secondary electrons emitted from the Faraday cage or to positive ions entering the Faraday cage. However, neither of these would be expected to show the maximum and decline with increase in retarding potential, unless, in the case of its being a positive ion current, the positive ions were formed in the neighborhood of slits S_4 and S_5 by the scattered electrons themselves. If this were true this current would be proportional to the square of the gas pressure. Fig. 1d shows this to be the case.[17] Curves A, B, and C are for a retarding potential of 86 volts (80-volts incident electrons) between slits S_3 and S_4, S_4 and S_5, S_5 and S_6, respectively. It is evident from this linearity that the positive ions from the main scattering region are not appreciably represented in the scattered current, though this might not be true for intense beam currents at angles near 90°.

When an accelerating potential is applied at the collector there is in general a small increase in the electron current. This is due to a retarding effect on the positive ions just mentioned, and perhaps also to a certain amount of penetration of the field into the scattering chamber to bring in low velocity electrons which would otherwise miss the collector. An accelerating field of 100 volts does not in general increase the measured current by more than a few percent. This effect has been reduced by the insertion of slit S_2.

If, instead of applying the field between slits S_4 and S_5, it is applied between S_5 and S_6, the same curves, within a few percent, as those in Fig. 1a are obtained. This is also true if the difference of potential is applied between S_3 and S_4, excepting in the case of high velocity electrons (say, 700 volts) when large fields cause a greater discrepancy due to penetration into the main scattering region.

[17] S. Werner, Proc. Roy. Soc. **A134,** 220 (1931), in studying the scattering at 90° in helium, also observed this negative current and found it proportional to the square of the pressure, but he attributed it as due to ionization near the collector slits by "long wave radiation" from the scattering region.

Likewise the same curves are duplicated by a constant factor, within a few percent, when the gas pressure is changed. This relation between the scattered current and pressure for 80-volt electrons is shown in Fig. 2c, for two angular settings and two retarding potentials. It is noted that these curves bend over slightly, as a result of the interception of the scattered electrons by gas molecules, and of the fact that the galvanometer current is a measure of the total electron current from the gun and not a measure of the

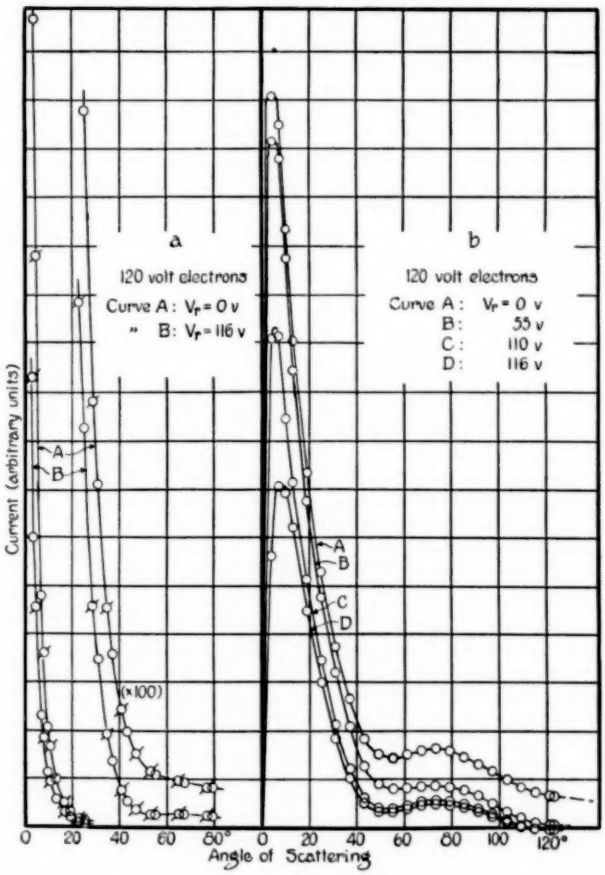

Fig. 3*a*, Current collected as a function of angular setting. To show symmetry of scattering (circles, scattering on one side of beam; circles with lines through them, scattering on the other side). *b*, Scattered current per unit angle (between θ and $\theta+d\theta$) as a function of angle.

beam current at the point of scattering. The curves taken with a retarding potential deviate more from a straight line than do the others which is probably due to the positive ion current discussed above.

The Faraday cage was made long to insure its being a good collector of electrons. It was at first thought that an accelerating field between S_5 and S_6 would increase its efficiency by retarding any slow secondary electrons which attempted to escape. But this was found to be unnecessary, and indeed quite inadvisable. In Fig. 2b is drawn the end of a velocity distribution curve for

80-volt incident electrons, with the retarding potential applied between slits S_4 and S_5. With this potential fixed at 80 volts, an accelerating potential was applied in one-volt steps between S_5 and S_6, giving the crosses from right to left. It is noticed that they practically retrace the first curve. Evidently there is a distinct penetration of this field into the region between S_4 and S_5. A similar result was obtained when the retarding potential was applied between S_3 and S_4 and the accelerating potential between S_5 and S_6, though in this case the new curve fell slightly below the original one. It is obvious that it is inadvisable to use this method to increase the efficiency of a collector.[18]

The symmetry of scattering to the right and left of the electron beam is shown for 120-volt electrons in Fig. 3a. The number of electrons collected by the Faraday cage is plotted as a function of the angular position of the electron gun. Curve A is for no retarding potential and curve B for a retarding potential of 117 volts. The circles are the experimental points for scattering say to the left of the beam and the circles with the lines through them to the right of the beam. It is seen that the criterion of symmetry is met very nicely.

As the ionization potential of mercury is 10.4 volts, when a 120-volt electron directly ionizes a mercury atom there remains about 110 electron-volts of energy to be divided between the incident and the ejected electrons. For every electron going off with an energy less than 110/2 volts there must be an electron with an energy between this value and 110 volts. Hence the total number of electrons scattered with energies between 0 and 55 volts should equal the number with energies between 55 and 110 volts. (This would be strictly true only if there were no multiple ionization and no inelastic impacts with energy loss greater than 10.4 volts which do not result in ionization in which case it would be impossible to say anything about the division of energy. Bleakney[19] has studied the formation of multiply charged ions in mercury vapor, and has found that approximately 15 percent of the ions formed by 120-volt electrons are double charged.) In Fig. 3b are given curves for the number of electrons scattered with different energies in a cone between θ and $\theta+d\theta$ from a definite length of the beam for 120-volt incident electrons. To obtain these curves the experimental curves are multiplied twice by $\sin\theta$, first to correct for the variation in the effective length of the beam with angular setting (Fig. 1) and second to change from scattering in units of "electrons scattered per unit solid angle" to "electrons scattered per unit angle." The area under curve A is a measure of the total number of

[18] Arnot, reference 6, in studying the angular distribution of elastically scattered electrons, has applied such additional accelerating potentials "to prevent any secondary emission of electrons from the Faraday cylinder." His collector was short and secondary emission might otherwise have been large. He has used from 12 to 21 volts, and as his slit system was similar in dimensions to ours it would seem that his measurements are subject to this error. When, for 80-volt electrons, a retarding potential of 77 volts is used to eliminate all but those electrons which are scattered elastically, and then a subsequent 12 volts accelerating potential is applied, the increased current is not due alone to increased collector efficiency but also to the addition of a number of *inelastically* scattered electrons which can now pass through the slit system.

[19] W. Bleakney, Phys. Rev. **35**, 139 (1930).

electrons scattered and the areas under curves B, C and D, the number of electrons scattered with energies in excess of 55, 110 and 116 volts, respectively. By numerical integration it is found that the number of electrons with energies between 0 and 55 volts is to the number with energies between 55 and 110 volts as 1.0 is to 1.1. Perhaps not quite all of the low velocity electrons are collected, probably because the readings could not be carried beyond 123°. The extrapolation to 0° is quite definite, as a bending over of the curves is discernible for small angles of deflection. On the whole, these tests indicate that the apparatus is quite satisfactory.

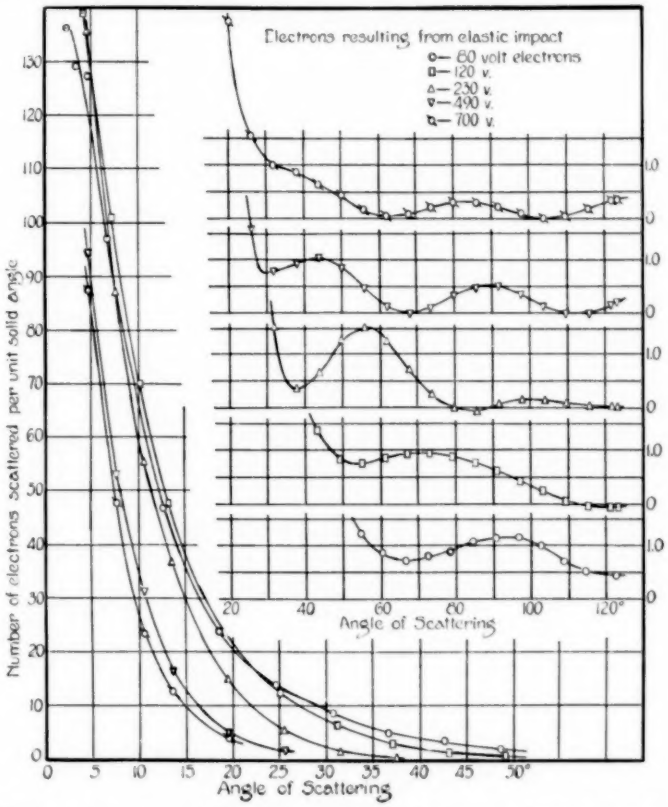

Fig. 4. Number of electrons elastically scattered (per primary electron, per unit solid angle, per cm path, per mm pressure at 0°C) as a function of angle.

The results to be presented are for the scattering of 80, 120, 230, 490 and 700-volt electrons in mercury vapor at a pressure of 1.17×10^{-3} mm. With the mercury frozen out with liquid air the scattered current at all angles was less than 2 percent of that at this pressure. This was the case up to within about 3° of the direction of the electron beam. In analyzing the velocities of the scattered electrons retarding potentials were applied between slits S_4 and S_5.

Elastic Scattering

The curves in Fig. 4 show the angular distribution of electrons scattered

elastically for the five velocities indicated. The ordinates are given in units of the number of electrons scattered per primary electron, per unit solid angle, per cm path, per mm pressure at 0°C. The method of converting scattering as experimentally measured in arbitrary units into the units given will be discussed later. The number of electrons scattered is seen to decrease very rapidly in the region of small-angle scattering with increase in the angle of deflection. This steepness of the curves is in general greater the higher the velocity of the incident electrons. Similar curves have been obtained by Arnot[6] for scattering in mercury vapor.

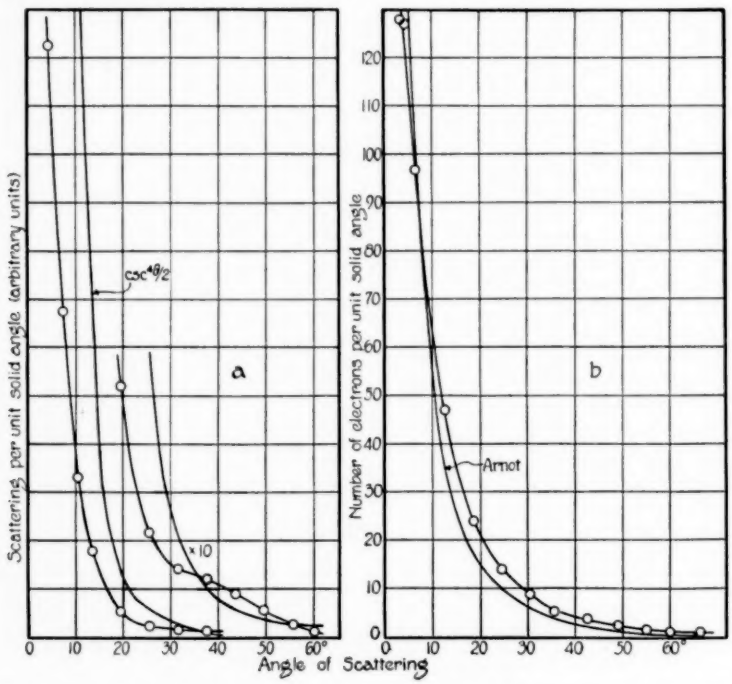

Fig. 5*a*, Comparison of elastic scattering of 700-volt electrons with cosec⁴ $\theta/2$ (Mott's theory). *b*, Comparison of elastic scattering of 80-volt electrons with Arnot's results for 82-volt electrons.

When the elastic scattering is studied at large angles a series of peaks is observed in the scattering curves. These are plotted to a different scale in the inset to Fig. 4. (It will be noted that some of the curves fall below the zero-axis at certain angles. This is due to the fact that no correction was made for the secondary positive ion current previously mentioned. Excepting for the scattering at large angles in the neighborhood of the minima this correction would have been inappreciable.) A single peak is observed in the 80-volt curve at about 95°. As the velocity increases this is seen to move in to smaller angles, finally merging with the main peak, and new maxima appear. There is also an indication of a "merged maximum" in the 80-volt curve at about 28°, which would show up as another order of diffraction for lower electron velocities. The angles at which these peaks occur agree well

with those obtained by Arnot.[6] There is no satisfactory theory of this effect, though in view of the many current experiments which confer the property of a wave upon a moving electron such diffraction phenomena are not entirely surprising. Bullard and Massey[7] have succeeded in a rough way in duplicating diffraction peaks for a limited range of velocities in argon, following a method due to Faxen and Holtzmark.[13] Arnot[6] has similarly fitted this theory to the scattering of 54-volt electrons in krypton, reproducing the 70° peak.

Mott[12] gives for the number of electrons elastically scattered per primary electron, per cm path, per unit solid angle, per atom in a unit volume, as a

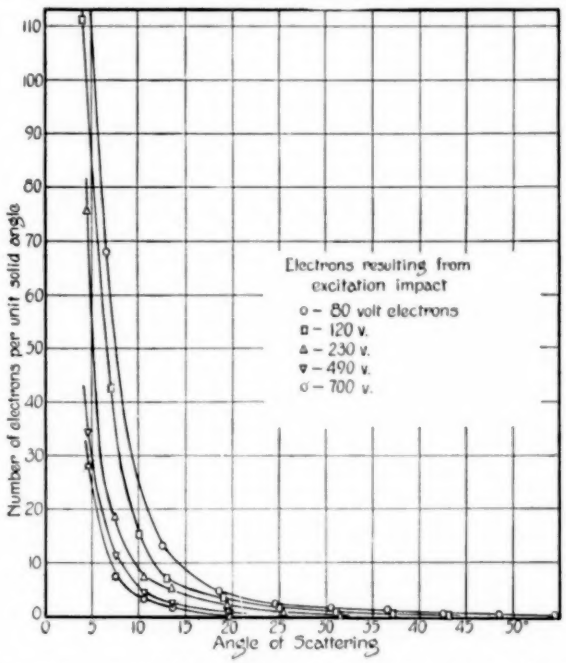
Number of electrons per unit solid angle
Angle of Scattering
Electrons resulting from excitation impact
o – 80 volt electrons
□ – 120 v.
Δ – 230 v.
▽ – 490 v.
○ – 700 v.

Fig. 6. Number of electrons scattered inelastically at excitation impact (per primary electron, per unit solid angle, per cm path, per mm pressure at 0°C) as a function of angle.

function of the angle of deflection, θ, and the velocity of the incident electron, v,

$$I(\theta, v) = \left(\frac{e^2}{2mv^2}[N - F]\,\mathrm{cosec}^2\frac{\theta}{2}\right)^2,$$

where N is the atomic number and F the atomic structure factor. The equation is supposedly good for high velocity electrons. For a particular gas and electron velocity the scattering should then be proportional to $\mathrm{cosec}^4\,\theta/2$. In Fig. 5a the experimental results for 700-volts electrons are compared with a curve of $\mathrm{cosec}^4\,\theta/2$, both in arbitrary units. It is seen that the theoretical curve is much steeper than the experimental curve out to 40°. Evidently Mott's theory is not applicable to the elastic scattering of electrons in mercury vapor for electrons with even as much as 700 volts velocity.

In Fig. 5b our curve for the elastic scattering of 80-volt electrons is compared with that of Arnot (for 82-volt electrons). The units are again the number of electrons scattered per primary electron, per unit solid angle, per cm path, per mm pressure at 0°C. It is to be noted that Arnot's curve is much steeper than ours. Due to the system of potentials used in his collector is is believed that Arnot collected not only electrons scattered elastically but also a large number of inelastically scattered electrons.[18] As electrons scattered inelastically exhibit a more decided preference for small angle scattering than do electrons scattered elastically (as will be seen in the next section), curves including them would of course be steeper.[20]

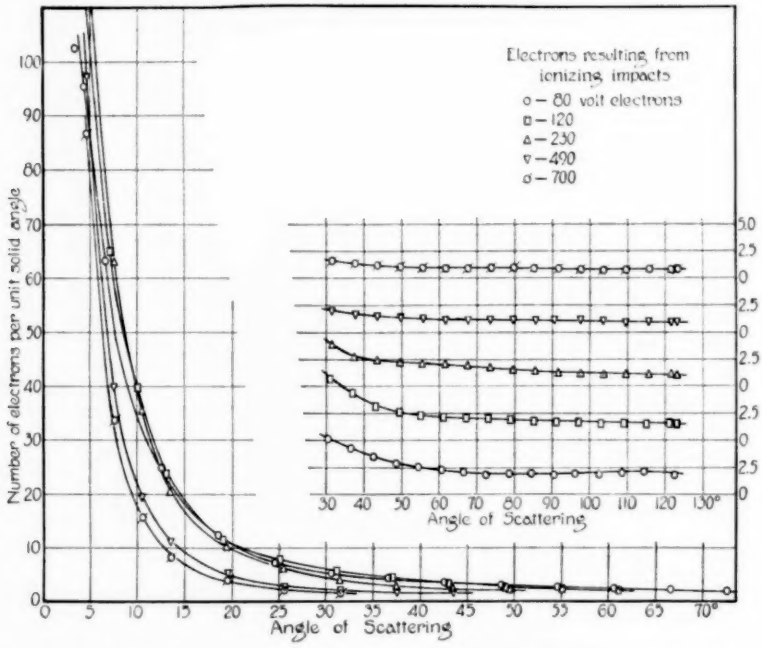

Fig. 7. Number of electrons scattered inelastically at ionizing impact (per primary electron, per unit solid angle, per cm path, per mm pressure at 0°C) as a function of angle.

Inelastic Scattering

In Fig. 6 are plotted the curves for the number of electrons scattered inelastically from a collision in which the mercury atom is excited. The ordinate is again in the conventional units given above. As was seen from the velocity distribution curves of Fig. 2, the energy loss suffered by electrons in this group was mainly 6.7 volts. Here it is again seen that forward scat-

[20] Though the curves are given in the same units the difference between the numerical magnitudes has no significance since it is difficult to transcribe the experimentally measured quantities into the conventional units. In particular, the effective length of the electron beam from which scattered electrons are collected and the effective solid angle for collection are difficult to ascertain,—in Arnot's case fields applied between the diaphragms which define these quantities enhance this difficulty. Arnot believes that he has "an estimate of the absolute scattering which is probably correct to within 50 percent."

tering is highly favored. The curves are much steeper in fact than are those for the elastically scattered electrons. In general they are also steeper the higher the velocity of the impinging electrons. These curves decrease to very small values of the ordinate for large angles, and do not show any pattern within the experimental error of the measurements.

Curves for the angular distribution of electrons scattered inelastically after impacts which have resulted in energy losses greater than the ionizing potential are also steeper than are those for elastic scattering but not so steep as those for the excitation group. Such curves are presented, in the usual units, in Fig. 7. These curves include all electrons scattered with en-

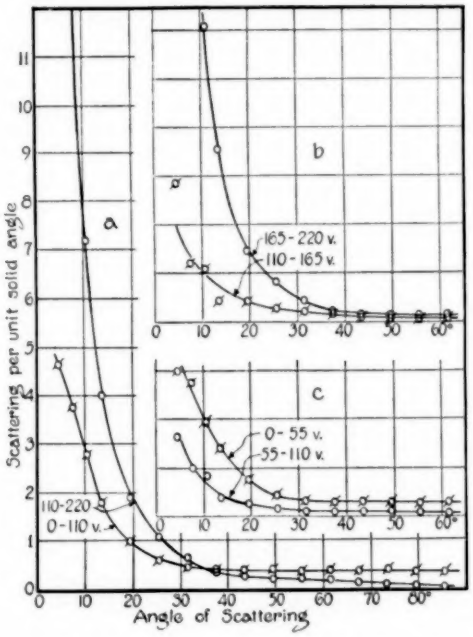

Fig. 8. Angular distribution of colliding and ejected electrons resulting from a 230-volt collision. (Energy range of scattered electrons is indicated.)

ergies between 0 and $(V_a - 10.4)$ volts, where V_a is the velocity of the incident electrons. They include both the scattered incident electrons and the ejected electrons. In general here again we have an increase in steepness with increase in velocity of the incident electrons. For large angles of scattering this group is relatively more prominent than either of the other two groups. In the inset these curves, plotted to a different scale, are carried to an angle of 123°. It is interesting to note the wide range at large angles over which the scattering is nearly constant.

After a 230-volt electron ionizes a mercury atom there remains approximately 220-electron volts of energy to be divided between the colliding and the ejected electrons. Following the procedure of Hughes and McMillen[9] we will label the slower of these two electrons the ejected electron, and the faster, the colliding electron. This is done as a matter of convenience, inasmuch as

there is supposedly no physical difference between any two electrons. In Fig. 8 we have divided the electrons resulting from a 230-volt ionizing collision into groups according to their energies. It is seen from *a* that the colliding electrons are greatly in excess of the ejected electrons at small angles, and that the reverse is the case at large angles. The two groups show decidedly different types of angular distributions. A numerical integration of these curves gives for the ratio between the number of ejected electrons and the number of colliding electrons: 1.0 to 1.1. In the insets of Fig. 8 these groups

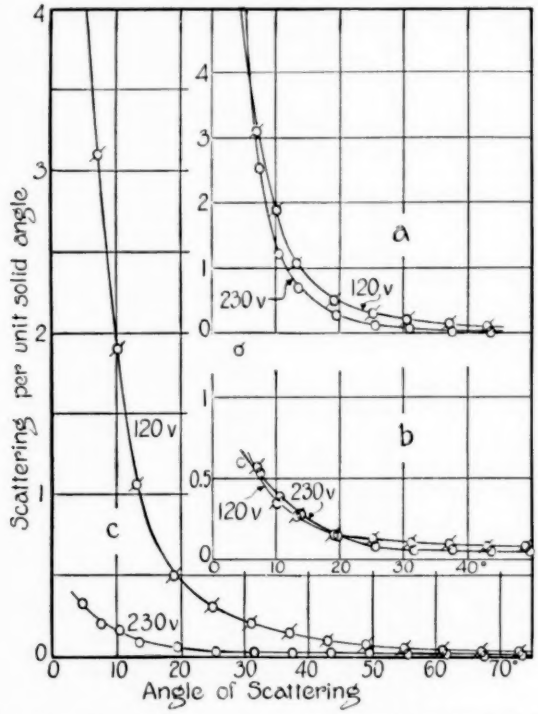

Fig. 9. Angular distribution of groups of electrons resulting from 120- and 230-volt collisions. *a*, Electrons which have lost from 0 to 55 volts in addition to the ionization potential. *b*, Electrons which emerge with from 0 to 55 volts velocity. *c*, Electrons which emerge from 55 to 110 volts velocity.

are further subdivided. It is to be noted that both groups of the faster electrons, *b*, have similar angular distributions, and that both groups of the slower electrons, *c*, also have similar distributions. Further, of the two subgroups in *b*, the faster group is much in excess of the other at all angles; of the subgroups in *c*, the slower is in excess at all angles. This indicates that the division of energy remaining after ionization takes place in such a way that one of the electrons emerges with most of the energy, and the other one with very little. There is thus not much probability that the energy will be shared approximately equally.

In Fig. 9a are plotted the angular distributions for electrons which have lost up to 55 volts in addition to the energy necessary to ionize the

mercury atom. Thus, for a particular range of energy loss, the higher the velocity of the incident electron the steeper the angular distribution curve, as was also observed by Hughes and McMillen[9] for a narrow range of energy loss.

It is interesting to examine the angular distribution curves for electrons emerging with a particular velocity as a function of the velocity of the incident electron. In Fig. 9b are curves for electrons scattered with energies from 0 to 55 volts. Evidently it is of little consequence to electrons in this range of energies as to whether they result from 120 or 230-volt impacts. On the other hand, for the same two incident velocities, when we consider the angular distributions for electrons emerging with velocities between 55 and 110 volts, the effect of the velocity of the incident electron is quite apparent,—the

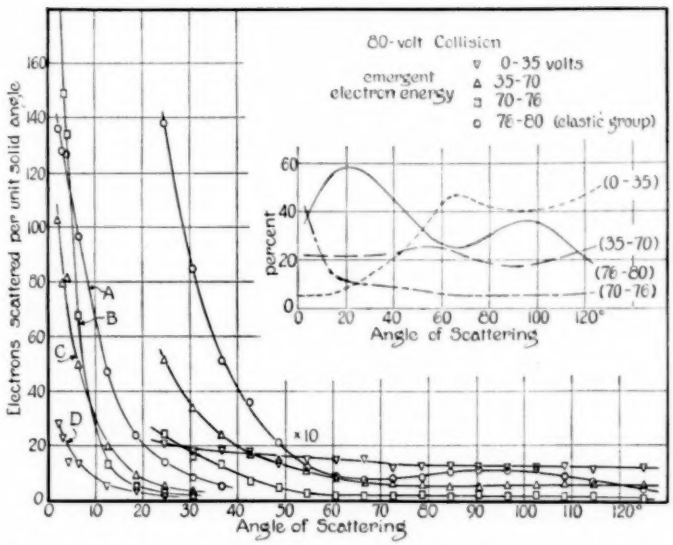

Fig. 10. Angular distribution of various groups of electrons resulting from an 80-volt collision in units of number of electrons per primary electron, per unit solid angle, per cm path, per mm pressure at 0°C. Inset: percent of total scattering due to these various groups.

curves of Fig. 9c are decidedly different. We note that these electrons (emerging with from 55 to 110 volts velocity) are what we have chosen to call colliding electrons for 120-volt collisions, and ejected electrons for 230-volt collisions, whereas the electrons of *b* (emerging with from 0 to 55 volts velocity) are in both cases ejected electrons. These results, and those of Fig. 8, indicate that when we are dealing with scattered electrons which are ejected electrons we get a different type of angular distribution than when these electrons are the colliding electrons. Such results tempt one to go farther than merely to label these two groups as colliding and ejected electrons—one is tempted actually to identify them as such.

For purposes of comparison, the angular distribution curves for the four groups of electrons resulting from 80-volt collisions are plotted in Fig. 10. These curves are given in the conventional system of units. In the region of

small angle scattering it is seen that the electrons scattered at excitation impacts exhibit the most decided tendency to persist in the forward direction. In general, for the three inelastic groups, the smaller the energy loss the steeper the distribution curve. These curves are extended out to 123°, drawn to a larger scale, as is indicated. It is to be noted that at large angles the slower group of electrons, the ejected electrons, predominate, whereas there are very few which have resulted from excitation impacts. These relations between the four groups are further exhibited in the inset of Fig. 10. Here the percentage of the total scattering at a particular angle which is due to a particular group is plotted as a function of the angle.

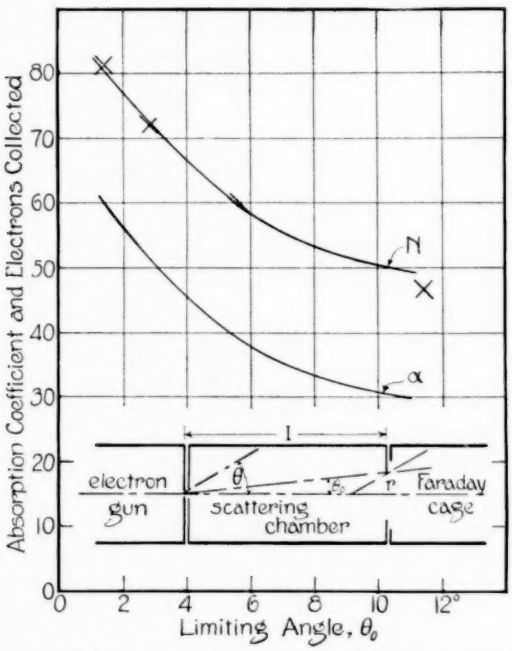

Fig. 11. Absorption coefficient, α, as a function of limiting angle of collection, θ_0, for 80-volt electrons, using apparatus of inset. (Results of Palmer, reference 15.) Total number of electrons collected N, as a function of θ_0.

Absolute Scattering

The scattering curves have been presented in units of the number of electrons scattered per primary electron, per unit solid angle, per cm path, per mm pressure at 0°C. The current ratios measured experimentally were of course in arbitrary units, and to obtain the absolute scattering the following method was used.

In Fig. 11 are presented some of the results of a series of measurements by one of us[15] on the effect of resolving power on measurements of the absorption coefficient α, of electrons in gases. The radius r, of the exit-diaphragm of a scattering chamber in a conventional Mayer type of apparatus (see inset to Fig. 11) could be changed, giving a limiting angle θ_0, below which if electrons were deflected by gas molecules they would not be counted

as having collided. The value of α thus determined for 80-volt electrons is plotted as a function of θ_0. By taking into consideration the ions formed which drift to the walls of the scattering chamber (and neutralize the effect of a certain number of electrons) it is possible to calculate the total number of electrons actually collected. This gives the curve N,[21] in units of number of electrons scattered per primary electron, per cm length of scattering chamber, per mm pressure at 0°C. This may be obtained for any value of r by a numerical integration of the experimentally determined angular scattering curve for the total scattering of 80-volt electrons, $K \cdot F(\theta)$. The number of electrons collected by the scattering chamber in the above units will then be

$$N = \int_{\theta_0}^{\pi} (1 - r/l \tan \theta) \cdot 2\pi \sin \theta \cdot K \cdot F(\theta) \cdot d\theta$$

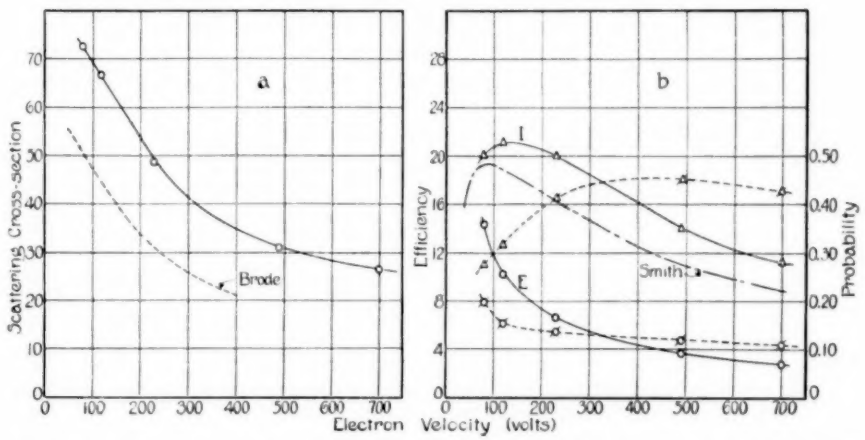

Fig. 12. *a*, Scattering cross-section (absorption coefficient) as a function of primary electron velocity, in cm^2/cm^3 per mm pressure at 0°C, obtained by numerical integration. *b*, Efficiency of ionization I, in number of units of positive charge formed per primary electron, per cm path, per mm pressure at 0°C, obtained by numerical integration. Efficiency of excitation, E, in number of molecules excited per primary electron, per cm path, per mm pressure at 0°C, obtained by numerical integration.

where θ_0 is $\tan^{-1} r/l$. Such a numerical integration was performed for four different diaphragm openings, and with an appropriate constant, K, the four crosses in Fig. 11 were obtained. This constant was then applied to the experimentally measured ratio to give the angular scattering curves in the conventional units. It should be emphasized that the good agreement between the crosses and the curve of Fig. 11 serves as an additional check on the validity of the angular scattering curves.

Cross-section for Interception, Excitation, and Ionization

By a numerical integration of our angular distribution curves it is possible to obtain curves for the cross-section area for the interception of electrons,

[21] We have used the efficiency of ionization data of P. T. Smith, Phys. Rev. **37**, 808 (1931) in this calculation, partially for reasons of internal consistency. The original curve for N was obtained from the data of Bleakney.[19]

and for the efficiencies of excitation, and ionization by electron impact. From Bleakney's work[19] one can calculate the fraction of the electrons resulting from ionizing impacts which are ejected electrons. This fraction of the number of electrons obtained by a numerical integration of the curves of Fig. 7 represents the number of ejected electrons and is hence a measure of the efficiency of ionization. This assumes that all impacts which result in energy losses greater than the ionization potential actually ionize the atom. An integration of the curves of Fig. 6 gives the number of electrons scattered due to excitation collisions. An integration of the curves for the total scattering less the ejected electrons gives the number of primary electrons scattered, or, which is numerically the same, the cross-sectional area for interception. This latter is plotted in Fig. 12a for the five electron velocities studied. The units are cm^2/cm^3 blocked off by gas molecules per mm pressure at 0°C, or the number of collisions per electron, per cm path, per mm pressure at 0°C. The curve obtained by Brode[22] with a Ramsauer type of apparatus is also presented. His values are lower than ours because his absorption coefficient is defined by an apparatus with finite slits such that electrons which are deflected through a small angle are not counted as having collided. It should be noted that our value for 80-volt electrons agrees quite well with the value of α which would be obtained from Fig. 11 by an extrapolation back to $\theta_0 = 0°$.

The curve I of Fig. 12b gives the efficiency of ionization in terms of the number of units of positive charge formed per electron, per cm path, per mm pressure at 0°C, obtained as outlined above. The curve obtained by Smith[21] in a straight-forward manner is presented for comparison. Probably the agreement is as good as could be expected because of the uncertainty in the extrapolation to 180°—there is an appreciable number of slow electrons scattered at large angles. The curve E represents the number of excited molecules formed per primary electron, per cm path, per mm pressure at 0°C, also obtained as outlined above.

From these curves and the absorption coefficient curve one can calculate the actual probability that a collision will result in an excited atom or a unit of positive charge. These probabilities are given by the two dashed curves. As the energy loss due to excitation is mainly 6.7 volts, it is interesting that the probability should be so high. Brattain[23] has measured the probability of excitation of the 6.67-volt energy level in the mercury atom for electron velocities in the neighborhood of this value. He finds that the probability reaches a maximum and begins to fall at about 7.0 volts, having a peak value of about 0.06 (in the same units as we have used). Evidently the probability rises again for higher velocity electrons. The probability for ionization shows a maximum of about 0.45 at about 400 volts.

Further work is in progress which will enable a study of the scattering of lower velocity electrons, and larger angles of deflection.

[22] R. B. Brode, Proc. Roy. Soc. **A125,** 134 (1930).
[23] W. H. Brattain, Phys. Rev. **34,** 474 (1929).

On the Quantum Correction For Thermodynamic Equilibrium

By E. WIGNER
Department of Physics, Princeton University
(Received March 14, 1932)

The probability of a configuration is given in classical theory by the Boltzmann formula $\exp[-V/kT]$ where V is the potential energy of this configuration. For high temperatures this of course also holds in quantum theory. For lower temperatures, however, a correction term has to be introduced, which can be developed into a power series of h. The formula is developed for this correction by means of a probability function and the result discussed.

1

IN classical statistical mechanics the relative probability for the range p_1 to p_1+dp_1; p_2 to p_2+dp_2; $\cdots$; p_n to p_n+dp_n for the momenta and x_1 to x_1+dx_1; x_2 to x_2+dx_2; $\cdots$; x_n to x_n+dx_n for the coordinates is given for statistical equilibrium by the Gibbs-Boltzmann formula

$$P(x_1, \cdots, x_n; p_1, \cdots, p_n)dx_1 \cdots dx_n dp_1 \cdots dp_n = e^{-\beta\epsilon}dx_1 \cdots dx_n dp_1 \cdots dp_n \quad (1)$$

where ϵ is the sum of the kinetic and potential energy V

$$\epsilon = \frac{p_1^2}{2m_1} + \frac{p_2^2}{2m_2} + \cdots + \frac{p_n^2}{2m_n} + V(x_1 \cdots x_n) \quad (2)$$

and β is the reciprocal temperature T divided by the Boltzmann constant

$$\beta = 1/kT. \quad (3)$$

In quantum theory there does not exist any similar simple expression for the probability, because one cannot ask for the simultaneous probability for the coordinates and momenta. Moreover, it is not possible to derive a simple expression even for the relative probabilities of the coordinates alone—as is given in classical theory by $e^{-\beta V(x_1 \cdots x_n)}$. One sees this by considering that this expression would give at once the square of the wave function of the lowest state $|\psi_0(x_1 \cdots x_n)|^2$ when $\beta = \infty$ is inserted and on the other hand we know that it is not possible, in general, to derive a closed formula for the latter.

The thermodynamics of quantum mechanical systems is in principle, however, given by a formula of Neumann,[1] who has shown that the mean value of any physical quantity is, (apart from a normalizing constant depending only on temperature), the sum of the diagonal elements of the matrix

$$Qe^{-\beta H} \quad (4)$$

where Q is the matrix (operator) of the quantity under consideration and H is the Hamiltonian of the system. As the diagonal sum is an invariant under

[1] J. von Neumann, Gött. Nachr. p. 273, 1927.

transformations, one can choose any matrix or operator-representation for the Q and H. In building the exponential of H one must, of course, take into account the non-commutability of the different parts of H.

2

It does not seem to be easy to make explicit calculations with the form (4) of the mean value. One may resort therefore to the following method.

If a wave function $\psi(x_1 \cdots x_n)$ is given one may build the following expression[2]

$$P(x_1, \cdots, x_n; p_1, \cdots, p_n) = \left(\frac{1}{h\pi}\right)^n \int_{-\infty}^{\infty} \cdots \int dy_1 \cdots dy_n \psi(x_1 + y_1 \cdots x_n + y_n)^* \psi(x_1 - y_1 \cdots x_n - y_n) e^{2i(p_1 y_1 + \cdots + p_n y_n)/h} \quad (5)$$

and call it the probability-function of the simultaneous values of $x_1 \cdots x_n$ for the coordinates and $p_1 \cdots p_n$ for the momenta. In (5), as throughout this paper, h is the Planck constant divided by 2π and the integration with respect to the y has to be carried out from $-\infty$ to ∞. Expression (5) is real, but not everywhere positive. It has the property, that it gives, when integrated with respect to the p, the correct probabilities $|\psi(x_1 \cdots x_n)|^2$ for the different values of the coordinates and also it gives, when integrated with respect to the x, the correct quantum mechanical probabilities

$$\left| \int_{-\infty}^{\infty} \cdots \int \psi(x_1 \cdots x_n) e^{-i(p_1 x_1 + \cdots + p_n x_n)/h} dx_1 \cdots dx_n \right|^2$$

for the momenta $p_1, \cdots, p_n$. The first fact follows simply from the theorem about the Fourier integral and one gets the second by introducing $x_k + y_k = u_k$; $x_k - y_k = v_k$ into (5).

Hence it follows, furthermore, that one may get the correct expectation values of any function of the coordinates or the momenta for the state ψ by the normal probability calculation with (5). As expectation values are additive this even holds for a sum of a function of the coordinates and a function of the momenta as, e.g., the energy H. In formulas, it is

$$\int_{-\infty}^{\infty} \cdots \int \int_{-\infty}^{\infty} \cdots \int dx_1 \cdots dx_n dp_1 \cdots dp_n [f(p_1 \cdots p_n) + g(x_1 \cdots x_n)] P(x_1 \cdots x_n; p_1 \cdots p_n) = \int_{-\infty}^{\infty} \cdots \int \psi(x_1 \cdots x_n)^* \left[f\left(\frac{h}{i}\frac{\partial}{\partial x_1}, \cdots, \frac{h}{i}\frac{\partial}{\partial x_n}\right) + g(x_1 \cdots x_n) \right] \psi(x_1 \cdots x_n) dx_1 \cdots dx_n \quad (6)$$

for any ψ, f, g, if P is given by (5).

[2] This expression was found by L. Szilard and the present author some years ago for another purpose.

Of course $P(x_1, \cdots, x_n; p_1, \cdots, p_n)$ cannot be really interpreted as the simultaneous probability for coordinates and momenta, as is clear from the fact, that it may take negative values. But of course this must not hinder the use of it in calculations as an auxiliary function which obeys many relations we would expect from such a probability. It should be noted, furthermore, that (5) is not the only bilinear expression in ψ, which satisfies (6). There must be a great freedom in the expression (5), as it makes from a function ψ of n variables one with $2n$ variables. It may be shown, however, that there does not exist any expression $P(x_1 \cdots x_n; p_1 \cdots p_n)$ which is bilinear in ψ, satisfies (6) and is everywhere (for all values of $x_1, \cdots, x_n, p_1, \cdots, p_n$) positive, so (5) was chosen from all possible expressions, because it seems to be the simplest.

If $\psi(x_1, \cdots, x_n)$ changes according to the second Schrödinger equation

$$ih\frac{\partial\psi}{\partial t} = -\sum_{k=1}^{n}\frac{h^2}{2m_k}\frac{\partial^2\psi}{\partial x_k^2} + V(x_1, \cdots, x_n)\psi \tag{7}$$

the change of $P(x_1, \cdots, x_n; p_1, \cdots, p_n)$ is given by

$$\frac{\partial P}{\partial t} = -\sum_{k=1}^{n}\frac{p_k}{m_k}\frac{\partial P}{\partial x_k} + \sum\frac{\partial^{\lambda_1+\cdots+\lambda_n}V}{\partial x_1^{\lambda_1}\cdots\partial x_n^{\lambda_n}}\frac{(h/2i)^{\lambda_1+\cdots+\lambda_n-1}}{\lambda_1!\cdots\lambda_n!}\frac{\partial^{\lambda_1+\cdots+\lambda_n}P}{\partial p_1^{\lambda_1}\cdots\partial p_n^{\lambda_n}} \tag{8}$$

where the last summation has to be extended over all positive integer values of $\lambda_1, \cdots, \lambda_n$ for which the sum $\lambda_1+\lambda_2+\cdots+\lambda_n$ is odd. In fact we get for $\partial P/\partial t$ by (5) and (7)

$$\begin{aligned}\frac{\partial P}{\partial t} &= \frac{1}{(h\pi)^n}\int\cdots\int dy_1\cdots dy_n e^{2i(p_1y_1+\cdots+p_ny_n)/h}\\ &\cdot\Big\{\sum_k\frac{ih}{2m_k}\Big[-\frac{\partial^2\psi(x_1+y_1,\cdots,x_n+y_n)^*}{\partial x_k^2}\psi(x_1-y_1,\cdots,x_n-y_n)\\ &+\psi(x_1+y_1,\cdots,x_n+y_n)^*\frac{\partial^2\psi(x_1-y_1,\cdots,x_n-y_n)}{\partial x_k^2}\\ &+\frac{i}{h}[V(x_1+y_1,\cdots,x_n+y_n)\\ &-V(x_1-y_1,\cdots,x_n-y_n)]\psi(x_1+y_1,\cdots,x_n+y_n)^*\psi(x_1-y_1,\cdots x_n-y_n)\Big\}.\end{aligned} \tag{9}$$

Here one can replace the differentiations with respect to x_k by differentiations with respect to y_k and perform in the first two terms one partial integration with respect to y_k. In the last term we can develop $V(x_1+y_1, \cdots, x_n+y_n)$ and $V(x_1-y_1, \cdots, x_n-y_n)$ in a Taylor series with respect to the y and get

$$\begin{aligned}\frac{\partial P}{\partial t} &= \frac{1}{(\pi h)^n}\int\cdots\int dy_1\cdots dy_n e^{2i(p_1y_1+\cdots+p_ny_n)/h}\\ &\cdot\Big\{\sum_k\frac{p_k}{m_k}\Big[-\frac{\partial\psi(x_1+y_1,\cdots,x_n+y_n)^*}{\partial y_k}\psi(x_1-y_1,\cdots,x_n-y_n)\end{aligned}$$

$$+\psi(x_1+y_1,\cdots,x_n+y_n)^*\frac{\partial\psi(x_1-y_1,\cdots,x_n-y_n)}{\partial y_k}\Big]$$

$$+\frac{i}{h}\sum_{\lambda}\frac{\partial^{\lambda_1+\cdots+\lambda_n}V}{\partial x_1^{\lambda_1}\cdots\partial x_n^{\lambda_n}}\frac{y_1^{\lambda_1}\cdots y_n^{\lambda_n}}{\lambda_1!\cdots\lambda_n!}\psi(x_1+y_1,\cdots,x_n+y_n)^*$$

$$\cdot\psi(x_1-y_1,\cdots,x_n-y_n)\Big\}, \tag{10}$$

which is identical with (8) if one replaces now the differentiations with respect to y_k by differentiations with respect to x_k. Of course, (8) is legitimate only if it is possible to develop the potential energy V in a Taylor series.

Eq. (8) shows the close analogy between the probability function of the classical mechanics and our P: indeed the equation of continuity

$$\frac{\partial P}{\partial t}=-\sum_k\frac{p_k}{m_k}\frac{\partial P}{\partial x_k}+\sum_k\frac{\partial V}{\partial x_k}\frac{\partial P}{\partial p_k}$$

differs from (8) only in terms of at least the second power of h and at least the third derivative of V. Expression (8) is even identical with the classical when V has no third and higher derivatives as, e.g., in a system of oscillators.

There is an alternative form for $\partial P/\partial t$, which however will not be used later on. It is

$$\frac{\partial}{\partial t}P(x_1,\cdots,x_n;p_1,\cdots,p_n)=-\sum_k\frac{p_k}{m_k}\frac{\partial}{\partial x_k}P(x_1,\cdots,x_n;p_1,\cdots,p_n)$$

$$+\int_{-\infty}^{\infty}\cdots\int dj_1\cdots dj_n P(x_1,\cdots,x_n;P_1+j_1,\cdots,P_n+j_n)J(x_1,\cdots,x_n; \tag{11}$$

$$j_1,\cdots,j_n)$$

where $J(x_1,\cdots,x_n;j_1,\cdots,j_n)$ can be interpreted as the probability of a jump in the momenta with the amounts $j_1,\cdots,j_n$ for the configuration $x_1,\cdots,x_n$. The probability of this jump is given by

$$J(x_1,\cdots,x_n;j_1,\cdots,j_n)$$

$$=\frac{i}{\pi^n h^{n+1}}\int_{-\infty}^{\infty}\cdots\int dy_1\cdots dy_n[V(x_1+y_1,\cdots,x_n+y_n)$$

$$-V(x_1-y_1,\cdots,x_n-y_n)]e^{-(2i/h)(y_1j_1+\cdots+y_nj_n)} \tag{11a}$$

that is, by the Fourier expansion coefficients of the potential $V(x_1,\cdots,x_n)$. This form clearly shows the quantum mechanical nature of our P: the momenta change discontinuously by amounts which would be half the momenta of light quanta if the potential were composed of light.[2a] To derive (11) one can insert both for P and J their respective values (5) and (11a) on the right hand side of (11). In the first term one can replace $p_k e^{2i(p_1y_1+\cdots+p_ny_n)/h}$ by

[2a] Cf. F. Bloch, Zeits. f. Physik **52**, 555 (1929).

$(h/2i)(\partial/\partial y_k)e^{2i(p_1y_1+\cdots+p_ny_n)/h}$ and then perform a partial integration with respect to y_k. Then one can replace the differentiation with respect to y by differentiation with respect to x, upon which some terms cancel and the rest goes over to

$$\sum_k \frac{h}{2im}\int\cdots\int dy_1\cdots dy_n\left[\frac{\partial^2\psi(x_1+y_1,\cdots,x_n+y_n)^*}{\partial x_k^2}\psi(x_1-y_1,\cdots,x_n-y_n)\right.$$
$$\left.-\psi(x_1+y_1,\cdots,x_n+y_n)\frac{\partial^2\psi(x_1-y_1,\cdots,x_n-y_n)}{\partial x_k^2}\right]e^{2i(p_1y_1+\cdots+p_ny_n)/h} \quad (12)$$

which is just what we need for the left side of (11). By integrating the second term on the right side of (11)

$$\int\cdots\int dy_1\cdots dy_n\psi(x_1+y_1\cdots x_n+y_n)^*\psi(x_1-y_1\cdots x_n-y_n)$$
$$\cdot\int\cdots\int dj_1\cdots dj_n e^{(2i/h)[(p_1+j_1)y_1+\cdots+(p_n+j_n)y_n]}$$
$$\cdot\frac{i}{\pi^n h^{n+1}}\int\cdots\int dz_1\cdots dz_n\left[V(x_1+z_1\cdots x_n+z_n)\right.$$
$$\left.-V(x_1-z_1\cdots x_n-z_n)\right]e^{-2i(z_1j_1+\cdots+z_nj_n)/h}$$

with respect to z and j one gets because of the Fourier theorem[3]

$$(i/h)\int\cdots\int dy_1\cdots dy_n\psi(x_1+y_1\cdots x_n+y_n)^*\psi(x_1-y_1\cdots x_n-y_n)$$
$$e^{2i(p_1y_1+\cdots+p_ny_n)/h}\cdot[V(x_1+y_1\cdots x_n+y_n)-V(x_1-y_1\cdots x_n-y_n)] \quad (12a)$$

and this gives the second part of the left side of (11).

3

So far we have defined only a probability function for pure states, which gives us the correct expectation values for quantities $f(p_1\cdots p_n)+g(x_1\cdots x_n)$. If, however, we have a mixture,[4] e.g., the pure states ψ_1, ψ_2, ψ_3, $\cdots$ with the respective probabilities w_1, w_2, w_3, $\cdots$ (with $w_1+w_2+w_3+\cdots=1$) the normal probability calculation suggests a probability function

$$P(x_1,\cdots,x_n,p_1,\cdots,p_n)=\sum_\lambda w_\lambda P_\lambda(x_1,\cdots,x_n,\cdots,p_n) \quad (13)$$

where P_λ is the probability function for ψ_λ. This probability function gives obviously the correct expectation values for all quantities, for which (5) gives correct expectation values and therefore will be adopted.

For a system in statistical equilibrium at the temperature $T=1/k\beta$ the relative probability of a stationary state ψ_λ is $e^{-\beta E_\lambda}$ where E_λ is the energy of ψ_λ. Therefore the probability function is a part from a constant

[3] Cf. e. g., R. Courant und D. Hilbert, Methoden der mathematischen Physik I. Berlin 1924. p. 62, Eq. (29).

[4] J. v. Neumann, Gött Nachr. 245, 1927. L. Landau, Zeits. f. Physik **45**, 430 (1927).

$$P(x_1 \cdots x_n;\ p_1 \cdots p_n)$$

$$= \sum_\lambda \int \cdots \int dy_1 \cdots dy_n \psi_\lambda(x_1 + y_1 \cdots x_n + y_n)^* \cdot e^{-\beta E_\lambda} \psi_\lambda(x_1 - y_1 \cdots x_n - y_n) e^{2i(p_1 y_1 + \cdots + p_n y_n)/h}. \quad (14)$$

Now

$$\sum_\lambda \psi_\lambda (u_1 \cdots u_n)^* f(E_\lambda) \psi_\lambda (v_1 \cdots v_n)$$

is that matrix element of the operator $f(H)$, (H is the energy operator) which is in the $u_1 \cdots u_n$ row and $v_1 \cdots v_n$ column. Therefore (14) may be written as

$$P(x_1 \cdots x_n;\ p_1 \cdots p_n)$$

$$= \int_{-\infty}^{\infty} \cdots \int dy_1 \cdots dy_n e^{i[(x_1+y_1)p_1 + \cdots + (x_n+y_n)p_n]/h} \left[e^{-\beta H}\right]_{x_1+y_1 \cdots x_n+y_n;\, x_1-y_1 \cdots x_n-y_n} \cdot e^{-i[(x_1-y_1)p_1 + \cdots + (x_n-y_n)p_n]/h}. \quad (15)$$

so that we have under the integral sign the $x_1+y_1 \cdots x_n+y_n;\ x_1-y_1 \cdots x_n-y_n$ element of the matrix $e^{-\beta H}$ transformed by the diagonal matrix $e^{i(p_1 x_1 + \cdots + p_n x_n)/h}$. Instead of transforming $e^{-\beta H}$ we can transform H first and then take the exponential with the transformed expression. By transforming H we get the operator (the p are numbers, not operators!)

$$H = e^{i(x_1 p_1 + \cdots + x_n p_n)/h} \left(- \sum_k \frac{h^2}{2m_k} \frac{\partial^2}{\partial x_k^2} + V(x_1 \cdots x_n) \right) e^{-i(x_1 p_1 + \cdots + x_n p_n)/h}$$

which is equal to

$$\tilde{H} = \epsilon + \sum_{k=1}^{n} \left(\frac{ihp_k}{m_k} \frac{\partial}{\partial x_k} - \frac{h^2}{2m_k} \frac{\partial^2}{\partial x_k^2} \right) \quad (16)$$

where

$$\epsilon = \sum_{k=1}^{n} \frac{p_k^2}{2m_k} + V(x_1, \cdots, x_n). \quad (17)$$

So we get for (15)

$$P(x_1, \cdots, x_n;\ p_1, \cdots, p_n)$$

$$= \int \cdots \int dy_1 \cdots dy_n \left[e^{-\beta \tilde{H}}\right]_{x_1+y_1 \cdots x_n+y_n;\, x_1-y_1 \cdots x_n-y_n}. \quad (18)$$

By calculating the mean value of a quantity $Q = f(p_1, \cdots, p_n) + g(x_1, \cdots, x_n)$ by (18) one has to obtain the same result as by using the original expression (4) of Neumann.

If we are dealing with a system, the behavior of which in statistical equilibrium is nearly correctly given by the classical theory, we can expand (18) into a power of h and keep the first few terms only. The term with the zero power of h is $\sum_r (-\beta)^r \epsilon^r / r!$ Now ϵ^r is the operator of multiplication with the r

power of (17). Its $x_1+y_1, \cdots, x_n+y_n; x_1-y_1, \cdots, x_n-y_n$ element is consequently

$$\epsilon(x_1 + y_1, \cdots, x_n + y_n)^r \delta(x_1 + y_1, x_1 - y_1) \cdots \delta(x_n + y_n, x_n - y_n).$$

As δ (also δ', δ'', $\cdots$) only depends on the difference of its two arguments, one can write $\delta(-2y_1) \cdots \delta(-2y_n)$ for the last factors and perform the integration by introducing $-2y_1, \cdots, -2y_n$ as new variables. The terms with the zero power of h, arising from the first part of (16) only, give thus

$$(1/2^n) \sum_r (-\beta)^r \epsilon(x_1, \cdots, x_n)^r / r! = e^{-\beta\epsilon}/2^n \tag{19}$$

which is just the classical expression.

The higher approximations of the probability function can be calculated in a very similar way. The terms of $e^{-\beta\tilde{H}}$, involving the first power of the second part of $\tilde{H}$ only, are

$$\sum_{r=0}^{\infty} \frac{(-\beta)^r}{r!} \sum_{\rho=1}^{r} \epsilon^{\rho-1} \sum_k \left(\frac{ihp_k}{m_k} \frac{\partial}{\partial x_k} - \frac{h^2}{2m_k} \frac{\partial^2}{\partial x_k^2} \right) \epsilon^{r-\rho} \tag{20}$$

By replacing all operators by symbolic integral-kernels one gets for the $x_1+y_1, \cdots, x_n+y_n; x_1-y_1, \cdots, x_n-y_n$ element of the operator (20)

$$\sum_r \frac{(-\beta)^r}{r!} \sum_{\rho=1}^{r} \epsilon(x_1 + y_1, \cdots, x_n + y_n)^{\rho-1}$$

$$\cdot \sum_k \left[\frac{ihp_k}{m_k} \delta(-2y_1) \cdots \delta'(-2y_k) \cdots \delta(-2y_n) \right.$$

$$\left. - \frac{h^2}{2m_k} \delta(-2y_1) \cdots \delta''(-2y_k) \cdots \delta(-2y_n) \right] \epsilon(x_1 - y_1, \cdots, x_n - y_n)^{r-\rho}.$$

Now

$$\sum_{\rho=1}^{r} \epsilon_+^{\rho-1} \epsilon_-^{r-\rho} = \sum_{\rho=1}^{r} \epsilon_-^{r-1} \left(\frac{\epsilon_+}{\epsilon_-} \right)^{\rho-1} = \frac{\epsilon_+^r - \epsilon_-^r}{\epsilon_+ - \epsilon_-}$$

so that the summation over ρ and r can be performed in (21). By introducing again new variables $w_1, \cdots, w_n$ for $-2y_1, \cdots, -2y_n$ and performing the integration one has

$$\frac{1}{2^n} \sum_k \left[\frac{ihp_k}{m_k} \frac{\partial}{\partial w_k} - \frac{h^2}{2m_k} \frac{\partial^2}{\partial w_k^2} \right]$$

$$\frac{e^{-\beta\epsilon(x_1, \cdots, x_k - w_k/2, \cdots, x_n)} - e^{-\beta\epsilon(x_k, \cdots, x_k + w_k/2, \cdots, x_n)}}{\epsilon(x_1, \cdots, x_k - \frac{1}{2}w_k, \cdots, x_n) - \epsilon(x_1, \cdots, x_k + \frac{1}{2}w_k, \cdots, x_n)}$$

where $w_k = 0$ must be inserted after differentiation. The first differential quotient vanishes at $w_k = 0$, as the expression to be differentiated is an even function of w_k. The second part gives

$$\frac{e^{-\beta\epsilon}}{2^n} \sum_k \frac{h^2}{m_k}\left(-\frac{\beta^2}{8}\frac{\partial^2\epsilon}{\partial x_k{}^2}+\frac{\beta^3}{24}\left(\frac{\partial\epsilon}{\partial x_k}\right)^2\right). \tag{21}$$

In principle it is possible to calculate in the same way the terms involving the higher powers of the second part of $\tilde{H}$ also, the summation over r and the quantities corresponding to our ρ can always be performed in a very similar way. In practice, however, the computation becomes too laborious. Still it is clear, that if we develop our probability function for thermal equilibrium in a power series of h

$$P(x_1, \cdots, x_n; p_1, \cdots, p_n) = e^{-\beta\epsilon} + hf_1 + h^2 f_2 + \cdots \tag{22}$$

(we can omit the factor $1/2^n$ before $e^{-\beta\epsilon}$, as we are dealing with relative probabilities anyway) all terms will be quite definite functions of the p, V and the different partial derivatives of the latter. Furthermore it is easy to see, that f_k will not involve higher derivatives of V than the k-th nor higher powers of p than the k-th. These facts enable us to calculate the higher terms of (22) in a somewhat simpler way, than the direct expansion of (18) would be.

The state (22) is certainly stationary, so that it would give identically $\partial P/\partial t = 0$ when inserted into (8). By equating the coefficients of the different powers of h in $\partial P/\partial t$ to zero one gets the following equations:

$$\sum_k -\frac{p_k}{m_k}\frac{\partial e^{-\beta\epsilon}}{\partial x_k} + \sum_k \frac{\partial V}{\partial x_k}\frac{\partial e^{-\beta\epsilon}}{\partial p_k} = 0 \tag{23, 0}$$

$$\sum_k -\frac{p_k}{m_k}\frac{\partial f_1}{\partial x_k} + \sum_k \frac{\partial V}{\partial x_k}\frac{\partial f_1}{\partial p_k} = 0 \tag{23, 1}$$

$$\sum_k -\frac{p_k}{m_k}\frac{\partial f_2}{\partial x_k} + \sum_k \frac{\partial V}{\partial x_k}\frac{\partial f_2}{\partial p_k} - \sum_k \frac{\partial^3 V}{\partial x_k{}^3}\frac{h^2}{24}\frac{\partial^3 e^{-\beta\epsilon}}{\partial p_k{}^3} - \sum_{k\neq l} \frac{\partial^3 V}{\partial x_k{}^2 \partial x_l}\frac{h^2}{8}\frac{\partial^3 e^{-\beta\epsilon}}{\partial p_k{}^2 \partial p_l} = 0 \tag{23, 2}$$

and so on. The first of these equations is an identity because of (17), as it must be; (23, a), (23, 2), $\cdots$ will determine $f_1, f_2, \cdots$ respectively. All Eqs. (23, a) are linear inhomogeneous partial differential equations for the unknown f. From one solution f_a of (23, a) one obtains the general solution by adding to it the general solution F of the homogeneous part of (23, a), which is always

$$\sum_k -\frac{p_k}{m_k}\frac{\partial F}{\partial x_k} + \sum_k \frac{\partial V}{\partial x_k}\frac{\partial F}{\partial p_k} = 0.$$

This equation in turn is the classical equation for the stationary character of the probability distribution $F(x_1, \cdots, x_n; p_1, \cdots, p_n)$. It has in general only one solution which contains only a finite number of derivatives of V, namely

$$F(x_1, \cdots, x_n; p_1, \cdots, p_n) = F\left(\sum_k \frac{p_k{}^2}{2m_k} + v(x_1 \cdots x_n)\right) = F(\epsilon).$$

In fact, if it had other integrals, like

$$F(p_1, \cdots, p_n; V, \partial V/\partial x_1, \partial V/\partial x_2, \cdots) \tag{24}$$

then all mechanical problems would have in addition to the energy-integral further integrals of the form (24) which, of course, is not true.

One solution of (23, 1) is $f_1 = 0$ and the most general we have to consider is therefore $f_1 = F(\epsilon)$. We have to take however $F(\epsilon) = 0$ as f_1 has to vanish for a constant V. So we get $f_1 = 0$, as we know it already from the direct expansion of (18). The same holds consequently for $f_3, f_5, \cdots$, as the inhomogeneous part of the equation for f_3 only contains f_1, the inhomogeneous part of the equation for f_5 only f_1 and f_3, and so on.

For f_2 one easily gets

$$f_2 = e^{-\beta\epsilon}\left[\sum_k\left(-\frac{\beta^2}{8m_k}\frac{\partial^2 V}{\partial x_k{}^2} + \frac{\beta^3}{24m_k}\left(\frac{\partial V}{\partial x_k}\right)^2\right) + \sum_{k,l}\frac{\beta^3 p_k p_l}{24m_k m_l}\frac{\partial^2 V}{\partial x_k \partial x_l}\right] \tag{25}$$

as a solution of (23, 2) and it is also clear, that this is the solution we need. The first two terms of f_2 we have already directly computed (21), the third arises from terms with the second power of the second part of $\tilde{H}$. Similarly f_4 is for one degree of freedom ($n = 1$)

$$\begin{aligned} 64m^2\beta^{-2}\, e^{\beta\epsilon} f_4 = {} & H_4(q)\left[\beta^2 V'''^2/72 - \beta V''''/120\right] \\ & + H_2(q)\left[\beta^3 V'^2 V''/18 - 2\beta^2 V'''^2/15 - \beta^2 V' V'''/15 + \beta V''''/15\right] \\ & + H_0(q)\left[\beta^4 V'^4/18 - 22\beta^3 V'^2 V''/45 + 2\beta^2 V'''^2/5 + 8\beta^2 V' V'''/15\right. \\ & \left. - 4\beta V''''/15\right] \end{aligned} \tag{26}$$

where H_r is the r-th Hermitean polynomial and $q = \beta^{1/2} p/(2m)^{1/2}$.

It does not seem to be easy to get a simple closed expression for f_k, but it is quite possible to calculate all of them successively. A discussion of Eqs. (23) shows, that the g in

$$P(x_1, \cdots, x_n; p_1, \cdots, p_n) = e^{-\beta\epsilon}(1 + h^2 g_2 + h^4 g_4 + \cdots) \tag{27}$$

are rational expressions in the derivatives of V only (do not contain V itself) and all terms of g_k contain k differentiations and as functions of the p are polynomials of not higher than the k-th degree. The first term in (27) with the zero power of h is the only one, which occurs in classical theory. There is no term with the first power, so that if one can develop a property in a power series with respect to h, the deviation from the classical theory goes at least with the second power of h in thermal equilibrium. One familiar example for this is the inner energy of the oscillator, where the term with the first power of h vanishes just in consequence of the zero point energy. The second term can be interpreted as meaning that a quick variation of the probability function with the coordinates is unlikely, as it would mean a quick variation, a short wave-length, in the wave functions. This however would have the consequence of a high kinetic energy. The quantum mechanical probability is therefore something like the integral of the classical expression $e^{-\beta\epsilon}$ over a finite range of coordinates of the magnitude $\sim h/\bar{p}$ where $\bar{p}$ is the mean momentum $\sim (kTm)^{1/2}$. The correction terms of (27) have, among other effects,

the consequence that the probability for a particle being in a narrow hole is smaller than would be in classical statistics. From now on we will keep only the first two terms of (27).

4

From (25) one easily calculates the relative probabilities of the different configurations by integration with respect to the p:

$$\int \cdots \int dp_1 \cdots dp_n P(x_1 \cdots x_n; p_1 \cdots p_n)$$

$$= e^{-\beta V}\left[1 - \frac{h^2\beta^2}{12} \sum_k \frac{1}{m_k}\frac{\partial^2 V}{\partial x_k{}^2} + \frac{h^2\beta^3}{24} \sum_k \frac{1}{m_k}\left(\frac{\partial V}{\partial x_k}\right)^2\right]. \tag{28}$$

Hence the mean potential energy is

$$\bar{V} = \frac{\int V e^{-\beta V} dx}{\int e^{-\beta V} dx} + \frac{h^2\beta^2}{24} \frac{\int \sum_k \frac{1}{m_k}\frac{\partial^2 V}{\partial x_k{}^2} e^{-\beta V} dx \int V e^{-\beta V} dx}{\left(\int e^{-\beta V} dx\right)^2}$$

$$+ \frac{h^2\beta}{24} \frac{\int \sum_k \frac{1}{m_k}\frac{\partial^2 V}{\partial x_k{}^2}(1 - \beta V) e^{-\beta V} dx}{\int e^{-\beta V} dx} \tag{29}$$

where dx is written for $dx_1 \cdots dx_n$ and the higher power terms of h are omitted. Similarly the mean value of the kinetic energy is

$$\sum_k \frac{\overline{p_k{}^2}}{2m_k} = \frac{n}{2\beta} + \frac{h^2\beta}{24} \frac{\int \sum_k \frac{1}{m_k}\frac{\partial^2 V}{\partial x_k{}^2} e^{-\beta V} dx}{\int e^{-\beta V} dx}. \tag{30}$$

This formula also is correct only within the second power of h; in order to derive it one has to perform again some partial integrations with respect to the x. Eqs. (28), (29), (30) have a strict quantum mechanical meaning and it should be possible to derive them also from (4). One sees that the kinetic energy is in all cases larger than the classical expression $\frac{1}{2}nkT$.

5

One fact still needs to be mentioned. We assumed that the probability of a state with the energy E is given by $e^{-\beta E}$. This is not true in general, since the Pauli principle forbids some states altogether. The corrections thus introduced by the Bose or Fermi statistics even give terms with the first power of h, so that it seems, that as long as one cannot take the Bose of Fermi statistics into account, Eq. (25) cannot be applied to an assembly of identical par-

ticles, as, e.g., a gas. There is reason to believe however, that because of the large radii of the atoms this is not true and the corrections due to Fermi and Bose statistics may be neglected for moderately low temperatures.

The second virial coefficient was first calculated in quantum mechanics by F. London on the basis of his theory of inneratomic forces.[5] He also pointed out that quantum effects should be taken into account at lower temperatures. Slater and Kirkwood[6] gave a more exact expression for the inneratomic potential of He and Kirkwood and Keyes[7] calculated on this basis the classical part of the second virial coefficient of He. H. Margenau[8] and Kirkwood[9] performed the calculations for the quantum-correction. The present author also tried to calculate it by the method just outlined. He got results, which differ from those of Margenau and Kirkwood in some cases by more than 100 percent.[10] It does not seem however to be easy to compare these results with experiment, as the classical part of the second virial coefficient is at low temperatures so sensitive to small variations of the parameters occurring in the expression of the interatomic potential, that it changes by more than 20 percent if the parameter in the exponential (2.43) is changed by ½ percent and it does not seem to be possible to determine the latter within this accuracy.

[5] F. London, Zeits. f. Physik **63,** 245 (1930).

[6] J. C. Slater and J. G. Kirkwood, Phys. Rev. **37,** 682 (1931).

[7] J. G. Kirkwood and F. G. Keyes, Phys. Rev. **38,** 516 (1931).

[8] H. Margenau, Proc. Nat. Acad. **18,** 56, 230 (1932). Cf. also J. C. Slater, Phys. Rev. **38,** 237 (1931).

[9] J. G. Kirkwood, Phys. Zeits. **33,** 39 (1932).

[10] I am very much indebted to V. Rojansky for his kind assistance with these calculations. The reason for the disagreement between our results and those of Margenau and Kirkwood may be the fact that they did not apply any corrections for the continuous part of the spectrum.

In a paper which appeared recently in the Zeits. f. Physik (**74,** 295 (1932)) F. Bloch gets results which are somewhat similar to those of the present paper. (*Note added at proof.*)

The Hyperfine Structure of Lead

By JOHN L. ROSE AND L. P. GRANATH
New York University, University Heights

(Received April 25, 1932)

The hyperfine structure of several lines of Pb I and Pb II in the violet and ultraviolet regions has been determined. λλ4168, 4062, 4058, 4019, 3739, 3683, 3671, 3639, 3572, 2873, 2833, 2823, 2802 of Pb I, and λλ4386, 4245, 3786, 3016, 2948 of Pb II were found to have structure. λλ2663, 2614, 2613, and 2577 of Pb I were observed and found to be simple. Exposures with uranium-lead showed that all of the above lines are single for Pb^{206}. It was also found from the line patterns that there is a larger abundance of Pb^{207} than Pb^{208} in uranium-lead (Belgian Congo). The hyperfine splittings of $s^3P_{0,1}$ and $p^3P_{0,1,2}$ of Pb^{207} I were calculated. The center of gravity of the Pb^{207} terms and the single Pb^{206} and Pb^{208} terms for these levels were found to fall in the order of their masses. Much larger isotope displacements were observed for Pb II than for Pb I.

Variations in the relative intensities of certain lines of Pb I with excitation conditions made it appear that there may be something wrong in the classification of some of the lines with initial levels, $d^3D_{1,2}$ and $d^3F_{2,3}$. A change of several of the line patterns was observed with a variation of voltage and temperature.

INTRODUCTION

WITH a Paschen-Schüler tube[1] as a source, the hyperfine structure of Pb I and Pb II for ordinary and uranium-leads has been investigated from λ4386 to λ2393 by the use of two quartz Lummer-Gehrcke plates[2] (197×30×6.55 mm and 130×15×4.40 mm). The lines, λλ4168, 4062, and 4019, reported single by Janicki,[3] Luneland,[4] Wali Mohammed,[5] and Wali Mohammed and Sharma,[6] and λλ3740, 3683, 3671, 3572, 2873, 2823, and 2802, found simple by the latter, have been observed to have structure. The line, λ4058, found by all of the above investigators to have three components and by Murakawa[7] to have five, appeared with four components which is in agreement with Kopfermann;[8] λλ2833 and 3639, observed by Wali Mohammed and Sharma with three components, were found to have four and five components, respectively. They have also reported two components for λ2614 which we have found to be single. In addition to the above lines of Pb I, λλ4386, 4245, 3786, 3016, and 2948 of Pb II, which appeared on the photographic plates when the pressure of He in the tube was high, were found to have structure. The measurements for λ4245 agree with those made by Janicki, Wali Mohammed, and Murakawa. The separation of the two com-

[1] Schüler, Zeits. f. Physik **35**, 323 (1926).
[2] Kindly loaned by R. W. Wood.
[3] Janicki, Ann. d. Physik **29**, 833 (1909).
[4] Luneland, Ann. d. Physik **34**, 505 (1911).
[5] Wali Mohammed, Astrophy. J. **39**, 185 (1914).
[6] Wali Mohammed and Sharma, Phil. Mag. **12**, 1106 (1931).
[7] Murakawa, Zeits. f. Physik **72**, 793 (1931).
[8] Kopfermann, Naturw. **19**, 400 (1931); **19**, 675 (1931).

ponents of λ4386 agrees qualitatively with that found by Murakawa for this line.

Apparatus

Two tubes, one for ordinary lead and the other for uranium-lead, were mounted at right angles to each other. No auxiliary heater was required to vaporize the lead in the hollow cathode since the discharge developed sufficient heat for this purpose. With large currents it was possible to bring the iron cathode to a red heat. The tubes were connected in series with a vacuum system in which He could be admitted and purified. The He with pressures from 2 mm. to 0.01 mm of Hg was continuously circulated through the two tubes and a trap filled with chabazite at liquid air temperature. The chabazite was very effective in cleaning up the nitrogen in the He and the gases given off by the metal parts of the discharge tube.

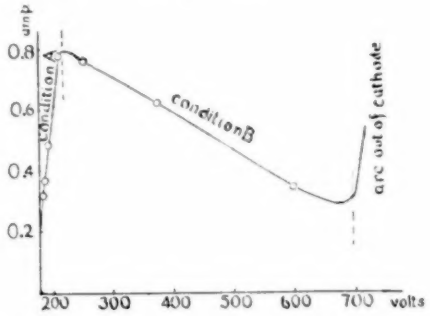

Fig. 1. Curve showing the variation of current with increasing voltage across the Paschen-Schüler lamp.

The source of excitation was a d.c. 3 k.w. motor-generator capable of producing voltages up to 1500 volts. A 450 ohm resistance was kept in series with the lamp which was being operated.

The Lummer-Gehrcke plates were used with a Hilger E2 quartz spectrograph. The light from the source, which was rendered slightly convergent by a large crystal quartz lens, entered the prism of the Lummer-Gehrcke plate after passing through a Wollaston prism. The fringes due to the extraordinary ray were brought to a focus by a quartz-fluorite lens[2] on the slit of the spectrograph. A brass slide was arranged in front of the wide slit which allowed the line patterns for two exposures to be photographed side by side on the same photographic plate. Since very long exposures were required for some of the lines, the Lummer-Gehrcke plates were mounted in a large, electrically heated, double wall, Beaver-board box whose temperature was kept constant to within 0.01° C by an ether thermostat.

Variation of Relative Intensities of Lines with Excitation Conditions

A study of the general appearance of the spectra of Pb and He as the voltage of the generator was increased led to rather interesting results. Start-

ing with 180 volts across the tube as measured directly by an electrostatic voltmeter and a current of 0.2 amp., an increase of the generator voltage caused a considerable increase of current through the tube with a very small increase of voltage across it. The voltage of the generator was steadily increased until the current was 0.8 amp. while the voltage on the tube went up to 210 volts. A further increase of generator voltage caused a decrease in the current with a large increase in the voltage across the tube. As shown in Fig. 1, it was possible to increase the generator potential until the current dropped to 0.3 amp. and the voltage of the tube increased to 700 volts before the discharge jumped out of the inside of the cathode and arcked from the outside of the cathode to the walls of the tube.

For convenience the condition with increasing current and cool cathode will be called condition A, and with decreasing current and very hot cathode will be called condition B. The He spectrum was more intense than that of the lead in condition A with a small vapor pressure of lead while the lead spectrum was relatively stronger than the He in condition B with larger pressures of lead vapor. See Fig. 2. In A the lines, λλ2873, 2833, 2802, and 2614, were quite strong and of nearly equal intensities while λλ2823 and 2613 were several times less intense. The relative intensities of these lines varied on changing to condition B in such a manner that λλ2613 and 2823 appeared as intense as λλ2873, 2802 and 2614, and at the same time λ2833, which was the strongest in condition A, became the least intense of this group.

The variation of the relative intensities of these lines together with the fact that λ2657 ($p^3P_1-d^3D_2$) was very faint in both conditions makes it appear that there may be something incorrect in the classification[9] of some of the lines. This line would be expected to appear with intensity comparable to that of λ2873 ($p^3P_2-d^3D_2$), provided there are no strong perturbations due to other terms.* The classification does not explain why λ2613($p^3P_1-d^3D_1$) and 2823 ($p^3P_2-d^3F_2$) should be so much weaker than λλ2802 ($p^3P_2-d^3F_3$), 2873 ($p^3P_2-d^3D_2$), and 2614 ($p^3P_1-d^3F_2$) in condition A and finally approach the same intensities in condition B. If the final levels for all of these lines are members of the triplet $p^3P_{0,1,2}$ there should be no variations in the relative intensities of the above lines which have been classified with common initial levels. Furthermore, since λ4019 ($p^1D_2-d^3F_3$) appeared, there should be expected a line, λ4063.4 ($p^1D_2-d^3F_2$) which has never been reported for Pb I. Also since λλ2613 ($p^3P_1-d^3D_1$) and 2170 ($p^3P_0-d^3D_1$) appeared, the third member of this triplet, λ2822.6 ($p^3P_2-d^3D_1$), is certainly expected. This line has also never been reported, nor observed by us. It is also difficult to see how λ2393, a very strong line in both conditions, should be omitted from the classification. The way in which the more intense components of λλ4058, 3683, 3639, and 2833 reversed with an increase of lead vapor pressure shows, however, that these lines are associated with the lower states of Pb I. This is in agreement with the classification. In Fig. 3 the series of photographs made with an increasing temperature of the cathode shows

[9] Gieseler and Grotrian, Zeits. f. Physik **39**, 377 (1926).

* The possibility of such a perturbation has been indicated to us by Professor A. G. Shenstone.

Fig. 2. *A*, cool cathode; *B*, hot cathode.

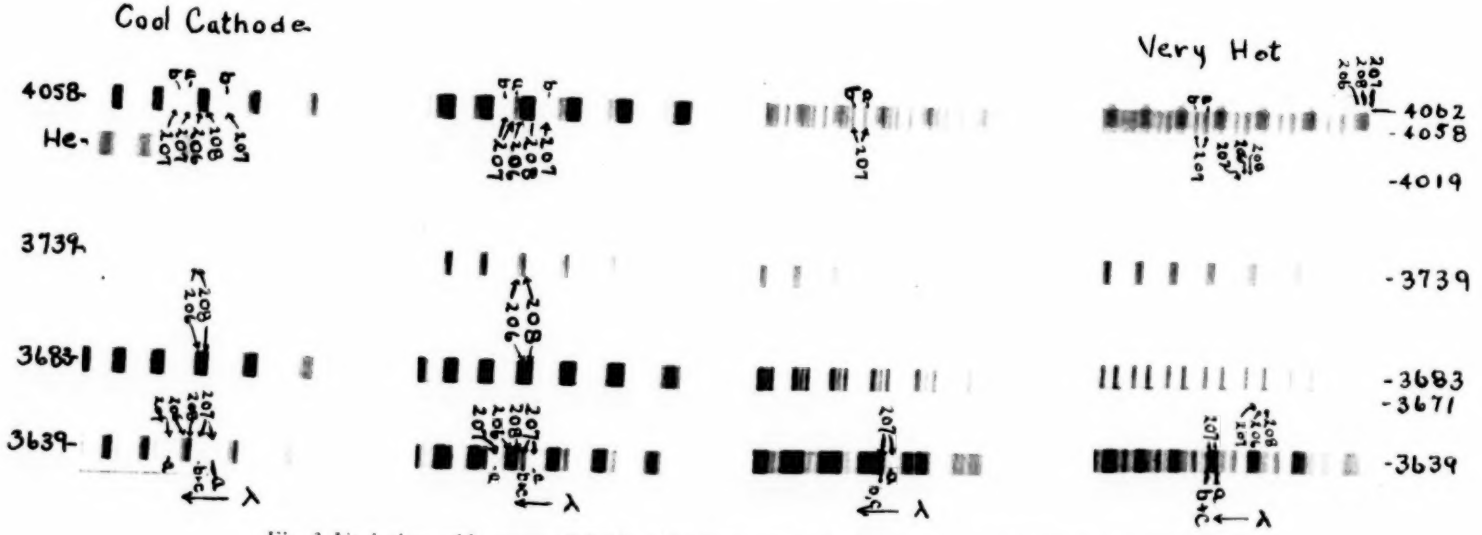

Fig. 3. Variations of Lummer-Gehrcke plate patterns with increasing temperature of the cathode.

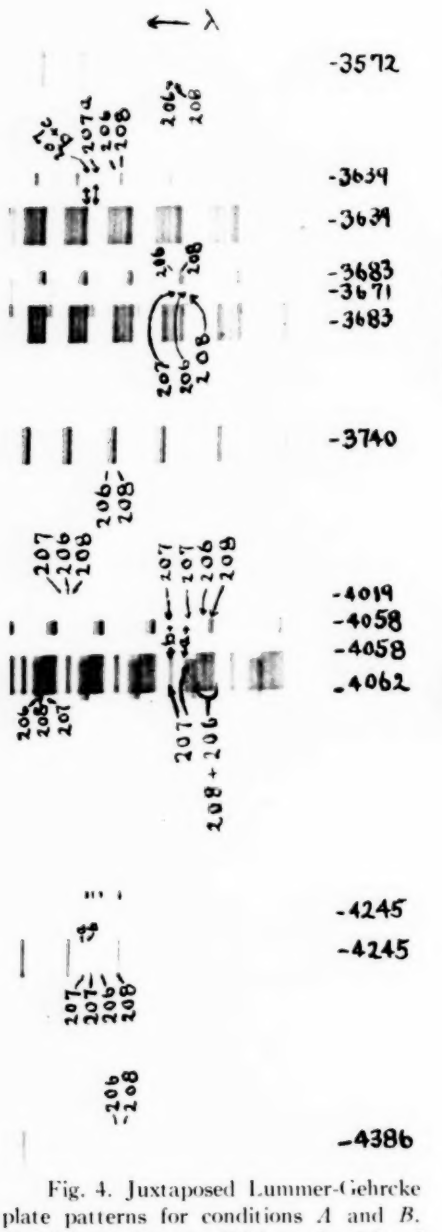

Fig. 4. Juxtaposed Lummer-Gehrcke plate patterns for conditions *A* and *B*. Condition *A* (narrow slit) is on the right of condition *B* (wide slit). Several weak lines appear only in condition *B*.

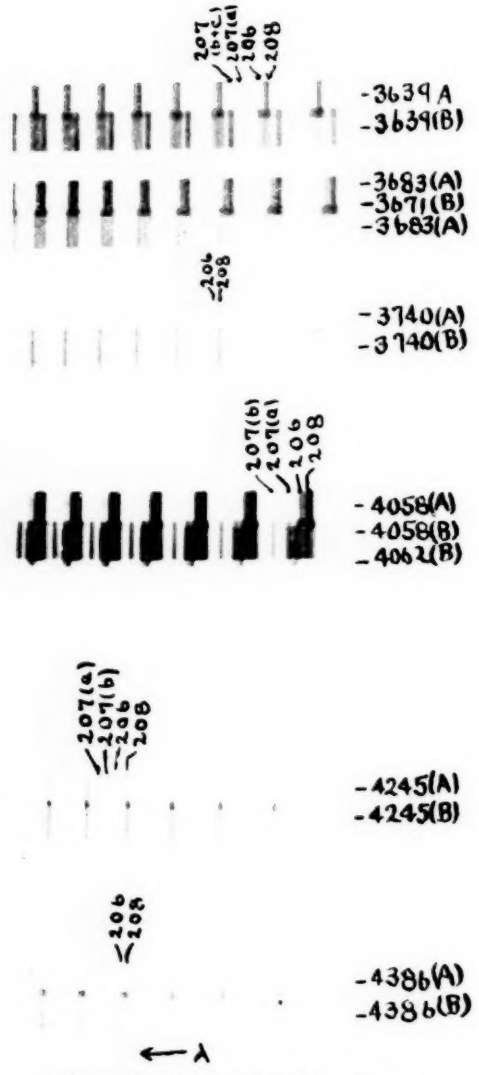

Fig. 5. Condition *A* (right) and condition *B* (left) photographed with equal slit widths.

the changes due to self reversal of the line patterns of λλ4058, 3683 and 3639.

Because of the complexity of the line patterns and the apparent change of the relative intensities of the components of certain lines in condition *B*, it is difficult to interpret the patterns in Fig. 3, which were photographed with a very hot cathode. Schüler and Keyston[10] have observed that a variation of the excitation conditions of the same hollow cathode discharge tube produced large changes in the relative intensities of the hyperfine structure lines of Cd, Tl, and Hg. These changes of intensity were not thought by them to be due to self reversal and have not as yet been explained. Although intensity measurements have not been made on our photographs obtained with different conditions of excitation, it appears that there may be a variation in the relative intensities of the components of some of the Pb I lines, exclusive of the absorption observed for the stronger components of several lines. In order to be more certain of the interpretations of the complicated patterns with a very hot cathode, the line structures with high and low temperatures were photographed side by side on the same photographic plate. This was done by allowing the Lummer fringes for one condition to enter a vertical portion of the wide slit of the spectrograph; another vertical portion of the slit was used for the second condition. The juxtaposed patterns in Figs. 4 and 5 with different slit widths show the relative positions of the components for conditions *A* and *B*.

Uranium-Lead

An exposure in condition *A* with uranium-lead (atomic weight 206), derived from ore of the Belgian Congo, showed that the Pb^{206} lines are single. See Fig. 6A. By juxtaposing the patterns of ordinary and uranium-leads in condition *A* it was found that the single Pb^{206} line corresponded to the next to the strongest component of ordinary lead for all of the Pb I and Pb II lines above λ2802, with the exception of λλ2873, 2823 and 2802 of Pb I. See Fig. 7. The single line of Pb^{206} for the above three lines appeared very close the strongest component of ordinary lead. It has been previously shown by Kopfermann[8] that the strongest and the next to the strongest components of λλ4058, 4242, 4245, and 5373 were due to isotopes Pb^{208} and Pb^{206} respectively, with nuclear spin, $i=0$, while the other components belong to Pb^{207} which has a nuclear spin, $i=\frac{1}{2}$.

In condition *B* when uranium-lead was used, the lines of Pb^{206} with low term values were found reversed. See Fig. 6B. In this condition faint components of Pb^{207} were also observed for some of the more intense lines. Because of the large isotope displacements and the small amount of reversal for λ4245, it was very easy to compare the relative intensities of the components of this line for ordinary lead with the components for uranium-lead. The two patterns of this line, side by side on the same photographic plate, have been reproduced in Fig. 8. These photographs show a larger abundance of Pb^{207} than Pb^{208} in uranium-lead.[11] This observation is in agreement with

[10] Schüler and Keyston, Zeits. f. Physik **71**, 413 (1931).

[11] Rose and Granath, Phy. Rev. **39**, 1017 (1932).

Aston's[12] mass-spectragraph determination of the relative abundance of isotopes of uranium-lead derived from uranium bearing Norwegian bröggerite. Rutherford[13] in commenting upon Aston's results, suggests that Pb^{207} is the end product of protactinium which in turn may be due to the disintegration of an isotope of uranium of atomic weight 235.

Measurements of the Line Patterns of Pb I

Practically all of the measurements of the separations of the hyperfine structure components were made from the photographed line patterns which

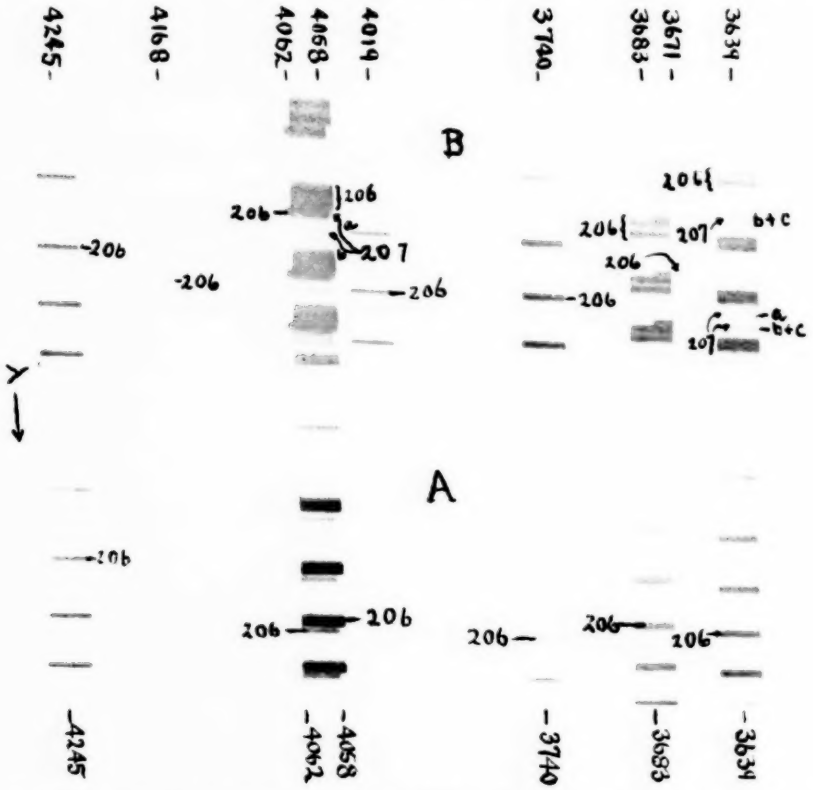

Fig. 6. Line patterns for uranium-lead (Belgian Congo). A, only single lines of Pb^{206} appear with cool cathode. B, in addition to the self reversed Pb^{206} line, components of Pb^{207} appear for some of the lines when the cathode is very hot.

were obtained by using the Lummer-Gehrcke plate of thickness, $t = 6.55$ mm. The lines were measured by a Fuess comparator which could be read to 0.001 mm, and the calculated separations of the components are considered accurate to at least ± 0.005 cm^{-1}. Table I gives the measurements on the line patterns of Pb I in terms of both frequency and wave-length differences. The line of the pattern from which the differences are measured is the most intense one, which in general is due to Pb^{208}. The isotopes to which the

[12] Aston, Nature **123,** 313 (1929).
[13] Rutherford, Nature **123,** 313 (1929).

TABLE I. *Hyperfine structure of Pb I lines.*

λ	Classification	Components	$\Delta\nu$ cm^{-1}	$\Delta\lambda$A	Order of intensities	(Theoretical) Expected relative intensities for Pb^{207} components
4168.045	$p^1D_2-d^3D_2$	208	0.000	0.000	1	(9, 1, 1, 14)
		206	−0.065	+0.011	2	
		207	−0.157	+0.027	3	
4062.149	$p^1D_2-d^3D_1$	207	+0.090	−0.015	3	(5, 1, 9)
		208	0.000	0.000	2	
		206	−0.075	+0.012	1	
4058.826	$p^3P_2-s^3P_1$	207(b)	+0.213	−0.035	4	(5, 1, 9)
		208	0.000	0.000	1	
		206	−0.093	+0.015	2	
		207(a)	−0.217	+0.036	3	
4019.644	$p^1D_2-d^3F_3$	208	0.000	0.000	1	(14, 1, 20)
		206	−0.069	+0.011	2	
		207	−0.153	+0.025	3	
3739.947	$p^1D_2-s^3P_2$	208	0.000	0.0000	1	(9, 1, 1, 14)
		206	−0.089	+0.0125	2	
3683.471	$p^3P_1-s^3P_0$	208	0.000	0.000	1	(1, 2)
		206	−0.085	+0.012	2	
		207	−0.12(?)	+0.02(?)	3	
3671.506	$p^1D_2-s^3P_1$	208	0.000	0.000	1	(5, 1, 9)
		206	−0.092	+0.012	2	
		207	−0.230	+0.031	3	
3639.583	$p^3P_1-s^3P_1$	207(b)	+0.135	−0.018	3	(2, 1, 1, 5)
		208	0.000	0.000	1	
		206	−0.088	+0.012	2	
		207(a)	−0.304	+0.040	5	
		207(c)	−0.429	+0.057	4	
3572.737	$p^1D_2-s^1P_1$	208	0.000	0.0000	1	(5, 1, 9)
		206	−0.069	+0.0088	2	
2873.324	$p^3P_2-d^3D_2$	207(b)	+0.218	−0.018	2(?)	(9, 1, 1, 14)
		208, 206	0.000	0.000	1	
		207(a)	−0.248	+0.020	2(?)	
2833.071	$p^3P_0-s^3P_1$	207(b)	+0.097	−0.0078	3	(1, 2)
		208	0.000	0.0000	1	
		206	−0.079	+0.0063	2	
		207(a)	−0.337	+0.027	4	
2823.199	$p^3P_2-d^3F_2$	207(b)	+0.195	−0.0155	3	(9, 1, 1, 14)
		208, 206	0.000	0.0000	1	
		207(a)	−0.166	+0.013	2	
2802.009	$p^3P_2-d^3F_3$	208, 206	0.000	0.000	1	(14, 1, 20)
		207	−0.231	+0.018	2	
2614.200	$p^3P_1-d^3F_2$		single			(5, 1, 9)
2613.678	$p^3P_1-d^3D_1$		single			(2, 1, 1, 5)

components belong are listed in the third column of the table. Where more than one component due to Pb^{207} was observed, small letters, *a*, *b*, *c*, etc., are used in describing the Pb^{207} components. No quantitative estimate of the relative intensities of the components has been made. In the next to the last column of the tables, however, the order of the intensities is given, the number 1 being assigned to the strongest component. The theoretical relative intensities for the components of Pb^{207} with nuclear spin, $i=\frac{1}{2}$, which would be expected from the classification by Gieseler and Grotrian[9] are given in the last column. These intensities were found by use of the Kronig-Sommerfeld -Höul intensity formulas as first applied to hyperfine structure by Hill.[14]

λλ 4168, 4062, 4019, and 3671

The strongest line of this group is λ4062. Since its pattern almost completely overlaps with the pattern of the very intense line, λ4058, it was very difficult to measure. In condition *A* the two strong components due to Pb^{208} and Pb^{206} appeared with very long exposures for all of these lines, while in condition *B* with a hot cathode the third component, presumably due to Pb^{207}, appeared on the plate intense enough to measure. No self reversal was noted for the stronger components with condition *B*. For this group at least two relatively strong Pb^{207} components are expected for each line, but only one was observed. It may be that the other Pb^{207} component is too close to one of the stronger components to be resolved. If both of the stronger Pb^{207} components were masked by Pb^{206} and Pb^{208} in these lines, the weak component may be the least intense one expected for Pb^{207}, or perhaps belong to another isotope of lead. Schüler and Jones[15] working in the red and green regions have recently reported evidence of Pb^{204}.

λλ 3739 and 3572

These lines appeared with the same patterns with either a cool or a very hot cathode. With high temperatures there seems to be a slight tendency for the two components of λ3572 to fuse together. No trace of a third component could be found.

λ 4058

This line with high lead vapor pressure could be photographed in one to five minutes, but the two strongest components were usually reversed. It required an exposure of one and one half hours with a low lead vapor pressure to photograph the unreversed line pattern, which consisted of four components. Components of Pb^{208} and Pb^{206} were seen as three in the former condition with component Pb^{207} (a) appearing the most intense in the pattern. The component due to Pb^{208} was the first to reverse with increasing temperature. This component was not as easily reversed as the corresponding component of λλ2833, 3683, and 3639.

[14] Hill, Proc. Nat. Acad. Sci. **15**, 779 (1929).
[15] Schüler and Jones, Naturw. **20**, 171 (1932).

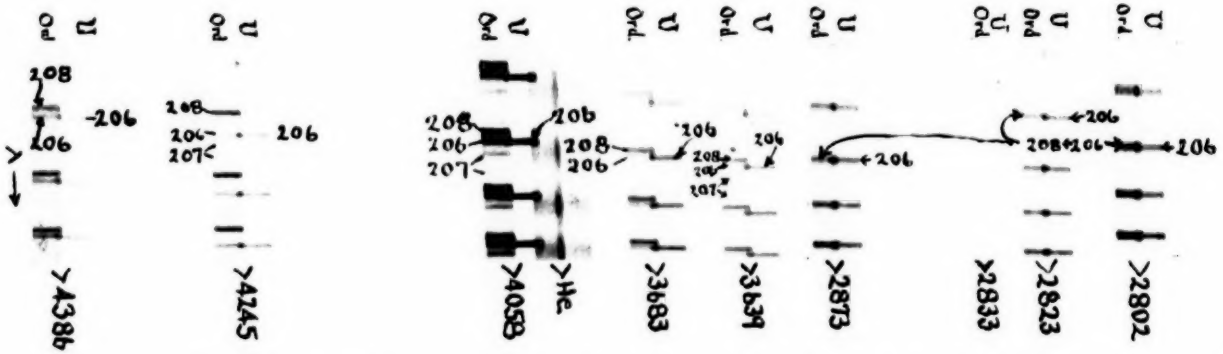

Fig. 7. Juxtaposed Lummer-Gehrcke plate patterns with cool cathode for uranium-lead (right) and ordinary lead (left). The exposure for λλ2873, 2823, and 2802 with ordinary lead was too short to show the Pb^{207} components. The reproductions for the lines above and below λ3639 were made from different photographic plates.

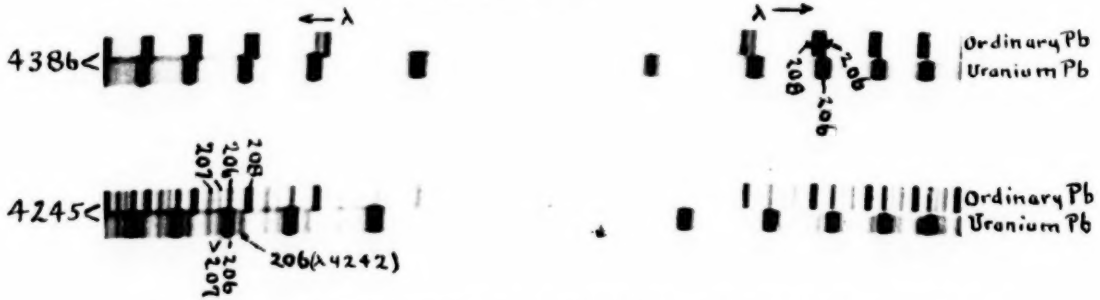

Fig. 8. A moderate exposure of ordinary lead (left) with cool cathode and a very long exposure of uranium-lead (right) with very hot cathode. The pattern of λ4245 for uranium-lead consists of the very intense Pb^{206} line and two components of Pb^{207}; no trace of Pb^{208} can be detected. The line which appears displaced slightly to the right of λ4245 is λ4242 (Pb^{206} for uranium-lead). No components of λ4242 for ordinary lead can be seen in this reproduction.

λ 3683

A very faint component appeared near the Pb^{206} line with a very long exposure and with low currents in condition *A*. It was impossible to measure this component, but it was estimated to be not over 0.12 cm^{-1} from Pb^{208}. A small increase of current in condition *A* was sufficient to cause the two main lines to fuse together and to appear as one very broad line. A further increase of current made this very broad line appear as three sharp equally spaced lines; with a very hot cathode the center one of the triplet nearly vanished and the outside ones were separated still farther and quite intense. See Fig. 3. A much cooler cathode must be used for this line than for λλ4058 or 3639.

λ 3639

The patterns for λ3639, reproduced in Figs. 3, 4, 5, and Fig. 7, were obtained by the Lummer-Gehrcke plate of thickness, $t = 6.55$ mm. The orders for (b) and (c) of Pb^{207} overlapped with this plate and these two components appeared as one. The fourth component of Pb^{207} was too close to a strong component to be observed with either plate.

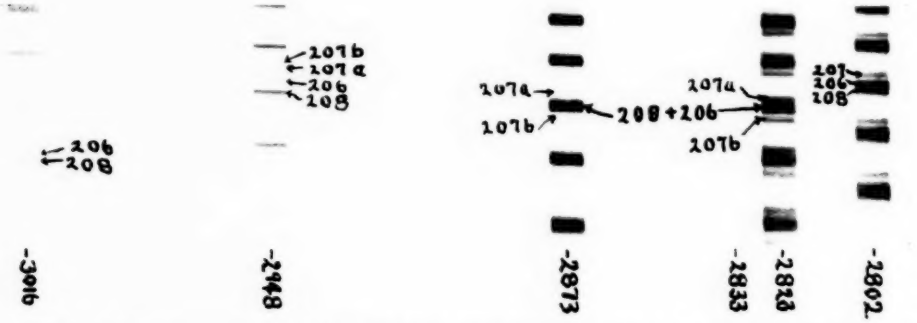

Fig. 9. These patterns were obtained by a long exposure with a hot cathode. The strong component of λ2802 appears to be slightly reversed. A very faint trace of λ2833 can be seen.

λλ 2873 and 2802

One very weak component for λ2802 and two very weak components of about equal intensity for λ2873 could be photographed with a twelve hour exposure in condition *A* and a one hour exposure in condition *B*. The principal component for each of these lines was very broad and intense. It appeared on the photographic plates with a short exposure in either condition. The patterns of these lines did not seem to change with the temperature of the cathode, although in some photographs there is evidence that λ2802 is subject to reversal before λ2873. See Fig. 9. The single Pb^{206} line of uranium-lead was thought to fall on the long wave wide of the center of the broad ordinary lead component. The above separations are from the center of the very heavy principal component.

λ 2833

This resonance line, the most difficult to obtain without reversal, has four components. With currents as low as 0.1 amp. and exposures up to fifteen

hours it was possible to obtain the pattern of this line without reversal. Its pattern changed with larger currents in such a way that it could not be recognized as the same line; with still larger currents, on the border of condition *B*, it practically disappeared. See Figs. 7 and 9.

λ 2823

This line is too weak to obtain its Lummer pattern when conditions are the best for getting good photographs of λ2833. In condition *B* exactly the reverse is true. On one plate the conditions were such that the patterns of both lines were of equal intensity. In conditions *A* and *B*, when its pattern appeared, it has three components. See Fig. 9. Its main component is broad but not as broad as λλ2873 and 2802, although its two weaker components are relatively much stronger than the weak components of λλ2873 and 2802. No marked reversal was observed even though the lead vapor pressure was very high. The uranium-lead line coincided with the main component; so it should be expected that this apparent component is unresolved and due to both Pb^{206} and Pb^{208} as in the case of λλ2873 and 2802. The intensities of Pb^{207} (a) and Pb^{207} (b) are sufficient to account for the two stronger components of Pb^{207} predicted by theory; this does not seem to be the case with the other two lines. Although components Pb^{207} (a) and Pb^{207} (b) of λ2823 were fairly intense, it was possible for them not to appear on a photographic plate even though the main component appeared quite dense. See Fig. 7.

λ 2614

It was difficult to measure this line since it and λ2613 almost completely overlapped each other. Measurements made on plates which were taken when the tube was being run with considerable power showed two components of nearly equal intensities with separation of 0.190 cm^{-1}. One heavy broad component was observed with smaller currents in condition *A* with long exposures. The previously observed separation must have been due to self reversal.

λ 2613

This line, which was many times weaker than λ2614 in condition *A*, became nearly as strong as λ2614 in condition *B*. It did not seem to be subject to any great reversal and appeared single and broad on all plates.

λλ2663, 2577, and all other strong lines down to λ2393 have appeared on a few plates in one condition or the other with fair intensity. All of them have a very broad single component with no suggestion of any weaker components. The strong lines below 2600A were less intense than those above and it was more difficult to use a Lummer plate in this region; so it might be that the principle component is a combination of the single components of Pb^{206}, Pb^{208}, and the strongest one of Pb^{207}, while other components due to Pb^{207} were too weak to appear with the exposes which have been used.

Measurements of the Line Patterns of Pb II

λλ 4386 and 3016

These lines, members of the same series, showed only two components. The Pb^{207} components must be very close together and nearer to Pb^{206} than

TABLE II. *Hyperfine structure of Pb II lines.*

λ	Classification	Components	$\Delta\nu$ cm^{-1}	$\Delta\lambda$A	Order of intensities	(Theoretical) Expected relative intensities for Pb^{207} components
5372.11*	$6p^2D_{5/2}-5f^2F_{7/2}$	207(b)	+0.388	−0.111	4	(27, 1, 20)
		208	0.000	0.000	1	
		206	−0.275	+0.079	2	
		207(a)	−0.576	+0.166	3	
4386.57	$6d^2D_{3/2}-5f^2F_{7/2}$	208	0.000	0.000	1	(14, 1, 9)
		206	−0.086	+0.017	2	
4244.99	$6d^2D_{5/2}-5f^2F_{7/2}$	207(b)	+0.286	−0.051	4	(27, 1, 20)
		208	0.000	0.000	1	
		206	−0.199	+0.036	2	
		207(a)	−0.424	+0.076	3	
3786.24	$6p^2D_{3/2}-5f^2F_{5/2}$	207(b)	+0.330	−0.047	4	(14, 1, 9)
		208	0.000	0.000	1	
		206	−0.415	+0.060	2	
		207(a)	−0.571	+0.082	3	
3016.61	$6d^2D_{3/2}-6f^2F_{5/2}$	208	0.000	0.0000	1	(14, 1, 9)
		206	−0.078	0.0071	2	
2948.72	$6d^2D_{5/2}-6f^2F_{7/2}$	207(b)	+0.293	−0.029	4	(27, 1, 20)
		208	0.000	0.000	1	
		206	−0.199	+0.017	2	
		207(a)	−0.416	+0.036	3	

* From the measurements of Janicki.

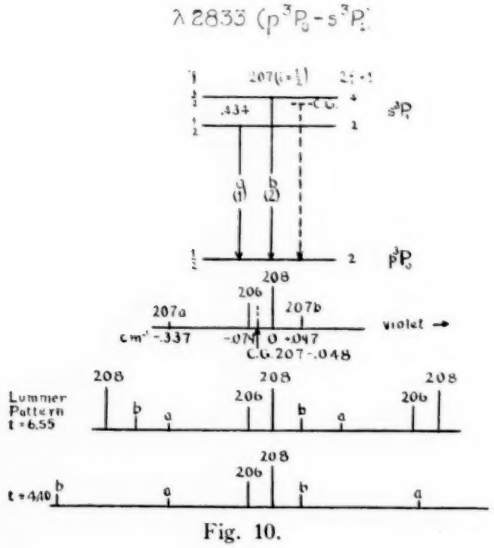

Fig. 10.

to Pb^{208} since they can not be seen in the photographs with uranium-lead, when Pb^{208} is absent. This is shown for λ4386 in Fig. 8 with the strong exposure of uranium-lead for which Pb^{207} components appeared in the pattern of λ4245.

λλ 4245 and 2948

These members of another series have also nearly identical patterns. The line structure of λ4245 reproduced in Figs. 4, 5, 7, and 8 was obtained by use of the large Lummer-Gehrcke plate while that of λ2948 in Fig. 9 was obtained with the small plate, which has a larger spectral range.

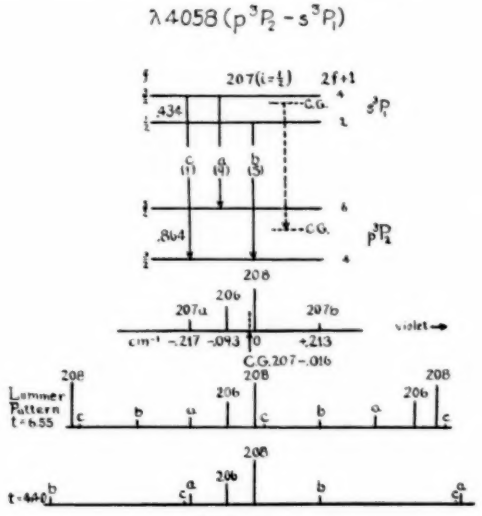

Fig. 11.

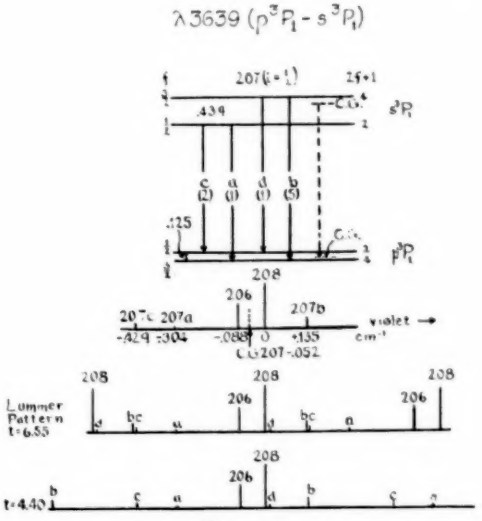

Fig. 12.

λ 3786

Only two photographs of λ3786, one with each Lummer-Gehrcke plate, were sufficiently good for measuring the separations of the components. The above values for the displacements of the Pb^{207} components are not as accurate as that for Pb^{206} with respect to Pb^{208}.

λ 5372

The measurements of this line by Janicki[3] have been included in order to compare the isotope displacement of Pb^{206} with respect to Pb^{208} with the displacements found in other lines.

Assignments of Levels to Pb^{207} I Lines

In the Figs. 10, 11, and 12 the theoretically determined values of the relative intensities of the components of Pb^{207} for $i=\frac{1}{2}$ and the possible transitions are indicated for λλ4058, 3639, and 2833. The line patterns of the two quartz Lummer-Gehrcke plates ($t=6.55$ mm and 4.40 mm) are also shown. With these data it is possible to find the hyperfine splitting of the $p^3P_{0,1,2}$ and $s^3P_{0,1}$ levels of Pb^{207} I.

The above measurements for the pattern of λ2833 give the separation of s^3P_1 to be 0.434 cm^{-1} since the final level of this line has no splitting. Although the weakest component, Pb^{207} (c) of λ4058 can not be seen with either Lummer plate, the separation of the final level can be found, however, by using the above value of the initial level, determined from λ2833, and the separation of components, Pb^{207} (a) and Pb^{207} (b) of λ4058. A separation of 0.864 cm^{-1} for p^3P_2, the final level for λ4058, agrees with the patterns and in addition explains why Pb^{207} (c) was not observed. This weak component in the case of each Lummer pattern would appear too close to a very strong component to be seen. From λ3639 the splitting of s^3P_1 is found to be 0.439 cm^{-1}; the levels of p^3P_1 are inverted and separated 0.125 cm^{-1}. This shows that component Pb^{207} (d) of λ3639 practically coincides with a very strong component and would not be expected to appear. The splitting of p^3P_1 could also be determined from λ3683 if the two predicted components of Pb^{207} had been seen, in as much as the initial level for this line has no splitting. It was observed, however, in the pattern of this line that the maximum separations of the components could not be more than 0.12 cm^{-1}, which in turn should be the maximum separation of the final level. This observation qualitatively agrees with the result for p^3P_1 obtained from λ3639.

Table III. *Separation of the hyperfine levels of Pb^{207} I.*

Term	Separation	Nature of term
s^3P_0	0.000 cm^{-1}	——
s^3P_1	0.436 "	regular
p^3P_0	0.000 "	——
p^3P_1	0.125 "	inverted
p^3P_2	0.864 "	regular

The separation for s^3P_1 is in agreement with 0.430 cm^{-1} found by Schüler and Jones[15] from the pattern of λ7228 $p^1D_2-s^3P_1$. The above separations and the patterns of λλ2873, 2823, 2802, 2614, 2613, 4168, 4062, and 4019 should enable one to find the nature of $d^3D_{1,2}$, $d^3F_{2,3}$, and p^1D_2. Two independent calculations for d^3F_2 and three for p^1D_2 were made. Very poor agreement for the several possible values for these levels was obtained. This appears to be further evidence of something incorrect in the classification of some of the lines discussed above.

Isotope Displacement

Measurements showed that the displacement of Pb^{206} with respect to Pb^{208} did not vary directly with the wave-length, although the separation was much larger for Pb I above 3500A than below with the exception of λ2833. The displacements above 3500A varied from 0.065 cm^{-1} to 0.092 cm^{-1} for the different lines with the Pb^{206} component always on the long wave side of Pb^{208}. Even though these displacements are much larger than that expected from the Bohr mass correction to the Rydberg constant, it has been found in the spark spectrum that the displacements for λλ5372, 4245, 3786, and 2948 are several times the maximum displacement found in the arc lines.

With the line patterns and the splitting of the levels known for λλ3639, 4058, 2833, and 3683, the Pb^{207} displacements with respect to Pb^{208} and Pb^{206} can be calculated. This was done by considering the center of gravity of the initial and final term levels of each line, and the displacement as the result of the splitting of the terms was calculated for one of the components of Pb^{207}. By the center of gravity of a split term is meant the weighted mean of the terms values of the sublevels, each sublevel being given the relative weight $2f+1$ (its statistical weight). The center of gravity of the hyperfine levels of Pb^{207} coincides with the position which the term would have were it not split. The broken line in Figs. 10, 11, and 12 represents the Pb^{207} line for

TABLE IV. *Isotope displacement of Pb^{206} and Pb^{207} with respect to Pb^{208}.*

λ	Pb^{206} $\Delta\nu$ cm^{-1}	C.G. of Pb^{207} $\Delta\nu$ cm^{-1}
Pb I		
7228*	−0.088	−0.055
4168	−0.065	
4062	−0.075	
4058	−0.093	−0.016
4019	−0.069	
3739	−0.089	
3683	−0.085	−0.04‡
3671	−0.092	
3639	−0.088	−0.052
3572	−0.069	
2873	Very small	
2833	−0.079	−0.048
2823	Very small	
2802	" "	
2663	" "	
2614	" "	
2613	" "	
2577	" "	
Pb II		
5372†	−0.275	
4386	−0.086	
4245	−0.199	
3786	−0.415	
3016	−0.078	
2948	−0.199	

* The measurements for this line were made by Schüler and Jones.
† The measurements for this line were made by Janicki.
‡ This result is only an estimate since the positions of the Pb^{207} components for λ3683 could not be measured. The uncertainty is estimated to be ±0.01 cm^{-1}.

TABLE V. *Term displacement with respect to Pb^{208}.*

Term	C.G. Pb^{207} $\Delta\nu$ cm^{-1}	Pb^{206} $\Delta\nu$ cm^{-1}
s^3P_0	−0.01*	−0.003
s^3P_1	0.000	0.000
p^3P_0	−0.048	−0.079
p^3P_1	−0.052	−0.088
p^3P_2	−0.016	−0.093

* The uncertainty of this result is ±0.01 cm^{-1} since the displacement for the center of gravity of Pb^{207} for λ3683 was used; cf. isotope displacement of λ3683 in Table IV.

no splitting of the terms. The results for the displacements of Pb^{207} and Pb^{206} with respect to Pb^{208} are given in Table IV.

The above isotopes displacements for λλ4058, 3683, 3639, and 2833 are in very good agreement with the displacements of Pb^{206}, Pb^{207}, and Pb^{208} found by Schüler and Jones[15] from the pattern of λ7228.

The relative displacements of the terms, $s^3P_{0,1}$ and $p^3P_{0,1,2}$, for Pb^{206}, Pb^{207}, and Pb^{208} can be determined from the isotope displacements in the line patterns of λλ4058, 3683, 3639, and 2833. The term displacements given in Table V were found by arbitrarily considering no displacements for s^3P_1. The way in which the terms, with the exception of Pb^{207} for s^3P_0, fall in the order of their masses is in agreement with the results of Schüler and Keyston[16] for Hg. Since the uncertainty for Pb^{207} of s^3P_0 is much greater than the given displacement for Pb^{206}, the order of this term can not be definitely determined. The results for s^3P_0 do show, however, that the displacements for this term are approximately the same as those for s^3P_1. With the exception of Pb^{207} for p^3P_2, the relative isotope separations for the triplet term, $p^3P_{0,1,2}$, are found to be of the same order of magnitude.

In conclusion the authors wish to express their appreciation to Professor G. Breit, who suggested this problem, for his generous interest and advice throughout the progress of the investigation. We are also indebted to Professor R. W. Wood of Johns Hopkins University for the loan of the two Lummer-Gehrcke Plates and a quartz fluorite lens, to Professor J. P. Simmons of the Chemistry Department for the use of chemical equipment, to Dr. E. W. Riblett for the purification and reduction of the uranium-lead, and to all who have assisted us in obtaining samples of uranium-lead. Thanks are also due to Mr. Herman Beck for the construction of the discharge tubes.

Note added in Proof: May 14, 1932

After the manuscript for this article was sent to the editor, an article on the hyperfine structure of lead by Kopfermann[17] was received. Practically all of his measurements of the line patterns agree with those reported by us. He was able apparently, to resolve and measure the separations of Pb^{208} and Pb^{206} for several lines which we reported to be very small. Two components of Pb^{207} for λ4062 were observed by him in which case we had seen only one,

[16] Schüler and Keyston, Zeits. f. Physik **72,** 433 (1931).

[17] Kopfermann, Zeits. f. Physik **75,** 363 (1932).

while the Pb^{207} components for λλ4168 and 4019 measured by us were not included in his measurements. The principal difference in the results of the two articles is in the value for the regular splitting of p^3P_2 given by him to be approximately 0.220 cm^{-1}. Our value, 0.864 cm^{-1}, was found by considering the two visible Pb^{207} components of λ4058 to be those with relative intensities 9 and 5. Kopfermann considered them to be the components, predicted by theory, with relative intensities 5 and 1. He was able to see the strongest component with intensity 9 in the position of Pb^{208} when uranium-lead was used. This was possible since uranium-lead contains a smaller abundance of Pb^{208} than Pb^{207}.

With a sample of uranium-lead we have tried to see this component of Pb^{207}. Several high resolving power instruments and different types of photographic plates have been used. Due to the large difference in the relative abundance of Pb^{207} and Pb^{206}, the Pb^{206} line had to be very much overexposed in order to see this component of Pb^{207}. Since the component is very close to Pb^{206} it could be easily masked by the photographic broadening of the intense Pb^{206} line caused by overexposure. From over twenty five photographic exposures of λ4058 with uranium-lead, only two or three plates seemed to indicate the presence of the Pb^{207} component which was observed by Kopfermann. One of these plates is better than any of the others as judged by the sharpness of other lines, and makes us believe that Kopfermann's interpretation is correct. The patterns of this line for ordinary lead were again observed. With a very cool cathode it is possible that the relative intensities of Pb^{207} (a) and Pb^{207} (b) may be 5 and 1, but on plates taken with a slightly higher temperature of the cathode the ratio of the relative intensities of these components is certainly less than 5 to 1. Using the interpretation of the line pattern of λ4058 given by Kopfermann, the regular splittings of s^3P_1 and p^3P_2 from our measurements of λ4058 are 0.430 cm^{-1} and approximately 0.213 cm^{-1}, respectively. With this value for p^3P_2 the isotope displacement of Pb^{207} with respect to Pb^{208} becomes -0.058 cm^{-1} instead of -0.016 cm^{-1} as given above. This result fits in better with the displacements of Tables IV and V.

The splittings of d^3D_2, d^3F_3 and d^3F_2 were found by Kopfermann to be 0.255 cm^{-1} (regular), 0.250 cm^{-1} (regular), and 0.130 cm^{-1} (inverted), respectively. Considering the splittings of p^3P_2 to be 0.213 cm^{-1}, our measurements for the line patterns of λλ2873 and 2823 give splittings for d^3D_2 and d^3F_2 to be of the same order as that above. The relative intensities of the components of λ2802 on our plates are such that a regular splitting of 0.250 cm^{-1} for d^3F_3 does not appear to be correct. For λ2802 three components of Pb^{207} with relative intensities 20, 14, and 1 are predicted by theory. With a splitting of 0.250 cm^{-1} for d^3F_3 the two stronger components of Pb^{207} would nearly coincide in the line pattern of λ2802. Only one apparent component of Pb^{207} was observed by us, and its intensity with a cool cathode is much too small to account for both of the stronger components of Pb^{207}. A hotter cathode, which does not seem to give the correct relative intensities for the components of λ4058, shows an increase in the intensity of the apparent Pb^{207} component. A comparison of the relative intensities of the components of

λλ2823 and 2802 in Fig. 9, a reproduction of a plate obtained by using a very hot cathode, shows that the apparent Pb^{207} component of λ2802 can not account for both of the stronger components of Pb^{207}. If it should be due to the stronger components, the center of gravity of Pb^{207} would not fall between Pb^{208} and Pb^{206} as it does for other lines.

Kopfermann's results for d^3D_2 and d^3F_3 could be verified however, by observing another Pb^{207} component for each of the lines λλ4168 and 4019 since Schüler and Jones[15] have found a regular splitting for p^1D_2, the final level for these lines, to be 0.049 cm^{-1}. The second Pb^{207} component for these lines would fall near Pb^{208} and should be observed by a long exposure with uranium-lead.

With the above data it is possible to make a comparison with theory. Defining with Goudsmit[18] the interaction constant A by

$$W(j) = [A(j)/2]\ [f(f+1) - i(i+1) - j(j+1)]$$

letting a', a'' be respectively the values of A for $ap_{3/2}$, $p_{1/2}$ electron moving in the same central field as each of the two equivalent p electrons, $(6p)^2$, responsible for the normal set of levels of Pb, the following relations hold:

$$3a' = A(^3P_1) + A(^3P_2) + A(^1D_2)$$

$$3a'' = 5A(^3P_2) + 5A(^1D_2) - 7A(^3P_1).$$

We obtain using $\Delta W(^3P_1) = -0.125$ cm^{-1}, $\Delta W(^3P_2) = 0.215$ cm^{-1}, $\Delta W(^1D_2) = 0.049$ cm^{-1} for $a'' = 0.370$ cm^{-1}, $a' = 0.007(4)$ cm^{-1}. It is very curious that the values obtained by Goudsmit[18] for the $(6p)^3$ configuration of Bi are $a'' = 0.375$ cm^{-1}, $a' = 0.007$ cm^{-1}. The value of a' is very sensitive not only to experimental errors but also to corrections which must be applied to the above simple theory on account of the energy differences of the three terms involved. On the other hand a'' is much less sensitive to such corrections. Thus even though a''/a' is greater than the possible theoretical value,[19] $5 \times 3.4 = 17$, it may be that these values are not real indications of disagreement with the theory. The agreement of a'' for Pb^{207} and Bi indicates on the other hand that the ratio of the magnetic to the mechanical moment is nearly the same for the two nuclei. It is also of interest that a'' for Tl is 0.71 cm^{-1}, a value nearly twice as large as the above.

[18] S. Goudsmit, Phys. Rev. **37,** 663 (1931); See table p. 675 and theory of pp. 668–669. Note that on account of intermediate coupling only sum rules are applicable without calculating complex parameters. See also G. Breit and F. W. Doermann, Phys. Rev. **36,** 1732 (1930); Discussion on p. 1750 and G. Racah, Zeits. f. Physik **71,** 431 (1931), the latter for discussion of intermediate coupling.

[19] G. Breit, Phys. Rev. **38,** 463 (1931); **37,** 1182 (1931); G. Racah, Cim. **8,** 178 (1931).

Mean Lives of Mercury Lines λ2537 and λ1849

By PAUL H. GARRETT
Physics Laboratories, Columbia University
(Received April 19, 1932)

The mean life of the mercury line λ2537 was measured by the alternating voltage method previously described by Webb. The radiation was excited in a quartz tube by impact with electrons from a hot cathode. The photoelectric system was contained in a separate tube also of quartz. The photoelectric surface was zinc evaporated on a nickel plate. Measurements of the apparent life were made with diminishing mercury vapor pressures until further reduction of pressure produced no change in the measured rate of decay of the radiation. At these low pressures (below 3×10^{-4} mm, for the geometry used) the absorption and reemission of the radiation was negligible and the true life of a single excitation process was measured. This was found to be 1.08×10^{-7} sec. with an estimated precision of one percent.

Absorption coefficient of λ1849. An absorption cell with a one mm thick absorbing layer of mercury vapor was mounted so as to move in and out between the excitation and photoelectric tubes used in the above measurements. The absorption of λ1849 was measured at pressures such that the absorption of λ2537 was negligible. From this the atomic absorption coefficient for the main component of the line was found to be 6.2×10^{-11} from which the mean life of the 2^1P_1 state was calculated to be 2.9×10^{-10} sec. with an estimated precision of 25 percent.

SEVERAL determinations have been made of the mean life τ of the 2^3P_1 state in mercury, which results in the radiation of λ2537. Eldridge,[1] v. Keussler,[2] Olson[3] and Hanle[4] measured the depolarizing effect of a steady magnetic field on the light from a mercury resonance lamp illuminated with polarized light and from the rate of the Lamor precession and its effect on the polarization of the radiation calculated τ. They give the values 0.88×10^{-7} sec., 1.13×10^{-7} sec., 0.98×10^{-7} sec., and approximately 10^{-7} sec. respectively. Fermi and Rasetti[5] and Breit and Ellett[6] determined τ to be of the order of 10^{-7} sec. by finding the period of the alternating magnetic field at which the depolarizing effect disappeared. Tolman[7] derived a formula relating τ to the absorption of the line and from the absorption measurements of Fuchtbauer, Joos and Dinkelacker[8] calculated τ to be 1.03×10^{-7} sec. Kopferman and Tietze[9] and Zemansky[10] used Tolman's formula but assumed the shape and breadth of both the emission and absorption lines in calculating

[1] J. A. Eldridge, Phys. Rev. **24,** 234 (1924).
[2] V. v. Keussler, Ann. d. Physik **82,** 793 (1927).
[3] H. F. Olson, Phys. Rev. **32,** 443 (1928).
[4] W. Hanle, Zeits. f. Physik **30,** 93 (1924).
[5] E. Fermi and F. Rasetti, Zeits. f. Physik **33,** 246 (1925).
[6] G. Breit and A. Ellett, Phys. Rev. **25,** 888 (1925).
[7] R. C. Tolman, Phys. Rev. **23,** 693 (1924).
[8] Chr. Füchtbauer, G. Joos and O. Dinkelacker, Ann. d. Physik **71,** 204 (1923).
[9] H. Kopferman and W. Tietze, Zeits. f. Physik **56,** 604 (1929).
[10] M. W. Zemansky, Phys. Rev. **36,** 219 (1930).

τ and found it to be 1.04×10^{-7} sec., and of the order of 10^{-7} sec., respectively. Ladenburg and Wolfsohn[11] measured the index of refraction of mercury vapor for wave-lengths very close to 2537A and calculated τ from a dispersion formula to be 1.14×10^{-7} sec. These methods are somewhat indirect. The first direct observation of the decay of the radiation was made by Wien.[12] The intensity of the radiation from the ions in a canal ray tube was found to fall off exponentially and from this rate of decay the mean life was calculated as 0.98×10^{-7} sec. Interpretation of his results is somewhat difficult since, due to the method of excitation, it is impossible to determine when and how the atom is excited to the state in question.

Webb and Messenger[13] investigated the persistence of λ2537 excited in mercury vapor by electron impact using the method described below. Due to absorption and reemission of the radiation the persistence changed with the concentration of mercury atoms through which the radiation passed. As the concentration was reduced the persistence approached a limiting value which is the mean life of the excited 2^3P_1 state. However the construction and sensitivity of their experimental tube did not permit a precise determination of τ. The present investigation was undertaken to make a more precise determination of τ using more sensitive and more advantageously designed apparatus.

Method

The method used was one previously developed in this laboratory[14] in which the excitation was produced by electron impact excited by alternating voltages in such a way that excitation occurred only during the positive half cycles. The radiation was detected by a photoelectric system to which were applied alternating voltages of the same frequency and phase as those applied to the excitation system so that there was practically no current to or from the photoelectric surface during the negative half cycles. For very low frequencies ("zero frequency") practically all the energy is radiated during the positive half cycle and there is a maximum photoelectric current; while as the frequency is increased, due to persistence of the radiation, an increasing fraction of the energy arrives at the photoelectric system during the negative half cycles, so that the resulting electrometer current is decreased. For the photoelectric system used, at infinite frequency the current dropped to approximately 50 percent of its value at "zero frequency." The relation of the electrometer current to the frequency is usually expressed as the variation with the frequency of the ratio, R, of the electrometer current at any given frequency to that at "zero frequency," and will be referred to below as the "R-frequency" curve. To calculate τ from this relation it is necessary to assume the law governing the falling off of the radiation after the instant of excitation. It is assumed throughout that this law follows an exponential rela-

[11] R. Ladenburg and G. Wolfsohn, Zeits. f. Physik **65,** 207 (1930).

[12] W. Wien, Ann. d. Physik **73,** 483 (1924).

[13] H. W. Webb and H. A. Messenger, Phys. Rev. **33,** 319 (1929).

[14] H. W. Webb, Phys. Rev. **24,** 113 (1924); F. G. Slack, Phys. Rev. **28,** 1 (1926); reference 13; R. H. Randall, Phys. Rev. **35,** 1161 (1930).

tion and from the form of the excitation-time curve of the excitation system and the characteristics of the photoelectric system the value of τ may be determined by suitable integrations from the R-frequency curves. In the simple case where the excited radiation varies with the time according to a sine law during the positive half cycle and the photoelectric current falls from saturation value to zero immediately after the reversal of the voltage, these integrations can be made analytically and we find that:[15]

$$1/\tau = 2\pi f_{1/2} \tag{1}$$

where $f_{1/2}$ is the frequency at which the R-frequency curve has dropped halfway to its final value at infinite frequency. If the above conditions do not obtain then the integrations involved in calculating τ must be done either partially or completely by graphical methods. However in most cases τ is given by Eq. (1) to within 10 percent.

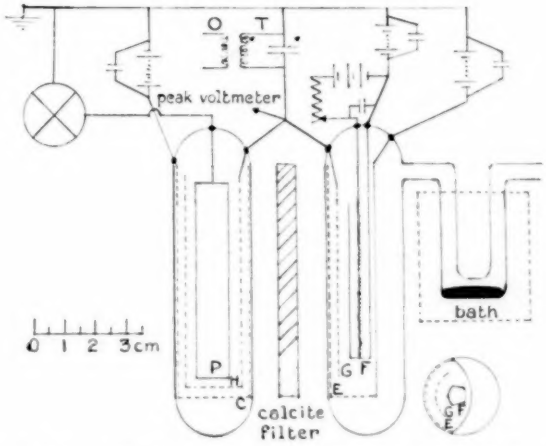

Fig. 1. Schematic diagram of apparatus and electrical circuits.

Apparatus

The excitation and photoelectric systems were put in separate experimental tubes. This had the advantage that no metastable atoms excited by electron impacts could reach the photoelectric surface and there set electrons free, and the further great advantage that the path through mercury vapor traversed by the radiation was shortened and hence the chance of absorption and reemission was greatly reduced. Fig. 1 is a schematic diagram of the apparatus showing the essential parts drawn to scale.

The excitation system was in a tube of fused quartz containing three electrodes, F, G and E. F was a hollow, unipotential, hot cathode made of platinum sheet with a tungsten heater down the center. The surface facing G was coated with oxide. G was an accelerating grid made of 0.17 cm mesh nickel gauze. E was a shielding grid made of 0.34 cm mesh nickel gauze with a nickel sheet portion back of F. This experimental tube was connected to a

[15] Reference 13, pp. 321–322.

mercury diffusion pump which was operating whenever observations were being taken. Between this tube and the pump, surrounded by a bath in a Dewar flask, was a mercury well which controlled the vapor pressure in the excitation system. The temperature of the bath was thermostatically controlled so that it could be held constant to within 0.3°C at any given temperature from 0°C to −40°C. When the bath was used at temperatures below environment the necessary cooling was obtained by a copper rod which made thermal connection between the bath and a hopper filled with carbon dioxide snow. The size of the rod was so chosen that it carried off heat a little more rapidly than the bath gained heat from the surroundings which difference was supplied by a small electric heater controlled by the thermostat. A mechanical stirrer was used.

The photoelectric system was in a tube of fused quartz and contained three electrodes *P*, *II* and *C*. *P* was the light sensitive surface and was a nickel cylinder onto which a film of zinc had been evaporated. *II* was a collecting grid of 0.17 cm mesh, and *C* a shielding grid of 0.34 cm mesh nickel gauze. In preparing this tube it was baked at 450°C and pumped for several hours before the zinc was deposited. While depositing the zinc the cylinder *P* was cooled by passing water through a reentrant tube (not shown on the diagram) while the rest of the system was kept hot. A freeze-out trap between the tube and the pump was immersed in liquid air which prevented any mercury from going into the photoelectric system. This tube was sealed off with residual gas at a pressure of less than 10^{-5} mm of mercury.

Zinc was chosen for the surface *P* since radiations of wave-length longer than about 3000A do not effect it appreciably. Between the excitation and photoelectric tubes was placed a filter 10.5 cm long 2.0 cm wide and 0.7 cm thick made of calcite split from a large block so that the surfaces were unscratched. Calcite absorbs radiations shorter than about 2100A. Hence only radiations from the excitation tube lying between 2100A and 3000A produced any appreciable photoelectric current.

The cathode was heated by a 12 volt storage battery and all other d.c. voltages were supplied by small dry cells. The alternating voltages were supplied by two vacuum tube oscillators, 0, using the Hartley circuit. One had a fixed frequency of 40,000 cycles (equivalent to "zero frequency" for the mean life of λ2537) and the other one was variable from 10^5 to 10^7 cycles. Care was taken to keep the wave form of these voltages simple sinusoidal. The voltage applied to the experimental tubes was the drop across the condenser in a tuned circuit, *T*. This circuit was tuned sharply and was coupled inductively to the oscillators with the coupling very loose. In order that the a.c. component of the emission current which passed through this circuit should not effect the wave form of the voltage applied to *G* and *H*, the coil was made with very few turns and the condenser was correspondingly large. The tests for wave form described in earlier papers[16] were made for each frequency. These tests are very necessary when high frequencies are used. They indicated that at no time was error introduced due to faulty wave form.

[16] H. W. Webb, reference 14, pp. 119–120.

G and H were connected directly and given the same a.c. voltage since with any other circuit indeterminable phase shifts between them were difficult to avoid when using high frequencies. A peak voltmeter with a microammeter in the grid circuit was used to measure the amplitudes of these voltages. With this circuit the peak voltage could be measured to one percent and when determining the ratio of the electrometer current at high to that at the reference low frequency the peak voltages at the two frequencies could be made the same to within one tenth of one percent. The frequency was measured to within one half of one percent with a wavemeter which was calibrated against the harmonics of a known oscillator.

The photoelectric currents were measured with a Compton quadrant electrometer of about 8000 mm per volt sensitivity.

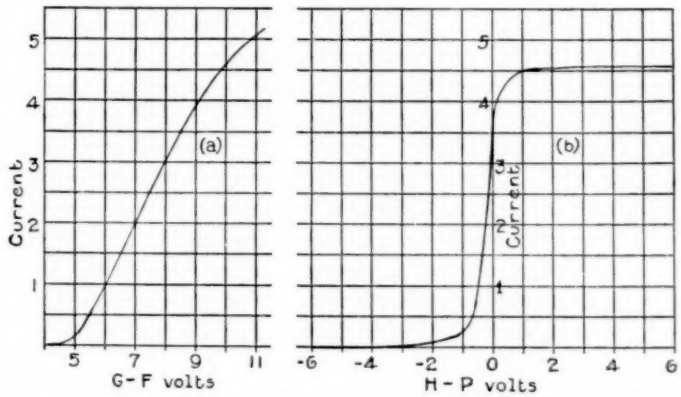

Fig. 2. Curve (a), typical excitation curve. Curve (b) photoelectric characteristic.

Experimental and Results

In determing the R-frequency curves the procedure was as follows. With liquid air around the mercury well the excitation tube was baked at 400°C for several hours to make sure that no drops or films of mercury remained in the tube. The mercury well was then immersed in the bath which had previously been set at the desired working temperature which was held constant throughout a series of observations. To ensure equilibrium no observations were taken until at least twleve hours after immersion in the bath. The steady current characteristics of the excitation and photoelectric tubes were then found. Typical curves showing these characteristics are reproduced in Fig. 2. In determining the characteristic excitation curve, (a) Fig. 2, which gives the relation of the accelerating voltage of the electrons in the excitation system to the excitation of radiation as measured by the photoelectric effect, E and F were always at the same voltage which voltage was negative and variable. The other voltage conditions were: $G=0$, $C=7.5$, $H=9.0$, and $P=0$ volts. For the photoelectric characteristic curve, (b) Fig. 2, which shows the variation of the photoelectric current with the voltage $H-P$ for constant radiation falling on the surface, the conditions were: $E=F=-10.0$, $G=0$, $C=7.5$, $P=0$, and H variable from -6.0 to $+6.0$ volts. After making the

tests for wave form and proper functioning of the apparatus, the electrodes, F and E were set at -5.1 volts, G, H and P at zero volts and an alternating voltage, usually 6.0 volts peak value, was impressed on G and H. The ratio R of the electrometer current at high frequency to that at the reference low frequency was then determined as a function of the frequency. An example of the resulting R-frequency curve is shown in (a) Fig. 3 where the ordinates are the current ratios and the abscissas are the frequencies. From this curve τ was calculated by the use of Eq. (1).

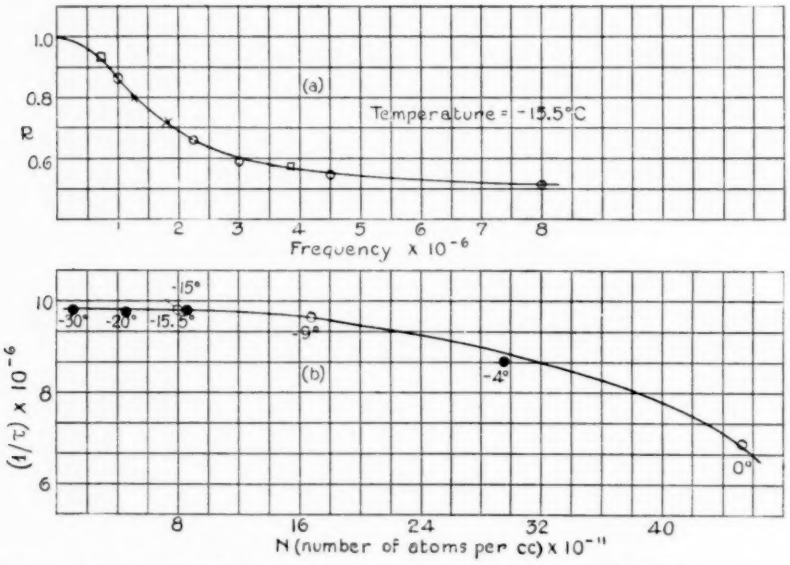

Fig. 3. Curve (a), typical R-frequency curve. Curve (b) persistence of $\lambda 2537$ vs. concentration.

Following the same procedure as above τ was determined for different mercury vapor pressures in the excitation tube. Its variation with the concentration of mercury atoms is shown in curve (b) Fig. 3 where the values of the reciprocal of τ are the ordinates and the mercury vapor concentrations are the abscissas. The temperatures marked on the curve are those of the mercury well while N is the concentration after correcting for the temperature of the excitation tube. It will be noted from the curve that for values of N greater than 8×10^{11} τ begins to increase being about 40 percent larger at 0°C than at -15°C. The rate of increase of τ with vapor pressure (due to absorption and reemission which lengthens the apparent life) is determined by the depth and shape of the layer of mercury vapor passed through by the radiation and is therefore dependent on the geometry of the excitation tube. The particular curve shown includes data from excitation tubes in which the emergent radiation had traversed layers of vapor of approximately the same thickness. This curve shows that at well temperatures less than about -15°C a further decrease in pressure produces no measureable change in τ so that the persistence measured at these pressures is the mean life associated with the initial excitation and radiation process. It should be noted that the values of τ

shown on this curve are uncorrected for the departure from a simple sinusoidal form of the excitation-time curve (i.e., the relation of the excitation to the time during the positive half cycle) and for the difference of the actual photoelectric current characteristic from the ideal one assumed in deriving Eq. (1). (Actually this current dropped from maximum to zero in about one sixth of a period instead of immediately after the reversal of the voltage.)

A precise determination of the mean life was then made. With a well temperature of $-20°C$ the steady current characteristics of the experimental tubes were carefully determined. It was found that the excitation-time curve could be expressed with necessary precision by the first three terms of a sine series extending through the positive half cycle. Assuming that radiation excited at time $t=0$ decreased according to the exponential $e^{-t/\tau}$, and integrating over the excitation-time curve the emission of the radiation as a function of the time was found for a given frequency. This integration was done analytically. By multiplying the radiation arriving at the photoelectric surface at successive times by the corresponding ordinates of the experimentally determined photoelectric characteristic, the relation of the photoelectric current to the time was then found. The integration of this curve gave the electrometer current. This latter integration was necessarily done graphically. This calculation was carried out for the reference low frequency and for several frequencies near the half value ($f_{1/2}$) so that the form of the R-frequency curve as a function of the product of this frequency and the unknown τ, was accurately known in this region. The ratio R was then determined experimentally for several frequencies near the half value. Thirty observations of R were taken for each frequency which determined the values of this ratio with a precision of one percent. From these values and the calculated curve the value of τ, the mean life of the 2^3P_1 state, was found to be 1.08×10^{-7} sec. with an estimated precision of one percent.

These measurements of τ might be in error if transitions other than $1^1S_0-2^3P_1$ were present in sufficient amounts. If the radiation associated therewith produced appreciable photoelectric action and the mean life were different from that being measured, or if the transitions were to the 2^3P_1 state whether the corresponding radiation effected the photoelectric surface or not, the persistent radiation would vary with the time in a more complex way (due to the several lives involved) and the R-frequency curves would not have the form calculated above. The lines $\lambda2655$, $2^3P_1-4^1D_2$ and $\lambda4358$, $2^3P_1-2^3S_1$, are two possible cases of transitions followed by $1^1S_0-2^3P_1$. We know that the mean life of $2^3P_1-2^3S_1$ is approximately one half of that of the 2^3P_1 state[17] and would expect a measureable delay in the emission of $\lambda2537$ if the 2^3S_1 state were excited to a marked degree. Experimentally however these curves were always found to have the calculated form. A further test was made by determining the ratio R at a given frequency with the peak value of the alternating voltage at 6.0; 5.0, 4.0, and 2.5 volts in turn. If transitions other than $1^1S_0-2^3P_1$ were effecting τ appreciably R would change with the above changes in voltage. No such change was observed. These tests indi-

[17] R. H. Randall, reference 14, p. 1167.

cate then that the persistence measured is the true mean life of a single atomic process in question.

Absorption Coefficient of λ1849

The apparatus used in the measurement of the life time of λ2537 was, with minor changes, found to be adaptable for the measurement of the absorption coefficient of mercury vapor for λ1849, and so a determination of this quantity was made in order to form an estimate of the mean life of the 2^1P_1 state. The calcite filter used cut out 30 to 60 percent (depending on the excitation voltage) of the total radiation excited in the excitation tube. This radiation was of wave-length shorter than about 2100A, for the most part λ1849. As found above the absorption of λ2537 is negligible by layers of mercury vapor not thicker than 3 or 4 mm and concentrations not greater than 8×10^{11} atoms per cc, while the absorption of λ1849 is of a convenient magnitude for measurement.

A screen with a 1.3 cm aperture was put immediately in front of the photoelectric tube which was placed 7.5 cm from the excitation tube. Midway between the photoelectric and excitation tubes was placed the absorption cell which was made by cementing into a metal frame two circular plates of crystal quartz 3 mm thick and 50 mm in diameter. The inner surfaces were one mm apart so that this was the thickness of the absorbing layer of mercury vapor. The absorption cell was connected to a mercury well, similar to that described above, which was connected to a mercury diffusion pump. The absorption cell, the well and the pump were mounted together on a slide so that the absorption cell could be readily moved in and out from between the excitation and photoelectric tubes. To compensate for the absorption of the quartz walls, when the cell was out two plates of quartz identical with the walls of the absorption cell were substituted.

Before the absorption cell was sealed into the system the well was cooled to a temperature below the environment and kept thereafter at a low temperature in order to prevent the formation of films or drops of mercury in the cell. In order to insure equilibrium, whenever the pressure in the absorption cell was changed the bath was held at the desired temperature for at least 24 hours before observations were taken.

The voltages used on the excitation and photoelectric tubes were: $P=E=F=0$, $G=85.0$, $C=9.0$ and $H=6.0$.

With a calcite filter, the absorption-wave-length characteristics of which were known, it was found that about 45 percent of the radiation was greater than λ2100, that is λ2537 and possibly some λ2200, the balance being λ1849 and other radiation of wave-length less than λ2100, probably the spark line λ1942. Of these only λ1849 suffered appreciably absorption in the cell. The amount of λ1849 was approximately 35 percent but as it was not possible to determine this value with sufficient precision the measurements were so made that this was unnecessary.

Let E_0 be the amount of λ1849 which falls on the photoelectric surface when the absorption cell is not in and let C be the amount of unabsorbable

radiation which falls on the photoelectric surface (which amount is constant), E_0 and C being measured in terms of photoelectric response. The total radiation falling on the photoelectric surface when the cell is out (i.e., when there is no absorption) is then E_0+C. Let E be the total amount of λ1849 falling on the absorption cell (also measured by photoelectric response) and let A be the fraction of it which is absorbed. Then the radiation falling on the photoelectric surface when the cell is in, is composed of three parts: (1) the unabsorbed portion of E_0 (2) the unabsorbable radiation C and (3) the part of AE which when reradiated reaches the photoelectric surface. If it is assumed that half the absorbed radiation goes forward and the other half goes back upon reradiation then this third part would be given by βAE where β is a fraction depending on the geometry of the apparatus. Let f be a function of the concentration in the cell which gives the ratio of the reradiated light which goes forward to that which would go forward if the above assumption were true. Then the radiation falling on the photoelectric surface when the absorption cell is in is: $E_0(1-A)+C+f\beta AE$ and the ratio r of the photoelectric response with the absorption cell in to that with the absorption cell out is:

$$r = \frac{E_0(1-A)+C+f\beta AE}{E_0+C} \tag{2}$$

from which:

$$A = \frac{(1-r)(1+C/E_0)}{(1-f\beta E/E_0)}. \tag{3}$$

Since the line has hyperfine structure A does not depend in a simple manner upon the absorption coefficients. If the components of the line do not overlap appreciably:

$$A = \frac{I_1A_1+I_2A_2+I_3A_3+\cdots}{I_1+I_2+I_3+\cdots} \tag{4}$$

where $I_1, I_2, \cdots$ are the intensities of the components and $A_1, A_2, \cdots$ are the absorptions experienced by each. Now if $(k_0l)_n$ is the product of the absorption coefficient for the center of the line and the thickness of the absorbing layer for the nth component it has been shown that:[18]

$$A_n = 1 - \frac{\int_{-\infty}^{\infty} \exp\left\{-\left[\omega^2(k_0l)_n e^{-(\Delta\nu_E/\Delta\nu_A\cdot\omega)^2}\right]\right\} d\omega}{\int_{-\infty}^{+\infty} \exp(-\omega^2)d\omega} \tag{5}$$

where l is the thickness of the absorbing layer and $\Delta\nu_E/\Delta\nu_A$ is the ratio of the breadths of the emission and absorption lines. Zemansky has evaluated the expression (5) for different values of $\Delta\nu_E/\Delta\nu_A$.[19] In the present experiments the breadth of both emission and absorption lines were due to Doppler

[18] M. W. Zemansky, reference 10.

[19] Reference 10, pp. 222–224.

effect (since the natural breadth may be neglected within the precision of the experiment) and $\Delta\nu_E/\Delta\nu_A$ was calculated to be 1.2. In curve (a) of Fig. 4 A_n is plotted against $(k_0l)_n$ for this value of $\Delta\nu_E/\Delta\nu_A$.

From the work of Schuler and Keyston[20] we find for λ1849 a hyperfine structure of six resolved lines of relative intensities: 5.5:6.8:69.9:4.5:11.0:2.3 The first and fifth are due to isotope 199, the second, fourth and sixth to isotope 201 and the third is due to the five even isotopes unresolved. The fourth and fifth lie close together and may be taken as a single line in calculating absorption, but the others are sufficiently separated that with the Doppler breadths met with in this experiment their overlapping may be neglected.

If the absorptions of the different isotopes be assumed proportional to their concentrations and if the relative absorptions of the components from one isotope be assumed proportional to the statistical weights of the end states involved, we find, after combining the values for the fourth and fifth

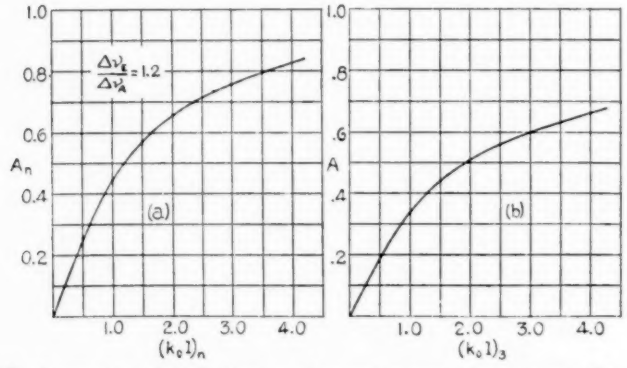

Fig. 4. Curve (a), absorption of single line vs. absorption coefficient. Curve (b), total absorption of λ1849 vs. absorption coefficient of strongest component.

lines, the relative values of (k_0l) for the components to be: 0.079:0.098:1.00 :0.22:0.033. Using Eq. (4) and curve (a) Fig. 4 we can now compute A as a function of $(k_0l)_3$, the absorption coefficient of the strongest component. The result is shown in curve (b) of Fig. 4, the total absorption A being plotted as ordinates and $(k_0l)_3$ as abscissas.

To find the value of $(k_0l)_3$ as a function of Nl, the product of the total concentration of mercury atoms and the thickness of the absorbing layer, the procedure was as follows. The ratio r was measured for several concentrations in the absorption cell. The results are shown in curve (a) of Fig. 5 where the ordinates are the values of r and the abscissas are the products of the number of atoms per cc times the thickness of the absorbing layer. The three points indicated by circles were taken with a pressure in the excitation tube corresponding to a well temperature of $-30°$C. The points shown by the square and the triangle were taken with the pressure in the excitation tube decreased by 60 percent and increased by 60 percent respectively. That these points

[20] H. Schüler and J. E. Keyston, Zeits. f. Physik **72**, 423 (1931).

fall on the same curve as the others shows that pressure effects such as broadening and reversal of the line in the excitation tube were negligible. The value of $\beta E/E_0$ was calculated from the geometry of the apparatus with a precision of about 15 percent. The function f was found by graphical integrations. With concentrations such that the absorption was very small f was unity and decreased slowly with increasing concentration, approaching zero as the concentration approached infinity. The value of C/E_0 could not, however, be obtained by measurements at very large values of N (for which A would be unity and f zero) since the absorption of λ2537 became appreciable and therefore C was no longer constant. Measurements of C/E_0 by means of filters was also subject to too large errors. Consequently C/E_0 was found by trial and was taken as the value which substituted in Eq. (3) and combined with the data of curve (a) Fig. 5 and curve (b) Fig. 4 gave most nearly a linear rela-

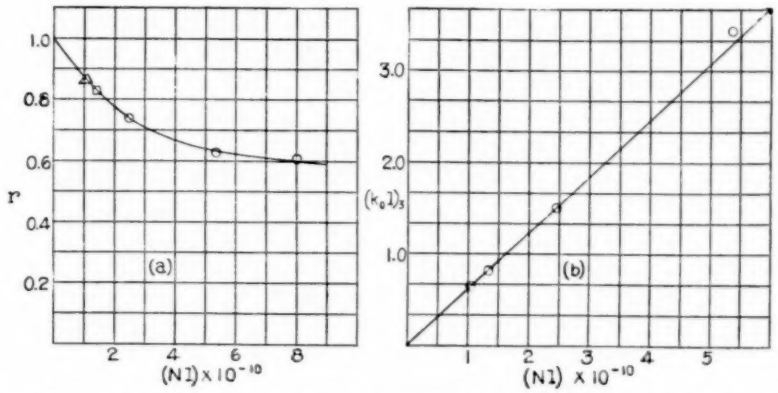

Fig. 5. Curve (a), ratio of photoelectric response with absorption cell in to that with it out vs. concentration times thickness of absorbing layer. Curve (b), absorption coefficient of strongest component vs. concentration times thickness of absorbing layer.

tion between $(k_0l)_3$ and Nl. The result is shown in curve (b) Fig. 5 which gives a value of $(k_0l)_3/Nl$ of 6.2×10^{-11}, or $(k_0)_3=6.2\times10^{-11}N$. From the steps taken in obtaining this value the precision is estimated as 25 percent.

It has been shown that[21]

$$\sum(k_0l)_\kappa = \frac{2}{\Delta\nu_A}\left(\frac{ln\,2}{\pi}\right)^{1/2}\frac{\lambda_0^2}{8\pi\tau}\cdot\frac{g_2}{g_1}\cdot Nl$$

where $\Delta\nu_A$ is the Doppler breadth of the absorption line, λ_0 is the wavelength of the center of the line g_2 and g_1 are the apriori probabilities of the states which give rise to radiation λ_0, and τ is the mean life of the excited state. Now $\Delta\nu_A=1.5\times10^9$ sec.$^{-1}$, $\lambda_0=1.85\times10^{-5}$ cm, and $g_2/g_1=3/1$.

Since the even isotopes have only one unresolved component we may obtain the value of τ for them (we have already assumed τ to be the same for all the isotopes) by putting on the left-hand side of the above equation the value of $(k_0l)_3$ found above and for N the concentration of the even isotopes, which is 0.699 times the total concentration of mercury atoms. We get then:

[21] W. Zehden and M. W. Zemansky, Zeits. f. Physik **72**, 442 (1931).

$$\tau = 2.9 \times 10^{-10} \text{ sec.}$$

As estimated above the precision is about 25 percent. Ladenburg and Wolfsohn[22] by fitting constants into a three term dispersion formula found an f-value which led to a life for the 2^1P_1 state of 1.6×10^{-9} sec. The reason for the large disagreement between these two values is not evident.

The author wishes to express his thanks to Professor Harold W. Webb for suggesting this investigation and for his many suggestions and continued help throughout the experiment.

[22] Reference 11.

Wave-Lengths of the Tungsten K Series Spectrum with the Double Spectrometer

By JOHN H. WILLIAMS*
Ryerson Physical Laboratory, University of Chicago.

(Received April 25, 1932)

With a Société Genovoise double spectrometer and the method devised by Compton the K series wave-lengths of tungsten were determined from the diffraction angles in the first order from calcite. The results, corrected for slit heights and reduced to 18°C are:

Line	Angle	Wave-length in x.u.
W $K\alpha_2$	2° 01′ 06.3″	213.37
W $K\alpha_1$	1° 58′ 22.3″	208.56
W $K\beta_3$	1° 44′ 51.4″	184.75
W $K\beta_1$	1° 44′ 24.8″	183.97
W $K\gamma$	1° 41′ 37.7″	179.06

The wave-lengths are calculated assuming a grating constant $d=3.02904$A at 18°C. The separation of α_1, α_2 agrees exactly with the energy difference $L_{II}-L_{III}$. The β_1, β_3 lines are easily resolved in the first order and give a separation of 0.78 x. u. agreeing closely with the energy difference $M_{II}-M_{III}$. Some remarks are made on the measurement of the natural widths of W K series lines.

INTRODUCTION

ACCURATE measurements of the x-ray wave-lengths of the K series lines of tungsten and higher elements have not been published in recent years. Siegbahn[1] gives the values obtained by Stephenson and Cork[2] as the most acceptable. Recently Seemann[3] has partially resolved β_1 and β_3 in the third order by his photographic method and gives their wave-lengths relative to α_1. Earlier measurements are those of Cork,[4] Siegbahn,[5] and Réchou.[6] The accurate measurement of these short wave-lengths by the usual methods is complicated by the small angle diffraction and more particularly by the large penetration into the crystal. With the present method the former of these difficulties is overcome partially since the beam is twice diffracted. The latter difficulty is not inherent in the double spectrometer method.

APPARATUS

The spectrometer and method have been described by Compton[7] and his observations establish the method as one of precision. The first crystal is set to reflect the line in question over the main axis of the spectrometer. This axis bears the second crystal and its rotation is read on a precision circle to

* National Research Fellow.
[1] M. Siegbahn, Spektroskopie der Roentgenstrahlen, Berlin, Julius Springer, 1931.
[2] B. R. Stephenson and J. M. Cork, Phys. Rev. **27**, 138 (1926).
[3] H. Seeman, Zeits. f. Physik **73**, 87 (1931).
[4] J. M. Cork, Phys. Rev. **25**, 197 (1925), corrected by reference 2.
[5] M. Siegbahn, Phil. Mag. **38**, 639 (1919).
[6] G. Réchou, C. R. **180**, 1107 (1925).
[7] A. H. Compton, R. S. I. **2**, 365 (1931).

seconds of arc. Calibrations of these circles show random errors in the rulings of $\pm 0.4''$ so that the angle measurements can be relied on to that accuracy. The second crystal reflects the wave-length in the (1, −1) and (1, +1) orders,[8] one half of the difference giving the diffraction angle from calcite in the first order. The intensity was observed by ionization methods with a pressure ionization chamber filled with argon. The temperature was recorded at three times during the observation of any two consecutive curves and never varied more than 0.2°C during that short interval of time.

Measurements

Typical curves obtained are shown in Fig. 1. These are seen to be smooth and symmetrical so that the maximum of an intense line could be located to

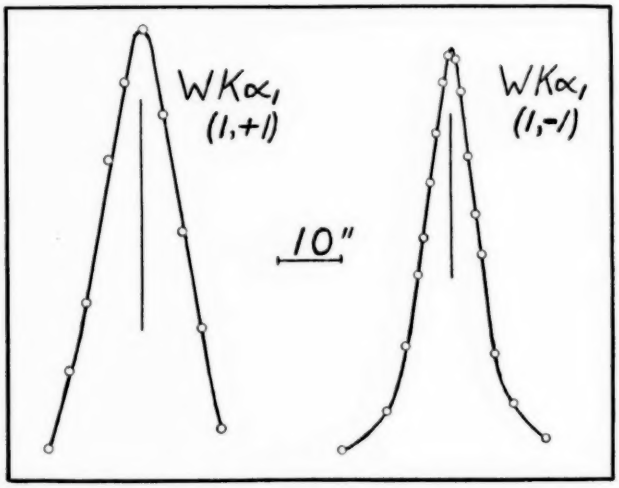

Fig. 1. Ionization curves of the tops of the peaks of W $K\alpha_1$ in the (1, +1) and (1, −1) positions against the indicated angular scale. The vertical scale is not the same for both curves.

within $\pm 0.1''$. Curves were always taken in the order (1, +1), (1, −1), (1, −1), (1, +1), (1, +1) etc. to eliminate the effect of any gradual shifts of the apparatus.

The observed angle is to be reduced to 18°C by the equation

$$\delta\theta_T = -1.04 \times 10^{-5} (18 - T) \tan \theta. \tag{1}$$

The second correction to be applied is that due to the effective height of the vertical stops,[9] and reduces the observed angle by an amount

$$\delta\theta_{\text{eff.}} = \frac{a^2 + b^2}{24 L^2} \tan \theta \tag{2}$$

where a and b are the slit heights at a distance L apart and θ is the Bragg angle. Thus the true diffraction angle is given by

[8] S. K. Allison and J. H. Williams, Phys. Rev. **35**, 149 (1930).
[9] J. H. Williams, Phys. Rev. in press.

$$\theta = \theta_{\text{obs.}} + \delta\theta_T - \delta\theta_{\text{eff.}}. \quad (3)$$

Table I is a record of the observed diffraction angles for W $K\alpha_1$ in the first order from calcite. The instrument was thrown out of adjustment and re-

TABLE I.

Curve No.	$\theta_{\text{obs.}}$	$\delta\theta_T - \delta\theta_{\text{eff.}}$	$\theta^r{}_{\text{es.}}$
12, 13	1° 58′ 22.3″	0.2″	1° 58′ 22.5″
15, 16	" 22.1	0.2	" 22.3
17, 18	" 21.1	0.2	" 21.3
19, 20	" 21.6	0.2	" 21.8
21, 22	" 22.5	0.2	" 22.7
28, 29	" 22.4	0.2	" 22.6
30, 31	" 22.4	0.1	" 22.5
32, 33	" 22.1	0.1	" 22.2
42, 43	" 22.5	−0.1	" 22.4
44, 45	" 22.5	0.1	" 22.6
55, 56	" 22.1	0.3	" 22.4

adjusted between curves Nos. 22 and 28, 33 and 42, 45 and 55. It is seen that the adjustment of the instrument can be made so perfect as not to influence appreciably the resultant diffraction angles.

RESULTS

Table II contains the calculated angles and the wave-lengths based on the grating constant $d = 3.02904$A at 18°C, compared with earlier observations.

TABLE II.

Line	Angle	λ in x.u.	Other observers
W $K\alpha_2$	2° 01′ 06.3″	213.37	213.45[2], 213.45[4] 213 52[5], 213.48[6]
W $K\alpha_1$	1° 58′ 22.3″	208.56	208.62[2], 208.60[4] 208.85[5], 208.50[6]
W $K\beta_3$	1° 44′ 51.4″	184.75	184.83[3]
W $K\beta_1$	1° 44′ 24.8″	183.97	184.02[3]
W $K\gamma$	1° 41′ 37.7″	179.06	178.98[2], 178.87[4] 179.40[5], 179.00[6]
W $K\beta_1$, β_3	Present results averaged with intensities 2/1	184.23	184.22[2], 184.35[4] 184.37[5], 184.16[6]

The results are seen to be in fair agreement with previous measurements but are somewhat smaller for the more intense lines. Seemann's[3] values for β_1 and β_3 are recalculated on the basis of $\alpha_1 = 208.56$x.u. The preferred measurements of Stephenson and Cork[2] and those of Cork[4] were taken with a Rutherford-Andrade method,[10] the x-rays passing through a thin crystal,

[10] E. Rutherford and Da Andrade, Phil. Mag. **28,** 263 (1914).

which is an experimental method quite unlike the present double-crystal method.

An ionization curve of the W $K\beta_1$, β_3 doublet is shown in Fig. 2. The doublet is seen to be almost completely resolved. The only previous satisfactory resolution of this doublet in tungsten or any heavy element was obtained by Seemann.[3] The resolution in his work is possibly one-third as complete as shown here.

Theoretically the K_γ line is a close doublet, the transitions being M_{II}, M_{III} to K. No evidence of a doublet structure was secured except that the K_γ line was broader than the other lines.

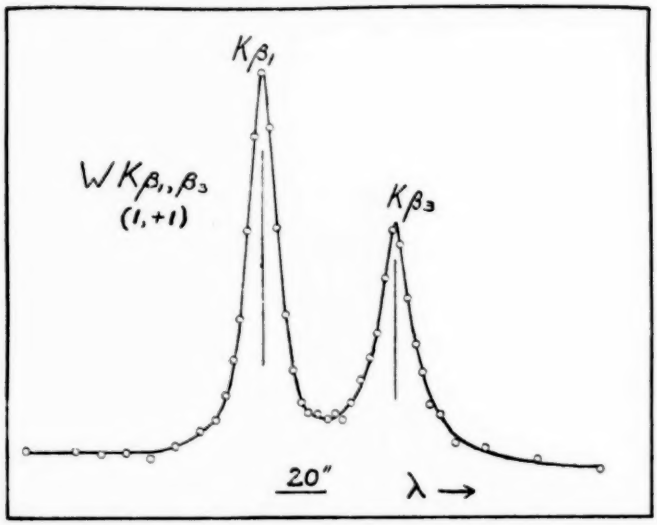

Fig. 2. Ionization curve of W $K\beta_1$, β_3 in the (1, +1) position. Ordinates are proportional to ionization currents, abscissae to angular settings of crystal B to the indicated scale.

Table III records the wave-length separations of the α and β doublets together with the experimentally observed and calculated energy separations. The experimental values are compared to those of other observers.

TABLE III.

Doublet	Observer	λ in x.u.	$\Delta\nu/R_{obs.}$	$\Delta\nu/R_{calc.}$
α_1, α_2	Present	4.81	98.58	98.56
	St. & Cork	4.83	99.0	
β_1, β_3	Present	0.78	20.94	21.71
	Seemann	0.81	21.72	

The wave-length separations are seen to agree within a few hundredths of an x.u. or to within about a second of arc. The $\Delta\nu/R$ calculated values are from Idei's[11] measurements on the L series wave-lengths of tungsten. There is almost exact agreement, well within experimental error in the α_1, α_2

[11] S. Idei, Sci. Rep. Tohoku Imp. Univ. **19**, 560 (1930).

separation. The β_1, β_3 separation does not agree so well; the exact agreement between Seemann's separation and the calculated value may be in part fortuitous since his resolution was far from complete.

Remarks on the Widths of Lines

It was hoped that this research would lead to accurate values of the natural widths of the K series lines of tungsten. In order to obtain such values one must use fairly perfect crystals and measure the rocking curves in parallel positions.[12] The crystals used were very large, 13×6 cm, in order to allow an appreciable width of slit at small angle reflection. The rocking curves in the $(1, -1)$ position gave half-widths at half maximum of from 4.5 to 5.0 seconds under various adjustments.

Schwarzschild[13] has developed the mathematical theory of the double spectrometer and has given the expressions for the reduction of the observed widths to give the natural widths of the lines. However, these expressions are based on the assumption that the natural shape of both the line in the antiparallel position and the rocking curve in the parallel position are Gaussian error curves. These assumptions are known to be at best only poor approximations, in the former case from several observers[14,15,16] and in the latter from the work of Allison.[17] Thus when a line is observed in several orders of the instrument and the corrections are made according to the methods of Schwarzschild[13] and Allison and Williams[12] one would not expect agreement between the orders[18] for lines whose natural widths are comparable to the crystal diffraction pattern widths, because the theory is not accurate under these conditions. In the case of the tungsten K series lines the finite width of the crystal diffraction pattern, W_C, in the first order is of the same order of magnitude as the natural widths of the lines themselves. Agreement between the calculated widths in first and second order particularily is not to be expected because the order of magnitude of the correction term, W_C, changes greatly and the error introduced by the approximate theory becomes large. One can, therefore, only expect to obtain relative and not natural widths of these very narrow lines unless a more extensive study is made with highly perfect crystals and the results are calculated by a more accurate theory. The relative widths in the $(1, +1)$ position of the lines observed are given in Table IV.

Table IV.

Line	α_2	α_1	β_3	β_1	γ
Relative width	21	19	18	17	25

[12] S. K. Allison and J. H. Williams, Phys. Rev. **37**, 1476 (1930).
[13] M. Schwarzschild, Phys. Rev. **32**, 162 (1928).
[14] J. H. Williams, Phys. Rev. **37**, 1431 (1931).
[15] R. C. Spencer, Phys. Rev. **38**, 630 (1931).
[16] A. Hoyt, Bull. Am. Phys. Soc. **7**, 11 (1932).
[17] S. K. Allison, Phys. Rev. in press.
[18] F. K. Richtmeyer, Washington Meeting Am. Phys. Soc. (1931).

The failure to measure line widths under these conditions does not necessarily invalidate previous work on wider lines, especially that on the much greater widths in the L series,[14,15] where the correction terms become almost negligible.

In conclusion I wish to express my thanks to Professor S. K. Allison for the use of his laboratory facilities and for his helpful interest during this research. My thanks are also due Professor A. H. Compton for the use of one of his double crystal spectrometers.

A Lower Limit for the Ground State of the Helium Atom

By D. H. WEINSTEIN
California Institute of Technology

(Received April 21, 1932)

A method of obtaining a lower limit for the ground state of any system in terms of the energy difference between the ground state and the next highest state is given. Applied to the helium atom this gives a rough value of $-6.2R$ as compared to the experimental value of -5.818R.

1.

LET the Schrödinger equation describing a system in the n'th state, having energy W_n be

$$H\psi_n = W_n\psi_n \tag{1}$$

where H is the energy operator. Then it is well known that

$$I_1 = \int \xi H \xi^* d\tau \geqq W_0 \tag{2}$$

where ξ is any function satisfying the condition $\int \xi\xi^* = 1$. This is the basis of the Ritz method in which one guesses at a function with suitable parameters which are adjusted so as to make I_1 a minimum. This method has been applied by Kellner[1] and Hylleraas[2] to the ground state of the helium atom, who obtain values only a few hundredths of a percent above the experimental value. Such agreement does not necessarily mean that the true theoretical value agrees with the experimental value, although it is quite certain that this is so in this case. Nevertheless, in many cases it would be valuable to have a lower limit for the ground state. We assume ξ (ξ is taken to be real for simplicity) to be an approximate solution of the Schrödinger equation in the ground state. Analytically this means that $a_1, a_2, \cdots, a_n, \cdots$, are small compared to a_0 in the expansion

$$\xi = a_0\psi_0 + a_1\psi_1 + \cdots a_n\psi_n \cdots \tag{3}$$

where

$$\sum_{n=0}^{\infty} a_n^2 = 1. \tag{4}$$

Now

$$I_1 = \int \xi H \xi d\tau = \sum_{n=0}^{\infty} W_n a_n^2 \tag{5}$$

[1] Kellner, Zeits. f. Physik **44**, 91 (1927).
[2] Hylleraas, Zeits. f. Physik **48**, 469 (1928).

in virtue of the orthogonality properties of the ψ's

$$\int \psi_n \psi_m^* d\tau = \begin{cases} 0 & m \neq n \\ 1 & m = n \end{cases} \tag{6}$$

We shall suppose the W's are arranged in order, so that

$$W_0 < W_1 < W_2 \cdots .$$

Using Eq. (4) we have

$$I_1 = W_0 + \sum_{n=1}^{\infty} (W_n - W_0) a_n^2. \tag{7}$$

Note that

$$\sum_{n=1}^{\infty} (W_n - W_0) a_n^2 = \Delta_1 \geqq 0. \tag{8}$$

Making use of our assumption about ξ so that we may neglect powers of a_n higher than the second, we have

$$I_1^2 = W_0^2 + 2W_0 \sum_{n=1}^{\infty} (W_n - W_0) a_n^2. \tag{9}$$

Let

$$\int \xi H^2 \xi d\tau = I_2 = \sum_{n=0}^{\infty} a_n^2 W_n^2 = W_0^2 + \sum_{n=1}^{\infty} (W_n^2 - W_0^2) a_n^2. \tag{10}$$

Now

$$I_2 - I_1^2 = \Delta_2 = \sum_{n=1}^{\infty} (W_n - W_0)^2 a_n^2 \geqq 0. \tag{11}$$

$$\Delta_1 \leqq \Delta_2 / W_1 - W_0. \tag{12}$$

Hence substituting in Eq. (7) we obtain our fundamental equation

$$I_1 - \frac{\Delta_2}{W_1 - W_0} \leqq W_0. \tag{13}$$

2. Application to Helium

We have

$$H = - a_0 e^2 / 2(\Delta_1 + \Delta_2) - \frac{Ze^2}{r_1} - \frac{Ze^2}{r_2} + \frac{e^2}{r_{12}} \tag{14}$$

where a_0 is the first Bohr orbit $a_0 = h^2/4\pi me^2$, Ze the charge on the nucleus, and r_1 and r_2 the radial distances of the two electrons from the nucleus. We take for ξ the hydrogen eigenfunction of the ground state

$$\xi = \frac{\alpha^3}{\pi} e^{-\alpha(r_1 + r_2)}$$

$$\alpha = \frac{Z}{a_0} .$$

Now it is well known (see Frenkel, Einfuhrung in die Wellenmechanik) that

$$I_1 = W_H + e^2 \int \xi^2 \frac{1}{r_{12}} d\tau = W_H + \tfrac{5}{8}\alpha e^2 = -5.5R \tag{15}$$

$$W_H = -4e^2/a_0.$$

Also

$$I_2 = \int \xi H \left(W_H + \frac{e^2}{r_{12}}\right)\xi = W_H{}^2 + e^2 \int \xi^2 \frac{1}{r_{12}} d\tau$$

$$- a_0 e^2/2 \int \xi(\Delta_1 + \Delta_2)\left(\frac{e^2}{r_{12}}\xi\right) d\tau$$

$$+ \int \xi^2 \frac{e^2}{r_{12}}\left(-\frac{Ze^2}{r_1} - \frac{Ze^2}{r_2} + \frac{e^2}{r_{12}}\right) d\tau. \tag{16}$$

Now by Green's theorem, since the surface integrals vanish

$$\int \xi(\Delta_1 + \Delta_2)\left(\frac{e^2}{r_{12}}\xi\right) d\tau = \int \frac{e^2}{r_{12}} \xi(\Delta_1 + \Delta_2)\xi d\tau. \tag{17}$$

Hence

$$I_2 = W_H{}^2 + 2e^2 \int \xi^2 \frac{1}{r_{12}} d\tau + e^4 \int \xi^2 \frac{1}{r_{12}{}^2} d\tau \tag{18}$$

and

$$I_2 - I_1{}^2 = \Delta_2 = e^4 \int \xi^2 \frac{1}{r_{12}{}^2} - e^4 \left[\int \xi^2 \frac{1}{r_{12}} d\tau\right]^2. \tag{19}$$

Being unable to obtain its exact value, it was found that

$$e^4 \int \xi^2 \frac{1}{r_{12}{}^2} \approx 7/16 e^4\alpha^2$$

$$\Delta_2 \approx 3/64 e^4\alpha^2.$$

While there are methods of obtaining the theoretical value of $W_1 - W_0$ to a sufficiently good approximation, we take the experimental value $W_1 - W_0 = 16$ volts $= 0.56\, e^2/a_0$. We thus obtain

$$\frac{\Delta_2}{W_1 - W_0} \approx 0.34 e^2/a_0 = 0.68R$$

$$I_1 - 0.68R = -6.2R.$$

This may be compared with the experimental value of $-5.818R$.

I wish to thank Professor Pauling, who called attention to this problem in his lectures, for his very kind advice.

The Shift of the Transmission Band of Silver by Cold Working

By HENRY MARGENAU
Sloane Physics Laboratory, Yale University

(Received April 11, 1932)

It is pointed out that the shift of the reflection minimum of silver, occurring as a consequence of cold working the silver surface, can be understood on the basis of Kronig's theory of metallic dispersion as a result of the change in the lattice constant. Correlation with known values of the density changes leads to satisfactory agreement.

THE position of the well-known ultraviolet minimum of reflecting power of silver has been found to depend on the degree of strain in the silver surface.[1] Polishing the surface, for instance, produced a measurable shift of the minimum to higher wave-lengths, while a release of the strain by heating appeared to reverse the shift. When this result was reported it was interpreted on the basis of Drude's theory of metallic conduction.

Meanwhile, Kronig's theory of dispersion in metals has provided a more adequate basis for an explanation of this phenomenon. To suggest a very simple interpretation, and to correlate it with observed density changes of the metal, is the purpose of this note.[2] According to Kronig,[3] the limiting frequency of the conduction band, ν_1, which will be considered as coinciding with the limit of the transmission band and the minimum of reflecting power, is given by

$$\nu_1 = C/a^2, \tag{1}$$

where a is the lattice constant and C contains, beside numerical constants, Bloch's parameter β' which measures the firmness of binding of the conduction electrons, and N, their number per atom. We wish to point out that it is possible to understand the effect of cold working upon the metal without assuming a change in β' or in N, that is, by regarding the change of the lattice constant as mainly responsible for the effect.

Cold working is known to decrease the density of a metal. Honda and Shimizu[4] have subjected silver specimens to high pressures and found the density ρ to change permanently by as much as 0.5 percent. Since their measurements give average values for the total specimen it may well be argued that the surface regions of a highly polished silver plate exhibit even greater changes.

If only a is considered to vary, (1) is equivalent to

$$\Delta\nu_1/\nu_1 = -2\Delta a/a;$$

[1] H. Margenau, Phys. Rev. **33**, 1035 (1929).

[2] The argument follows that presented by J. V. Pennington, Phys. Rev. **39**, 953 (1932) to account for the temperature shift of the transmission band.

[3] R. de L. Kronig, Proc. Roy. Soc. **124**, 409 (1929).

[4] K. Honda and Y. Shimizu, Science Reports Tohoku Imp. Univ. **20**, 460 (1931).

but

$$\Delta a/a = -\Delta\rho/3\rho,$$

since

$$\rho = \text{const.}/a^3.$$

Hence

$$\Delta\nu_1/\nu_1 = 2\Delta\rho/3\rho. \tag{2}$$

The largest shift of the minimum in our experiment was +20A, and the minimum lies at approximately 3150A. Thus $\Delta\nu_1/\nu_1 \leqq -6\cdot 10^{-3}$. By (2) this would correspond to $\Delta\rho/\rho = -9\cdot 10^{-3}$. The maximum value found by Honda and Shimizu is $\Delta\rho/\rho = -5\cdot 10^{-3}$, as stated. This, it appears, represents a satisfactory correlation between the two phenomena in question.

The Depth of Origin of Photoelectrons

By HERBERT E. IVES AND H. B. BRIGGS
Bell Telephone Laboratories

(Received April 9, 1932)

Previous work has shown that the photoelectrons from a silver plate covered with an equilibrium film of alkali metal follow the wave-length distribution of energy just above the silver surface, i.e., in the alkali metal. This question has been further investigated with particular references to alkali metal films in their early stages of development, where their average depth is less than one atom. Computations made on the absorption of light just within the silver surface show that there should be very definite and striking differences in the wave-length distribution of photoemission if emission occurs due to light absorption in the silver, as contrasted with emission from a film on the silver. Experimental tests made with sodium and caesium films show that in the earliest measurable state the emission exhibits characteristics peculiar to the light absorption in silver, and that as the films build up the emission becomes characteristic of the energy above the silver. It is concluded that the photoelectrons originate partly in the underlying metal and partly in the alkali metal film, the relative proportions varying with the film thickness.

IN PREVIOUS papers[1] we have described photoelectric experiments with alkali metal films on silver and on platinum, which show that the photoelectric currents follow the characteristics of the light energy immediately above the supporting metal surface. We have interpreted these experiments as evidence that the photoelectrons originate in the alkali metal film.

The films heretofore studied had reached their complete equilibrium development, and were therefore an atom or more thick, completely covering the supporting metal surface. It is however possible to study photoelectric currents from surfaces during the process of deposition of the alkali metal film, when the average depth may be much less than one atom, in other words, while the surface has upon it isolated atoms or groups of atoms of alkali metal, with uncovered spaces between. Under these conditions, do the photoelectrons originate in the alkali metal, or, as some theories indicate, is the function of the alkali metal centers that of facilitating the escape of electrons released in the underlying metal, but prevented from emerging ordinarily by its high work function?

The experiments described below were made chiefly on partly developed alkali metal films on silver, in the belief that the correlation of optical and photoelectric properties which had proved so informative in the case of fully developed films would here again indicate the place of origin of the photoelectrons. The reasons for expecting information on this point appear from a study of the light energy conditions both above and within the surface of the supporting metal, for these exhibit striking and decisive differences.

[1] Ives, *The Vectorial Photoelectric Effect*, Phys. Rev. **38**, 1209–1218 (1931).
Ives and Briggs, *The Photoelectric Effect from Thin Films of Alkali Metal on Silver*, Phys. Rev. **38**, 1477–1489 (1931).

In order to make clear these differences, we have in Fig. 1a, reproduced data from an earlier paper showing the computed energy densities above a silver surface, for a range of wave-lengths extending through the ultraviolet absorption band, for perpendicularly incident light ($\perp\!\!\!\perp$) and for light incident at 60°, polarized with the electric vector parallel ($\|$) and perpendicular ($\perp$) to the plane of incidence. In Fig. 1c we show the bulk absorbing power, or the fraction of the incident light which is subtracted by an infinitely thick layer of silver. In Fig. 1b we show the "lamellar" absorbing power, or relative amounts of energy absorbed by a thin layer of silver, *just inside* the surface.[2] In view of our conception that the photoelectrons can only escape from the topmost layer of metal it is our expectation that it is this lamellar or surface

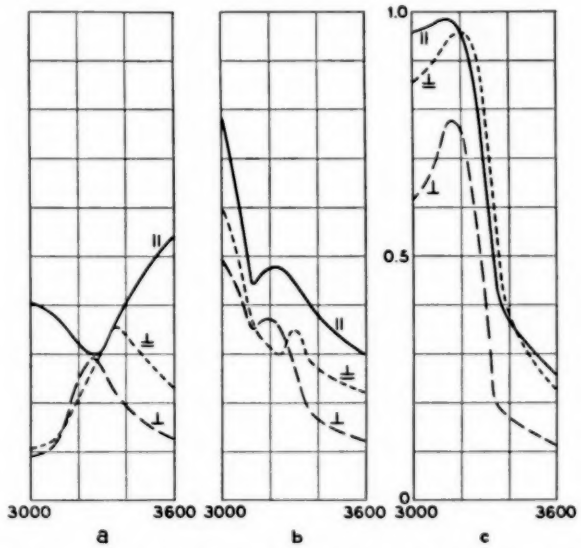

Fig. 1. Optical properties of silver near ultraviolet absorption band, plotted for perpendicular incidence of light ($\perp\!\!\!\perp$) and for light incident at 60°, polarized with electric vector parallel to plane of incidence ($\|$) and perpendicular to plane of incidence ($\perp$). (a) Energy density just above surface; (b) Absorption just inside metal; (c) bulk absorbing power.

absorption—which in many respects is transitional in character between the bulk absorption and the energy density above the surface—which would impose its peculiarities on photoemission originating in the silver. Before discussing the significant differences between these curves, we note that of the three sets of curves only Fig. 1c is on an absolute scale, as shown, all absorbing powers lying between zero and unity. The absolute amount of the surface absorption shown in Fig. 1b depends on the thickness of the layer, which enters as a multiplier, while the absorption taking place in a film lying above the surface is a function both of the energy densities shown in Fig. 1a, and of the absorbing power of the film material through this wave-length region.

[2] We are here using data derived from a study of the absorption of light in thin and thick layers of metal, which will be published shortly by Mr. T. C. Fry. An abstract appears in the program of the meeting of the Optical Society of America of February 27, 1932 under the title, *Plane Waves of Light III.*

Hence, insofar as the absorption of energy is concerned Figs. 1b and 1c give complete information as to relative values from wave-length to wave-length, while Fig. 1a represents relative energy absorbed in the film only if the film absorbs uniformly at all wave-lengths (and conditions of polarization). If the film material has optical singularities, such as absorption bands, in the region under study, they can mask to greater or less degree the characteristic forms of the curves shown. As a further caution on the interpretation of these curves we must recognize as well that the intrinsic photoelectric emission per unit of absorbed light at each wave-length, also enters as a multiplier. Both this factor and the optical constants of the film material, must be known before the problem can be completely elucidated. Nevertheless, by working with films of an alkali metal which shows no evidence of optical singularity in the wave-length interval under observation (as appears to be substantially the case with sodium), and confining our attention chiefly to the *positions* of the

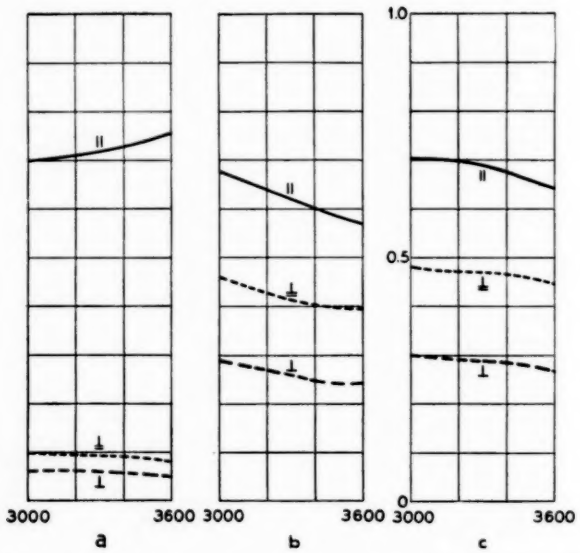

Fig. 2. Optical properties of platinum corresponding to those shown for silver in Fig. 1.

characteristic maximum and minimum of absorption and photoemission, rather conclusive information can be derived.

Taking up now in some detail the differences between the silver absorption just inside the surface, and the energy densities just above the surface, consider first the curves for light at 60° incidence polarized with the electric vector parallel to the plane of incidence (∥). In these, the minimum or cleft at 3260A characteristic of the energy above the surface, and which was found so strikingly in the fully developed alkali metal films, disappears inside the surface and is replaced by a small peak at 3200A. For light polarized in the other plane, (⊥), the maximum at 3260A found above the surface is shifted to 3200A and greatly reduced in size. The curves representing the surface absorption both rise steeply toward shorter wave-lengths, as compared with the energy above the surface. For light incident perpendicularly (⊥) the

computed curves for the two cases are also materially different. The broad high maximum in the energy above the surface is replaced by a small peak, shifted toward shorter wave-lengths, and the whole curve for the surface absorption rises more steeply toward the shorter wave-lengths.

Before proceeding to describe the experiments on silver, we also show, in Fig. 2, the corresponding computed data for platinum, on which we have also obtained data of some significance. No absorption band, such as that exhibited by silver, is present in the wave-length interval shown, and the differences in the three sets of curves are not so spectacular. There is however one of great importance; while the energy above the surface (Fig. 2a) exhibits very large ratios for the two planes of polarization at 60° incidence (about 12:1) immediately the surface is entered the relative absorptions drop to low values (between 2 and 3 to 1), being substantially the same as in the bulk absorbing power. Now in earlier work[3] on thin films of alkali metal on platinum we have found that a characteristic of the very thin, or partly developed films is that they show *low* ratios; in fact the "angle curves" approximate in shape to the bulk absorptions as plotted against angle. These angle curves might then be considered as evidence that with partially developed films the photoelectrons do originate in the absorption of light in the surface of the underlying metal. We shall see however that the experimental data indicate that such an explanation is inadequate and that some additional cause for the low ratios between emission as the plane of polarization is changed, is called for, where the films are very thin.

Apparatus and Experimental Procedure

The majority of the experiments were made with sodium films on silver, and for these the apparatus and methods of observation were in all essentials similar to those described earlier. The tungsten filament quartz-windowed lamp was the only light source used, since as before the significant wave-length region, to which the measurements were restricted, lies between the nearest mercury arc lines. The energy distribution of the lamp was as before determined by interpolated photoelectric measurements on a sodium-on-platinum perpendicular incidence cell, which is presumed to be free of irregularities of emission in this region. With sodium the rate of growth of the films is so slow that, after the introduction of the alkali metal, or after it had been driven off the plate by electron bombardment, ample time was available to make reliable measurements at any stage of development. In order to have some indication of the thickness to which the film had grown, the long wave limit was usually found. This, as is well established,[4] moves toward long wave-lengths as the film develops, reaching the resonance potential value (5893A for sodium) and then recedes somewhat for the final equilibrium film. In the present experiments the long wave limits noted are only approximate, as no

[3] Ives, *Photoelectric Properties of Thin Films of Alkali Metals*, Astrophysical Journal, **LX**, 4 (1924).

[4] Ives and Olpin, *Maximum Excursion of the Photoelectric Long Wave Limit*, Phys. Rev. **34**, 117–128 (1929).

precautions were taken to cut out stray short wave energy, such as the use of exceedingly fine slits, or color filters.

It was planned to supplement the sodium film measurements by a series on caesium, which because of its greater intrinsic sensitiveness, would permit measurements at much earlier stages of film development. Accordingly, a (60°) tube was designed and built, which in addition to a plate of silver had a platinum plate and twin quartz windows, so that comparative data might be obtained with the two different underlying metals. The caesium was distilled into a bulb on a side tube, and was allowed to diffuse slowly into the main tube. Caesium films are however exceedingly difficult to work with, and our results are quite incomplete, due, first of all, to the rapidity of growth of the film at the earliest stages, and second to the rapid development of surface leakage inside the tube, which completely swamped the small photoelectric currents long before the equilibrium stage was reached. Nevertheless, incomplete as they are the caesium data bring out points of considerable interest.

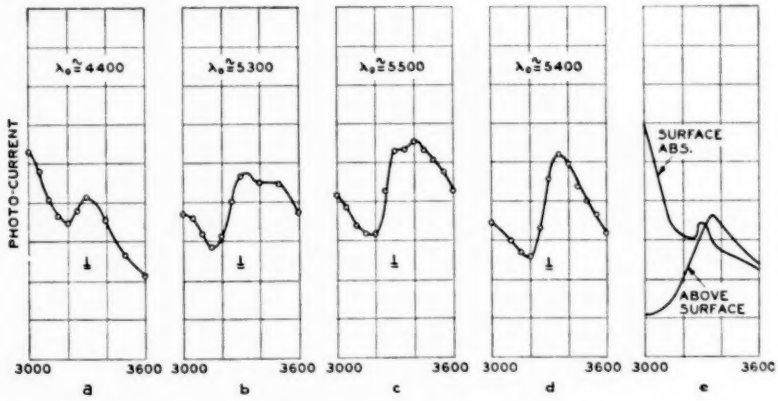

Fig. 3. Photocurrents from thin films of sodium on silver, light incident perpendicularly. Figs. a, b, c and d show successive stages, as indicated by the approximate long wave limits. Fig. e reproduces from Fig. 1, a and b, the surface absorption and supra-surface energy density.

Experimental Results

Silver

As a preliminary to the discussion of the photoemission from silver plates on which alkali metal films are allowed to form, it is pertinent to record that silver itself shows no detectable photoemission in this wave-length interval. All the photoelectric emission is due, whatever the exact mechanism may be, to the presence of the alkali metal film.

Sodium, perpendicular incidence, Fig. 3

The earliest stage of film deposition for which reliable measurements could be obtained exhibited a long wave limit at approximately 4400A. In this condition, (a), the photocurrent rises steeply toward short wave-lengths, showing however a well marked maximum at 3300A. As the film grows and the long wave limit increases (b) and (c) the short wave emission decreases

relatively to the maximum value, and the long wave side of the emission maximum builds up. For the fully developed film (d) this process has continued until the position of the maximum has shifted to 3350A, and the emission on the short wave side is nowhere as great as at the maximum.

At (e) are shown the computed surface absorption and supra-surface energy density, copied from Fig. 1, (a) and (b), for this condition of illumination. Comparing these with the experimental results we note that the final state (d) is clearly dominated by the supra-surface energy density, that is, as previously concluded, the photoelectrons originate in the alkali metal film. Now, comparing (e) and (a) we see that the film in its earliest measured state definitely shows characteristics peculiar to the absorption in the silver surface. These are, the trend upward toward short wave-lengths, and, of greater significance, a maximum at 3300A. It is true that the "fine structure" of this maximum as computed in (e) is not shown in (a), but it is to be remembered on the one hand, that the experimental observations are of necessity made with spectrometer slits of considerable width, and on the other hand, that the computed curves themselves rest on experimental determinations of the optical constants of silver, which must not be accepted as infallible. Bearing these facts in mind, the data present clear evidence, we believe, that *in the earlier stages of film deposition the photoelectrons come from the underlying metal.*

Sodium, oblique incidence, Fig. 4

Inspection of the data shown in the curves, (a) to (e), reveals that we have here again the same general shift of characteristics from those of the silver surface to those of the space immediately above the surface. In the earliest stages both planes of polarization show a maximum at 3200A, characteristic of the absorption just inside the silver surface. In the completely developed film (e) the one plane of polarization ($\parallel$) exhibits the deep minimum at 3300A, the other ($\perp$) the maximum between 3200A and 3300A characteristic of the energy density above the surface. There are however several features in the structure of the curves which complicate the simple interpretation indicated by the perpendicular incidence data.

One peculiarity is that the characteristics of both regions of absorption are always present to some degree. Thus in the fully developed film the silver absorption peak at 3200A still shows its influence, by a small shoulder on the $\parallel$ curve,[5] and by the fact that the $\perp$ maximum is shifted to somewhat shorter wave-lengths than the computed curve (3230A as against 3270A). At the first stage of deposition measured, which is considerably earlier than for perpendicularly incident light, ($\lambda_0 \leqq$ 4000A as against 4400A) the $\parallel$ curve shows definite indication of the depression at 3300A characteristic of the energy density above the surface. In immediately succeeding stages, not here reproduced, the $\parallel$ curve quickly takes the shape shown in (b), where the minimum at 3300A is pronounced. It is not of course out of order that there should be

[5] This shoulder is shown by the points in the previously published curves (reference 1 above) but its significance was not understood.

a transition from one set of characteristics to the other, however there is one feature in which this transition does not fit the computed curves of Fig. 1. According to the || curve in Figs. 1a and 1b, the early maximum at 3200, and the final minimum at 3300 are of such breadth that if both are present together they should very nearly neutralize each other, resulting in a nearly smooth emission curve. Actually the behavior is as if the maximum and minimum in question were very much sharper than the computations show so that they do not overlap to such an extent as to neutralize. Here again the caution with regard to accepting the optical constants as infallible must be stressed. For one thing these were determined from silver plates in air, while our plates were outgassed and worked with in vacuo; this difference in conditions may of itself, quite apart from experimental uncertainties, be sufficient explanation for the much narrower singularities which our photoelectric data appear to reflect. In any event there is no reason to modify the general conclusion already drawn from the data at perpendicular incidence, that *the photoelectrons come largely from the silver in the early stages, and chiefly from the sodium film in the later stages of deposition.*

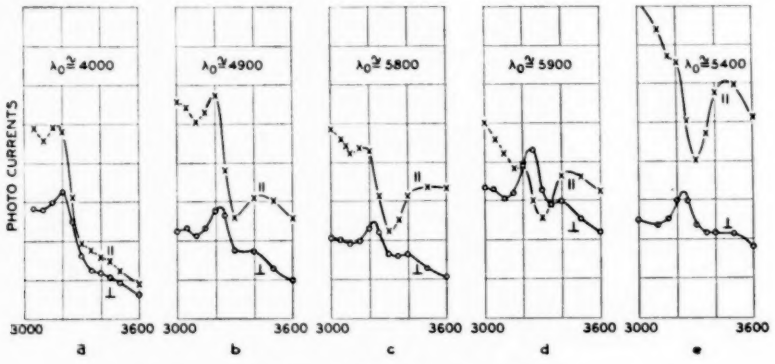

Fig. 4. Photocurrents from thin films of sodium on silver, light incident at 60°, successive stages.

Directing our attention to Fig. 4d we find a condition which has a vital bearing on the question whether the low ratios of || to ⊥ emission found with partially developed films are to be ascribed to the emission originating in the supporting metal, for which these ratios are low. We observe here that around 3300A this ratio is actually *inverted*, there is a smaller emission for light polarized with the electric vector parallel to the plane of incidence than when it is perpendicular thereto. Now the occurrence of such an inversion is not characteristic of the silver, for which this ratio is always greater than unity. Moreover it occurs at a late stage of film formation, where the characteristics with respect to wave-length of the energy density above the surface are predominant. It is not a characteristic of the unmodified energy density above the silver, for which the ratio in question is nearly unity at 3270A. It must, in accordance with our previous findings depend upon the optical properties of the alkali metal occupying the space just above the silver. The occurrence of low ratios in partially developed films must therefore be due in part to peculiar optical properties of such films.

Caesium, oblique incidence, Fig. 5

Our results for caesium are incomplete for reasons already stated, but are recorded partly because they confirm the sodium results and partly because they exhibit some new phenomena which are interesting in connection with our general study of the correlation of optical and photoelectric properties.

Referring to Fig. 5 we have at (a) again the exhibition in the earliest stages of film development of maxima of emission at 3200A for both planes of polarization of incident light. As the film grows (b to e) the maximum for ⊥ light shifts to longer wave-lengths and the emission curve is lower in relative value on the short-wave side, following in general the behavior of the sodium film. For ∥ light the growth history presents new features. The maximum at 3200A

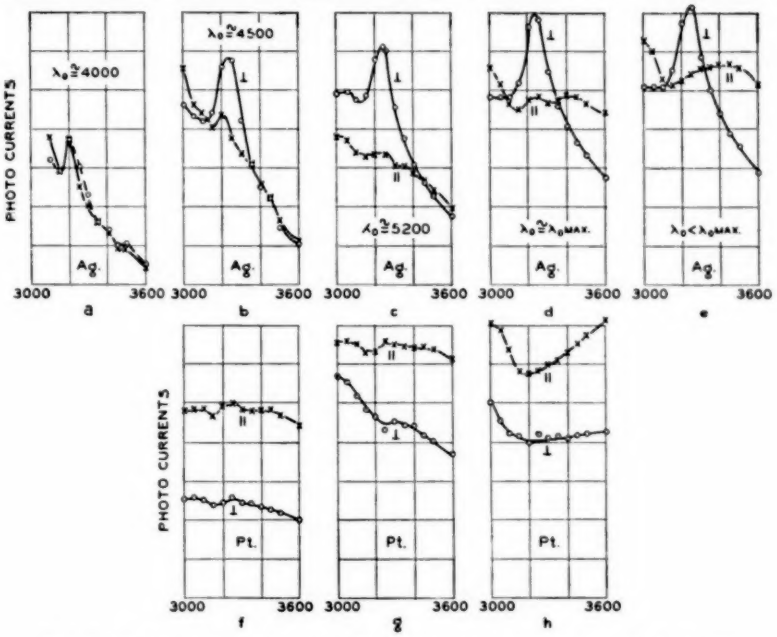

Fig. 5. Photocurrents from thin films of caesium on silver and platinum; light incident at 60°, successive stages.

quickly irons out, the whole curve drops, showing the inverted ∥/⊥ ratio over a wide wave-length region; the minimum at 3300, which is so striking in the sodium film, is merely suggested for a period, to be lost in the appearance of a new minimum at 3150A as the film passes its maximum long wave limit condition.

The behavior of the ∥ emission in its later stages appears to have little relationship to the optical properties of silver plotted in Fig. 1. For the explanation of the inverted ratio of ∥/⊥ emission, we must, as with sodium, ascribe it to a property of the alkali metal, on which more will be said later. For the peculiar shape of the curve we derive an explanation from data taken on a platinum plate in the same tube, shown in Fig. 5 (f) (g) (h) at intervals between (b) (c) (d) and (e) approximately as their positions with respect to the upper diagrams show. The significant fact shown by these curves is that,

in the later stages of film deposition (h) the caesium film on platinum exhibits precisely the same minimum of emission at 3150A as on silver. We have here a clear indication that caesium has in this spectral region an optical singularity (probably an absorption band) which is masking the silver characteristic. We have earlier emphasized the necessity for working with films which possess no optical singularities in the wave-length region under study if the indications of our guiding theory are to be tested without ambiguity. This condition is met with sodium, but not with caesium. Insofar however as we are asking the question, where the photoelectrons originate, this complication has not affected the answer. The minimum of emission at 3150A is shown by its occurrence both with platinum and silver to be a characteristic of caesium.

Discussion of Results

By comparison of the experimental data of Figs. 3, 4 and 5 with the computed supra-surface energy and surface absorption curves of Figs. 1 and 2, the following broad conclusions may be drawn:

1. At the very earliest stages of alkali metal film deposition the photoelectric emission exhibits a spectral distribution containing characteristics of the absorption of the underlying metal. These characteristics become less noticeable as the film builds up.

2. During the greater part of the film growth period the photoelectric emission clearly exhibits spectral distribution features characteristic of the energy distribution above the supporting metal surface. These characteristic features dominate in the final stages of film growth.

In terms of the title of this communication, these conclusions may be recast as follows:

In the initial stages of alkali metal film growth photoelectrons are emitted which originate in the supporting metal; as the film increases in thickness more and more photoelectrons originate in the alkali metal; in the completely covered surface practically all the photoelectrons come from the alkali metal film.

These experimental results lend support to the idea that the alkali metal atoms (or ions) on the surface of another metal decrease the work function of the surface, extend the long wave limit and allow electrons originating in the underlying metal to escape. They show however that only a part (and during most of the development history of the film only a small part) of the photoelectrons are thus to be accounted for. On the face of the evidence at least equal emphasis should be placed on the conception that restraining forces due to the underlying metal act upon the electrons originating in the alkali metal film and cause the limitation of the long wave response while the film is only partially developed.

Accepting these conclusions, we must now recur to one of the original questions asked, namely, why is the ratio of the emissions for excitation by obliquely incident light polarized in the two chief planes ($\parallel$ and $\perp$) low (such as 2 or 3 to 1) in the partially developed films, when the energy density above

the supporting metal calls for high ratios, such as 10 or 20 to 1? Our experimental results show the possibility that these low ratios are due, in the very early stages of film growth, to the emission originating in the supporting metal. But that this explanation is not adequate is very clear from the data of Figs. 4 and 5, in which a stage of film development appears where the ratio of $\parallel$ to $\perp$ emission is actually *inverted*, that is, the $\perp$ emission is greater than the $\parallel$, a condition which does not occur in the absorption in the silver. It is apparent that some other contributory cause for these low (and inverted) ratios of emission for partially deposited films, must be found.

Now the occurrence of an inverted ratio, while surprising at first glance, is actually entirely in accord with our previously found explanation of the low ratios occurring in the long wave visible region for all of the alkali metals.[1] A ratio lower than that exhibited by the energy density above the surface follows at once when the refractive index N and the extinction coefficient K_0 have such values that $1/(N+iK_0)^2$ is less than unity. In the case of sodium on platinum as the underlying metal, this factor in the long wave region reduced ratios of 30:1 down to 4 or 5 to 1. This same kind of reduction, applied to an energy density ratio of approximately unity, as in silver near 3250A would at once give ratios less than unity. What does require further explanation however is the fact that this ratio rises again with increasing film deposition, as shown in Fig. 4e, for sodium, and (as we have verified by angle curves) with caesium.

It is possible that an explanation is to be found in the peculiar optical constants of the alkali metals exhibited when they are in a dispersed form. Garnett[6] has shown that the colors of glass containing dissolved metals, and of alkali metal films on glass, can be correlated with new optical constants which bear a complicated relationship to the bulk constants, varying with the amount of material per unit volume. The alteration of values in the perpendicular electric vector upon entering the alkali metal film—which has been previously shown to explain the variation of the vectorial effect with wave-length—will of necessity be calculated for partially deposited films only in terms of optical constants applying to such film structures as arrived at by studies similar to those of Garnett. The optical constants which Garnett calculates for isolated aggregates of atoms call for sharp singularities of absorption, both as to wave-length and as to state of development of the film. The constants can moreover be different depending on the plane of polarization of the light. While Garnett's assumed film structures may not correspond exactly to those with which we are dealing[7] his work at any rate indicates the possibility that the low ratios in question may find their explanation in part

[6] Phil. Trans. Royal Soc. A, **V203,** 385–420 (1904); **205,** 237–288 (1905).

[7] Inverted ratios, which we have noted on several occasions, appear to occur under rather special conditions, not reproducible at will, and apparently dependent on the way in which the alkali metal film builds up, as conditioned by vapor pressure, temperature and preparation of the underlying metal. Thus we observed this condition in very thin films of sodium which showed a departure from Lambert's law (Phys. Rev. **35,** 669, (1930)). A departure from Lambert's law is one of the effects to be expected from isolated aggregates of metal, which is the condition studied by Garnett.

in the properties of the alkali metal film in its partially developed state. The complete elucidation of thin film photoemission in its early stages must wait upon more complete knowledge than we now have of the optical constants of the alkali metals. Our conclusions as to the depth of origin of the photoelectrons are however not dependent on the complete explanation of this phase of the problem, and remain unaffected.

The Intensity of Infrared Absorption Bands

By LORNE A. MATHESON
University of Michigan

(Received April 23, 1932)

An experimental method of measuring the absolute intensities of infrared absorption bands in gases has been used in which the absorbed energy was measured directly by the volume change in the absorbing gas due to the heat evolution in it. The absorption cell was traversed by radiation from a specially constructed infrared monochromator arranged for evacuation. The incident energy density was found through a calibrated thermocouple and galvanometer and the optical characteristics of the monochromator. Measurements were made with various path-lengths of absorbing gas. The absorption was extrapolated to zero by using a logarithmic graph which has many advantages. Line-width forms were investigated. It was found that for CO, $\alpha = \int \alpha_\nu d\nu$ was 1.18×10^{13} for the fundamental vibration band at 4.66μ and 1.54×10^{11} for the harmonic. The corresponding Einstein coefficients and the amplitudes of electric moment were calculated. The results of the analysis show that the Lorentz collision broadening type of line shape satisfies the experimental data much better than other line shapes. The line widths of the fundamental and harmonic bands were observed as 0.10 and 0.12 cm^{-1} at atmospheric pressure which would arise from collision diameters of 5.5A and 6.1A respectively. These line widths are smaller than have been previously reported for infrared lines.

IN THE study of spectroscopy two measurables are encountered, frequency and intensity. The qualitative part of the intensity variation with frequency, that is the position of spectral lines has been much more thoroughly investigated than the quantitative, partly because of its greater ease of accurate measurement and partly because the theory concerning line frequencies has been more completely developed and has proved very fruitful. Only a relatively small amount of work has been done on the determination of intensities in spectra. The present article describes the measurement of the absolute intensity of infrared absorption lines.

In the study of the infrared absorption spectra of gases, methods must be used which complicate the calculation of intensities and the only work which can lay claim to accuracy is that of Bourgin[1] and of Dunham[2] on the intensities of the HCl lines. This article describes the application of an unusual method for the measurement of intensity in the infrared, that of the measurement of the heat evolved in the gas itself during the absorption.

The intensity of absorption in a spectral region is defined as:

$$\alpha = \int \alpha_\nu d\nu \tag{1}$$

where α_ν is the absorption coefficient at frequency ν, that is, the coefficient of the path-length in the expression

[1] Bourgin, Phys. Rev. **29**, 694 (1927).
[2] Dunham, Phys. Rev. **34**, 438 (1929).

$$I_x = I_0 e^{-\alpha_\nu x} \tag{2}$$

which gives the intensity after the radiation of frequency ν has traversed a path-length x of absorber. This α is related to the Einstein coefficients of the transition causing the absorption by the relations:[3]

$$\alpha_{ij} = h\nu N B_{ij}/c \tag{3}$$

$$\alpha_{ij} = c^2 A_{ij}/8\pi\nu^2 \tag{4}$$

where the subscripts denote the states involved in the transition, and thence to the matrix component of the amplitude of the electric moment associated with the transition.

$$\alpha_{ij} = 2\pi^3 N^\nu (p_{ji})^2/3hc. \tag{5}$$

Because of the exponential character of the absorption, of inability to work in the infrared with slit-widths less than the line-width and of ignorance of the line-shape, one cannot find the intensity from measurements of the absorption at a single path-length.[2] It is, rather, necessary to take readings at several path-lengths x and then extrapolate to $x=0$. To extrapolate with any degree of accuracy sufficiently small values of x must be used. In practice this means the greatest value of α_ν must be less than $\frac{1}{2}$. Since the line-width in the infrared, of the order of 0.2 cm^{-1}, is much smaller than the slit-widths used (about 2.0 cm^{-1}), the absorbed energy is only about 1/20th the incident. In the usual type of absorption measurement the incident and the transmitted radiation are measured and from these the absorbed radiation is calculated. The absorption is thus the difference between two much larger quantities, a small error in either of which causes a relatively large error in the result and hence in the determination of intensity.

The present method is an attempt to decrease the large cause of error mentioned above by measuring the absorbed energy directly. This absorbed energy is determined by a micromanometer which measures the volume change in the absorbing gas due to its temperature increase. The incident energy is obtained in absolute measure by means of a calibrated thermocouple. The method suffers from the disadvantage that the absorbed and incident energy must be measured by different means. Many measured quantities enter multiplicatively into the result and thus errors of standardization as well as errors of measurement may exist. In the usual type of absorption measurement the dimensionless absorption is given immediately by the ratio of two galvanometer deflections and no other quantities enter except the path-length. The method employed here does however possess great sensitivity and we believe that the results obtained by it are fully as reliable as those obtained by the usual procedure.

The heat energy liberated in the gas can be taken as a measure of the absorbed energy, since very little energy is reradiated. The mean life of an unperturbed molecule in the vibrational state to which it is lifted by the absorption of infrared radiation is about 10^{-2} secs. Under experimental

[3] Tolman, "Statistical Mechanics," (1927 Ed.) p. 175.

conditions used here the molecule suffers 10^8 collisions during this time and it is quite certain that its vibrational energy will become rotational or translational through impact rather than be re-emitted as scattered radiation. The number of molecules having a translational energy greater than $h\nu$ for the fundamental band is about 10^{-4} of the total number of molecules at room temperature.

Gerlach[4] has investigated this point experimentally in the case of CO_2 and was unable to detect scattered radiation when CO_2 at atmospheric pressure was absorbing infrared. An approximate wave-mechanical solution has been carried through by Zener[5] in which it is found that the probability of a 1–0 vibration transition of an N_2 molecule due to a head-on collision with an He atom is 6×10^{-8} at room temperature. The fact that this calculated probability is so small does cast some doubt on the assumption which underlies the present work, namely that only a small portion of the radiation escapes measurement by re-emission. The final results may thus be said to form only a lower limit to the value of α. However the large value of α found for CO seems to indicate with considerable definiteness that in this case practically all of the absorbed radiation does become heat and thus also that the vibrational state of the molecule is changed by less than 10^8 collisions.

The absorbed energy ΔE is given by:

$$\Delta E = \int J_\nu(1 - e^{-\alpha_\nu x})d\nu \tag{6}$$

where J_ν is the incident energy stream density lying between the frequencies ν and $\nu+d\nu$. If J_ν is constant over the absorption region and we expand the exponential:

$$\Delta E = J_\nu \int [x\alpha_\nu d\nu + \tfrac{1}{2}x^2(\alpha_\nu)^2 d\nu + \tfrac{1}{3}x^3(\alpha_\nu)^3 d\nu \cdots] \tag{7}$$

or

$$\lim_{x=0} \Delta E/xJ_\nu = \alpha. \tag{8}$$

Experimental measurements were taken for various values of x and the results extrapolated to $x=0$.

The Measurement of the Absorbed Energy

The absorption cell and its accessories are shown in Figs. 1 and 2. The monochromator B with the exit slit s_2 and the rocksalt window w_2 furnished the incident beam J. This passed through the absorption cell A via the salt windows and the remaining portion was absorbed by the receiver F. In good thermal contact with A was an almost identical compensating chamber C.

[4] Gerlach, Ann. d. Physik 5, **4–5,** 371 (1930). Some deductions of interest here from the work of Kneser, (Phys. Zeits. **32,** 179, 1931) on ultrasonic wave velocity in gases have been published recently by Heil (Zeits. f. Physik **74,** 31, 1932). In the case of CO_2 the oscillation corresponding to the 14.9μ band is affected by approximately 10^{-6} of the molecular collisions.

[5] Zener, Phys. Rev. **37,** 556 (1931).

The two chambers were well insulated from external thermal effects and between them the micromanometer was connected so that it might be relatively unaffected by external temperature and pressure fluctuations.

The volume change ΔV due to the radiation was limited by the thermal conductivity of the gas in the absorption cell. With the size of cell used, a

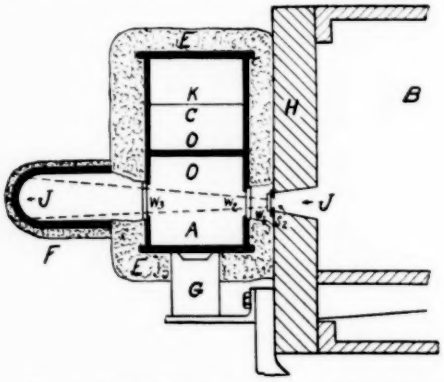

Fig. 1. Lateral section of absorption cell.

10 cm cube, the change in volume was 85 percent completed in 30 secs. after the heat source conditions in the gas were changed; a result which agrees with calculations based on the Fourier theory of heat conduction.

The connection between ΔE and the micromanometer indication can be approximately calculated, but to supplement this calculation a Pt wire 5.65×10^{-3} cm in diameter was placed in the compensating chamber in the position corresponding to that of the beam in the other chamber. The micromanometer was then calibrated by developing a known ΔE in the wire electrically. It can be shown that the line source of the wire and the volume distribution of the beam differ only slightly in their effect on $\Delta E/\Delta V$. Difference in end effect and heat conduction along the wire may also be neglected. No

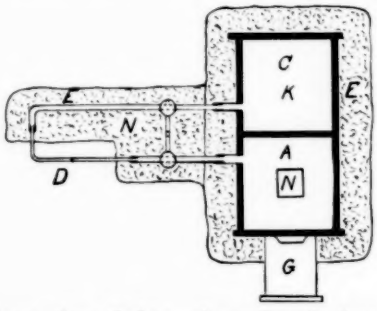

Fig. 2. Front view of absorption cell and micromanometer.

change was found in the resistance of the wire over the range of the currents used. A specially calibrated milliameter was used to determine the current in absolute measure.

Convection appeared to play no role in the range of extrapolation. Heat transfer by it is proportional to the square of the temperature differences

involved and an approximate calculation showed that the ratio of convected to conducted energy was much less than 2 percent at a value of ΔV equal to 10 times the usable sensitivity of the micromanometer, at which point the measurements had the greatest bearing on the final results. Also no decrease of $\Delta V/\Delta E$ with increase of ΔE which would result from convection was observed within the range of measurements.

The micromanometer consisted of an oil drop in a capillary tube as shown at D in Fig. 2. The drop motion was measured on the eyepiece scale of a telemicroscope focussed on the meniscus. The drop consisted of a higher boiling fraction of kerosene which had sufficiently low vapor pressure and vapor diffusion so that its infrared absorption in the cell was not noticeable. It possessed a viscosity which was sufficiently small so that its position indicated the value of ΔV with no appreciable lag. The sensitivity was $dV = 10^{-5}$ cm^3; $dp = 3 \times 10^{-2}$ dynes/cm^2; $dT = 10^{-5}$°C. and $dE = 1.0$ erg per second developed in the cell which corresponded to a linear movement of the drop of 5×10^{-4} cm.

Capillary forces acting on the drop were about 10^3 times the gas forces to be measured so slight inhomogeneities in the surface of the tube or drop might disturb the readings considerably. Even after thorough cleaning of specially chosen capillary tubing the readings showed small variations which could be traced to this cause. There was also a type of hysteresis in the motion of the drop which was unfortunately most noticeable at small deflections where the readings were most desired.

Small unsteady drifts of the oil drop occurred due to chemical activity, adsorption or thermal leaks through the insulation surrounding the cell. To eliminate the effect of these as well as the variations mentioned above many readings had to be taken. The radiation was allowed to pass through the cell during alternate 30 sec. intervals and readings taken at each movement of the shutter. The difference between a reading and the mean of its two neighbors was taken as the effect of the radiation. This eliminates the effect of uniform drift and when the mean of such differences was taken, the higher derivatives of drift with respect to time tended to disappear because of their variability. All readings of which records are shown represent such averages.

To eliminate the uncertainty caused by the hysteresis in the oil drop motion, readings were taken for various currents, i, in the compensating wire and a graph plotted between i^2 and "s," the drop deflection. Both positive and negative s's were used and the intercept on the $s = 0$ axis of the best mean straight line through the points gave the value of i^2 corresponding to the radiation. As an aid in determining these lines, those for various absorbing path lengths were plotted on the same graph. The slopes should be the same, but the intercepts different. Readings could be reproduced to 1 erg per sec.

The Measurement of the Incident Energy

A monochromator as shown in Fig. 3 was constructed to select the required frequency range and to enable the measurement of the energy density

in it. The instrument was designed for use with wide slits to insure the maximum intensity of radiation J_ν but with small enough aberration so that the variation of J_ν with frequency ν of the beam issuing from the monochromator was known with sufficient accuracy. The path of the radiation from the Nernst glower N to the absorption cell A is shown by the dotted line. The mirror was of 50 cm focal length and the rocksalt prism P was of $17\frac{1}{2}°$ angle and had 10×15 cm faces.

All the monochromator parts were mounted on the head II. The cover Q was of heavy iron pipe furnished with a flange R which made a ground joint contact with the corresponding part of II and was mounted on rollers which fitted rails on the base so it could be rolled back from II. The slit widths and the prism table rotation could be controlled by micrometer screws projecting through cones in the head II. The radiation could be interrupted by a magnetically operated shutter t. The exit slit was covered with an NaCl window. The monochromator could be evacuated to 10^{-2} mm Hg pressure and thus the greater part of the H_2O and CO_2 removed from the path. This was not necessary however in the CO measurements as the CO bands do not overlap those of the above named gases.

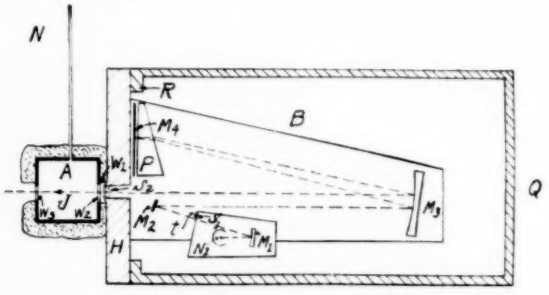

Fig. 3. Top view of monochromator.

The Nernst glower was preheated to start it, the monochromator sealed, evacuated and refilled with air drawn through a liquid air trap. The glower could be kept heated at a low temperature for long periods without deterioration. During readings the current could be kept constant to within 1 percent by manual adjustment. To decrease the effect of plastic movement of the glower its focus on the incident slit was made broad.

The monochromator was focussed by the use of the Na D lines. The breadth of focus due to aberration was 0.2 mm or 0.2μ at 3.0μ. The wavelength calibration of the micrometer controlling the prism rotation was accomplished by the use of the dispersion curve of NaCl and the micrometer readings for the Na D lines. This calibration predicted the position of the various absorptions. The dispersion was also used to calculate the slit widths in frequency units, a magnitude which enters directly into the final results. The slit widths in cms were measured with the micrometer screws which adjusted them externally, the calibration being checked with a microscope.

The above optical facts concerning the monochromator allowed the calculation of the shape and the position of the energy distribution curve shown

idealized in Fig. 4. In constructing this figure it has been assumed that the monochromator possessed an ideal focus, that the incident slit was uniformly illuminated and that I_ν, the radiation of the source per unit frequency interval, was a constant. The width of the wings g equals the frequency width of the narrower slit $\Delta\nu_2$ and h the width of the region of maximum J_ν equals $|\Delta\nu_1 - \Delta\nu_2|$.

$J = \int J_\nu d\nu$, the total radiation issuing from the monochromator was found by removing the absorption cell and focussing the exit radiation on a thermopile with a mirror. The thermopile and mirror combination was calibrated in absolute measure by illuminating the exit slit s_2 with a standard incandescent lamp from the Bureau of Standards. This allowed the thermopile calibration in situ with the same radiation distribution over the thermopile surface as in the actual measurements. Correction was made for the NaCl windows traversed.

From Fig. 4

$$J = \int J_\nu d\nu = J_\nu(\text{max.})\ \Delta\nu(\text{max.})$$

or

$$J_\nu(\text{max.}) = J/\Delta\nu(\text{max.}) \tag{9}$$

where $\Delta\nu$(max.) is the frequency width of the widest slit and J_ν(max.) is the greatest value of J_ν in Fig. 4.

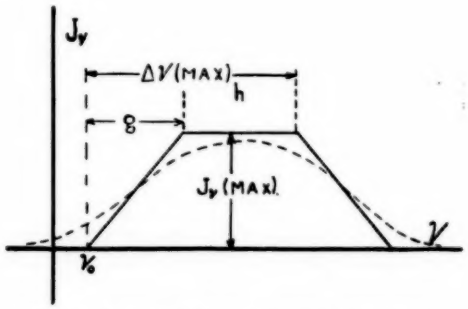

Fig. 4. Incident energy versus frequency.

Eq. (9) was used to calculate J_ν(max.) which is that operating on the absorbing gas. It was found that the variation of illumination density over the incident slit and the variation of I_ν with ν which would disturb the validity of (9) could be neglected. It should be noted here that it is I_ν which is considered rather than I_λ which would vary considerably with ν or λ. I_ν and J_ν are used because it is an α_ν and an $\int\alpha_\nu d\nu$ which is discussed. The correction for the effect of aberration and nonidealness of focussing will be noted later.

In some cases; i.e., that of CO, the band whose intensity is desired lies close to, but still does not overlap, an absorption band of the atmosphere. J_ν at the position of absorption is not changed, but (9) is not valid, since part of the area under Fig. 4 is removed. To enable results to be taken at

any ν a curve was made of J versus prism rotation and the regions of absorption bridged by interpolation.

The Measurement of $\Delta E/xJ_\nu$

The factor in (8) not yet treated is x, the effective path length of the absorbing gas. This was measured in units of cms at 76 cm Hg pressure and 300°K. The cell was evacuated with a Hyvac and Hg vapor pump and filled with the partial pressure of absorber giving the desired path length. The absorber was then diluted to atmospheric pressure with air which had been drawn through sodium hydroxide solution, sulfuric acid and a liquid air trap. This treatment decreases to negligible concentration all the polar constituents of air except CO.

The CO used was made by dropping formic acid on sulfuric and was drawn through sodium hydroxide solution, sulfuric acid and finally liquified with liquid air. The middle boiling fraction of this liquid was used. All sur-

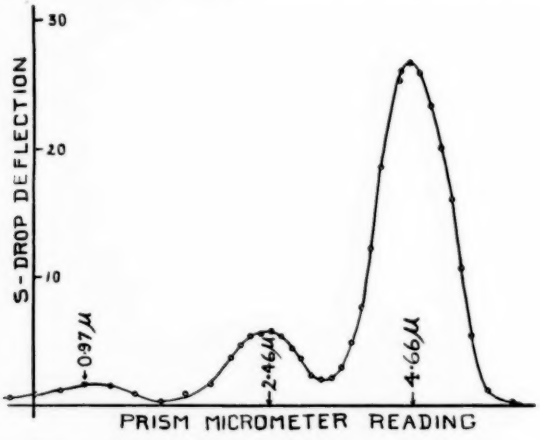

Fig. 5. Absorption versus incident wave-length.

faces in contact with the gas were of glass except for short lengths of protected rubber tubing and the inside surface of the copper absorption cell which was coated with ceresin. During a set of measurements x was halved after each reading and thus small x's reached with accuracy. The gases were removed by pumping and flushing the cell with air freed from CO_2 and H_2O. A small residual drop deflection remained which had to be corrected for. It was apparently due to absorption and scattering of the beam by the windows.

In beginning the study of any gas the slits were adjusted to resolve bands 1μ apart, the cell filled with the gas and an absorption spectrum of drop deflections plotted against prism rotation as shown in Fig. 5 for CO. The fundamental at 4.66μ and the harmonic at 2.35μ are present. The slight maximum at 1.0μ could not be explained and seemed to disappear with decrease in x of CO.

It is seen that the peak of the absorption curve is not flat, as Fig. 4 would lead one to believe it should be. Most of the width of this curve is due to the width of the absorption band itself, but part comes from the non-idealness

of the incident energy curve illustrated by the dotted line shown in Fig. 4. The correction for this non-idealness was found by increasing $\Delta\nu$(max.) or the greater slit width and finding how the maximum absorption as indicated in Fig. 5 increased. As s_2 is made large with respect to the aberrations J_ν(max.) approaches its ideal value. Curves, such as Fig. 5, were plotted for several values of $\Delta\nu$(max.). It was found that about 10 percent should be added to the maximum s's obtained when using $\frac{1}{2}$ and 1 mm slits in order that they represent the s's due to the J_ν calculated from Eq. (8).

When the absorption regions were located their wave-lengths were checked. Readings were then taken at the maxima in Fig. 5 for a series of x's. Thus as experimental data one possesses a series of i^2's corresponding to various x's. The most accurate method of obtaining α from these will be discussed in the next section.

The Theoretical Derivation of $\Delta E/xJ_\nu$

It is possible to calculate the variation of ΔE with x from α and the line width if one assumes a line shape and the relative intensity of the lines in a band. We shall indicate the results for a band, such as that of CO, with no zero branch. The line shape shall be assumed to have the form:

$$\alpha_{\nu j} = r_j b^2/\left[b^2 + (\nu - \nu_j)^2\right]. \tag{10}$$

Where r_j is the height or absorption coefficient at the peak of the line j, b is defined as the line width and ν_j is the center of the line. It is seen that b is the distance from ν_j to where $\alpha_{\nu j}$ has fallen to $\frac{1}{2}$ its value at ν_j.

$\Delta E_j = J_\nu \int (1 - e - \alpha_{\nu j}{}^x) d\nu$, where J_ν is treated as a constant.

$$= J_\nu \sum_{n=1}^{\infty} \frac{(-1)^{n-1}}{n!} \int (\alpha_{\nu j})^n d\nu. \tag{11}$$

Using (10) and considering only one line, we may integrate each term:

$$\Delta E_j = \pi b \sum_{n=1}^{\infty} d_n (l r_j)^n \tag{12}$$

where

$$d_n = \frac{(-1)^{n+1}(2n-3)(2n-5)\cdots 1}{n!(n-1)!2^{n-1}}.$$

The results may also be expressed in Bessel functions,[6] but this form was not found as apt for the purpose as the above.

The Energy Absorbed by a Band Branch

Let us consider the ΔE due to one branch of a band, taking b the same for all the lines and letting the relative intensities of the lines be given by:

$$r_j = cje^{-\sigma i^2}$$

where $\sigma = h^2/8\pi^2 IkT$. This arises from the application of old quantum theory but is sufficiently correct for the present purpose. Let $\sum_{j=1}^{\infty} r_j = R$. Then, if

[6] Ladenburg and Reiche, Ann. d. Physik **42**, 181 (1913).

we replace the summation by an integration which is allowable here, we find:

$$r_j = 2R\sigma j e^{-\sigma j^2}. \tag{13}$$

Substituting (13) in (10) we find:

$$\frac{\Delta E}{J_\nu} = \sum_{n=1}^{\infty} \frac{(-1)^{n+1}}{n!} x^n \int \left[\sum_{j=1}^{\infty} \frac{r_j b^2 d\nu}{b^2 + (\nu - \nu_j)^2} \right]^n.$$

We may now approximate

$$\left[\sum_{j=1}^{\infty} \alpha_{\nu j} \right]^n \quad \text{by} \quad \sum_{j=1}^{\infty} (\alpha_{\nu j})^n$$

This neglect of the cross product terms in the expansion is equivalent to neglecting the effect of line overlapping. In the case of CO it may be shown that the cross product terms may be neglected to $n = 10$ and $xr_j(\text{max.}) = 4.0$. This allows evaluation of the series for large enough values of x to overlap the region of experimental data in which the accuracy decreases with decreasing x.

We may now integrate with respect to ν after interchanging $\int d\nu$ with $\sum_j$.

$$\frac{\Delta E}{J_\nu} = \sum_{n=1}^{\infty} \pi b \frac{(-1)^{n+1}}{n!} \frac{(2n-3)(2n-5) \cdots 1}{(n-1)!\,2^{n-1}} \sum_{j=1}^{\infty} x^n \nu_j{}^n. \tag{15}$$

Substituting the value of r_j from (13) we may replace $\sum_j$ by $\int dj$ with an error less than 2 percent for each term, when n is less than 10. The integration with respect to j may now be carried out and gives:

$$\Delta E / J_\nu = \sum_{n=1}^{\infty} g_n x^n. \tag{16}$$

We must find the effect of this heat when it is liberated along the length of the beam in the absorption cell. The cube of 10 cm on an edge has a difficult heat conduction solution where sources are concerned, but the present situation can be approximated by a sphere of about 5 radius with the beam traversing a diameter.

Consider a sphere of radius a with its surface temperature constant which is filled with a gas of heat conductivity ρ. A heat source of strength ϵ at a distance b from its center causes a change in temperature ΔT which may be calculated at any point by image theory. The volume change due to this ΔT throughout the gas is then:

$$\Delta v = \int \Delta T dv / T \tag{17}$$

$$= \epsilon(a^2 - b^2)/6\rho T. \tag{18}$$

To find the effect due to the heat absorption taking place in the length of the beam, we introduce a coordinate q measured along the length of the

beam from its incident end; then (18) becomes:

$$\Delta v = \epsilon(2aq - q^2)/6\rho T. \tag{19}$$

The ΔE in (16) occurs over a length $2a$, i.e., the total beam length in the cell. For the absorption in any length q with an effective path length x in the cell we need merely substitute $qx/2a$ in (16) for x. Thus the heat absorbed between q and dq is:

$$\begin{aligned}\epsilon(q) &= \frac{\partial \Delta E(q)}{\partial q} \\ &= g_n \left(\frac{x}{2a}\right)^n n q^{n-1}\end{aligned} \tag{20}$$

Substituting (20) in (19) and integrating with respect to q

$$\Delta v = \frac{\pi b a^2}{18\rho T} \sum_{n=1}^{\infty} h_n U^n. \tag{21}$$

Where $U = 2Rx(\sigma)^{1/2}$ which corresponds to a mean absorption line height and

$$h_n = \frac{3(2n-3)(2n-5)\cdots 1[(n-1)/2]!}{(n+2)!(n-1)!n^{(n-1)/2}2^{n-2}} \text{for } n \text{ odd}$$

and

$$h_n = \frac{3\pi^{1/2}(2n-3)(2n-5)\cdots 1.3.5\cdots(n-1)}{2^{(3n-4)/2}(n+2)!(n-1)!n^{(n-1)/2}} \text{for } n \text{ even}.$$

The numerical values of h_n were calculated for values of n to 10. The value of $g = \sum_{n=1}^{10} h_n U^{n-1}$ was calculated for values of U ranging from 0.1 to 10 and was plotted versus U. This graph corresponds to the experimental graph of i^2/x versus x where i^2/x is proportional to the energy absorption per molecule.

The slope of this curve at the origin is definitely related to the line width b. One can deduce the connection from (21).

$$\left[\frac{x}{i^2}\frac{d}{dx}\left(\frac{i^2}{x}\right)\right]_{x=0} = \frac{\alpha}{16b}\left(\frac{\sigma}{2\pi}\right)^{1/2}$$

$$\text{or } b = \frac{\alpha}{16}\left(\frac{\sigma}{2\pi}\right)^{1/2} x_1 \tag{22}$$

where x_1 is the value of x at the intersection of the $i^2/x = 0$ line and the tangent to the i^2/x line at $x = 0$.

The experimentally determined values of i^2/x were plotted versus x, the graph being modeled after that of $g = h_n U^{n-1}$ versus U. The results for one set of readings are shown in Fig. 6.

It was found that for large values of x the absorption was quite accurately equal to a power of x. This immediately suggested plotting the data on logarithmic scales. Fig. 7 shows the resulting theoretical curve, and Fig. 8,

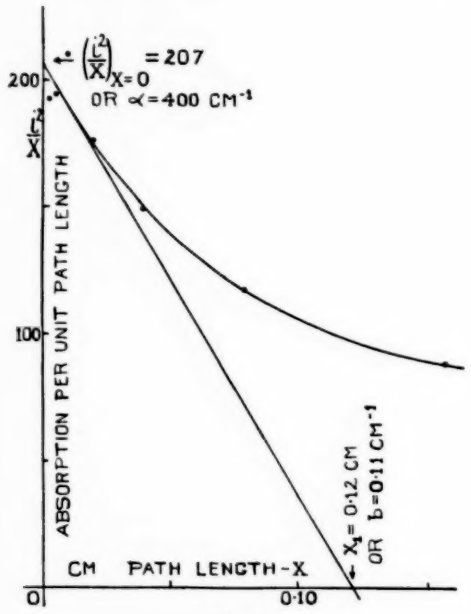

Fig. 6.

the experimental points with the best fitting theoretical curve superposed, determined by mere movement of Fig. 7 over the points of Fig. 8. It is seen that, for the larger values of x, the experimental curve is a straight line; i.e.,

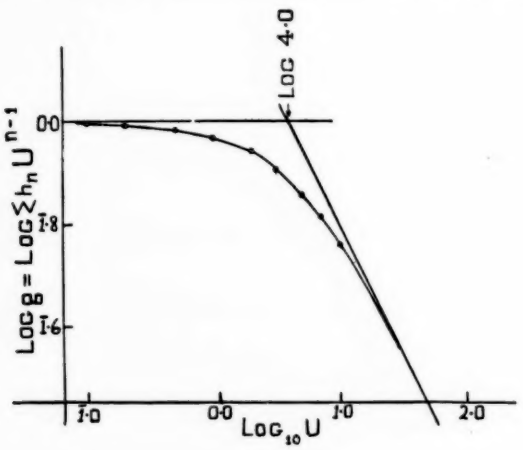

Fig. 7.

i^2/x is proportional to x^n where n is approximately equal to $-\frac{1}{2}$. The theoretical curve is provided with a like asymptote whose presence is justified on the grounds that all experimental curves taken for the CO fundamental had such

a behaviour for path lengths x greater than 1.0 mm and that the theoretical curve for a single line in the band given by Eqs. (11) and (12) has such a behaviour.[7]

With this type of plotting, the determination of α reduces to finding the position of the horizontal asymptote to the experimental curve at low values of x. The value of i^2/x of this line is that where the absorption is proportional to the number of atoms present and is proportional to α.

A comparison of Figs. 7 and 8 allows the scale factor in the abscissae; i.e., the ratio between U and x, to be found. As a reference point the intersection of the two asymptotes of each curve was used. The definition of U; i.e.,

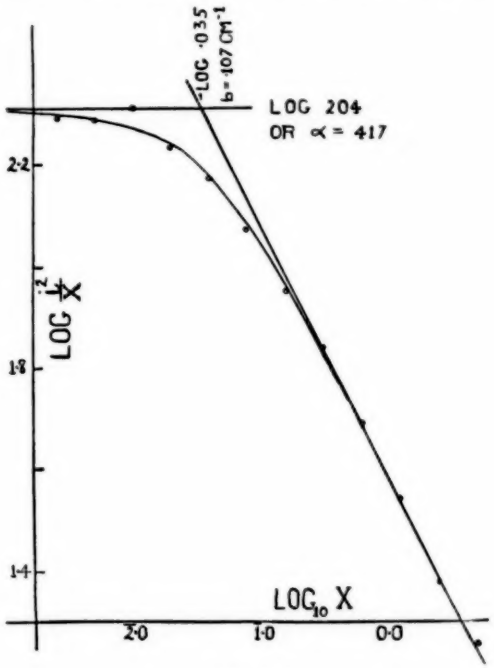

Fig. 8.

$U = 2R(\sigma)^{1/2}x$, allowed the calculation of R. b was then calculated from $\alpha = 2\pi Rb$. The value of b obtained in this way agrees numerically with that calculated from Eq. (22) applied to a different type of graph, i.e., Fig. 6.

It is seen that to determine α or the position of the horizontal asymptote, small enough x must be used so that x is not in the region where ΔE is proportional to $(x)^{1/2}$ but in the region where ΔE is at least beginning to be proportional to x. Not only must measurements be taken at several x's in any absorption measurement, but one must take some of them at a sufficiently small value of x, which is, as seen from Fig. (8), less than 1.0 mm of CO for the fundamental absorption band. This is smaller than has usually been employed heretofor in infrared absorption measurements. Results obtained with greater path length merely define a lower limit for α, since they determine a

[7] The asymptotic expansion of Eqs. (11) and (12) is proportional to $x^{1/2}$ for large x's.

lower limit for the position of the horizontal asymptote as can be seen immediately from Fig. 8. This result which is an important one applies also to measurements made on a single line. It appears that a rediscussion of some of the earlier experimental work on infrared intensities might be desirable.

The value of $\log \Delta E/xJ_\gamma$ from (11), that is for a single line, was plotted versus $\log x$. The experimental values of log (absorption/x) from several lines in the HCl absorption band at 3.5μ as determined by Bourgin[1] were plotted versus $\log x$ also. It was found that lower values of r were used in the present method than had been used by Bourgin; that is, the sensitivity of this method is greater. This does not however imply that the measurements based upon the older methods might not be improved as regards sensitivity. Recent developments in the field of amplification of thermoelectric currents would allow the use of narrower slits at shorter path lengths, thus permitting greater accuracy to be attained. Also there are a greater number of measurements with their possibilities of accompanying errors in the present method.

A set of data is shown below embodying the mean of the various determinations. The value of $\sigma = h^2/8\pi^2 IkT$ used was 0.0088 corresponding to a value[8] of $I = 1.50 \times 10^{-39}$ and a temperature of 300°K.

TABLE I.

	Fundamental, ($n = 1$) at $4.66\mu = 2150$ cm^{-1}	Harmonic, ($n = 2$) at $2.35\mu = 4260$ cm^{-1}
$J = \int J_\nu d\nu$ through slit	7.79×10^3 ergs/sec	4.24×10^4 ergs/sec
$\Delta\nu$ included in 1.0 mm slit	440 cm^{-1}	2200 cm^{-1}
J_ν(max.) corrected	14.7 ergs/sec. cm^{-1}	15.9
$\lim \frac{i^2 - (i^2)_0}{x}$ (i in m.a.)	204	2.87
$\alpha_{on} = \lim_{x=0} \frac{\Delta E}{xJ_\nu} = \frac{R}{J_\nu} \lim_{x=0} \frac{i^2 - (i^2)_0}{x}$	394 cm^{-1} = 1.182×10^{13}	5.13 cm^{-1} = 1.54×10^{11}
B_{on} from Eq. (3)	3.40×10^{16}	2.23×10^{14}
A_{no} from Eq. (4)	55.7	2.85
$\tau_{no} = \frac{1}{A_{no}}$	0.0180 secs.	
p_{no} from Eq. (5)	2.65×10^{-19}	2.15×10^{-20}
ϵ_{no}	3.9×10^{-10} e.s.u.	
R_{no}	610	9.8
$b_{no} = \alpha_{no}/2\pi R_{no}$	0.103 cm^{-1}	0.125 cm^{-1}
d_{no}	5.5Å	6.1Å

One may calculate an effective electric charge ϵ which, if it were concentrated on the nuclei and moved with them, would give the observed intensi-

[8] Snow and Rideal, Proc. Roy. Soc. **A125,** 462 (1929).

ties of absorption and emission from the formula:[9]

$$\alpha = \frac{\pi N \epsilon^2}{3c\mu} \cdot \tag{24}$$

Eq. (24) gives a value of $\epsilon_{01} = 3.92 \times 10^{-10}$ e.s.u. $= 0.82\ e$. This is quite large compared to the permanent effective charge of $0.022\ e$ calculated from the internuclear distance and from the permanent dipole moment obtained from dielectric constant measurements.[10] There is however no reason to suppose that any simple relation exists between these two effective charges.

An accurate wave mechanical analysis of the intensities in terms of the electric moment and its derivatives and the anharmonicities in the mechanical motions of the nuclei has been carried out by Dunham.[11] The values of α_{01} and α_{02} obtained above and the coefficients in the power series expansion of potential energy versus nuclear separation found for CO[8] were used in Eq. (9) of Dunham's article. The values of the first and second derivatives of the electric moment with respect to the nuclear separation were calculated assuming Dunham's a_3 and p''' equal to zero.

The results found were

$$p' = \pm 9.1 \times 10^{-18} \text{ e.s.u.}$$
$$p'' = \mp 3.4 \times 10^{-18} \text{ e.s.u.}$$
$$\text{or } \pm 3.7 \times 10^{-18} \text{ e.s.u.}$$

where the $+3.7$ and the -3.4 are to be taken with the positive value of p'. The derivatives appear large with respect to the equilibrium electric moment, $p = 0.118 \times 10^{-18}$ e.s.u.

In the method used no large error is expected in the derivation of R, since it does not depend on standardized measurements, but only upon x and relative i's. The probable errors in the various measurements were estimated and with liberal allowances the probable error in the result was about 30 percent. It is believed that the results are correct to within that order of magnitude at least.

The fact that at large values of x the absorption was proportional to $(x)^{1/2}$ leads definitely to a line shape of the form of Eq. (9). Other line shapes, for instance the error curve, not having the same behavior at large distances from the line center are definitely eliminated. Working over a smaller range of x's others have found that Eq. (9) gives a somewhat better representation of the absorption than other line shapes do. Curves such as Fig. 8 taken during this work furnish much more definite proof of this.

Classically this line shape arises from the Lorentz theory of collision broadening. During a collision the motion of the radiating body is changed in frequency or in phase, resulting in an effective chopping off of the monochromatic wave train being emitted or absorbed. The classical treatment

[9] Dennison, Phys. Rev. **31,** 510 (1928).
[10] Zahn and Miles, Phys. Rev. **32,** 497 (1928).
[11] Dunham, Phys. Rev. **35,** 1347 (1930).

of the effect on the absorption line of such an interruption assuming a definite cross-section of the molecules for collision, but allowing a distribution of velocities and mean free paths, has been worked out by Dennison.[9] He has shown that the resulting line shape is very closely given by a formula of the type (10) where the half width b can be related to σ the collision diameter, $\bar{v}$ the mean square velocity and N the number of molecules per cc. The actual formula is

$$b = n\sigma^2\left(\frac{7.60\,kT}{2\pi m}\right)^{1/2} = 0.78\,n\sigma^2\bar{v}. \tag{25}$$

The results of the application of Eq. (25) to the experimentally determined values of b are to be found in Table I. The values of σ found are somewhat larger than that calculated from gas kinetic data which is about 4.5A. However the magnitudes being measured in the two cases are not identical since a collision which is effective in determining the line shape may alter only the phase of a rotating molecule without affecting its energy. It should be emphasized that the line width is not an intrinsic property of the molecules as is intensity. The line width is determined by the type and frequency of the collisions. Also it might possibly be quite different for a CO molecule in an atmosphere of CO than in an atmosphere of N_2 even though the gas kinetic phenomena would be almost the same.

It is probable that most of the collision perturbation arises through its effect on the molecular rotation. The vibration is little affected by thermal collisions, while it appears that the rotational state is changed at about every gas kinetic collection.[5,12] However the collision diameter considered in these references need not be the same as that calculated here. A change of phase can affect a wave train but not an energy except in its uncertainty. It would seem that phase change may be a measurable quantity in line width determinations.

In conclusion it may be said that a method of measuring infrared absorption intensities has been tried and found satisfactory although somewhat cumbersome. It suffers from the fact that many absolute measurements must be made in which errors of standardization may easily arise. The final accuracy, while not large, appears to be definitely better than that previously attained owing to a greater sensitivity of the apparatus.

I wish to thank Professor D. M. Dennison for the suggestion and guidance of this problem and Professor W. F. Colby for many illuminating discussions.

[12] Oldenberg, Phys. Rev. **37**, 194 (1931).

Raman Spectra of a Series of Octanols

By GEORGE COLLINS
Rowland Physical Laboratory, The Johns Hopkins University

(Received April 4, 1932)

The Raman spectra of a series of nineteen octanols were obtained using Hg 4358 as the exciting line. These alcohols have structures which differ only in the relative position of a CH_3 and OH group along the side of a straight carbon chain seven atoms long. The Raman spectra consist in most cases of from seven to ten modified lines whose position and intensity vary considerably for the different compounds. A comparison of the Raman spectra and the molecular structure leads to an interpretation of most of the modified lines in terms of modes of vibration of the molecules. The lines which have been accounted for appear to be due to vibrations of the type C-H, CH_3–X, OH–X, and a C–C vibration in a plane at right angles to the length of the chain.

INTRODUCTION

INTEREST in Raman spectra has been confined largely to relatively simple cases where it has been possible to interpret the observed lines in terms of modes of vibration of the molecules. An approach to the problem

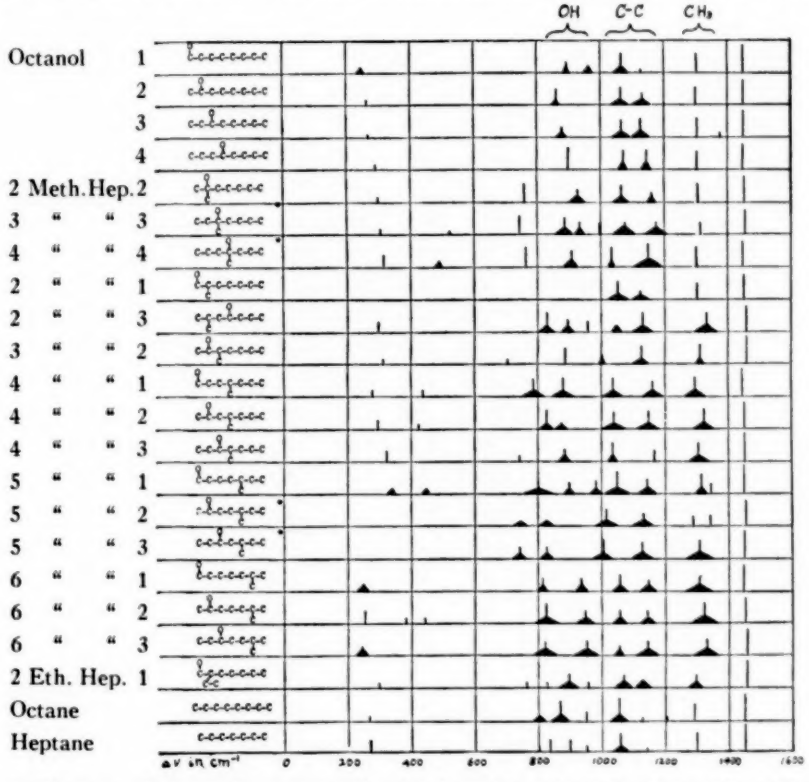

Fig. 1. Diagram of Raman frequencies showing breadth and relative intensities of lines.

of interpreting the Raman lines of more complicated molecules, however, was made possible by the synthesis here of a rather complete series of straight chain hydrocarbons. These were carefully prepared and purified under the direction of Professor Reid of this University by H. B. Glass, G. B. Malone and G. L. Dorough. The series consists of twenty-one octanols which differ from one another only in the relative positions of a methyl and hydroxyl group along the chain. Diagrammatic formula of these molecules are shown in Fig. 1. It is seen that the differences in their structure is slight and the investigation of their Raman spectra was undertaken with the hope that such a series would present an insight into the modes of vibration of long chain molecules. These octanols have already been the subject of considerable investigation and many of their physical and chemical properties have been determined.[1,2]

Procedure

The Raman spectra of these octanols were excited by Hg 4358. As they were available only in small quantities it was necessary to employ a special method of excitation devised by Wood.[3]

A filter composed of a concentration solution of quinine sulphate was introduced to absorb Hg 4047 which otherwise produced fluorescence, and an overlapping of the Raman spectra. The samples were prepared by slowly distilling the octanols, under a vacuum, without boiling. This freed them of suspended impurities which intensify the background on the photographic plate by direct scattering of the continuous spectrum of the mercury arc. Four of the octanols (indicated by an * in Fig. 1) decomposed under the action of the exciting light and in these cases the sample was repeatedly changed during excitation. The spectra were photographed with a small glass spectrograph having a disperion of 80A per mm. Little would be gained by photographing these spectra with an instrument of higher resolving power, as the natural width of the Raman lines seems to be several angstrom units. The increased intensity of the lines accompanying this low dispersion, on the other hand is a decided advantage. Exposure times varied from twelve to eighteen hours depending on the intensity of the continuous background. Wave-length determinations were made in duplicate and redetermined in cases where the agreement was not satisfactory. They were obtained by plotting a dispersion curve for each plate from the iron comparison spectrum and reading from this curve, by interpolation, the wave-length of the Raman lines. The frequency differences between these lines and Hg 4358.3A were then calculated using Kayer's "Tabelle der Schwingungszahlen." These frequency differences for relatively sharp lines are correct to about ± 5 cm^{-1}.

Results

Raman spectra of nineteen of the octanols were obtained and the results represented graphically in Fig. 1, and in tabular form in Table I. The height

[1] Crystal structure investigated by R. L. Edwards and G. W. Stewart, Phys. Rev. **35**, 291 (1930).

[2] A complete summary of the investigated properties of these octanols will soon be published by E. E. Reid.

[3] R. W. Wood, Jour. Franklin Institute 208 (1929).

TABLE I. *Raman frequencies expressed in $\Delta\nu$'s (cm^{-1})*

Octanol 1		264 (1)	894 (2)	966 (1)	1067 (3)	1129 (0)	1306 (3)	1449 (5)			
	1	274 (1)	862 (3)	1067 (3)	1134 (2)	1299 (3)	1447 (5)				
	3	269 (1)	879 (2)	1062 (3)	1129 (3)	1304 (3)	1448 (5)				
	4	292 (2)	898 (3)	1070 (3)	1143 (3)	1306 (3)	1446 (5)				
Meth. Hep.											
2	1	1055 (3)	1125 (2)	1305 (3)	1452 (5)						
2	2	292 (1)	356 (0)	762 (3)	937 (2)	1062 (3)	1162 (1)	1306 (3)	1452 (5)		
2	4	292 (1)	830 (3)	898 (1)	959 (1)	1048 (1)	1134 (3)	1334 (3)	1457 (5)		
3	2	315 (1)	707 (1)	886 (2)	1002 (1)	1131 (3)	1308 (3)	1457 (5)			
3	3	305 (1)	523 (0)	744 (3)	886 (3)	935 (2)	997 (2)	1077 (2)	1174 (2)	1313 (3)	1457 (5)
4	1	279 (1)	437 (1)	786 (3)	881 (3)	1038 (3)	1166 (2)	1294 (3)	1443 (5)		
4	2	299 (1)	427 (0)	828 (3)	876 (1)	1041 (3)	1155 (3)	1322 (3)	1455 (5)		
4	3	323 (1)	744 (0)	884 (2)	1036 (3)	1169 (2)	1304 (3)	1455 (5)			
4	4	315 (2)	488 (1)	769 (3)	903 (2)	1038 (3)	1155 (4)	1301 (3)	1443 (5)		
5	1	343 (1)	447 (1)	801 (2)	903 (2)	983 (2)	1048 (3)	1143 (2)	1317 (3)	1343 (1)	1448 (5)
5	2	747 (1)	825 (1)	1014 (3)	1134 (2)	1290 (2)	1346 (2)	1452 (5)			
5	3	747 (1)	825 (2)	1005 (3)	1129 (2)	1308 (3)	1446 (5)				
6	1	245 (1)	815 (2)	937 (2)	1055 (3)	1150 (2)	1308 (3)	1446 (5)			
6	2	251 (2)	381 (1)	442 (1)	823 (3)	947 (2)	1057 (2)	1141 (2)	1322 (3)	1452 (5)	
6	3	243 (1)	820 (2)	956 (2)	1055 (1)	1146 (2)	1336 (3)	1455 (5)			
2 Ethyl Heptanol 1		297 (1)	766 (1)	825 (1)	894 (2)	959 (1)	1069 (2)	1129 (1)	1294 (2)	1455 (5)	
Heptane		207 (2)	835 (2)	896 (2)	954 (1)	1060 (3)	1141 (0)	1304 (3)	1448 (5)		
Octane		271 (2)	804 (1)	862 (3)	952 (2)	1053 (3)	1131 (0)	1205 (0)	1290 (3)	1446 (5)	

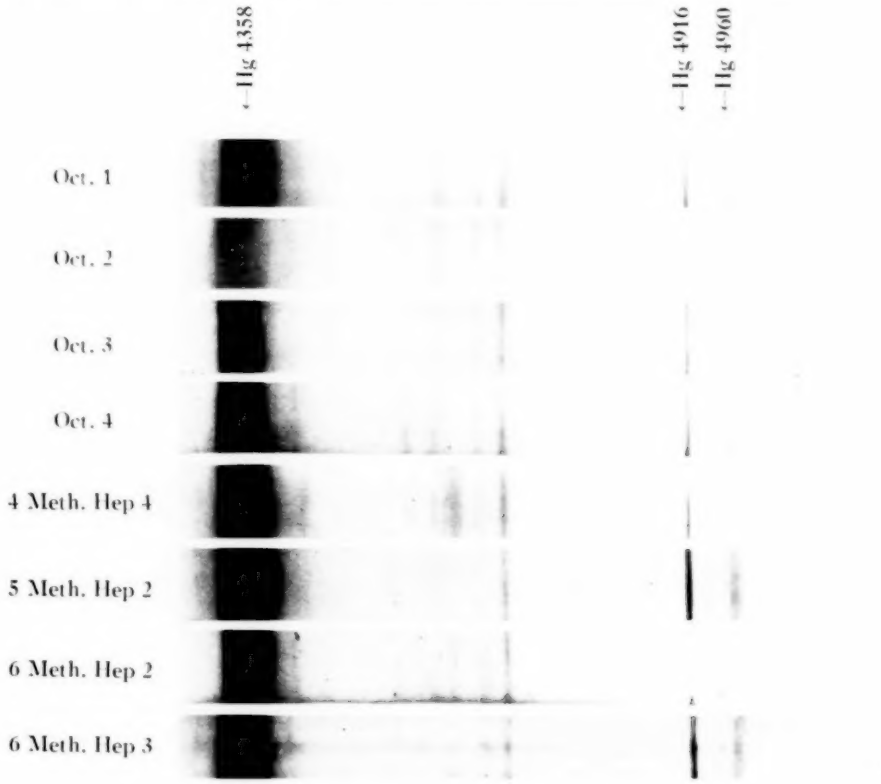

Fig. 2. Raman lines excited by Hg 4358.

of the lines in Fig. 1 indicates the relative intensity of the Raman lines as estimated by eye. The approximate width of the Raman lines is indicated on this diagram by the breadth of the line at its base. For purposes of comparison the Raman spectra of heptane, octane and two ethyl heptanol 1 were photographed with the same apparatus and the results included in Fig. 1 and Table I.

Fig. 2 shows the enlargements of some typical plates. It is to be noticed that there are considerable differences in the character of these spectra, in that the Raman lines show more clearly for some compounds than for others. In order to minimize the possibility of poor alignment being responsible for this, most of the spectra were photographed twice. It was found, however, that these differences are due largely to inherent differences in the compounds. All the lines showing in Fig. 2 are Raman lines with the exception of Hg 4358, Hg 4916 and Hg 4960 which are so marked.

An interpretation of some of these Raman lines in terms of modes of vibration of the molecules may be made. The strong line at 1450 cm^{-1} which appears in most hydrocarbons has been attributed by Dadieu and Kohlrausch[4] as due to vibrations of the hydrogen atoms of the

groups at right angles to the bond.

The lines which occur at about 1300 cm^{-1} have been attributed to the vibrations of a methyl group against the rest of the molecule. This explanation receives support from an examination of the character of this line as it appears in the different octanols reported here. For compounds which have methyl groups only on the end of their molecules this line is single and quite sharp. The examples of this are octanol 1, 2, 3, 4, heptane and octane. For compounds which have an additional methyl group attached to the side of the molecule this line is either broad or double. The inference is that methyl group attached to the end and middle of the molecules have slightly different frequencies of vibration which accounts for the broad or double character of this line. The compounds which have this characteristic are shown in Fig. 1 between two methyl heptanol 1 and 6 methyl heptanol 3. This interpretation would at first seem to suggest that the lines at 1300 cm^{-1} in the spectra of the three tertiary alcohols, 2 methyl heptanol 2, 3 methyl heptanol 3, and 4 methyl heptanol should be broad. As a matter of fact they are not. The explanation of this apparent discrepancy is that these compounds have a CH_3 and OH group attached to the same carbon atom. The presence of the OH group opposite the methyl group apparently results in a mutual vibration of the two with a frequency very much less than that of the CH_3 group against the carbon chain alone. The effect of this is to leave the line at 1300 cm^{-1} single and sharp and produces a new line in another region. This new frequency is to be found in the Raman spectra of these three compounds at about 755 cm^{-1} and does not appear in the spectra of any of the other compounds. A similar line is reported by Trumpy[5] for tertiary butyl alcohol at 748 cm^{-1} which obviously has the same origin.

The origin of the Raman lines which appear in Fig. 1 between 1000 cm^{-1} and 1200 cm^{-1} can be ascribed to vibrations of the carbon atoms. Straight

[4] Dadieu and Kohlrausch, Ber. der. Deutsch. Chem. Ges. **63,** 251 (1930).

[5] B. Trumpy, Zeits. f. Physik **62,** 806 (1930).

chain molecules of more than seven carbon atoms show a strong line or group of lines in this region, and their position does not change greatly with changes in the length of the molecule. Very recently the Raman spectra of the normal alcohols and bromides from C_9 to C_{13} have been obtained. They verify the observation that the position of these lines at about 1100 cm^{-1} is not greatly influenced by the length of the molecule and are but slightly influenced by the radical attached to the ends of the molecule. The vibration associated with these Raman lines must then be one which would be independent of the length of the molecule. From x-ray data, and the chemical behavior of organic compounds it has been well established that the carbon atoms of straight chain molecules do not lie in a line but have a zigzag formation. X-ray data[6] for the crystal structure of long-chain compounds indicates that the carbon atoms line in a plane and that the angle between the lines joining successive carbon atoms is nearly the tetrahedral angle of 108°28′. Assuming that this general structure is retained in the liquid state, a vibration which would be independent of the length of the molecule would be one in which the carbon atoms on one side of the chain vibrate as a whole with respect to those on the other wide of the chain (See Fig. 3). The frequency of such a vibration may be easily calculated. For an infinitely long molecule this frequency may be determined by considering simply two adjacent carbon atoms.

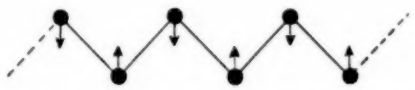

Fig. 3. Diagram illustrating type of vibration of carbon atoms responsible for lines between 1000 cm^{-1} and 1200 cm^{-1}.

The formulas used is

$$\omega = \frac{1}{2\pi}\left(\frac{2f\cos\theta/2}{\mu}\right)^{1/2}$$

where f is the force constant for the C-C bond, μ is the reduced mass of two carbon atoms, and θ is the angle between the C-C bonds. Using Kohlrausch's value of f for the C-C bond of 4.31×10^5 dynes/cm and $\theta=108°$, $\omega=1075$ cm^{-1}. This value lies nicely within the frequency range covered by the lines in question. For all the compounds shown in Fig. 1 with the exception of octane, heptane and octanol 1 the lines between 1000 cm^{-1} and 1200 cm^{-1} appear to be double in character. As only the normal compounds possess a single line in this region it seems likely that the presence of an OH or CH_3 group along the side of the chain is responsible for the doubling of this frequency.

The assumption that the structure of these molecules is the same in the liquid state as in the solid state is, of course, open to question. The difference to be expected is that in the liquid state the carbon atoms of the molecules will probably no longer lie in a plane. This may account for the extreme breadth of the lines.

[6] A. Müller, Proc. Roy. Soc. (London) **120A,** 437 (1928); **127A,** 417 (1930).

As in the case of the lines between 1000 cm^{-1} and 1200 cm^{-1} there seems to be a tendency for the lines between 800 cm^{-1} and 1000 cm^{-1} to exist in pairs. As shown by Trumpy this is the region in which Raman lines arising from vibrations of the OH group against a long carbon chain would be expected to occur. The fact that they are double seems again to be associated with the presence of the CH_3 group along the side of the molecule.

I am indebted to Professor R. W. Wood for his assistance and interest in this work, and to Professor E. E. Reid who kindly provided me with the octanols.

The Absorption Spectrum of Water Vapor Beyond 10μ

By LOUIS RUSSELL WEBER AND H. M. RANDALL
Physical Laboratory, University of Michigan.

(Received March 9, 1932)

The absorption spectrum of water vapor has been remeasured in the region 10–25μ, the dispersing agent being a 60° KBr prism with a Wadsworth-Littrow mounting. The recording vacuum spectrograph is described. The necessary amplification is obtained by means of the Moll or the Firestone amplifier. The increased dispersion of this spectrograph shows the spectrum to be very complicated in this region and not yet fully resolved. No decision has been reached as to the nature of this spectrum, whether it is a vibration-rotation band, the near end of the rotation spectrum, or an overlapping of the two.

THE new vacuum recording spectrometer,[1] recently described, possesses a range which extends to about 30μ. This increased spectral range in a region of the spectrum until now little explored, is due to the complement of prisms, made from single crystals grown in this laboratory from the fused salts. The materials so far successfully fashioned into prisms are potassium chloride, potassium bromide and potassium iodide. This instrument holds promise of usefulness, particularly in the region beyond 15μ, the limit set by the opacity of sodium chloride. The prism spectrometer possesses the obvious advantage in distinction to a grating of conserving the energy available in a single spectrum. By using one or more prisms in a train and reversing the beam, a dispersion approximating that of a grating may be obtained. The crystals besides making prisms, also furnish materials for windows of absorption cells, for vacuum thermopiles, etc.

The first extensive work with this instrument has been with water vapor. Its spectrum has been extensively studied in this laboratory[2] up to and through the band at 6μ which extends well beyond this central point. There appeared to be the possibility of deciding through the largely increased resolution of this instrument whether the bands known to exist beyond 10μ were pure rotation bands or were another vibration-rotation band. Moreover, it is necessary to know the water vapor spectrum as produced by this spectrometer whenever the instrument is used with other materials, provided any part of the beam from source to recording thermopile passes through the air of the room. This is because the water vapor of the air is always present in sufficient quantities to produce marked absorption lines, particularly beyond 15μ. To a lesser extent the carbon dioxide of the air presents a similar problem.

The self-recording spectrometer used in this work has some marked advantages. With the present instrument, it is possible to record a spectral

[1] Randall and Strong, Rev. Sci. Inst. **2,** 585 (1931).

[2] Sleator, Astrophys. Journ. **48,** 126 (1918); Sleator and Phelps, Astrophys. Jour. **62** 28 (1925); Sleator and Plyler, Phys. Rev. **37,** 1493 (1931).

range of 15μ in one and one-half hours. One can keep the conditions of the source, absorption cell, and spectrograph more constant than is possible when several days are required for one complete set of measurements. Furthermore, a recording spectrograph makes a continuous record, leaving nothing to the conjecture of the experimenter as to what takes place between circle readings taken at definite intervals. The saving in time thus gained can be used for making several records. This not only makes precise measurements possible but permits the elimination of extraneous influences with greater certainty.

The spectrometer Fig. 1 is a Wadsworth-Littrow combination, using a 60° prism of potassium bromide. The radiation enters the slit S and is reflected by the small mirror M''' to the parabolical mirror M, 14 cm in diameter. This mirror, M, is a segment cut from a larger paraboloidal mirror in such a manner that the axis of the paraboloid passes through the edge of the mirror, M. M is so adjusted that this axis passes midway between the slit S' and the virtual image of S. Since these are close together the aberration is reduced to a minimum. In order that the more essential features of the instrument may be seen readily, the supports which carry the slits S and S' are not shown in

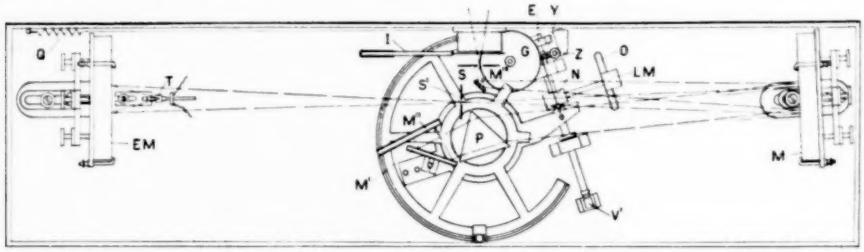

Fig. 1. Inner brass compartment of the spectrograph containing optical parts.

the figure. The rays after being made parallel by M, pass through the prism P at almost minimum deviation. The Wadsworth mirror M' which moves with the prism, reflects the rays to the Littrow mirror M'' which is stationary so that they strike the latter almost normally. Retracing their path, they again pass through the prism at nearly minimum deviation to the mirror M which brings them to focus on the exit slit S'. This slit of 25 mm length, is at one of the foci of the elliptical mirror EM, and the thermopile T is at the other focus. These foci are 43.75 and 8.75 cm from the mirror, so as to produce an image on the thermopile junctions one-fifth the size of the exit slit. The spectrograph as described is enclosed in a heavy brass case, which in turn can be rolled into a heavy welded steel case. This latter case is so designed that any deformations produced by evacuation can in no way affect the brass case. The complete spectrograph is evacuated to pressures varying from 10^{-3} to 10^{-4} mm using a fore pump working with two mercury diffusion pumps.

The thermopile and its mounting were designed by Firestone.[3] The three junctions are composed of bismuth and an alloy of bismuth and tin. Since the

[3] Firestone, Rev. Sci. Inst. **1**, 630 (1930).

linear thermopile was enclosed in a case only 10 mm long, it intercepted very little energy when placed in front of the elliptical mirror. The sensitivity increased approximately nine-fold when the case was evacuated to 10^{-3} mm.

The potassium bromide prism was made from a single crystal which was grown in the laboratory from the fused salt, and has a refracting angle of approximately 60°. The faces are 6.5 cm high and 7 cm long. The theoretical resolving power, computed from the indices of refraction recently measured by Gundelach,[4] is 366.8 at 10μ and 1295 at 25μ.

The practical resolving power in which we are primarily interested because of our finite slit widths is shown in Table I in which the slit-widths are

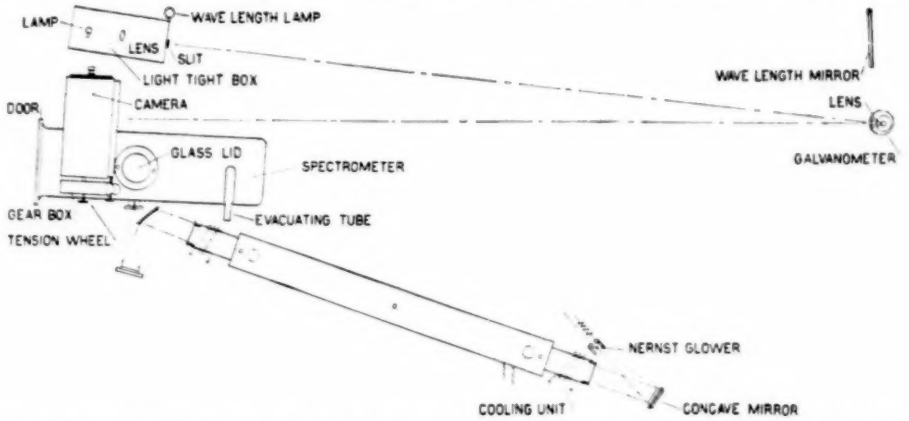

Fig. 2. Arrangement of apparatus showing the outer welded steel case containing the spectrometer, the camera, the absorption cell, and the registering equipment.

TABLE I. *Practical resolving power of spectrometer.*

Slit width	Region	Wave number	Angstroms	Seconds	Hettner
	10μ	5.90	590		700A
0.2 mm	17	1.18	340	20.7	3900
	23	0.43	240		17400
	10	11.80	1180		
0.4 mm	17	2.36	680	41.4	
	23	0.86	480		

given in terms of wave number, angstrom units, and seconds of arc. For comparison Hettner's slit widths are included. Thus, at 23μ, the interval included by the slit is 70 to 35 times smaller than that used by Hettner,[5] depending upon the slit used. At 17μ, the interval is 6 to 12 times smaller. The present determinations were made with these two slit widths 0.2 mm from 10 to 15μ and 0.4 mm from 15 to 25μ. The exit slit was kept at the same value as the entrance slit.

Two lengths of absorption cell were used, of two meters and three meters respectively. Fig. 2 shows one of the cells in detail. It was composed of several

[4] E. Gundelach, Zeits. f. Physik **66,** 775 (1930).

[5] Hettner, Ann. d. Physik **55,** 476 (1917).

lengths of galvanized iron pipe 6″ in diameter joined together rigidly by partly telescoping one section into the other. In each end a brass ring was fitted snugly and sealed with liquid porcelain. These rings had been prepared so that a shoulder extended beyond the end of the cell for the purpose of receiving the holders of the lacquer films used to close the ends. This permitted an airtight joint.

Besides the ends, the cell had three 1″ openings to receive thermometers, one at each end and one in the middle. The gas inlet and outlet were placed, one on top at one end, and one on the bottom at the other end to insure a more uniform filling of the cell. They were 3″ in diameter. The whole cell, except for 15 inches at each end, was covered with a layer of asbestos paper which was wound with resistance wire to permit heating the cell to 350°C if necessary. In order to reduce temperature changes in the room as much as possible and to keep the cell at a more uniform temperature, a cylinder of magnesium and asbestos was fitted around the cell. The whole was further covered with canvas.

Since the lacquer films were easily ruptured at high temperatures, it was necessary to cool the ends of the cell by running water through six or seven turns of lead tubing wound around each end. To make films whose diameters were five inches, we placed three small wires equispaced along diameters of the ring and in the plane of the ring. These intercept very little energy and make the film much more capable of standing up under its own weight or any vibrations to which it might be subjected.

The films were approximately 0.5μ in thickness and transmitted practically all the radiation in the region from 10μ to 25μ except at 12μ where the absorption amounted to about 80 percent. They were removed when this region was under investigation. In working with steam in the region from 10μ to 25μ, it is not absolutely necessary to have the ends of the cell closed, provided any mirrors near the cell are protected from condensation or are sufficiently removed so that no condensation takes place on them.

The source consisted of a small Nernst glower enclosed except for one side, in a small asbestos box. Although the glower was operated on the alternating current lighting circuit, no trouble was experienced in fluctuations. It was placed very near to the end of the cell as shown in Fig. 2 and at the principal focus of a concave silvered mirror whose diameter was 12 cm and whose focal length was 25 cm. Thus, the rays traversing the cell were parallel, and upon emerging from the cell, fell upon a plane silvered mirror 20 cm in diameter. This mirror was far enough from the end of the cell so that when no films were used, no condensation took place on it. The rays were then reflected to a gold plated concave mirror and brought to focus on the entrance slit of the spectrometer which was covered by a potassium bromide plate to make possible the evacuation of the spectrograph.

The main features of the recording system were as follows. The thermopile was connected to a Moll thermal relay for most of the work; later, to eliminate all drifts, an alternating current amplifier due to Firestone was used. This will be described in more detail below. The amplification used with the

Moll relay was approximately 45 which gave deflections of 50 cm at 10μ to 3 cm at 25μ for slits of 0.2 mm width. The distance from the galvanometer to the camera is 4.5 meters. The amplification was limited by the Brownian motions affecting the galvanometer coil and also by the drifts that might be present. By means of the lamp and optical system shown in Fig. 2, a point image of the slit in the end of the light-tight box was produced on the photographic paper in the camera. The drum holding the photographic paper moves perpendicular to the deflection of the galvanometer and in coordination with the prism.

The whole mechanism for causing the coördinated movement of drum and prism was driven by a small universal motor. A Veeder counter placed on the spectrograph allowed one to read the position of the prism in arbitrary numbers which were approximately equal to seconds of arc. Since the calibration to be described shortly, consisted in getting the wave-lengths as a function of these Veeder numbers, the Veeder counter was always used to set the prism for throwing radiation of a certain wave-length into the exit slit. For every 30 seconds of arc turned through by the prism, a contact was closed on the spectrograph case, causing the lamp labelled "wave-length lamp" to flash. The light from this lamp was reflected back by a plane mirror near the galvanometer and entered the camera producing a fine reference line on the photographic paper with the aid of a cylindrical lens whose length equals that of the camera box. Thus, as we shall see later, this makes the measurement in terms of wave-length quicker and limits the error due to a shrinkage of the paper to a negligible amount. The bromide paper sheets were 20×31 inches so that the region from 10 to 23.5μ could be recorded on one sheet during one revolution of the drum in 90 minutes of time. The drum was usually operated so that the time between reference lines on the paper was 15 seconds and the distance between them was 2.5 mm. Several records were taken with a time interval of 114 seconds and a distance between lines of approximately 8 mm. This interval still represented 30 seconds of arc with respect to the prism.

When the present investigation was near an end, Mr. Firestone had just perfected an amplifier which eliminated all drift of the zero. A full description of this has just appeared[6] so only a brief account will be included here. In merely by connecting a large condenser in series with the galvanometer (across which is a shunt resistance for critical damping), and then periodically interrupting the radiation falling on the thermopile. The galvanometer would then give an oscillating deflection, the amplitude of oscillation being proportional to the amount of radiation falling on the thermopile. But since the drifts can not pass through the condenser, the oscillations of the galvanometer will always take place about the same zero. However, any condenser to be found in the laboratory would have such a high impedance at these low frequencies that the sensitivity of the system would be too low. By using a photoelectric cell and vacuum tube in the system to amplify the deflections of the primary galvanometer, circuits of sufficiently high impedance are en-

[6] Firestone, Rev. Sci. Inst. **3**, 163 (1932).

countered that condensers may be connected in series with them without seriously imparing the sensitivity. Thus, although the primary galvanometer may be subject to a considerable amount of drift, the secondary galvanometer, which is making the record, receives only the periodic deflection, the drift not being passed through the amplifier. All galvanometer, amplifier, and thermopile leads were enclosed in copper sheathing to eliminate electrical disturbances either from circuits in the room or other apparatus in the building.

Although the spectrograph was equipped with a very good circle to be read by means of a sealed-in microscope, it was believed that a much quicker method of calibration would be an empirical one. Therefore, the absorption spectra of gases previously measured with a grating to 15μ were recorded and a curve was then plotted between the known wave-lengths and their Veeder numbers as read on the instrument.

TABLE II. *Substances used and their absorption wave-lengths.*

Substance	(Wave-length) μ in air	Veeder number	Wave-length	Veeder number
Ammonia[7]				
	10.32μ	42400	20.29**	47975
	10.71	42550	20.42	48062
Acetylene[8]	13.69	43810	20.62	48230
Methyl Iodide[9]	11.29	42765	20.82	48394
Methyl Iodide[9]	11.90	43000	21.12	48619
Methyl Bromide[10]	16.38	45260	21.34	48784
Carbon Dioxide[11]	14.97	44475	21.82	49203
Water Vapor*	15.991	45052	22.07	49401
	16.190	45181	22.88	50135
	16.667	45452	23.81	51004
	16.893	45593	24.61	52069
	17.102	45723		
	17.220	45799		
	17.360	45884		
	19.023	46999		

Data beyond 15μ has been kindly supplied by Mr. Norman Wright and Dr. E. K. Plyler, who were working with gratings in the region beyond 15μ. Mr. Wright had found water vapor absorption superimposed upon the energy curve of reststrahlen from quartz in the region of 20μ. The pattern was so unmistakably the same as obtained previously on the recording spectrograph when 0.8 mm slits were used that these series of points were used for extending the calibration curve. They were measured with a grating with an accuracy of 0.01μ. In taking "in and out" readings in the absorption spectrum of another gas in the near infrared, Dr. E. K. Plyler noticed that the "out" readings varied considerably due to atmospheric absorption. He very kindly

[7] Barker, Phys. Rev. **33,** 684 (1929).
[8] Meyer and Levin, Jour. Op. Soc. **16,** 137 (1928).
[9] Bennett and Meyer, Phys. Rev. **32,** 888 (1928).
[10] Sleator, Phys. Rev. **38,** 147 (1931).
[11] Martin and Barker, Phys. Rev. **37,** 1708 (1931).
* Checked from "out" curves of Plyler.
** Duplicated by Wright.

permitted the writers to plot these values and a number of these bands were found to correspond with those already found in our work. Dr. Plyler's readings are accurate to $\pm 0.001\mu$. It is believed the points can be taken from the dispersion curve with an accuracy of $\pm 0.01\mu$. An inspection of the entire calibration curve from 1 to 25μ shows that it follows the general characteristics of dispersion curves for other salt prisms.

The substances used and their wave-lengths of absorption are given in Table II.

Since this recording spectrograph is just coming into general use, its method of recording data will be described with some detail. The spectrograph was generally evacuated to 10^{-4} mm of mercury pressure before a record was made. If the region from 10μ to 15μ was under investigation, steam was led from the generator into the top of the cell at one end, the cell being heated to over 100°C. If, on the other hand, the region from 15μ to 25μ was to be recorded, a long trough containing water was placed in the bottom of the cell. This produced saturated water vapor at room temperature. After all conditions regarding amplifier, cell, and spectrograph were believed constant as learned by experience, the camera was loaded and the register lamp adjusted. The shutter in front of the camera was opened, exposing the cylindrical lens and the photographic paper. Finally, the metal shutter in front of the entrance slit was raised. The small driving motor was then started after the Veeder number had been recorded. For convenience, the instrument was always started when the circuit of the lamp used to record the reference lines was closed. By pausing a second after the camera shutter was opened, a darker reference line was produced on the paper than those made in the course of the record. Hence, there was no doubt about the initial Veeder number.

At intervals of about 1000 Veeder numbers, the motor was stopped and the metal shutter in front of the entrance slit was closed. This recorded the deflection photographically on the paper. Afterwards, a line drawn through these points furnished a base line with the aid of which percentage absorptions could be estimated. With the Firestone amplifier described above, the zero point of course always remained the same.

Sometimes, more than one record was obtained on the same sheet thus making a rapid comparison of curves possible. In this case, the reference lines were not put on a second time, experience having shown that the second set of reference lines either exactly coincided with the first set or were displaced at most by an amount corresponding to not more than one or two seconds of arc. The exact amount of this displacement could be determined by recording only a few of the subsequent sets of reference lines, and allowed for in reading the positions of the corresponding set of absorption lines.

Only those absorption lines that appeared on four or five records were accepted. The most intense lines always appeared; but the weakest ones could be influenced by the Brownian motion affecting the galvanometer so that care had to be exercised in making these determinations.

The greatest difficulty presents itself in the determination of percentage absorption. The energy is small at best and the percentage of spurious radia-

tion of shorter wave-lengths increases as 25μ is approached. If one can move the absorption cell in and out of the path, one can, by compensating devices, obtain the percentage absorption with a fair degree of precision. In the present case, the cell is too massive to lift out of the path and, furthermore, such a method is impossible with continuous recording. Also since carbon dioxide and the water vapor which is under investigation are always present in the atmosphere, the optical path cannot be entirely freed of them.

The method of determining the percentage absorption was as follows: (1) With the Moll relay. When employing this device, deflections were taken several times on a record by stopping the driving motor and closing the metal shutter in front of the entrance slit. A small dot was made on the paper in this way and the line of zero deflection of the galvanometer was found by drawing a smooth curve through these points. An envelope of the absorption curve was then drawn to determine the position the curve would have had

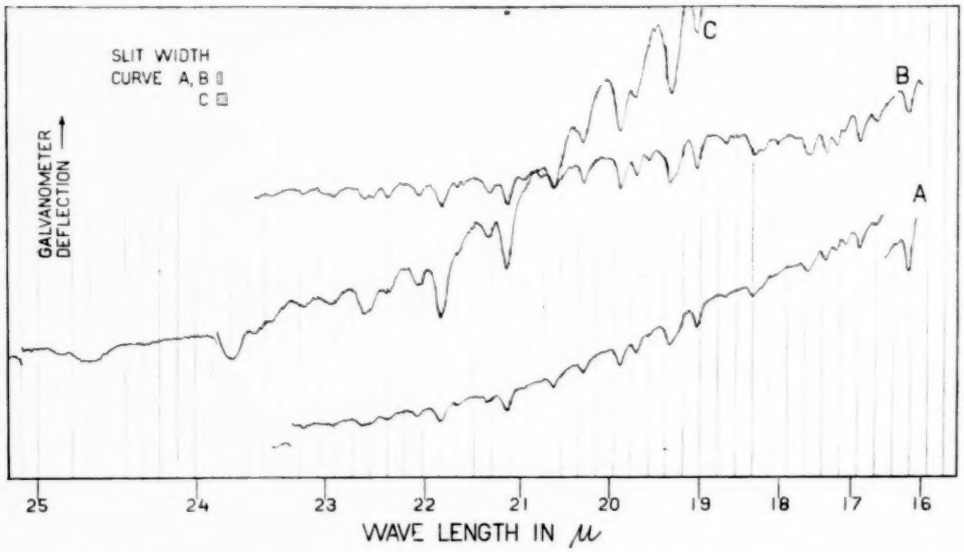

Fig. 3. Absorption lines in the region between 16μ and 25μ photographically registered, the amplification being by the Moll amplifier. Cell filled with saturated vapor at room temperature. Slit width curves *A* and *B*, 0.4 mm, *C*, 0.8 mm.

provided there were no absorption. The depth of the absorption was measured with respect to this envelope and the ratio of this distance to the distance between the envelope and the base line gave the percentage of absorption. Since there is always some scattered radiation of shorter wave-lengths, several deflections were taken in the region from 10μ to 20μ with a fluorite plate placed in the optical path before the entrance slit. Likewise a rocksalt plate was used in the region from 20μ to 25μ. Corrections were then applied to the apparent absorptions taking account, of course, of the loss of radiation due to the reflections from these plates and also a possibility of a slight change in focus. We believe that the percentage absorptions given later in the table will at least give the relative intensities with fair degree of accuracy. (2)

With the Firestone amplifier. Here the zero remains constant so that one can draw an envelope at the top and at the bottom of the recorded oscillations of the galvanometer. The available energy is then for any wave-length, one-half the distance between the envelopes while the transmitted energy is one-half the width of the record at the same wave-length. To get the percentage absorption, one merely subtracts the second value from the first one and divides this result by the first value. A correction for the scattered radiation must be made as before.

Figs. 3 and 4 show the curves obtained in the region from 10μ to 25μ as recorded with the Moll relay and the recording spectrograph. Of the three curves of Fig. 3, recording the region beyond 16μ, *A* and *B* were obtained when a slit width of 0.4 mm was used, while a slit width of 0.8 mm was used when *C* was recorded. The absorbing medium was saturated water vapor at room temperature obtained by placing a trough of water in the bottom of the

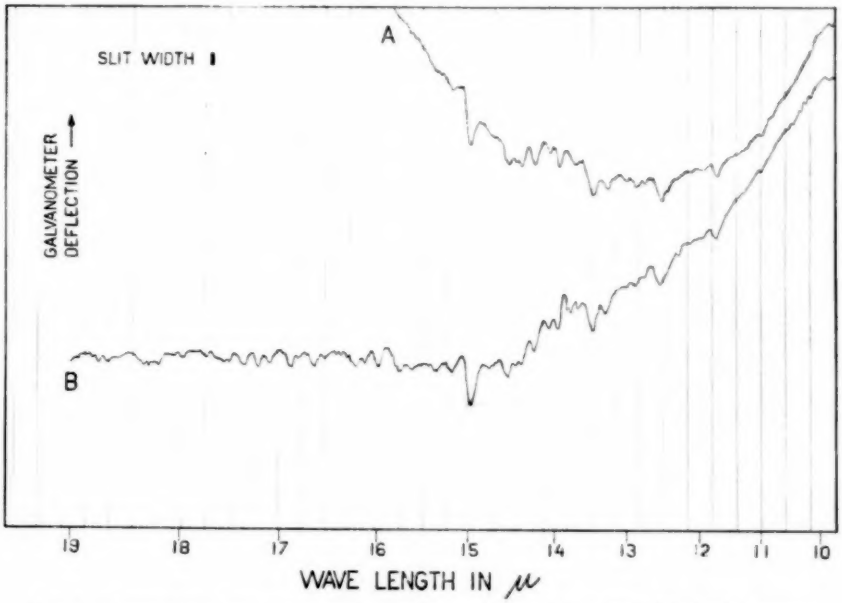

Fig. 4. Absorption lines in the region between 10μ and 19μ. Cell filled with steam for curves *A* and *B*. Slits 0.2 mm, Moll amplifier.

cell. The cell was not heated. *B* and *C* were recorded on the same sheet but *A* has been cut from another record and fitted for comparison. It is apparent that all of the lines repeat themselves very accurately. Curve *C*, however, which was obtained with twice the slit width of the other does not show as many lines resolved. In the reproductions of the original records only every fifth reference line has been drawn in.

The spectral region from 10μ to 19μ is recorded in Fig. 4. The curves shown were taken with slit widths of 0.2 mm since the available energy in this region was greater. With steam filling the three meter cell, and the cell heated to over 100°C, curves *A* and *B* were obtained. The fact that they do not have the slope of the other curves was due to a slight drift in the thermal relay

from the heat caused by the cell. Otherwise, they would have followed the energy curve of the glower except for the absorption present. If the drift is not too great, it is a distinct advantage, especially when one is in a region where the slope of the energy curve is great. As the curves clearly show, the falling off of energy is compensated by a drift so that the absorptions appear with less distortion than they otherwise would. As it was, the drift in *a* did become large enough to change the slope to one in the opposite direction.

Both Hettner's work and the present one, show the least absorption in the region from 10μ to 11μ. The strong line at nearly 15μ is due to CO_2 in the atmosphere. The region from 16μ to 19μ shows additional lines to those recorded in Fig. 3 since the resolution is larger here due to the narrower slit. It is unfortunate that lack of sufficient energy prevented a continuance of the curve out to 25μ with slits 0.2 mm wide. The ability of the instrument to repeat itself is shown by these curves and also those in the previous plates.

Several records, one of which is shown in Fig. 5, were obtained while using the Firestone amplifier already described. Due to the unvarying zero and the ease with which envelopes can be drawn to these curves, percentage absorptions can be obtained much more easily than with the Moll instrument. The results derived from them substantiate those of the previous work and add several new lines. Some of the records with the Firestone amplifier were made with the camera drum rotating three times as fast with respect to the prism as was the case when the curves of Fig. 5 were recorded. Then by running the driving motor so slowly that 114 seconds of time would elapse between reference lines instead of the usual 15, it was possible to obtain 30 instead of 4 complete oscillations of the galvanometer recorded between the reference lines, or one to each second of arc, since in terms of arc the reference lines are still but 30 seconds apart. Thus the spectrum was covered at much shorter intervals than is usually done when the circle is advanced by small steps without automatic recording.

Fig. 5 was obtained when the cell contained saturated water vapor at room temperature. The slit width was 0.5 mm. The increase in deflections at 16μ and again at 22μ is due to an increase of the amplification used. As in Fig. 4 very little absorption is evident in the region between 10μ and 15μ without having steam in the cell as the absorbing medium. That which is present is due mostly to CO_2.

Records in the region beyond 16μ, obtained when the slits were 0.2 mm with steam filling the cell, did not show sharper lines due undoubtedly to the fact that steam is too absorbing in this region. For this reason, only saturated water vapor at room temperature was used in this region to obtain the best records. Besides water vapor, the CO_2 content of the air also absorbed. Careful check experiments, in which the change in intensities of the lines were observed when the three meter cell was filled in turn with steam, CO_2, and dried air, determined which of the observed lines were due to water vapor and which to CO_2. Table III contains the results of this research.

The measurement of the water vapor spectrum as resolved by this recording spectrometer has been accomplished. But the question as to whether this

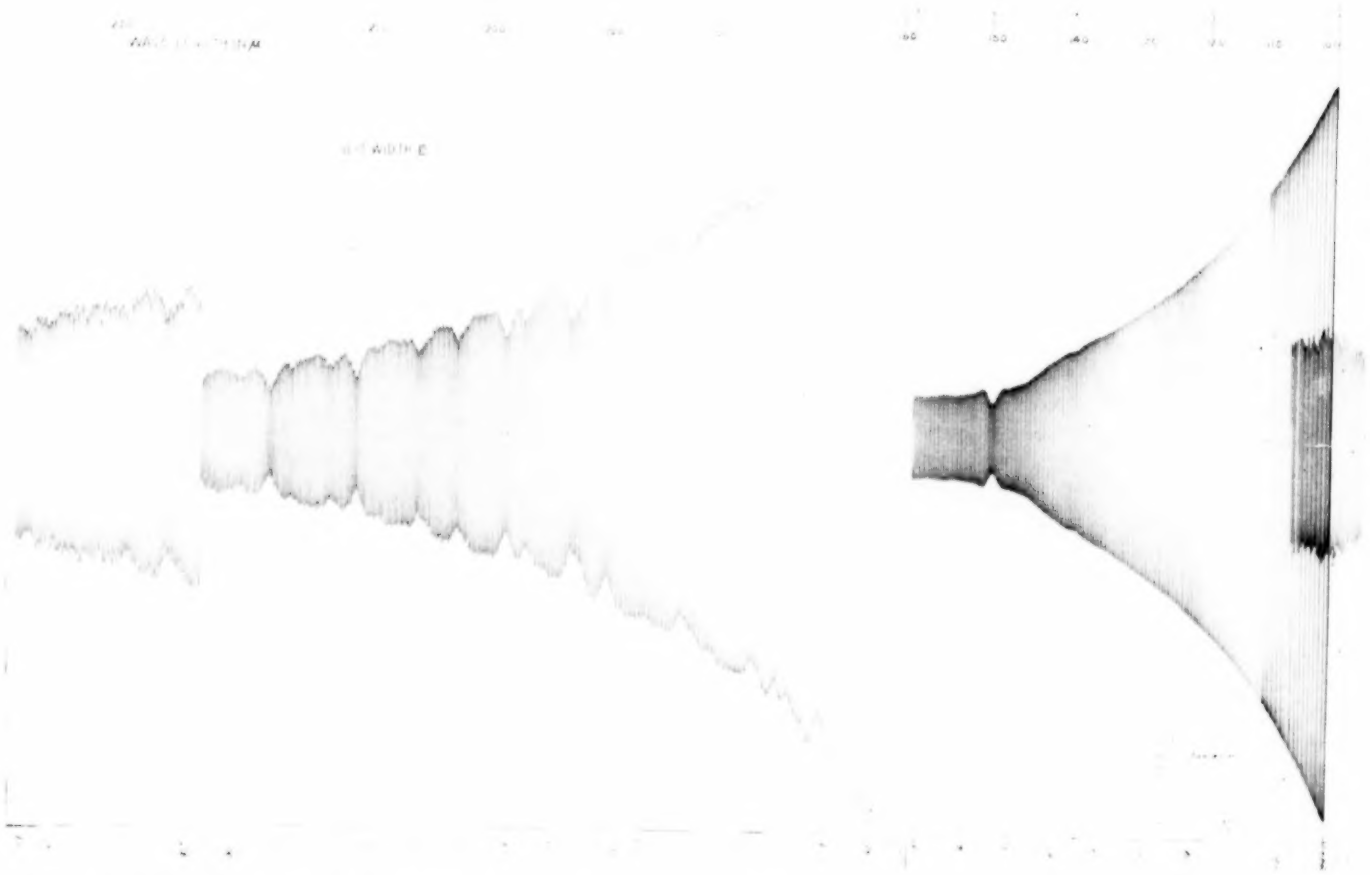

Fig. 5. Absorption lines in the region between 10μ and 23μ absorption cell filled with saturated water vapor at room temperature. Slits, 0.5 mm. Firestone amplifier used. Reference lines appear reproduced only at the extreme right of figure.

TABLE III. *Absorption spectrum of water vapor.*

Wave-length	Waves per cm	% Absorp. steam		Wave-length	Waves per cm	% Absorp. sat. vapor
10.13μ	987.2	1		16.58μ	603.1	2
10.20	980.4	1		16.667*	600.0	5
10.42	959.7	9		16.69	599.2	3
10.85	921.7	1		16.82	694.5	7
11.06	904.2	5		16.893*	592.0	14
11.22	891.3	1		17.102*	584.73	6
11.32	883.4	1		17.220*	580.72	13
11.55	865.8	1		17.360*	576.04	14
11.58	863.6	1		17.50	571.4	4
11.65	858.4	2		17.57	569.2	16
11.77	849.6	7		17.64	566.9	9
11.97	835.4	4		17.72	564.3	6
12.14	823.7	7		17.84	560.5	4
12.34	810.4	2		17.95	557.1	6
12.41	805.8	4		18.06	553.7	9
12.48	801.0	10		18.21	549.1	14
12.58	794.9	11		18.29	546.7	8
12.65	790.6	15		18.34	545.3	19
12.82	780.0	6		18.39	543.8	7
12.92	774.0	9		18.52	540.0	5
13.06	765.7	17		18.66	553.9	8
13.22	756.4	16		18.74	533.6	3
13.32	750.8	15		18.97	527.1	4
13.50	740.7	17		19.023*	525.68	21
13.74	727.8	9		19.10	523.6	5
13.95	716.8	18	CO_2	19.25	519.5	24
14.07	710.7	13		19.32	517.6	32
14.23	702.7	32		19.41	515.2	6
14.39	694.9	31		19.56	511.2	9
14.46	691.6	32		19.69	507.9	23
14.54	687.8	39		19.79	505.3	20
14.76	677.5	21		19.87	503.3	30
15.17	659.2	25		20.10	497.5	3
15.34	651.9	17		20.29*	492.9	24
15.40	649.4	23	CO_2	20.42*	489.7	4
15.55	643.1	23		20.53	487.1	7
15.62	640.2	24	% Absorp.	20.55	486.6	18
15.73	635.7	32	Sat. Vapor	20.62	485.0	28
15.92	628.1	22	1	20.76	481.7	9
15.991*	625.35	40	4	20.94	477.6	12
16.08	621.9	19	1	21.12*	473.5	53
16.11	620.7		6	21.14	473.0	43
16.190*	617.67	25	10 CO	21.18	472.1	23
16.38	610.5	9	2	21.29	469.7	22
16.53	605.0	14	1	21.34*	468.6	26
21.39	467.5	12		22.62	442.0	31
21.66	461.7	24		22.88*	437.0	21
21.74	460.0	39		22.98*	435.1	9
21.81	458.5	65		23.16*	431.8	10
21.85	457.7	42		23.44*	426.6	24
21.89	456.8	21		23.59*	423.9	42
22.07	453.1	35		23.81*	420.0	66
22.37	447.0	42		24.61*	406.3	28
22.39	446.6	42		24.72	404.5	38
22.55*	443.4	17		24.91	401.4	25

* Checked with grating.

system of lines belongs to the rotation spectrum or to the vibration-rotation spectrum, or an over lapping of the two, can not now be decided. Theory indicates that the pure rotation spectrum in this relatively short wave-length

region is very complicated. The interpretation of the rotation spectrum can probably best be approached from measurements at the long wave-length end of the spectrum. The experimental difficulties would then be greatly increased but the interpretation of the results would be correspondingly simplified. A plot giving the percentage of absorption as a function of the frequency shows an increasing absorption with increasing wave-length. Unfortunately circumstances have not permitted extending this investigation at this time beyond 25μ. If it could have proceeded to 30 or 35μ, it might have become definitely evident that the absorption was continuously increasing, or it might have shown a maximum. The first case would have indicated a rotation spectrum, the second a vibration-rotation band.

A slight appearance of symmetry, which is more evident in some of the other records than in those shown here, would indicate a vibration-rotation band with its center at 18.7μ approximately. On the other hand, such changes in intensity as occur in passing from saturated vapor at room temperature to steam at somewhat over 100°C are very irregular, a circumstance more in harmony with the supposition that the near end of the complicated rotation spectrum is involved than that a vibration-rotation band is concerned. It is possible that if a sufficiently high elevation of temperature of the absorbing vapor could be produced, such changes in the relative intensities of the observed lines would occur as would permit a decision as to which type of spectrum is involved, since the change in relative intensities would be quite different in the two types.

Some Physical Properties of Compressed Gases, III. Hydrogen

By W. Edwards Deming and Lola E. Shupe
Bureau of Chemistry and Soils, U. S. Department of Agriculture, Washington, D. C.

(Received April 20, 1932)

The compressibility data on hydrogen taken at the Reichsanstalt, the Leiden, and the Fixed Nitrogen Research Laboratories have been smoothed, averaged, and extrapolated to cover the range −215°C to 500°C and to 1200 atm. A sensitive graphical scheme for getting derivatives makes possible the calculation of some physical properties of gases; those on nitrogen and carbon monoxide have been published. The properties so calculated are specific volume, density, temperature and pressure expansion coefficients, fugacity, C_p, $C_p - C_v$, C_T, and μ. These are exhibited in graphs and a table that cover the temperature and pressure ranges mentioned above, except that it was not possible to calculate heat capacities and Joule-Thomson coefficient below −75°C. The expansion coefficients $(T/v)(dv/dT)_p$ and $-(p/v)(dv/dp)$ decrease monatonically from unity as the pressure increases from 0 to 1200 atm., along all isotherms within the range studied. This is in contrast with the behavior of nitrogen and carbon monoxide; with these gases the expansion coefficients along isotherms at low and ordinary temperatures at first increase with pressure, then drop back to unity and after that decrease as the pressure is increased. Fugacity is tabulated at integral temperatures and pressures throughout the entire range. The $C_p - C_v$ vs. p isotherms all show a maximum at about 500 atm. At −75°C, C_p increases 0.95 cal./mole deg. as the pressure changes from 0 to 1200 atm. The increase ΔC_p with pressure becomes less as the temperature is raised. At 500°C it amounts to only 0.08 cal./mole deg. in 1200 atm. ΔC_p is several times smaller for hydrogen than for nitrogen or carbon monoxide. The C_v vs. t isobars from 0 to 600 atm. form a family of almost parallel curves. At higher pressures a distinct maximum appears at about 50°C. The Joule-Thomson coefficient is +0.21 deg./atm. at −75° and zero pressure; it is 0 at −75° and 25 atm., and becomes negative at higher pressures. It is 0 at −62° and zero pressure. At higher temperatures it is negative at zero pressure and decreases still further with increase in pressure. μ vs. t isobars and p vs. t μ = constant curves exhibit the calculated values of the Joule-Thomson coefficient. The compressibility data from which these calculations are made are probably for a 1:3 para ortho mixture, though there may be some question about this, particularly at extremely low temperatures. Values for the second virial coefficient are given. They follow the equation $B = 17.42 + 314.7\ T^{-1} - 2111 \times 10^2 T^{-2}$ cc/mole from −75° to 500°C within 0.05 cc/mole.

THIS is the third of a series of papers on certain physical properties of compressed gases. The two previous publications[1,2] were on nitrogen and carbon monoxide, and the present one deals with hydrogen. The method used is applicable when compressibility data cover a temperature and pressure range so thoroughly that derivatives such as $(dv/dT)_p$ and $(dv/dp)_T$ can be determined in that range.

The method for determining these derivatives has been described in the two previous papers and need not be repeated. It has been supplemented,

[1] W. Edwards Deming and Lola E. Shupe, Phys. Rev. **37,** 638 (1931).

[2] W. Edwards Deming and Lola E. Shupe, Phys. Rev. **38,** 2245 (1931). The equations, figures, and tables are numbered consecutively through this series of papers.

modified, and refined from time to time to overcome the peculiar obstacles presented by each gas. In particular, for hydrogen it was found that a power series of three and four terms, depending on the temperature range, will fit the $\Delta \equiv v(pv/RT-1)$ vs. T^{-1} isobars from $-215°$ to 300°C, so that differentiation of these gives determinations of derivatives with respect to temperature that are supplementary to the mechanical determinations. Also, the functions $T(dv/dT)_p - v$ and $-p(dv/dp)_T + v$ plotted in isobars and isotherms were found to be well adapted to smoothing the expansion coefficients $(T/v)(dv/dT)_p$ and $-(p/v)(dv/dp)_T$ and for determining $-T(d^2v/dT^2)_p$.

The derivatives $(dv/dT)_p$, $(dv/dp)_T$, $(d^2v/dT^2)_p$ are employed as in the previous work to obtain the desired physical properties, which are presented in Table III and in the graphs.

The compressibility data that we have used for this work were taken chiefly at the Reichsanstalt, the Leiden, and the Fixed Nitrogen Research Laboratories.[3–16] Bartlett's data extend from $-70°$ to 300°C and to 1000 atm. thus constitute by far the most comprehensive measurements over that temperature range. It is probable that all the observers cited were working with a 1:3 para ortho mixture of the two forms of hydrogen. The departure from the 1:3 ratio would be especially slight above -75°C, where our calculations on heat capacity are made.

It is customary to publish p, v, T data in tables showing "compressibility factors" $(pv)/(pv)_s$, the ratio of pv at the given temperature and pressure to the pv product for the same mass of gas at S. T. P. In other words, these tables show the value of pv when v is expressed in Amagat units. The ratio of $(pv)_s : RT_0$ is taken here as 0.99939, as given by William Wild[17] and the I. C. T.; and 22414.1 cc is taken for the volume of a mole of an ideal gas at S. T. P.; whence the factor required to convert volumes in Amagat units to volumes in cc/mole is $22414.1/0.99939 = 22427.8$. The factor 2.0155 converts densities in moles/cc into densities in g/cc.

[3] Amagat, Ann. chim. Phys. (6), **29,** 68 (1893).

[4] Witkowski, Krahauer Anzeiger, 305 (1905); Landolt-Börnstein Tabellen **1,** 105 (1923).

[5] Kohnstamm and Walstra, Proc. Roy. Acad. Amsterdam **17,** 203 (1914).

[6] Schalkwijk, Comm. Phys. Lab. Univ. Leiden, No. 70, or Verslag Akad. Amsterdam, (June 1901).

[7] Onnes, Crommelin, Smid, Comm. Phys. Lab. Univ. Leiden, No. 146b, or Verslag Akad. Amsterdam, (June 1915).

[8] Onnes and Penning, Arch. Neerland Sci. (**III A**) **7,** 172 (1923).

[9] Crommelin and Swallow, Comm. Phys. Lab. Univ. Leiden No. 172 a (1924).

[10] Onnes and Van Urk, Comm. Phys. Lab. Univ. Leiden No. 169d (1924).

[11] Holborn and Otto, Zeits. f. Physik **33,** 1 (1925); **38,** 359 (1926).

[12] Verschoyle, Proc. Roy. Soc. **111 A,** 552 (1926).

[13] Bartlett et al, J. Amer. Chem. Soc. **50,** 1275 (1928).

[14] G. A. Scott, Proc. Roy. Soc. **125 A,** 330 (1929).

[15] Bartlett et al, J. Amer. Chem. Soc. **52,** 1363 (1930).

[16] J. A. Beattie and O. C. Bridgeman, Proc. Amer. Acad. Arts and Sci. **63,** 229 (1928) give an accurate compilation of the data published prior to Bartlett's papers, listed in isochores and isotherms. We have used this extensively.

[17] William Wild, Phil. Mag. **12,** 41 (1931).

TABLE III. *Some physical properties of compressed hydrogen derived from experimental data on compressibility.*

1 p	2 v	3 ρ	4 f	5 $-\frac{p}{v}\left(\frac{dv}{dp}\right)_T$	6 $\frac{T}{v}\left(\frac{dv}{dT}\right)_p$	7 ΔC_p	8 C_p	9 C_v	10 Δ
atm.	cc mole	g liter	atm.				calories mole degree		cc mole
				$t=-75°$ $C_p^*=6.508$ $C_v^*=4.522$					
25	661.4	3.047	25.42	.983	.1000	.08	6.59	4.53	11.19
50	336.7	5.986	51.72	.963	.9965	.15	6.66	4.54	11.90
75	228.7	8.814	78.99	.943	.9895	.22	6.73	4.55	12.53
100	174.8	11.53	107.3	.922	.9800	.29	6.79	4.57	13.16
150	121.3	16.62	167.3	.881	.9546	.40	6.91	4.61	14.41
200	94.67	21.29	232.2	.840	.9250	.49	7.00	4.64	15.57
300	68.31	29.51	379.1	.766	.8611	.64	7.14	4.72	17.78
400	55.30	36.45	552.2	.704	.8004	.72	7.23	4.77	19.93
500	47.52	42.42	756.2	.652	.7458	.77	7.28	4.80	21.91
600	42.36	47.58	996.0	.613	.6957	.80	7.31	4.86	23.86
800	35.84	56.24	1605	.544	.6063	.86	7.37	5.01	27.35
1000	31.95	63.08	2430	.487	.5337	.91	7.42	5.14	30.83
1100	30.54	66.00	2945	.460	.5013	.93	7.44	5.19	32.56
1200	29.38	68.59	3540	.435	.4718	.93	7.44	5.24	34.34
				$t=-50°$ $C_p^*=6.660$ $C_v^*=4.674$					
25	744.7	2.707	25.41	.983	.9956	.06	6.72	4.68	12.40
50	378.8	5.321	51.69	.965	.9889	.12	6.78	4.69	13.01
75	257.1	7.841	78.90	.946	.9802	.17	6.83	4.70	13.58
100	196.3	10.27	107.1	.927	.9695	.22	6.88	4.72	14.15
150	135.8	14.84	166.6	.890	.9455	.30	6.96	4.74	15.22
200	105.6	19.08	230.8	.854	.9183	.38	7.04	4.77	16.23
300	75.67	26.64	374.5	.788	.8619	.48	7.14	4.82	18.14
400	60.80	33.15	541.4	.732	.8074	.55	7.21	4.87	19.94
500	51.91	38.83	735.1	.684	.7571	.60	7.26	4.90	21.66
600	46.00	43.82	959.4	.643	.7102	.63	7.29	4.94	23.33
800	38.57	52.26	1517	.579	.6277	.68	7.34	5.07	26.42
1000	34.10	59.11	2252	.524	.5592	.72	7.38	5.18	29.39
1100	32.47	62.08	2700	.502	.5284	.73	7.39	5.24	30.85
1200	31.11	64.78	3211	.478	.4996	.74	7.40	5.28	32.32
				$t=-25°$ $C_p^*=6.765$ $C_v^*=4.779$					
25	827.6	2.436	25.40	.984	.9931	.05	6.81	4.79	13.28
50	420.6	4.792	51.63	.967	.9847	.09	6.85	4.80	13.82
75	285.2	7.068	78.74	.949	.9751	.13	6.89	4.80	14.35
100	217.6	9.265	106.7	.932	.9645	.17	6.93	4.81	14.87
150	150.0	13.43	165.8	.898	.9409	.23	7.00	4.83	15.81
200	116.4	17.31	229.1	.865	.9157	.29	7.05	4.85	16.71
300	82.93	24.30	369.6	.806	.8640	.37	7.14	4.89	18.39
400	66.23	30.43	531.0	.755	.8143	.43	7.19	4.92	19.93
500	56.25	35.83	716.0	.709	.7673	.46	7.23	4.95	21.44
600	49.61	40.63	927.6	.671	.7232	.49	7.26	4.99	22.90
800	41.27	48.84	1444	.608	.6472	.53	7.30	5.08	25.64
1000	36.23	55.64	2109	.558	.5821	.56	7.33	5.18	28.22
1100	34.38	58.62	2507	.536	.5526	.57	7.34	5.23	29.47
1200	32.84	61.37	2957	.516	.5253	.57	7.34	5.28	30.72
				$t=0°$ $C_p^*=6.841$ $C_v^*=4.855$					
25	910.3	2.214	25.38	.985	.9917	.04	6.88	4.86	13.94
50	462.3	4.360	51.55	.969	.9825	.07	6.91	4.87	14.43
75	313.1	6.437	78.56	.952	.9724	.10	6.94	4.88	14.92
100	238.6	8.447	106.4	.936	.9617	.13	6.97	4.88	15.41
150	164.2	12.27	165.0	.905	.9391	.18	7.03	4.90	16.25
200	127.1	15.86	227.4	.875	.9156	.23	7.07	4.91	17.07
300	90.12	22.37	365.1	.820	.8678	.30	7.14	4.94	18.58
400	71.62	28.14	521.6	.774	.8211	.35	7.19	4.98	19.92
500	60.56	33.28	699.2	.730	.7771	.38	7.22	5.00	21.26
600	53.19	37.90	900.2	.693	.7355	.40	7.24	5.04	22.54
800	43.95	45.86	1383	.634	.6644	.44	7.28	5.11	24.99
1000	38.35	52.56	1993	.586	.6026	.47	7.31	5.20	27.26
1100	36.29	55.54	2354	.567	.5745	.48	7.32	5.26	28.34
1200	34.57	58.30	2757	.548	.5482	.48	7.32	5.30	29.41
				$t=25°$ $C_p^*=6.892$ $C_v^*=4.906$					
25	992.8	2.030	25.36	.985	.9910	.03	6.92	4.91	14.45
50	503.8	4.001	51.48	.970	.9814	.06	6.95	4.92	14.91
75	340.9	5.912	78.37	.955	.9712	.08	6.98	4.92	15.36
100	259.6	7.765	106.1	.940	.9606	.11	7.00	4.93	15.82
150	178.3	11.30	164.1	.911	.9389	.15	7.04	4.94	16.60
200	137.7	14.63	225.8	.882	.9165	.19	7.08	4.95	17.35
300	97.26	20.72	360.9	.832	.8719	.24	7.14	4.97	18.73
400	76.97	26.18	513.2	.789	.8280	.28	7.18	5.00	19.90
500	64.85	31.08	684.6	.749	.7864	.31	7.20	5.03	21.10
600	56.75	35.52	876.8	.713	.7480	.33	7.22	5.06	22.23

TABLE III. (*Continued*).

1 p	2 v	3 ρ	4 f	5 $-\frac{p}{v}\left(\frac{dv}{dp}\right)_T$	6 $\frac{T}{v}\left(\frac{dv}{dT}\right)_p$	7 ΔC_p	8 C_p	9 C_v	10 Δ
atm.	cc/mole	g/liter	atm.			calories/mole degree			cc/mole
800	46.61	43.24	1332	.656	.6799	.36	7.26	5.12	24.43
1000	40.46	49.82	1899	.611	.6211	.39	7.28	5.21	26.44
1100	38.19	52.77	2229	.593	.5944	.39	7.29	5.25	27.39
1200	36.30	55.53	2596	.576	.5689	.40	7.29	5.30	28.33
			$t=50°$	$C_p^*=6.927$	$C_v^*=4.941$				
25	1075	1.874	25.34	.986	.9906	.02	6.95	4.95	14.85
50	545.2	3.697	51.40	.972	.9809	.05	6.97	4.95	15.28
75	368.6	5.468	78.19	.958	.9708	.07	7.00	4.96	15.71
100	280.4	7.187	105.8	.943	.9605	.09	7.02	4.96	16.15
150	192.3	10.48	163.3	.916	.9394	.12	7.05	4.97	16.87
200	148.3	13.59	224.3	.890	.9181	.15	7.08	4.98	17.57
300	104.3	19.32	357.1	.843	.8762	.20	7.13	5.00	18.81
400	82.30	24.49	505.7	.802	.8349	.24	7.16	5.02	19.88
500	69.12	29.16	671.6	.765	.7960	.26	7.19	5.05	20.96
600	60.30	33.43	856.4	.731	.7595	.28	7.21	5.07	21.97
800	49.26	40.92	1289	.676	.6941	.31	7.24	5.13	23.95
1000	42.56	47.36	1820	.634	.6379	.33	7.26	5.21	25.75
1100	40.09	50.27	2126	.617	.6127	.34	7.26	5.30	26.59
1200	38.03	53.00	2463	.600	.5878	.34	7.27	5.35	27.42
			$t=100°$	$C_p^*=6.969$	$C_v^*=4.983$				
25	1240	1.625	25.31	.988	.9905	.02	6.99	4.99	15.44
50	627.8	3.210	51.26	.975	.9809	.03	7.00	4.99	15.82
75	423.9	4.755	77.88	.962	.9712	.05	7.02	5.00	16.21
100	322.0	6.259	105.2	.949	.9614	.06	7.03	5.00	16.63
150	220.2	9.155	161.9	.924	.9419	.10	7.06	5.01	17.28
200	169.3	11.91	221.6	.901	.9225	.12	7.09	5.01	17.90
300	118.4	17.02	350.6	.861	.8846	.15	7.12	5.03	18.98
400	92.90	21.70	493.2	.824	.8481	.18	7.15	5.05	19.84
500	77.59	25.98	650.3	.791	.8130	.20	7.17	5.07	20.72
600	67.35	29.92	823.1	.760	.7795	.22	7.19	5.09	21.54
800	54.53	36.96	1221	.709	.7192	.24	7.21	5.14	23.16
1000	46.75	43.12	1696	.671	.6676	.26	7.23	5.21	24.62
1100	43.88	45.93	1966	.655	.6443	.26	7.23	5.25	25.30
1200	41.49	48.58	2260	.639	.6218	.26	7.23	5.28	25.97
			$t=200°$	$C_p^*=6.993$	$C_v^*=5.007$				
25	1569	1.285	25.26	.990	.9914	.01	7.00	5.01	16.14
50	792.6	2.543	51.04	.979	.9827	.02	7.01	5.01	16.47
75	534.0	3.775	77.36	.969	.9740	.03	7.02	5.01	16.81
100	404.7	4.980	104.2	.958	.9653	.03	7.03	5.01	17.19
150	275.5	7.316	159.7	.937	.9483	.05	7.04	5.01	17.76
200	211.0	9.554	217.6	.918	.9316	.06	7.05	5.01	18.30
300	146.4	13.77	341.0	.885	.8996	.08	7.08	5.02	19.15
400	113.9	17.70	474.9	.855	.8690	.10	7.09	5.04	19.76
500	94.42	21.35	619.9	.827	.8395	.12	7.11	5.05	20.39
600	81.36	24.77	776.6	.803	.8114	.13	7.12	5.07	20.94
800	65.00	31.01	1128	.757	.7594	.14	7.14	5.11	22.05
1000	55.08	36.59	1534	.724	.7142	.15	7.15	5.16	23.06
1100	51.44	39.18	1759	.708	.6937	.16	7.15	5.18	23.54
1200	48.40	41.65	2000	.696	.6748	.16	7.15	5.21	24.00
			$t=300°$	$C_p^*=7.006$	$C_v^*=5.020$				
25	1898	1.069	25.22	.991	.9923	.01	7.01	5.02	16.53
50	957.1	2.106	50.88	.982	.9846	.01	7.02	5.02	16.84
75	643.8	3.131	76.99	.973	.9769	.02	7.02	5.02	17.14
100	487.2	4.131	103.6	.964	.9692	.02	7.03	5.02	17.50
150	330.6	6.096	158.2	.947	.9542	.03	7.04	5.02	18.04
200	252.4	7.986	214.8	.930	.9395	.04	7.05	5.02	18.52
300	174.1	11.58	334.3	.902	.9115	.06	7.06	5.03	19.24
400	134.8	14.96	462.4	.877	.8849	.07	7.08	5.04	19.70
500	111.1	18.14	599.5	.853	.8595	.08	7.09	5.06	20.15
600	95.28	21.15	745.8	.832	.8352	.09	7.10	5.07	20.54
800	75.40	26.73	1068	.794	.7899	.10	7.11	5.11	21.31
1000	63.38	31.80	1432	.761	.7494	.11	7.12	5.14	22.03
1100	58.98	34.18	1630	.746	.7314	.11	7.12	5.15	22.38
1200	55.29	36.45	1841	.734	.7146	.12	7.12	5.17	22.72
			$t=400°$	$C_p^*=7.029$	$C_v^*=5.043$				
25	2226	.9054	25.19	.992	.9932	.00	7.03	5.04	16.78
50	1122	1.797	50.76	.985	.9863	.01	7.04	5.04	17.06
75	753.4	2.675	76.72	.977	.9794	.01	7.04	5.05	17.35
100	569.5	3.539	103.1	.969	.9726	.02	7.04	5.04	17.69
150	385.6	5.227	157.1	.953	.9591	.02	7.05	5.04	18.21

TABLE III (*Continued*).

1 p	2 v	3 ρ	4 f	5 $-\frac{p}{v}\left(\frac{dv}{dp}\right)T$	6 $\frac{T}{v}\left(\frac{dv}{dT}\right)_p$	7 ΔC_p	8 C_p	9 C_v	10 Δ
atm.	cc mole	g liter	atm.			calories mole degree			cc mole
200	293.7	6.862	212.8	.939	.9461	.03	7.06	5.04	18.66
300	201.7	9.992	329.5	.914	.9213	.04	7.07	5.05	19.29
400	155.5	12.96	453.5	.892	.8977	.05	7.08	5.06	19.65
500	127.8	15.78	585.0	.872	.8750	.06	7.09	5.08	19.99
600	109.1	18.47	724.1	.854	.8534	.07	7.10	5.09	20.25
800	85.77	23.50	1026	.820	.8130	.08	7.11	5.12	20.78
1000	71.65	28.13	1362	.790	.7767	.09	7.12	5.15	21.30
1100	66.50	30.31	1544	.776	.7606	.09	7.12	5.16	21.57
1200	62.19	32.41	1734	.763	.7454	.09	7.12	5.17	21.83
			$t = 500°$	$C_p^* = 7.052$	$C_v^* = 5.076$				
25	2554	.7891	25.16	.993	.9938	.00	7.06	5.08	16.94
50	1286	1.568	50.67	.986	.9876	.00	7.07	5.08	17.21
75	863.0	2.336	76.51	.980	.9814	.01	7.07	5.08	17.48
100	651.7	3.093	102.7	.972	.9753	.01	7.07	5.08	17.82
150	440.5	4.575	156.2	.959	.9632	.02	7.08	5.08	18.33
200	335.0	6.017	211.2	.946	.9514	.02	7.08	5.07	18.76
300	229.3	8.791	325.8	.924	.9290	.03	7.09	5.08	19.31
400	176.2	11.44	446.8	.904	.9076	.04	7.10	5.09	19.61
500	144.3	13.96	574.1	.886	.8873	.04	7.11	5.10	19.86
600	123.0	16.39	708.0	.870	.8678	.05	7.11	5.11	20.04
800	96.11	20.97	996.0	.842	.8313	.06	7.12	5.14	20.38
1000	79.91	25.22	1312	.814	.7987	.06	7.12	5.16	20.75
1100	74.01	27.24	1481	.802	.7839	.06	7.13	5.17	20.96
1200	69.07	29.18	1658	.787	.7701	.07	7.13	5.17	21.17

TABLE III. (*Continued*).

1 p	2 v	3 ρ	4 f	6 $\frac{T}{v}\left(\frac{dv}{dT}\right)_p$	10 Δ
atm.	cc mole	g liter	atm.		cc mole
			$t = -215°$		
25	168.8	11.94	22.12	1.469	−19.54
			$t = -200°$		
25	229.2	8.793	23.75	1.227	−10.45
50	112.9	17.85	45.73	1.319	−6.76
			$t = -175°$		
25	321.2	6.275	24.84	1.088	−1.02
50	161.7	12.46	49.69	1.140	.58
75	109.8	18.35	74.88	1.101	2.47
			$t = -150°$		
25	408.5	4.934	25.22	1.038	4.31
50	207.4	9.720	51.05	1.061	5.35
75	140.6	14.34	77.64	1.067	6.05
			$t = -125°$		
25	493.8	4.082	25.38	1.016	7.60
50	251.3	8.020	51.58	1.023	8.43
75	170.6	11.81	78.70	1.019	8.94
100	131.1	15.37	106.9	1.010	10.27
			$t = -100°$		
25	578.0	3.487	25.41	1.004	9.76
50	294.3	6.848	51.71	1.004	10.49
75	199.9	10.08	78.99	.998	11.01
100	153.2	13.16	107.3	.989	11.98

Second virial coefficients

$\Delta = v(pv/RT - 1)$ in cc/mole extrapolated to zero pressure

t°C	Δ cc mole	t°C	Δ cc mole
−215	−24.46	0	13.44
−200	−13.81	25	13.99
−175	−3.06	50	14.43
−150	2.90	100	15.06
−125	6.54	200	15.81
−100	8.92	300	16.23
−75	10.46	400	16.49
−50	11.77	500	16.66
−25	12.72		

Care has been taken in each entry of the table to give only as many figures as we consider significant. No points are shown on the curves because they are drawn through the plotted points at practically every determination. Each property listed will now be discussed.

Specific volume v, column 2; density ρ, column 3; Δ, column 10 and Fig. 19. $\Delta \equiv v(pv/RT-1)$ were calculated from the p, v, T data and plotted against p as isotherms and against T^{-1} as isobars. These two families of curves were smoothed and averaged simultaneously, and then extrapolated to higher pres-

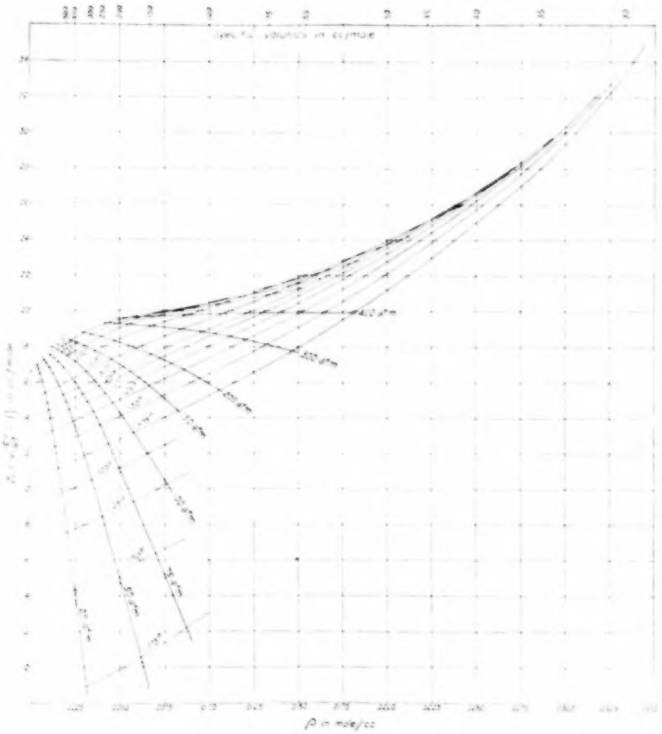

Fig. 19. Δ vs. ρ isotherms and isobars for hydrogen, plotted from column 10 of Table III. By means of this graph one can readily interpolate the p, v, T data. Thus, for $\rho = 0.005$ moles/cc and $p = 50$ atm., the temperature can be roughly estimated as $-153°$ or $-154°$C. By reading off $\Delta = 4.8$ cc/mole, at this point and using $v = 1/\rho = 200$ cc/mole, $p = 50$ atm., $R = 82.049$ cc atm./mole deg., the equation $\Delta = v(pv/RT-1)$ gives $T = 119.02°$, whence $t = 119.02 - 273.18 = -154.16°$C. Isobars above 400 atm. are omitted for clearness.

sures and temperatures. They were also extrapolated at the low temperature end the short distance from $-70°$ to $-75°$. The resulting smoothed values of Δ were read off at the desired temperatures and pressures. They are listed in column 10.

The second virial coefficients B listed at the end of Table III are the ordinates of the Δ vs. p isotherms at zero pressure, obtained by extrapolation. They follow the equation

$$B = 17.42 + 314.7T^{-1} + 2111 \times 10^2 T^{-2} \text{ cc/mole}$$

from $-75°$ to 500°C within 0.05 cc/mole. The B vs. T^{-1} curve departs considerably from a straight line. This means that second derivatives such as $(d^2v/dT^2)_p$ can not be obtained for hydrogen from van der Waals' equation, even at very low pressures.

Margenau[18] obtained the following equation for the second virial coefficient of a gas:

$$B = b(1 - 0.75y - 0.094y^2 - 0.014y^3 - 0.0019y^4 - 0.00022y^5 - 0.000022y^6 - \cdots) \tag{27}$$

where

$$b = 2\pi Nd^3/3, \quad y = \beta^2 V_i/d^6kT = 4\pi^2N^2\beta^2V_i/9kb^2T.$$

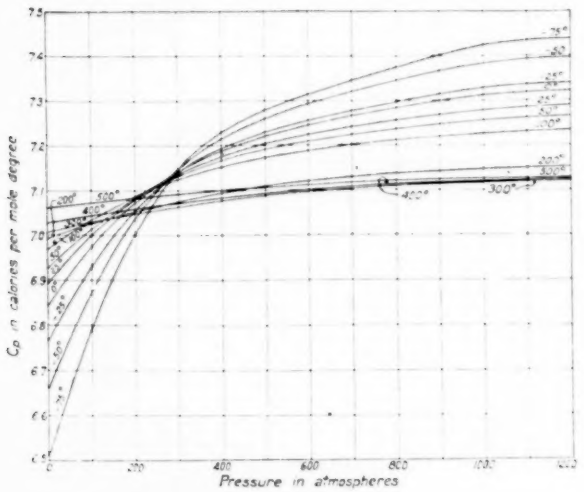

Fig. 20. Hydrogen, C_p vs. p isotherms.

β denotes polarizability of the molecule, V_i is the ionization potential. b is clearly four times the volume of N spheres of diameter d. If N is the number of molecules per mole, b is cc/mole. B can be evaluated by extrapolating the B vs. T^{-1} curve back to $T^{-1}=0$. The value so obtained is $b=17.42$ cc/mole. This with $V_i=15.34$ volts and $\beta=0.777\times10^{-24}$ cc per molecule gives $y=571.4T^{-1}$, for use in Margenau's equation. The values of B so calculated disagree with the experimental ones at the end of Table III. Margenau, having different data to compare with, reached the same conclusion for hydrogen. He pointed out that the zero point energy of H_2 and He probably renders his equation invalid for these gases. This difficulty would not be present in gases having heavier molecules. He found good agreement for N_2, CO, and several others, using the data then available. We later confirmed his conclusions for carbon monoxide[2] after determining b and B from compressibility data.

[18] Henry Margenau, Phys. Rev. **36,** 1782 (1930).

The relation $\Delta = v(pv/RT - 1)$ when solved for v gives the specific volume for any pressure and temperature at which Δ is known; thus the values of v were calculated. The densities in column 3 are in g/cc and were obtained by dividing 2.0155 by the corresponding v in cc/mole.

The Δ vs. ρ isotherms and isobars in Fig. 19 exhibit the p, v, T data for hydrogen in a form that makes interpolation convenient. Unfortunately the

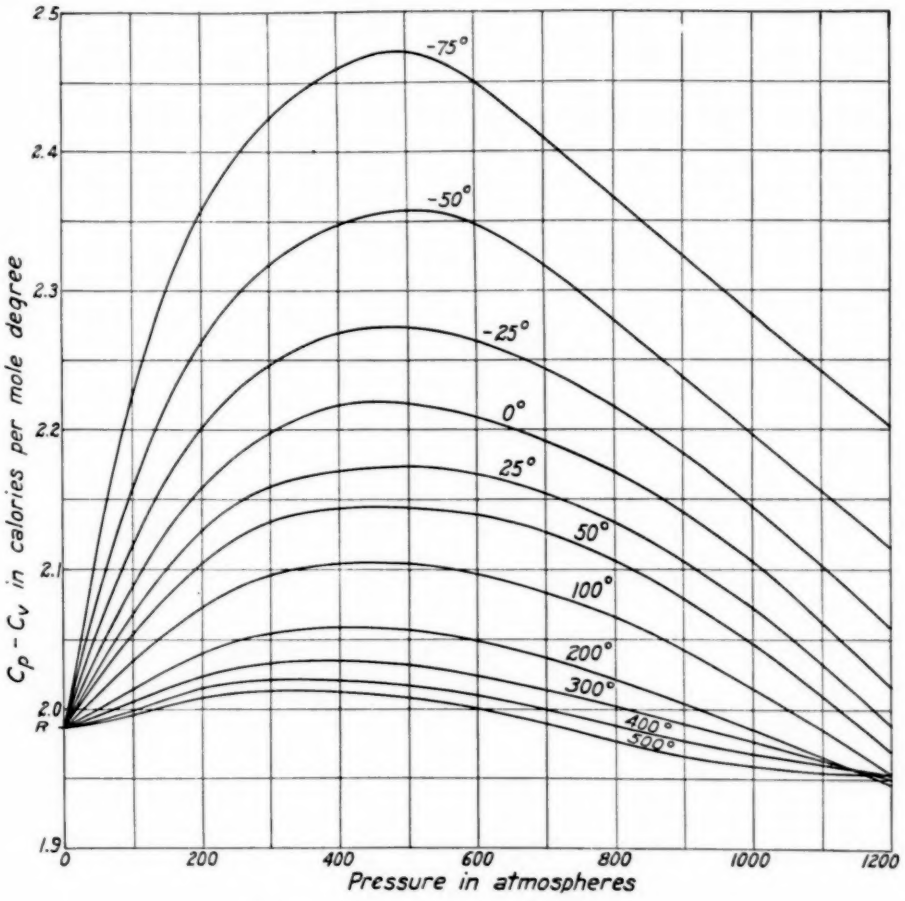

Fig. 21. Hydrogen, $C_p - C_v$ vs. p isotherms.

isobars above 400 atm. had to be omitted for clarity; this detracts somewhat from its usefulness at high pressures. This difficulty did not appear with carbon monoxide. A large scale graph can be made by anyone desiring greater accuracy; the necessary coordinates are in Table III. Fig. 19 shows the trends of the departure of hydrogen from the perfect gas law, since Δ is a measure of this deviation.

Fugacity f, column 4.

$\alpha \equiv (RT/pv - 1)$ were plotted in isotherms against p, and the expression

$$f = p \exp(-1/RT) \int_0^p \alpha dp \tag{28}$$

was evaluated by mechanical integration.

Expansion coefficients $-(p/v)(dv/dp)_T$ and $(T/v)(dv/dT)_p$, columns 5 and 6.

The Δ vs. p and α vs. p isotherms and the Δ vs. T^{-1} isobars are used to get these coefficients. The two determinations of $-(p/v)(dv/dp)_T$ at each point, obtained through Eqs. (6) and (7), were plotted in isotherms against pressure. The ordinates along these smoothed curves give the values recorded in column 5 of the table.

$(T/v)(dv/dT)_p$ in column 6 were evaluated through Eq. (15). The Δ and $(d\Delta/du)_p$ needed in this equation[19] were obtained from the power series

$$\Delta = a + bu + cu^2$$

that were found to fit the Δ vs. u isobars. a, b, and c are functions of pressure. At 25, 50, 75, and 100 atm. these isobars extended through a longer temperature range and it was necessary to add another term to the series. The values of $(T/v)(dv/dT)_p$ so determined were smoothed by plotting $v[(T/v)(dv/dT)_p - 1]$ against pressure.

Both expansion coefficients $-(p/v)(dv/dp)_T$ and $(T/v)(dv/dT)_p$ decrease monotonically from unity as the pressure increases from 0 to 1200 atm., along all isotherms within the range studied. This is in contrast with the behavior of nitrogen and carbon monoxide; with these gases the expansion coefficients along isotherms at low and ordinary temperatures at first increase with pressure, then drop back to unity and after that decrease as the pressure is increased.

ΔC_p, and the heat capacity C_p, columns 7 and 8 and Fig. 20.

ΔC_p is the change in C_p caused by a change in pressure at constant temperature. It is obtained through the thermodynamic equation

$$(dC_p/dp)_T = -T(d^2v/dT^2)_p, \tag{11}$$

which when integrated between 0 and p along an isotherm gives

$$C_p = C_p^* + \Delta C_p = C_p^* + \int_0^p -T(d^2v/dT^2)_p dp. \tag{12}$$

C_p^* is the heat capacity at zero pressure, and it is necessary to assume some value for it at each temperature in order to complete the calculations. In this matter we have sought the advice of Dr. W. M. D. Bryant of the Ammonia Division of the E. I. du Pont de Nemours Company, and have proceeded in the following manner. Giauque[20] calculated the heat capacity of hydrogen from 0°K to 298.1°K by utilizing spectroscopic data. This calculation does not depend on the behavior of a rigid molecular model, but includes the slight increase in heat capacity caused by molecular stretching. The rotational energy of hydrogen at low temperatures varies markedly with the ratio

[19] For convenience in writing derivatives, T^{-1} will be denoted by u.

[20] W. F. Giauque, J. Amer. Chem. Soc. **52,** 4821 (1930). Giauque's value at 225°K is evidently in error.

of para to ortho hydrogen. It is probable that the p, v, T data, at least those at $-70°C$ and above, were taken with a 1:3 para ortho mixture, since the ratio changes very slowly at low pressures in the absence of a catalyst. It is not known whether the rate of change increases much with pressure.

Hydrogen does not take on its full rotational heat until it reaches about 400°K. At this temperature the vibrational heat is extremely small but it attains appreciable values with sufficient increase in temperature. At high temperatures (above 400°K), where the molecule has taken up its full rotational heat capacity, the equation[21,22,23]

$$C_p^* = 6.954 + \phi(6100/T) + 0.00008T \text{ cal./mole deg.} \qquad (29)$$

probably gives the most reliable values. $6.954 = 7R/2$, the translational and rotational heat. $\phi(6100/T)$ is the Planck-Einstein function $R(6100/T)^2$

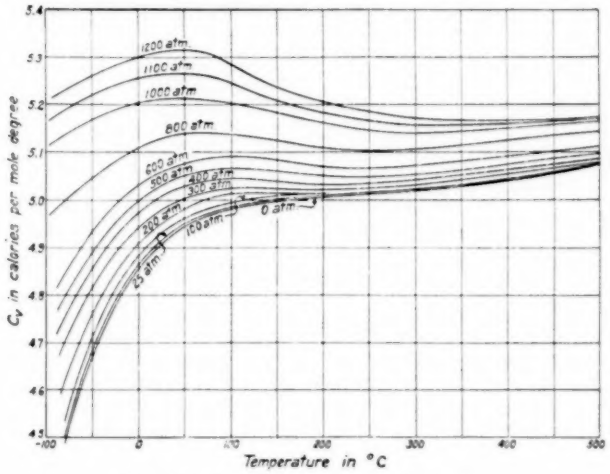

Fig. 22. Hydrogen, C_v vs. t isobars.

$e^{6100/T}/(e^{6100/T}-1)^2$, which takes care of vibrational energy. The term 0.00008 T is a correction for the small stretching, and was derived by Witmer from spectroscopic data. The characteristic temperature 6100°K was obtained by Eucken also from spectroscopic data. Rasetti[24] obtained 5960°K from the Raman spectrum, and this is in good agreement.

A curve of Giauque's values from 15°K to 298.1°K joins perfectly on to one calculated from Eq. (29) for temperatures above 400°K. Ordinates read from a curve so constructed gave the values of C_p^* used for this work. We here express our thanks to Dr. Bryant for his advice in selecting values of C_p^*.

As with nitrogen and carbon monoxide, the ΔC_p were obtained by a mechanical integration under the $-T(d^2v/dT^2)_p$ vs. p isotherms. The ordinates along these isotherms were calculated from the Δ curves by the relation

[21] A. Eucken, Wien-Harms Handbuch der Experimental Physik, Vol. VIII, part I, p. 445.
[22] E. Justi, Zeits. f. Tech. Mech. und Thermo. **2**, 120 (1931).
[23] E. E. Witmer, Proc. Nat. Acad. Sci., **12**, 238 (1926).
[24] F. Rasetti, Phys. Rev. **34**, 367 (1929).

$$-T(d^2v/dT^2)_p = -\frac{2u^2(d\Delta/du)_p + u^3(d^2\Delta/du^2)_p}{1+2\rho\Delta} + \frac{2pu}{R}\frac{(\Delta + ud\Delta/du)_p^2}{(1+2\rho\Delta)^3}. \quad (30)$$

The second derivative $(d^2\Delta/du^2)_p$ occurring here was obtained by differentiating the power series $\Delta = a + bu + cu^2$ that were found to fit the Δ vs. u isobars, and also by mechanical differentiation. These values of $-T(d^2v/dT^2)_p$ were

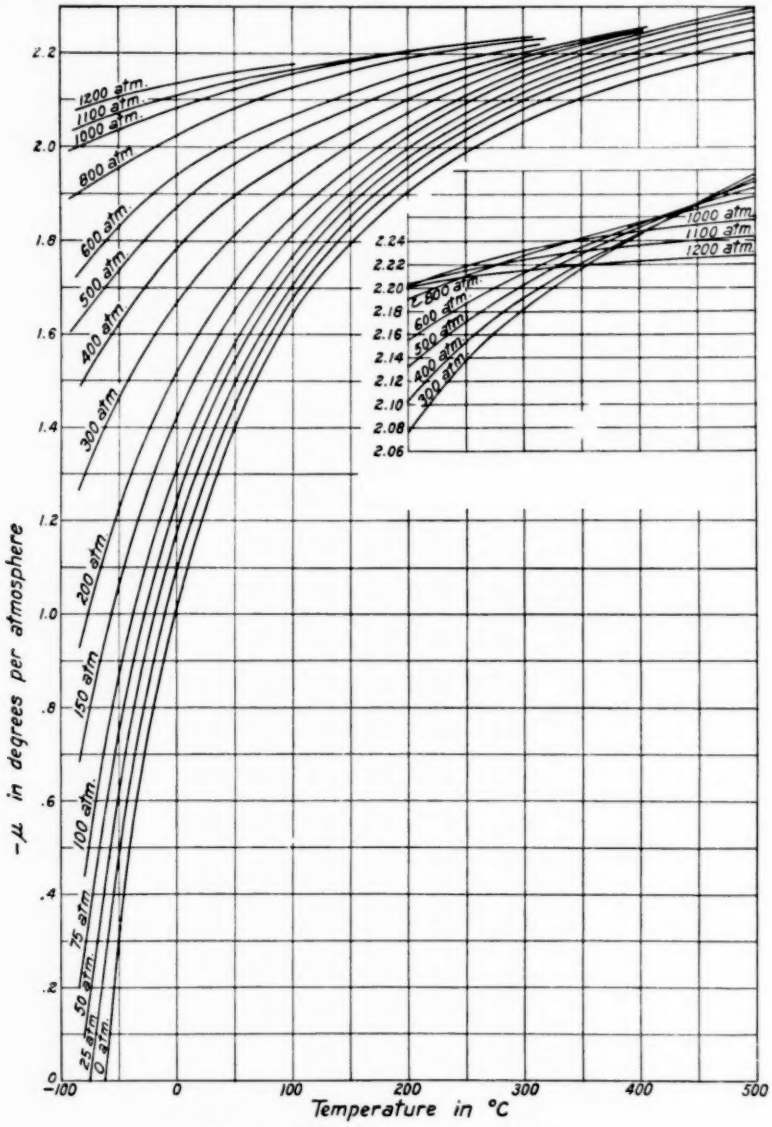

Fig. 23. Hydrogen, μ vs. t isobars.

found to agree well with determinations gotten by mechanical differentiation of the $v[(T/v)(dv/dT)_p - 1]$ vs. T isobars. They were smoothed by plotting them in isobars against T^{-2} before they were plotted in isotherms against pressure for the determination of ΔC_p by mechanical integration. The factor 0.02421 converts cc atm./mole deg. into cal./mole deg.

The quantity $C_p - C_v$, Fig. 21; the heat capacity C_v, column 9 and Fig. 22.

$$C_p - C_v = -T(dv/dT)_p^2/(dv/dp)_T. \tag{13}$$

Since the derivatives in columns 5 and 6 have been determined it is a simple matter to calculate $C_p - C_v$. This subtracted from C_p gives C_v. Some of the C_v vs. t isobars are drawn in Fig. 22. These are highly interesting for theoret-

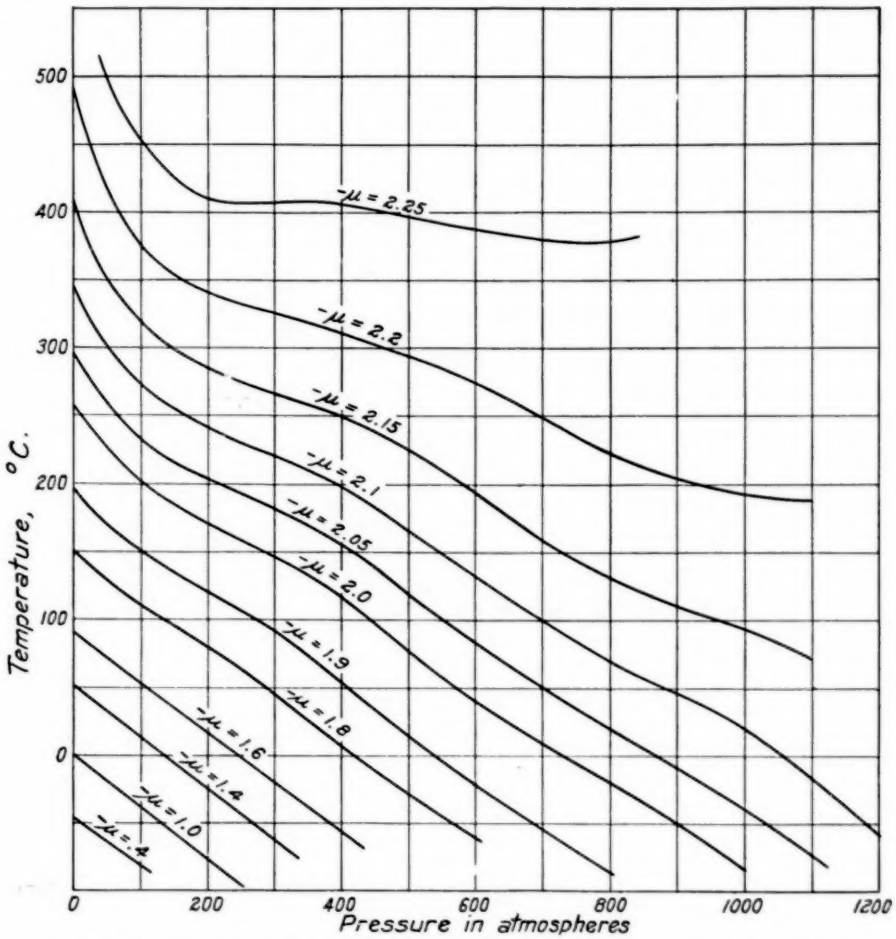

Fig. 24. Hydrogen, t vs. p, μ = constant curves. μ is given in centigrade degrees per atm. $\mu = (dt/dp)_H$.

ical work on the behavior of hydrogen molecules at various temperatures and pressures.

The Joule-Thomson coefficient μ, Figs. 23 and 24.

The Joule-Thomson coefficient was calculated from

$$\mu\rho C_p = (T/v)(dv/dT)_p - 1 \tag{14}$$

at each point, and the values so obtained are shown in Figs. 23 and 24. The inversion temperature for zero pressure appears to be about $-62°$.

Apparatus for Optical Studies at High Pressure

By THOS. C. POULTER
Department of Physics, Iowa Wesleyan College
(Received March 18, 1932)

The selection of materials for the construction of high pressure equipment is discussed. Simplified piston packing, electrode insulation, temperature control and a compact and safe type construction of pressure equipment is described with particular reference to systems for optical studies at high pressures. Equipment for optical studies at pressures as high as 30,000 atm. and some of their limitations and peculiarities are described.

INTRODUCTION

WHILE not intending to minimize the experimental difficulties encountered in research at extremely high pressure, it is the feeling of the author that much more work would be done in this field if the relative ease and safety with which such work can be carried on were more generally known. P. W. Bridgman[1] in his article, "The Technique of High Pressure Experimenting" and in his book "The Physics of High Pressures" gives a large number of very valuable methods of construction and techniques.

It is the intention in this paper to describe a number of pieces of high pressure equipment not already described in the literature, with particular attention to equipment involving windows for optical methods of attacking high pressure problems. In the treatment of the more important pieces an attempt will be made to give a sufficiently detailed description so that anyone wishing to construct and use them should not encounter great difficulty. These methods are presented as solutions of particular problems that have been encountered by the author during the past few years of designing and constructing high pressure equipment. It is not claimed that there are not other equally good solutions to these problems but only that the methods herein described have served very well.

SELECTION OF MATERIALS AND STEEL

The selection of the proper steel for the construction of high pressure equipment is of major importance from the standpoint of safety as well as that of obtaining experimental data.

Those parts of the equipment in contact with the material under high pressures are required to withstand either a great compressional force or a great tension. Steels that are specially developed for withstanding great compressional forces are of necessity too brittle to be used in places where a great tension is required. Likewise those having a high tensile strength must be sufficiently ductile so that they will adjust themselves to as nearly a uniform stress throughout their cross-sectional area as possible.

[1] P. W. Bridgman, Proc. Am. Acad. Arts and Sci. **49**, 627 (1913–14); The Physics of High Pressures, Macmillan Co., 1931.

After experiencing what might have been some very serious explosions from the use of carbon steels and some alloy steels of unknown physical properties, an attempt was made to find a steel better adapted to the purpose. Upon request the author was supplied specifications as to physical properties of a large number of different grades of steels from several manufacturers. The three physical properties upon which the steel for the construction of cylinders was based were tensile strength, yielding point, and elongation.

High tensile strength and yielding point are necessary for obtaining the pressure, while the elongation largely determines the safety of such equipment. The steel selected as most nearly meeting these requirements was the S. A. E. 3250, steel manufactured by the Republic Steel Corporation. A typical analysis of which is: C 0.50, Ms 0.56, P 0.017, S 0.022, Si 0.224, Ni 1.76, Cr 1.08. This steel has a tensile strength as high as 300,000 pounds, depending upon the seasoning treatment. It also has a remarkably high elongation of about 10 percent. After machining it is heat treated as follows: Neutralized at 1600° to 1700°F, quenched in oil at 1450°F and salt drawn to 750°F. This treatment produces a Brinell hardness of about 445.[2]

Bridgman mentions some difficulty in obtaining pieces of steel free from flaws, a difficulty which has never been encountered with this steel.

There is a certain cylinder-wall thickness, determined by the inside diameter of the cylinder and the steel from which it is constructed, beyond which additional thickness does not add to the pressure the cylinder will withstand. This thickness is reached when the elongation of the steel on the inside surface of the cylinder wall reaches a point where cracks develop before much stress is produced in the steel near the outer surface. For the above steel and an inside cylinder diameter of about 1.6 cm the maximum strength is obtained with a wall thickness of perhaps less than 6 cm.

This difficulty can be partially overcome by a seasoning process described by Bridgman which consists of stretching the cylinders by means of pressure and then regrinding them before they are put into actual service. If this procedure is carried to the point where optimum conditions are obtained for the outer surface of the cylinder, the steel near the center has been elongated to a point where it has been weakened. In order more nearly to obtain optimum conditions throughout the cylinder wall, it is necessary to construct the cylinder of coaxial shells. These shells are made of such a size that when they are pressed together the optimum elongation occurs. Cylinders of this kind are being constructed and studied with the hope of obtaining higher pressure than has yet been produced in the laboratory.

The selection of a steel for the construction of such pieces as pistons or window supports where they must withstand very great compressional forces was based upon hardness and crushing resistance. The steel selected for this purpose is the Rex AA or Rex AAA high speed steel, depending on the hard-

[2] The steel for the construction of our high pressure equipment was supplied through the courtesy of the Republic Steel Corporation. The heat treatment was done by them after the piece had been machined.

ness desired.[3] The hardness and crushing resistence of these steels are largely determined by the particular heat treatment to which they are subjected. The crushing resistence may run to more than a million pounds per square inch.

The pressure equipment used by the author is always constructed in such a way that parts made from high speed steel are completely inclosed by a less brittle steel. In this way it is possible to work close to the crushing limit of the steel without danger from flying pieces.

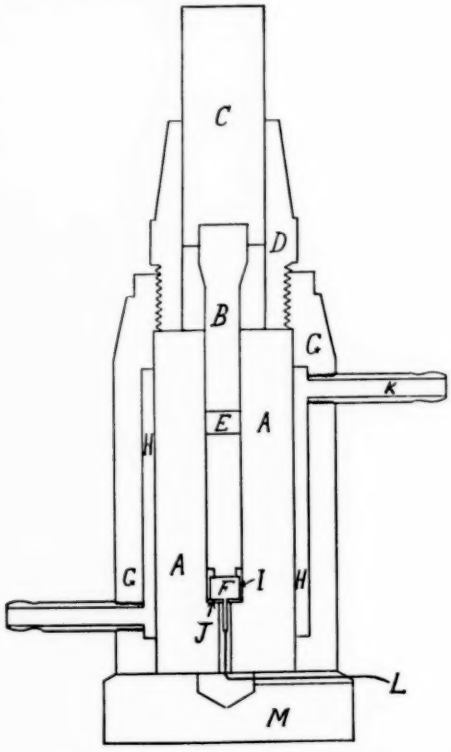

Fig. 1. High pressure cylinder with water jacket for temperature control and insulated electrode through the bottom of cylinder.

Construction of Pressure Chamber

The general method of developing the pressure is the same as that used by Bridgman and others; namely, the forcing of a small piston in a heavy cylinder by means of a hydraulic press.

The main body of the cylinder *A* Fig. 1 is constructed of S. A. E. 3250 steel, heat-treated to maximum tensile strength. The piston *B* is constructed of Rex AA or Rex AAA high speed steel. The piston guide *C* travels in the housing *D* thus preventing sidestrains on the piston. This is very important since even with the large four-rod two-hundred-ton hydraulic press used in this work sufficient sidestrains are produced to cause fracture of the pistons

[3] This steel is manufactured by and supplied through the courtesy of the Crucible Steel Company of America.

if such a guide is not employed. This housing also prevents flying pieces from getting out into the laboratory in case the piston shatters or a leak develops.

Fig. 2 shows the pieces of a piston which shattered while under 38,000 atmospheres pressure. Many pieces were imbedded in the soft steel housing surrounding the piston.

In one case an assistant received a severe bruise from flying oil and in another instance flying sulfuric acid penetrated two thicknesses of glass.

The rubber plug *E* makes a tight joint around the end of the piston. The housing *G* serves as a water jacket and as protection against flying pieces in case a cylinder splits. The cylinder is kept at constant temperature by circulating water from a thermostat around the pressure cylinder in the space *II* and the platins of the hydraulic press.

Fig. 2. Piston shattered at 38,000 atmosphere.

The body of the cylinder is machined from annealed steel allowing five or ten thousandths of an inch for grinding after being heat treated. They are ground on the inside with a high speed internal grinder.[4] This leaves the cylinder wall very smooth and reduces the friction of the piston to a minimum. The pistons are machined to a few thousandths of an inch oversize from annealed high speed steel. After machining they are heat treated and then ground to fit the cylinder tight enough so that from five to fifteen pounds are required to slip the piston in the cylinder. Before using, the center in the end of the piston used in supporting the piston in the lathe while machining should be ground off leaving the end of the piston flat. If this is not done the life of the piston is greatly reduced and the piston will usually split at the end before it has been used more than a few times. Leakage past the piston is prevented by placing a close fitting good grade rubber stopper from 5 to 10 mm in length, just ahead of the piston. This type of piston packing has four advantages over that used by Bridgman: (a) It can be used to a higher pressure because the entire cross-sectional area of the piston supports the pressure. There is no unsupported area in the center to make the pressure on the steel

[4] This grinder was purchased with a grant from the Iowa Academy of Science in 1928 and has been very valuable in the construction of pressure equipment.

of the end of the piston greater than the actual pressure in the cylinder. (b) Another advantage is that it offers less resistance to movements of the piston. (c) A rubber plug such as this is much more easily removed from the cylinder than the assembly used by Bridgman. (d) An important factor particularly in work of this type is its greater simplicity of construction and convenience of operation.

In this type of cylinder the material being studied under pressure is placed directly in the cylinder instead of in another chamber. This does away with the necessity of piping the liquid under pressure to the other chamber and thereby prevents difficulty due to leaks and transmission of pressure. When an electrical connection is necessary, a terminal is inserted through the bottom of the cylinder as shown in the figure.

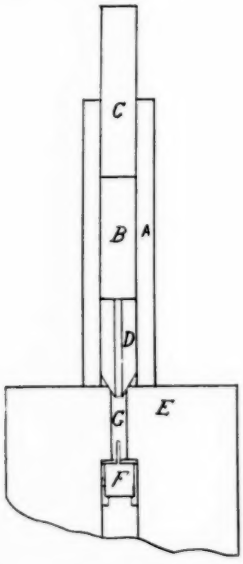

Fig. 3. Oil gun used to remove electrodes or pistons that have become fast in the cylinder.

The hardened high speed steel plug F is insulated from the sides of the cylinder by an enveloping shell of fiber I and from the end of the cylinder by a sheet of mica J about 0.5 mm or less in thickness. The insulated wire L is soldered to the plug F and is carried out through the hole in the bottom of the cylinder and through the groove in the base M. When the liquid in the cylinder is oil such electrodes serve very well at pressures as high as 30,000 atmospheres or higher and maintain a resistance of more than 300,000 ohms.

In case it is desired to remove such an electrode for any reason, a convenient method is to force it out with oil in the following manner. The cylinder is turned upside down and the wire pulled loose from F; a heavy walled tube A Fig. 3 having an inside diameter of 5/8 of an inch is placed over the center of the cylinder; the plug D having a 1/8 inch hole through the center is placed with its tapered end in the end of opening G through the bottom of the cylinder E; the tube is then partially filled with oil and the piston C put in

place; this piston is then driven in with a heavy hammer and the oil will force the electrode out. This method can be used to remove a piston in case one sticks in the cylinder.

When assembled, the cylinders are mounted in a vertical, four-rod hydraulic press. The pressure is developed by forcing the piston in with the press. The pressure in the high pressure cylinder can be calculated by the following equation in which P is the pressure in the high pressure cylinder, A is

$$P = \frac{(Ap) - (F + f)}{a}$$

the area of the press cylinder, p is the pressure in the press cylinder, F is the frictional force of the piston in the press cylinder, f is the frictional force of the high pressure piston, and a the cross-sectional area of the high pressure piston. If the pressure is being decreased the quantity $(F+f)$ has a plus sign in front of it instead of a minus. The diameter of the hydraulic press cylinder used in this work is about seven and one half inches.

The leather used in the hydraulic press cylinder is a self-acting leather packing which offers a frictional resistance less than 0.5 percent of the total force.[5] The friction of the small cylinder was determined by means of a cylinder having a piston in each end. This system is put under pressure and the force necessary to move the cylinder over the two pistons is measured. With carefully controlled conditions of metal surfaces the friction of the high pressure piston is reproducible to within 1 percent. In some particular designs this frictional force may run as high as 8 percent of the total force.

The corrected values check closely with those obtained by the manganin wire resistance method up to 13,000 atmospheres. The pressure effect of the resistance of manganin wire has never been measured directly at pressures above 13,000 atmospheres. Since extrapolated values are never safe, particularly to the extent that would be necessary in working with pressure as high as 30,000 atmospheres, the author has chosen what seems to be a more direct and reliable method.

Construction and Behavior of High Pressure Optical Systems

In this part will be given an outline of the work leading to the development of a satisfactory window mounting for either glass or quartz windows for withstanding pressures of occasionally as high as 30,000 atmospheres. The field of optical studies has been one of considerable investigation since the early work of E. H. Amagat in 1887–96.[6]

Amagat constructed a window mounting consisting of a piece of glass in the form of a truncated cone with an enveloping cone of ivory or other material as a gasket between the glass and the steel. This window was mounted in a tapered hole with the small end of the window in the direction of the ob-

[5] Hydraulic Engineering, Houghton Research Staff, Page 48–49 (1926).

[6] E. H. Amagat, Journ. Chem. Phys. [6] **29,** 68, 96, 505 (1893); Comptes Rendus **105,** 165 (1887); **117,** 507 (1893). Notice sur les Travoux Scientifiques de M. E. H. Amagat Paris, 1896.

server. Numerous other investigators have used modifications of Amagat's window-mounting with varying degrees of success.[7]

In the course of an investigation[8] that was being carried out in this laboratory, it was shown that glass capsules made from Pyrex or soft glass tubing (6 mm inside diameter) by sealing the ends off round would sometimes withstand an external hydrostatic pressure as great as 12,000 atmospheres. These capsules were about 20 to 30 mm in length and had a wall thickness of about 1.5 mm. This led us to believe that if the proper window support could be obtained it would be possible to use windows at pressures much higher than those reported in the literature. A review of the literature showed that in all window mountings previously employed a gasket material of some kind had been used between the glass and the steel support. Some experiments were then recalled in which samples of very hard steel were being tested with the view of using it for the construction of pistons. In these experiments, samples of the steel one half inch in diameter and one inch long were placed endwise between two blocks of hardened steel and pressure was then applied until the

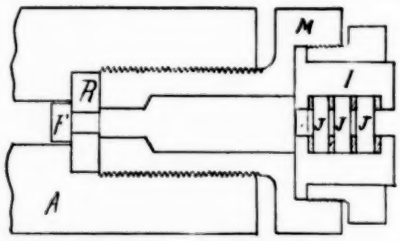

Fig. 4. Window mounting drawn to scale.

test pieces were crushed. Thinking that they would probably withstand a greater load if a thin sheet of soft steel were placed between the ends of the test pieces and the hardened steel blocks, sheets of soft steel 0.25 mm thick were so placed. Contrary to expectation, under these conditions, the test pieces were split at about half the load they had previously withstood.

Apparently in this case, the thin sheets of steel exerted lateral forces due to their flowing under pressure great enough to split the steel blocks. It seemed quite likely that a similar thing was happening in the case of the windows and the gasket material on which they were mounted. A window support must fulfill another condition, namely that its supporting surface must be perpendicular to the resultant force produced on it by the material in the cylinder. If such is not the case, the maximum strength of the glass cannot be utilized. With these facts as a guide the window mounting shown in Fig. 4 was constructed, in which the window *F* was mounted without a gasket and in contact with the polished surface of a very hard steel disk *R* about 10 mm in thickness with a 6 mm hole in the center.

The window and support were then mounted as shown in the figure and the cylinder and observation chamber filled with a light paraffin oil. Pressures

[7] Walter Wahl, Phil. Trans. Soc. **A212,** 117 (1913); Frances G. Wick, Proc. Am. Acad. Arts and Science **56,** 557–573 (1923).

[8] Thos. C. Poulter and Glen E. Frazer, paper in preparation.

were then applied in the usual way by forcing the piston in with the hydraulic press. The windows thus mounted would, in some cases, withstand a pressure of 30,000 atmospheres. The pressure in the observation chamber was determined as previously described. Thinking that this pressure was possibly in error as a result of the solidification of the oil, the following tests were made. These tests showed conclusively that there was but little pressure gradient in the oil and that therefore the pressures were substantially those computed.

For this investigation a number of other liquids, alcohol, ether, water, and glycerine were used to transmit the pressure. With alcohol, water, and ether the windows would usually break at pressures below 8000 atmospheres, whereas with glycerine the results were similar to those obtained with oil. Tests were then made to see if the piston was moving freely with oil or glycerine in the high pressure cylinder by means of the two-piston cylinder previously described. It was found that the pistons moved practically as freely with glycerine as with oil. Oil was then placed in the cylinder and observation chamber and its compressibility determined by means of the travel of the piston. There was detected no change in volume without a corresponding change in pressure such as would indicate a change of phase. However, such a change probably would not be expected for a material that is a mixture such as this paraffin oil. Some water was then placed in a thin walled rubber capsule in the observation chamber near the window, then with the remaining space filled with oil the piston travel was again measured as the pressure was built up. If the travel of the piston is measured as the pressure is built up, a decrease in volume is obtained with no increase in pressure between 10,500 and 11,000 atmospheres for a temperature of 30°C. This corresponds very closely to the pressure obtained by Bridgman for the formation of ice VI at that temperature. This shows that there is little or no pressure gradient in the paraffin oil below 11,000 atmospheres.

The freedom from a pressure gradient is probably to a large extent due to the compactness of the pressure system, which makes it necessary to transmit the pressure only a short distance. While it is not claimed that the viscosity of the oil has not reached a rather high value, the above experiments show that the plastic flow of the medium transmitting the pressure soon restores equilibrium.

In order further to test the ability of a window to withstand pressure a heavy-walled high-speed-steel tube was mounted in the pressure chamber of the cylinder shown in Fig. 1. One end of this tube is over the opening in the bottom of the cylinder and a window is mounted on the other end. This brought the window to within two centimeters of the end of the piston. In this case the pressure would be transmitted to the window even though the oil did solidify. Two windows were tested in this position, one breaking at 25,000 atmospheres and the other at 35,000 atmospheres. A window was then mounted with a little water in contact with it and the pressure was transmitted by means of oil. The oil and water were separated by a thin sheet of rubber. Under these conditions windows were again broken at pressures below 8000 atmospheres.

A window was then mounted in the middle of a piece of rubber tubing with oil on one side of the glass and water on the other. The two ends of the tube were then stoppered and this tube was placed in the observation chamber and surrounded with oil. A pressure of 21,000 atmospheres was built up and allowed to remain for about five minutes. It was then released and the side of the window that was in contact with the water was badly cracked and chipped while that in contact with the oil was intact. This shows that the breaking of the windows is in some way related to the material in contact with the glass as well as to the actual pressure employed. Now if a large pressure gradient does not exist, as has been shown, and the friction of the piston is corrected for, as described above, it is the belief of the author that the pressures used in this investigation are substantially those recorded.

Fig. 5. Diverging lens effect of fractured window.

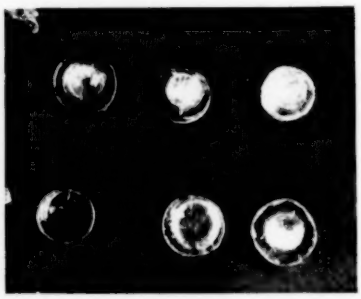

Fig. 6. Fractured windows before concentric shells have been removed.

Some valuable information relative to the difference in the behavior of windows when different liquids are used in contact with them can be obtained from the different types of fractures produced. A pressure window will frequently hold the pressure with but little leakage for some time after it has developed many cracks. Where such windows have been removed usually one of two general types of fracture has occurred.

The first is a spherical concentric shell fracture with the outside of the curvature towards the pressure. Sometimes four or five such shells break out leaving surfaces smooth enough to produce a diverging lens which will produce a fairly uniform image. Fig. 5 shows such a window mounted two inches in front of a printed page.

In all cases where such fractures have occurred the window has either been mounted on a gasket and the pressure transmitted by any of the five liquids used or with no gasket and the pressure transmitted by water, alcohol, or ether.

The second type of fracture occurs when no gasket is used and the pressure is transmitted with oil or glycerine. With this type of fracture only a thin layer of the glass which is over the opening in the window support is chipped off leaving a rough surface. Fig. 7 shows a group of such windows, placed fractured face down for photographing. The photograph also shows freedom

from other cracks. In either case the main portion of the window may be free from cracks. The above facts lead the author to suggest the following explanation for the difference in the behavior of pressure windows as different liquids are used to transmit the pressure. The concentric shell fracture, in cases where a gasket material is used, is probably due to the movement of the gasket as it flows under pressure. This would give the effect of a window supported on a moving surface. Since the fractures are of the same type with no gasket and the pressure being transmitted with water, alcohol, or ether, as those produced with a gasket and any of the liquids employed, the strains in the two cases must be similar. It may, therefore, be that these mobile liquids penetrate between the window and its support, thus producing the effect of a moving support. The relatively high viscosity of the oil and glycerine, particularly at the higher pressure, probably prevents such penetration thus making it possible to utilize the maximum strength of the glass or quartz.

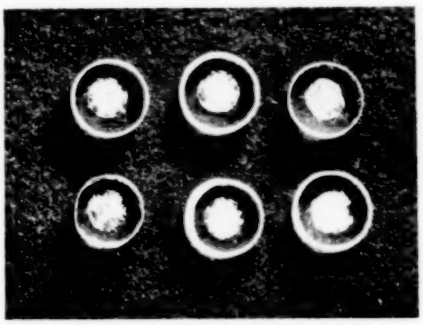

Fig. 7. Windows showing second type of fracture. Top row is quartz and bottom row is glass.

It is, therefore, the belief of the author that if glass or quartz windows are properly mounted they will withstand a pressure of 30,000 atmospheres provided that a light paraffin oil is used to transmit the pressures.

For work in which it is necessary to pass light into the material under pressure or make observations where windows are necessary, it has been found most convenient to construct the pressure cylinder and the observation chamber of a single piece of steel. In assemblies of this kind the end of the cylinder in which the pressure is developed opens into the observation chamber. This does away with the necessity of making connections to transmit the pressure from the cylinder to the observation chamber, and thus decreases the chances of leaks. This cylinder and observation chamber is enclosed in a water jacket for temperature control.

That portion of the cylinder in which the pressure is developed is identical with the corresponding part of the cylinder shown in Fig. 1. The observation chamber L contains the material being studied. The glass or quartz windows F are mounted against the polished surface of the high-speed-steel window supports R which are in turn held in place by means of the plugs M. The polished surface of the window support makes a tight joint with the shoulder

at the end of the observation chamber. The safety windows J are made of the same material as that used in the pressure windows and are mounted between fiber washers and held in place by the housing I. In earlier work only one safety window was used on each end but experience showed that one was insufficient. The purpose of the safety window is to catch flying pieces in case a pressure window shatters or a leak develops. The windows K are mounted in a metal tube which fits the inner end of the plug M. This puts them on the opposite side of the window support from the pressure windows. The intervening space is filled with a liquid having the same index of refraction as that of the pressure window. This corrects for the lens effects, due to the bulging of the pressure windows.[9]

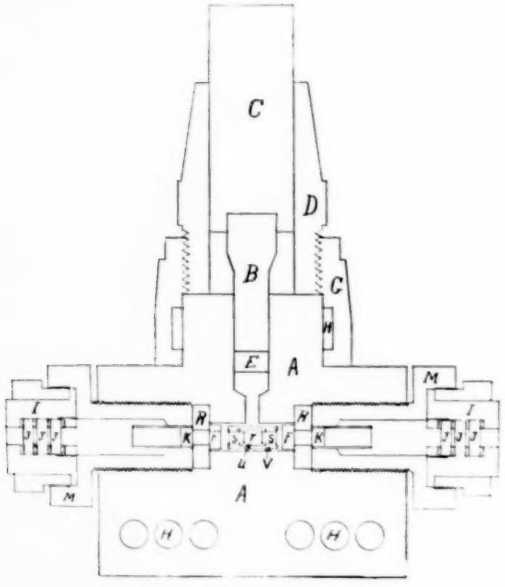

Fig. 8. Pressure equipment with windows in place, drawn to scale.

The window is a piece of glass or fused quartz approximately 11 mm in diameter and from 4 to 10 mm in thickness. The surface of the window support is ground flat to an accuracy of 1×10^{-4} cm which is measured by placing the window in contact with its surface and counting the interference fringes produced between them. These windows are held in place while assembling the cylinder by a small quantity of liquid balsam. The pressure is applied slowly so as to permit the balsam to flow out and allow the window to come in contact with the steel support. The liquid in the observation chamber has access to all sides of the window except its supporting surface thus producing as nearly a compressional force on the window as possible.

If it is desired to separate the oil in the cylinder from any other liquid being investigated, it is most convenient to place such a liquid in a small cell

[9] Thos. C. Poulter and Carl Benz. The Line Effect of Pressure Windows, Phys. Rev. 40, 872. (1932).

with windows in each end. This cell is placed in the observation chamber and surrounded with oil. If a constant quantity of material is desired in the light path it is necessary to use a telescoping cell.

If a constant length of a column of liquid is desired, the windows can be rigidly mounted in the ends of a hard steel tube. This tube can have a number of holes in the side which are covered by placing this tube in a thin walled

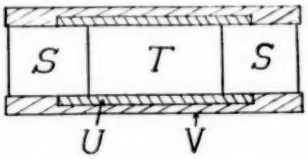

Fig. 9. Telescoping cell. U = high speed steel cell case with movable windows S. V = rubber tube surrounding cell and windows.

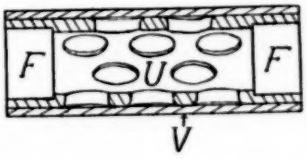

Fig. 10. Constant length cell. V = rubber tube stretched over outside of cell. F = windows cemented in place. U = high speed steel body of cell.

rubber tube. The compressibility of the hardened high speed steel is so small that very little error is introduced thereby.

While the author has had many experiences with explosions of high pressure apparatus that he does not care to have repeated, it is his belief that there is very little danger attached to investigation of this kind if the precautions herein described are carefully observed.

The author wishes to express his appreciation for the assistance in the form of a grant from the Bache Fund of the National Academy of Science.

The Lens Effect of Pressure Windows

By THOS. C. POULTER AND CARL BENZ
Department of Physics, Iowa Wesleyan College
(Received March 18, 1932)

The lens effect of high pressure optical systems involving glass or quartz windows has been studied and found to be due to four primary causes. (1) Pseudo-lens effects due to temperature gradients following changes of pressure. (2) Bulging of the outer surface of the pressure window. (3) Pseudo-lens effect due to unequal distribution of strain in the window. (4) The difference in index of refraction of the material in the cylinder and that of the window combined with the bulging of the inside surface of the window. These effects are measured and methods for their correction outlined.

INTRODUCTION

THE lens effect of pressure windows or of the entire optical portion of a pressure system as produced directly or indirectly by pressures has been studied with the view to determine the nature of the effect and if possible how to prevent or at least to correct for such effects. These lens effects were encountered in an attempt to measure the index of refraction of materials under pressure and this study wts found necessary before many optical investigations could be successfully carried on.[1,2,3,4]

APPARATUS AND PROCEDURE

The apparatus employed is a combination pressure cylinder and observation chamber which is so constructed that the observation chamber is located at the end of the pressure cylinder. The main body A, Fig. 1, is machined from a single piece of steel, thus preventing the possibility of leaks in connections between the pressure cylinder and the observation chamber. The safety windows J prevent danger from flying materials in case the pressure windows F blow out. The temperature is controlled by circulating water from the thermostat through the water jackets which cover both sides of the assembly and are connected by the openings marked H in the diagram. Water is also circulated through the platins of the hydraulic press. The material under investigation is placed in the observation chamber L and the pressure is developed by forcing the piston B into the pressure cylinder with a hydraulic press. The pressure in the high pressure cylinder is determined as in previous work by the authors.

The two ends of the observation chamber are fitted with glass or fused quartz windows F, mounted against the window supports. The rubber plug E makes a tight joint around the end of the piston.

[1] Thos. C. Poulter, Phys. Rev. **35,** 295 (1930).
[2] Thos. C. Poulter and Robert Wilson, Iowa Academy of Science **37,** 299–302 (1930).
[3] Thos. C. Poulter and Harold C. McComb, Iowa Academy of Science **37,** 311–12 (1930).
[4] Thos. C. Poulter, Apparatus for Optical Studies at High Pressures, Phys. Rev. 40, 860 (1932).

A light source *O* and lens *N* is placed at one end of the cylinder and adjusted so as to pass parallel light through the optical system, consisting of the two windows and the liquid within the observation chamber. A straight wire filament incandescent bulb is placed at the principal focus of the lens *N* for a light source. For large converging lens effects, the lens *P* is removed and a screen is placed at the other end of the observation chamber and adjusted so as to give a clear image of the filament. For diverging lens effect or small converging effects, a converging lens of known focal length is placed between the end of the chamber and the screen. The focal length of the combination is measured from which the lens effect of the pressure system can be calculated.

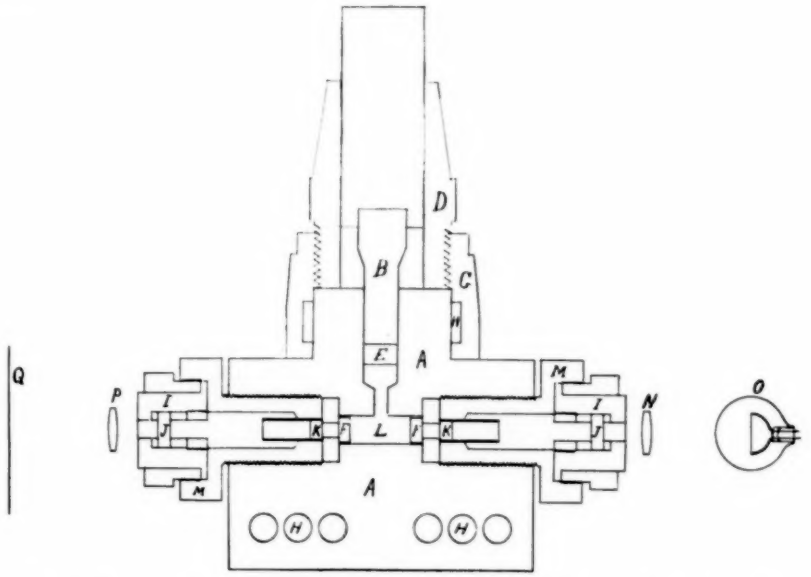

Fig. 1. Cross-section of pressure assembly and optical system drawn to scale.

Experimental Results

A large lens effect, being somewhat diffused at first but becoming sharply defined upon standing, is observed immediately following a pressure change. This is a diverging lens effect following an increase in pressure, and a converging lens effect following a decrease in pressure. These effects are of the order of magnitude that give a focal length of +4 cm or −4 cm. This value changes rapidly at first and becomes constant after standing for about five minutes. For a given pressure this constant value is the same regardless of whether the pressure has just previously been increased or decreased. A similar effect can be produced by rapidly changing the temperature of the observation chamber. If the observation chamber is rapidly heated by passing steam through the water jacket a converging lens effect is produced, whereas rapid cooling produces a diverging lens effect. If sufficient time is allowed following a pressure or temperature change (usually five minutes is sufficient)

for the lens effect to come to a constant value, this value is always that of a converging lens if the system is under pressure.

If another window K is then mounted just outside each of the pressure windows and the intervening space filled with a colorless liquid having an index of refraction the same as that of the window, most of the lens effect disappears.

For determining the remaining lens effect a lens P of known focal length is placed at the end of the cylinder opposite the source of parallel light. The focal length of the combination is then measured from which the focal length of the pressure system can be calculated. Table I contains a typical set of values for windows 4 and 8 mm in thickness. Experiments were carried out

TABLE I. *P—Pressure in atmospheres; F_1—Focal length of the pressure system uncorrected; F_2—Focal length of the pressure system calculated from R; F_3—Focal length of the pressure system using liquid correction window; F_4—Focal length of the liquid correction windows; R_1—Radius of curvature of the outside surface of the windows, optical method; R_2—Radius of curvature of the outside surface of the windows, plaster-of-paris method.*

	4 mm window						8 mm window				
P	F_1	F_2	F_3	F_4	R_1	R_2	F_1	F_2	F_3	F_4	R
1	∞	∞	∞	∞	∞	∞	∞	∞	∞	∞	∞
2000	24.1	16.2	−50	−16.2	15.6	16.0	55.0	36.2	−105	−36.2	35.5
4000	21.6	15.1	−50	−15.1	14.4		47.0	30.0	−105	−30.0	29.3
6000	18.9	13.7	−50	−13.7	13.1	13.0	38.9	28.4	−105	−28.4	27.8
8000	18.6	13.6	−50	−13.6	12.9		38.0	28.0	−105	−28.0	27.3
10,000	18.4	13.1	−50	−13.1	12.7	13.0	37.0	27.4	−105	−27.4	26.6
8000	18.5	13.5	−50	−13.5	12.8		38.0	28.0	−105	−28.0	27.3
6000	18.9	13.7	−50	−13.7	13.1	13.0	39.0	28.5	−105	−28.5	27.9
4000	21.5	15.0	−50	−15.0	14.3		40.0	29.0	−105	−29.0	29.2
2000	24.0	16.2	−50	−16.2	15.6	15.5	52.0	36.0	−105	−36.0	35.3
1	∞	∞	∞	∞	∞	∞	∞	∞	∞	∞	∞
30,000	15.2	11.7	−50	−11.7	11.0	11.0					

on 4 and 8 mm glass windows and 4 mm fused quartz windows. The values were the same within the limits of experimental error for the glass and quartz windows so only one set of data is given. These values are for windows 12 mm in diameter and placed over a 6 mm hole in the window support. In order to check the curvature of the glass or quartz by a more direct method, the opening in the window support was filled with freshly prepared plaster-of-paris. Pressure was then applied and the plaster-of-paris allowed to set, thus leaving the impression of the curved surface of the window. After allowing it to harden thoroughly, the curvature was measured by means of a micrometer. The values for the radius of curvature as obtained by this method check to within less than 5 percent of the values obtained by the optical method. This corresponds to an error in measuring of less than 0.001 cm, which is as close as measurements can conveniently be made to a plaster-of-paris surface.

DISCUSSION OF RESULTS

The nonexistence of a large pressure gradient in the oil used to transmit the pressure is definitely shown by the behavior of the optical portion of the system during, and for a few minutes following, a pressure change. During and immediately following a pressure change, the image of the filament through the pressure system is much less sharply defined than it is after

standing for about five minutes. If one observes the contents of the observation chamber during a pressure change, a distinct turbulent flow of material from the pressure cylinder to the observation chamber can be observed. This flow is visible due to the difference in the index of refraction accompanying the temperature change on compression. The contents of the observation chamber again become homogeneous on standing. This turbulent flow is even more easily observed if some finely divided solid material is suspended in the oil. Such a flow of material precludes the possibility of any very large pressure gradient.

The lens effect of the pressure system is probably due to a combination of several effects, the most important of which are:

1. The pseudo-lens effect due to a temperature gradient and thereby a density gradient of the material under pressure following a pressure change. This gradient existed between the walls of the observation chamber and a line through the center of the chamber.

2. The bulging of the outside surface of the pressure window.

3. The pseudo-lens effect due to the unequal but symmetrical distribution of strain in the glass or quartz of the window. This is due to the window support exerting a force around the edge on the supporting surface and not over the center.

4. The bulging of the inside surface of the window together with the difference in index of refraction of the window and the material under pressure.

The largest of these effects and the easiest one to correct for is the pseudo-lens effect following a change in pressure. At first thought it might appear as though this were due to a pressure gradient rather than a temperature gradient. If it were a pressure gradient it would likely extend between the center of the observation chamber and the windows. Any lens effect thus produced would be likely to be of the reverse nature, namely, a converging effect following an increase of pressure and diverging effect following a decrease in pressure. Furthermore, if it were a pressure gradient due to the materials becoming stiff under pressure, it would be most pronounced at the higher pressures, whereas it is much greater at pressures below 2000 atmospheres. That it is due to a temperature and thereby a density gradient is suggested by the fact that as soon as sufficient time is allowed for constant temperature to be established, the effect disappears. This is further confirmed by the fact that if the observation chamber is rapidly heated by running steam through the water jacket, an effect is produced similar to that produced by a decrease in pressure. Rapid cooling produces the same effect as an increase in pressure. The temperature of the material in the cylinder is suddenly increased due to compressibility during an increase in pressure. Since it is then at a higher temperature than the walls of the observation chamber, the material in contact with the walls is cooled first, producing a greater density around the outside than that through the center, hence the diverging effect. The reverse is true following a decrease in pressure. Since this effect completely disappears within five to ten minutes following a pressure change, it is automatically corrected for by allowing that time before making observations.

The next largest effect and also the next easiest to correct for is that of the bulging of the outer surface of the window. This effect is largely corrected by placing a liquid of about the same index of refraction as the window in contact with its outer surface. The radius of curvature of the outside surface of the pressure windows is determined in the following manner. The pressure windows and the intervening pressure liquid produces a lens of focal length F_1 whose thickness is the distance between the two outside surfaces of the windows. Now there is placed a layer of liquid on both curved surfaces which produces two diverging liquid lenses at the ends of the pressure system. The focal length of this combination F_3 is measured from which the focal length F_4 of the liquid correction windows alone can be calculated. Since we know the focal length F_4 of this pair of diverging liquid lenses and the distance between their curved surfaces C, their curvature, and hence, the radius of curvature of the outside surface of the pressure windows, can be calculated by means of the following equation

$$\frac{1}{F_3} = (\mu - 1)\left\{\frac{2}{R} - \frac{(\mu - 1)C}{\mu R}\right\} + \frac{1}{F_1}$$

in which μ is the index of refraction of the liquid used as correction window.

At pressures of 30,000 atmospheres, glass and quartz windows 4 mm in thickness will bend to a radius of curvature of as small as 11 cm. Glass windows will withstand such bending sometimes as many as five to ten times without apparent damage. Windows made of fused quartz are usually cracked after one or two such pressure runs.

The third and fourth effects are small as compared to the first two and are much more difficult to measure individually. The third could be measured by measuring the change in focal length of the system as materials of different indices of refraction are used in the observation chamber, if the effect of the pressure upon the index of refraction of such liquids were known. Since very little or no such data are available, usually the third and fourth effects are measured together with that due to any other cause if there be such. The magnitude of these latter two effects is indicated by the difference in focal length of the pressure system F_1, and F_2 the focal length as it would be if these factors did not enter.

If a liquid of the proper index of refraction is selected to place in contact with the outer surface of the pressure windows, an optical system can be obtained with almost no lens effect. If the remaining lens effect, after the first two have been corrected for, is that of a converging lens, a liquid of index of refraction greater than that of the window is required, whereas if it is a diverging effect, a liquid of index of refraction less than that of the window is required. In this way optical pressure system have been obtained whose focal length only changes from ∞ to 10 meters in changing from 1 to 30,000 atmospheres.

The authors wish to express their appreciation for the assistance in the form of a grant from the Rumford Fund of the American Academy of Arts and Science.

The Permeability of Glass and Fused Quartz to Ether, Alcohol, and Water at High Pressure

By Thos. C. Poulter and Robert O. Wilson
Department of Physics, Iowa Wesleyan College

(Received April 16, 1932)

The permeability of glass and fused quartz to water, alcohol and ether and its relation to pressure windows has been studied. These liquids are shown to penetrate to considerable depths if the pressure is maintained for as long as fifteen minutes, in which case the pieces of glass or quartz are shattered if the pressure is rapidly released. However, if the pressure is released over a period of several days little or no breakage occurs. It is, therefore, likely that much of the difference in the behavior of pressure windows as different liquids are used in contact with the windows is due to their ability to penetrate the glass or quartz.

Introduction

During the past several years the writer has been engaged in experiments involving very high pressures. This work has been described in a number of papers.[1–8]

Pressures up to 30,000 atmospheres were employed in cylinders with glass or quartz windows. In the course of these investigations it became necessary to study the properties of glass and quartz when in a liquid at high pressures.

The difference in the behavior of different liquids on pressure windows has suggested that in some cases the liquid was penetrating the glass or quartz of the window. P. W. Bridgman[9] found that hydrogen at 9000 atmospheres would penetrate the walls of a steel container and that cylinders containing hydrogen under high pressure would be frequently broken at less than half the pressure they had previously withstood. This has been encountered many times by the authors. Bridgman also found that if mercury were allowed to come in contact with the inner surface of the cylinder at very high pressure the cylinder wall would be weakened. Pressure windows will withstand several times as much pressure if oil or glycerine is used to transmit the pressure as they will if water, alcohol or ether, is employed. Windows surrounded by water, alcohol, or ether would frequently break on lowering the pressure even though they had previously withstood much

[1] Thos. C. Poulter and Robert Wilson, Iowa Acad. of Sci. **36,** 295–6 (1929).
[2] Thos. C. Poulter, Phys. Rev. **35,** 295 (1930).
[3] Thos. C. Poulter and Robert Wilson, Iowa Acad. of Sci. **37,** 299–302 (1930).
[4] Thos. C. Poulter and Harold C. McComb, Iowa Acad. of Sci. **37,** 311–312 (1930).
[5] Thos. C. Poulter and Carl A. Benz, Phys. Rev. **40,** 872 (1932).
[6] Thos. C. Poulter, Phys. Rev. **40,** 860 (1932).
[7] Thos. C. Poulter and Glen E. Frazer, paper in preparation.
[8] Thos. C. Poulter and Carter Ritchey, Phys. Rev. **39,** 816 (1932).
[9] P. W. Bridgman, Rec. trav. chim. **42,** 568–71 (1923); Proc. of Am. Acad. Arts Sci. **59,** No. 8, 177–221 (1924).

greater pressures. This investigation was undertaken in order to determine the nature of this difference in behavior.

Apparatus and Procedure

The pressure equipment used in this work is the vertical type cylinder used in other investigations by the author. This cylinder has an inside diameter of 1.6 cm and a capacity of about 17 cm^3. The pressure was produced and measured as in previous work.

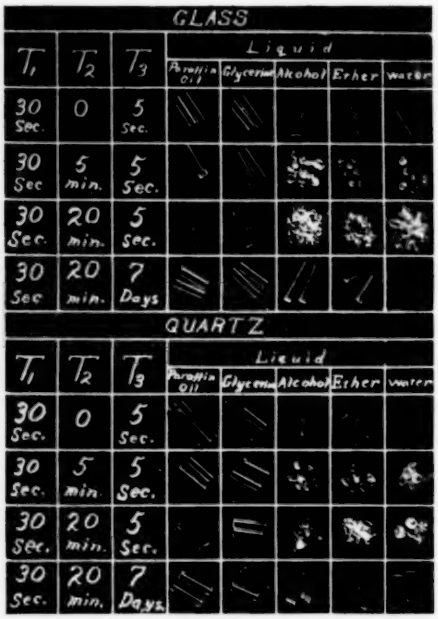

Fig. 1. Type of fractures occurring under various conditions: T_1, time required to develop the pressure, T_2, time the pressure was maintained, T_3, time consumed in reducing the pressure to atmospheric.

The samples to be tested were pieces of glass or quartz rod 3 to 4 mm in diameter and about 15 mm long. These pieces were placed in a piece of rubber tubing 5 cm long and 6 mm inside diameter. This tube was filled with the desired liquid and stoppered at both ends. It was then placed in the pressure cylinder and the pressure applied.

The manner in which the pressure is built up seems to have nothing to do with the behavior of the glass or quartz and the breakage usually occurs as the pressure is released. Little difference was noticed in the behavior of glass and quartz except that the quartz does not break with as regular a surface as does the glass. Oil and glycerine produce no fracturing of the glass of quartz. In the case of water, alcohol, and ether the following results were obtained. If the pressure was built up to any value above 15,000 atmospheres and immediately dropped to zero, the pieces would usually not be broken; occasionally they would be broken into two or three pieces. If the pressure was built

up above 15,000 atmospheres and held there for five minutes and then released, the rod would be broken in rather regular plates, the fractures running perpendicular to the length of the piece. The plates thus produced would be from one half to two or three millimeters in thickness. If the pressure was built up and allowed to stand for fifteen minutes or longer and then released rapidly the fractures would be irregular and the pieces usually much smaller. If the pressures were built up and released very slowly over a period of five to ten days very few if any fractures would occur. However, if the pieces of glass or quartz were surrounded with oil or glycerine and all of the above procedure carried out it is very unusual for any fracture to occur. The results of these experiments are shown in Fig. 1.

A glass disk such as those used for pressure windows is mounted in the center of a rubber tube with oil on one side and water, alcohol or ether on the other side and the two ends of the tube stoppered. This assembly is then placed in a pressure cylinder and surrounded with oil. If a pressure of 20,000

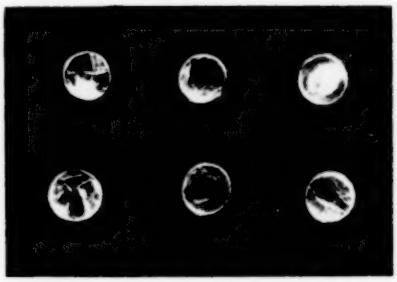

Fig. 2. Showing the fracture of the surface of glass and quartz in contact with water, alcohol or ether. Pieces are layed with fractured side down for photographing. The upper three are quartz and the lower three are glass.

atmospheres is developed and maintained for from 5 to 10 minutes and then rapidly released the side of the glass in contact with the water will be shattered while that in contact with the oil will remain intact. Fig. 2 shows such a group of fractured pieces.

Discussion of Results

The difference in the behavior of glass or quartz when surrounded by different liquids cannot be explained on the basis of temperature changes accompanying the rapid pressure changes, although these are large, sometimes amounting to as much as 100°C. If it were a temperature change the glass only would be effected, whereas the quartz is just as susceptible to the fracturing as the glass. Neither can it be explained on the basis of a differential compressibility of the solid modification of the water and the glass or quartz for no solid modification is known for alcohol or ether at these pressures and temperatures.

The fact that in cases where the glass has water on one side and oil on the other, only that side in contact with the water is shattered eliminates the

possibility of the fracturing being due to a compressibility hysteresis effect due to the glass or quartz being under extreme pressure. This is further shown by the fact that glass or quartz pressure windows four millimeters thick and twelve millimeters in diameter can be bent to a radius of curvature of eleven centimeters and return without fracturing. In the case of glass this has been done as many as ten times with a single window and with quartz it has been done as many as four times.

The most probable explanation of the fracturing of these materials after having been subjected to pressure while surrounded by water, alcohol, or ether is that the liquids while compressed actually penetrate the glass or quartz. Then as the pressure is released the cohesive force of the glass or quartz is not great enough to retain the liquids under this compressed condition. This explanation of the fracturing is in agreement with all the facts at hand:

(a) Little or no breakage occurs if insufficient time is allowed for the liquid to penetrate.

(b) Breakage occurs as the pressure is released rather than when it is being built up or retained at a high pressure.

(c) Little or no breakage occurs if the pressure is allowed to drop slowly enough to permit the gradual escape of the liquid.

(d) No breakage occurs if liquids of relatively large molecules and high viscosity are used such as oil or glycerine.

(e) The fracturing is determined by the type of liquid and not by the pressure alone, as is shown when different liquids are on opposite sides of the same piece of glass or quartz. In this case the pressures are necessarily equal.

The authors wish to express their appreciation for the assistance in the form of a grant from the Rumford Fund of the American Academy of Arts and Science.

LETTERS TO THE EDITOR

Prompt publication of brief reports of important discoveries in physics may be secured by addressing them to this department. Closing dates for this department are, for the first issue of the month, the twenty-eighth of the preceding month; for the second issue, the thirteenth of the month. The Board of Editors does not hold itself responsible for the opinions expressed by the correspondents.

The Loss of Energy by Fast Electric Particles

In a recent letter to the Physical Review[1] Carlson and Oppenheimer consider the problem of the relativity effect on the rate of loss of energy by very fast particles—with energy $T=\epsilon Mc^2 \gg Mc^2$, M being the rest mass—and apply their results to the particles associated with penetrating radiation. The writer considered these questions in a paper published some time ago,[2] and in the present note desires in the first place (paragraph *a*) to point out that the result concerning light collisions arrived at by Carlson and Oppenheimer is already contained in a formula given in that paper. In paragraph *c* of this note the writer's method of deriving the relativity correction, which is somewhat different from that of Carlson and Oppenheimer, is outlined. *d* discusses the relation with experiment, and in particular points out an error in Watson and Terroux's recent letter to the Physical Review,[3] and also shows that we are not yet compelled to postulate (as Carlson and Oppenheimer do) an unknown particle to explain the ionization produced by the particles of penetrating radiation. *e* concludes with a consideration of the energy lost in heavy collisions, in which results are indicated which do not agree with those of Carlson and Oppenheimer.

a. Carlson and Oppenheimer consider that for ultrafast particles only collisions with comparatively small energy transfer, Q, need be taken into account. To compare my calculations with theirs we take the formula 10a, p. 341, in the above mentioned paper. This formula gives the loss of energy $d_W T$ in light collisions—defined by $Q<W$ where ionization potential, $J \ll W \ll mc^2$ (m = electronic mass). The formula actually refers to β-particles, but applies to particles with charge $z\times e$, and any mass, if, in one place, we replace e^2 by z^2e^2. It then gives

$$d_W T/dx = (2\pi z^2 e^4 N/mv^2)\{\log (W\beta^2/k_1 J^2) - \beta^2 + \log (1-\beta^2)^{-1}\} \quad (1)$$

v = velocity of moving particle. $\beta = v/c$. N = number of atomic electrons/cc. Now $T=\epsilon Mc^2 = Mc^2\{(1-\beta^2)^{-1/2}-1\}$, so that for the case of *very* large ϵ considered by Carlson and Oppenheimer, (1) becomes

$$dT/dx = (4\pi z^2 e^4 N/mc^2)\log \epsilon. \quad (2)$$

This is identical with their formula.

b. In the nonrelativity region, (1) reduces to the nonrelativity formula derived by Gaunt.[4] Since the time of Gaunt's calculation a more accurate quantum theory formula for the nonrelativity region has been given by Bethe.[5] Bethe deals with the primary ionization as well as the loss of energy. In a paper, now in the press, the writer applies the relativity correction in (1) to Bethe's formulae obtaining

$$d_W T/dx = (2\pi z^2 e^4 N/mv^2)\{\log (2Wmc^2\beta^2/E^2) + \log (1-\beta^2)^{-1}\} \quad (3)^*$$

(E/h is a characteristic frequency of the atoms traversed) and a primary ionization per cm (for hydrogen atoms) of

[1] Carlson and Oppenheimer, Phys. Rev. **38**, 1787 (1931).

[2] Williams, Roy. Soc. Proc. **A130**, 328 (1931).

[3] Watson and Terroux, Phys. Rev. **38**, 2291 (1931).

[4] Gaunt, Camb. Phil. Soc. Proc. **23**, 732 (1927).

[5] Bethe, Ann. d. Physik. **5**, 325 (1930).

* $-\beta^2$ in (1) is numerically unimportant, especially for large ϵ. It is omitted from (3) and (4).

$$I = (2\pi z^2e^4N/mv^2J)\,0.285\{\log(42mc^2\beta^2/J) + \log(1-\beta^2)^{-1}\}. \quad (4)$$

c. The relativity correction in (3) and (4), as derived by the writer, depends upon a relativity increase in the 'radius of action' of the moving particle. The radius of action, ρ, is equal to the impact parameter, p, for which the time of collision is comparable with the smallest natural period of the atomic electron. For collisions with $p \gg \rho$ the conditions are adiabatic and the energy transfer is insignificant. For $p \ll \rho$ energy transfer takes place 'freely,' the average transfer, $\bar{Q}$, being, in the case where p is also greater than atomic dimensions, actually equal to the classical energy transfer to a free electron viz., $2z^2e^4/mv^2p^2$. The relativity increase in the radius of action is due to the Fitzgerald contraction of the field of the particle. The latter, in light collisions, may be assumed to move with uniform velocity. The Fritzgerald contraction then reduces the time of collision, for a given impact parameter, by $(1-\beta^2)^{-1/2}$; and as a result the radius of action is correspondingly increased, from ρ_0, say, to $\rho_0(1-\beta^2)^{-1/2}$. The Fitzgerald contraction leaves the time integral of the perturbing force unaltered, from which it may be shown that, in the light collisions dealt with, the relativity effect is entirely represented by the increase in the radius of action. This gives rise to an extra dissipation of energy dT_R/dx equal to

$$\int_{\rho_0}^{\rho'} (2z^2e^4/mv^2p^2)2\pi p\,dp\,N = (2\pi z^2e^4N/mv^2)\log(1-\beta^2)^{-1} = (4\pi z^2e^4N/mv^2)\log(1+\epsilon). \quad (5)$$

(This gives (2) for large ϵ). The extra energy loss dT_R is concentrated in *very* light collisions, with energy loss of the order of the ionization potential J. It follows that if $W \gg J$, dT_R is all to be included in d_WT. The nonrelativity value of d_WT/dx according to Bethe's calculations is $(2\pi z^2e^4N/mv^2)\log(2Wmc^2\beta^2/E^2)$. The addition of dT_R to this gives (3). For hydrogen atoms the extra primary ionization corresponding to dT_R is $0.285\ dT_R/J$. (4) represents the addition of this to Bethe's nonrelativity formula for the primary ionization.

It is of interest that since dT_R all goes into light collisions with $Q \sim J$, the frequency $\phi(Q)$ of light collisions with $Q \gg J$ is unaffected, and is therefore given by the nonrelativity expression for $\phi(Q)$ viz.,

$$\phi_0(Q) = 2\pi z^2e^4N/mv^2Q^2. \quad (6)$$

It might be mentioned that the derivation of the results given in this paragraph can be put in exact mathematical language, and it is hoped to publish in due course the details of the calculations.

d. Comparison with experiment. From (3) and (4) the variation with velocity of both the energy loss, d_WT, and the primary ionization, is represented by an expression $F(\beta)$ of the form $\beta^{-2}\log\{k\beta^2/(1-\beta^2)\}$. In terms of energy, ϵMc^2, this expression is $F(\epsilon) = (1+\epsilon)^2(2\epsilon+\epsilon^2)^{-1}\log\{k'(2\epsilon+\epsilon^2)\}$. As ϵ increases $F(\epsilon)$ decreases approximately as $1/\epsilon$ for small ϵ, passes through a minimum at $\epsilon \sim 3$, and then increases approximately as $\log k'\epsilon$, which for very large ϵ increases as $\log \epsilon$. In comparing with experiment, Watson and Terroux[3] apparently assume the latter variation, viz., increase with $\log \epsilon$, to hold for all ϵ, and actually apply it to the region $0.25 < \epsilon < 3$. It is no wonder that these writers conclude very decisively against the theory, for the primary ionization observed by Terroux and myself[6] (which they quote) *decreases* quite rapidly with increasing ϵ for most of this region. To make a legitimate comparison with experiment in this region we must take the full expression for $F(\epsilon)$. We then find reasonable agreement. It requires however more accurate data than were aimed at in the above experiments to decide whether the relativity correction in (4) is adequate, but it is in the right direction and of the right order of magnitude. A detailed comparison of (3) and (4) with experiment is given in a paper by the writer which is now in the press.

The minimum effect referred to above, which takes place at $\epsilon \sim 3$, corresponds approximately to a primary ionization of about $20z^2$/cm, and a total ionization approximately double this, viz., $40z^2$/cm, when the gas traversed is air at N.T.P. and where ze is the charge of the moving particle. The most quantitative information we have about the ionization produced by the particles associated with penetrating radiation is due to Skobelzyn,[8] who records a total ionization of about 40/cm in air. From the foregoing it follows that no particle, whatever its velocity, with more than a single electronic charge (i.e., $z > 1$) can produce so little ionization. The

[6] Williams and Terroux, Roy. Soc. Proc. **A126,** 289 (1930).

ionization is however equal to the minimum ionization produced by particles with $z=1$, i.e., electrons and protons. The energy which gives this minimum is $3Mc^2$, i.e., 1.5×10^6 volts for electrons, and 3×10^9 volts for protons. From other evidence the ionizing particles of penetrating radiation have energy at least of the order of 10^9 volts. Electrons are therefore ruled out, but not protons.

It is interesting to note that the total ionization observed by Skobelzyn (40/cm) is equal to the theoretical primary ionization due to electrons with about 10^{10} volts. The writer, who has for some time been aware of the position concerning this question,[7] wrote to Dr. Skobelzyn, some time ago (Nov. 1929), to make sure that the ionization observed by him was not conceivably primary ionization, in which case it would follow that the particles concerned might be 10^{10} volt electrons. In his reply Dr. Skobelzyn however confirmed the statement in his paper.

We must mention recent observations of a similar kind to Skobelzyn's made by Mott-Smith and Locher.[9] Carlson and Oppenheimer conclude from these that the particles concerned cannot be any known electric particle. The experimental data are however too qualitative for such a conclusion to be drawn. In fact, as far as it goes, the data are not inconsistent with Skobelzyn's, and it therefore leaves the above conclusions unaffected. Mott-Smith and Locher say that the 'penetrating' particles they observe produce about one half of the ionization produced by an average recoil electron from scattered hard $RaC\gamma$ rays. The latter is very indefinite. A rough estimate gives a total ionization by such recoil electrons of about 90 per cm, and half this agrees with Skobelzyn's result of 40/cm. This agreement however confirms no more than the order of magnitude of the results.

e. Heavy collisions. The primary ionization, and $d_W T$, depend only on light collisions. To obtain the energy lost in all collisions we must add to $d_W T$ a quantity $d^W T = \int_W^{Q_{\max}} Q\phi(Q)dQdx$. This integral involves large Q for which magnetic forces and relativity variation in the mass of the "knocked" electron may be important—these effects are neglected in the treatment of light collisions in *c*, Carlson and Oppenheimer state that the contribution of the heavy collisions to the total stopping power is unimportant. Now as far as protons (and heavier particles) are concerned, the problem of the loss of energy in traversing free electrons* is the same as the problem of the nuclear scattering of electrons, which has already been worked out on the quantum theory by Mott.[10] Using Mott's results we find that for very heavy particles, except for Q close to its maximum value of $2\epsilon^2 mc^2$, $\phi(Q)$ is the same as its nonrelativity value $\phi_0(Q)$ given by (6). It follows that if ϵ is very large, $d^W T/dx$ is approximately $(2\pi Nz^2e^4/mc^2)$ $\log(\epsilon^2 mc^2/W)$. Adding this to $d_W T/dx$ (Eq. (3)) we obtain a total dissipation of

$$dT/dx = (4\pi z^2 e^4 N/mc^2)\{\log(mc^2/E) + 2\log\epsilon\} \quad (7)$$

According to this and (2) the dissipation for *very* large ϵ is just doubled by the inclusion of heavy collisions—in contradiction with the above supposition of Carlson and Oppenheimer.

It is surprising that $\phi(Q)$ maintains the same form for $Q \gg mc^2$ as for $Q \ll mc^2$, since for the former the knocked electron is effectively a heavy particle. A change in the region $Q \sim mc^2$, however, requires a change in the nuclear scattering formula in the region of scattering angle $\theta \sim (1-\beta^2)^{1/2}$, and in Mott's formula there is no such change. The contribution of heavy collisions is negligible only if the scattering is negligible for $\theta > (1-\beta^2)^{1/2}$.

E. J. WILLIAMS

The Physical Laboratories,
Manchester University,
January 26, 1932.

[7] E.g., reference, 2, p. 336.

[8] Skobelzyn, Zeits. f. Physik **54,** 686 (1929).

[9] Mott-Smith and Locher, Phys. Rev. **38,** 1399 (1931).

* In the region $Q > W$ the atomic electrons may be treated as free since $W \gg J$.

[10] Mott, Roy. Soc. Proc. **A124,** 425 (1929).

Zeeman Effect in the Spectrum of Pb III.

We have been studying the Zeeman effect of the spectra of Pb II, Pb III, and Pb IV with a view to checking the classifications in these spectra. The patterns found are in general

agreement with the classification of Gieseler[1] on Pb II and Smith on Pb III[2] and Pb IV.[3]

Of these spectra, Pb III is the most interesting, since we have the possibility of checking the Houston[4] theory of intermediate coupling. In the case of the $6s7p$ configuration, ($^3P_0$, $^3P_1$, $^3P_2$, $^1P_1$) the g-sum of $^3P_1+{}^1P_1$ yields a value slightly higher than the 5/2 it should be according to Pauli's g-sum rule, while the $^3P_2$ level, which should be unaffected by coupling (to first order terms) yields a g-value of about 1.35 instead of 3/2. This might be accounted for by incorrect assignment, but there is no other level in the neighborhood that would fit. It seems then, that the abnormal g-value must be attributed to perturbations caused by the proximity of $6p^2$ and $6s7d$ configurations.

The work was done with the aid of the new 30,000 line 21-ft. grating in the Paschen-Ruage mounting, and the Weiss-type magnet recently completed at this laboratory, with fields of about 41,000 gausses. A complete report will appear in the late summer.

J. B. GREEN
R. A. LORING
Mendenhall Laboratory of Physics,
Ohio State University, Columbus, Ohio,
May 4, 1932.

[1] Gieseler, Zeits. f. Physik **42,** 265 (1927).
[2] Smith, Phys. Rev. **34,** 393 (1929).
[3] Smith, Phys. Rev. **36,** 1 (1930).
[4] Houston, Phys. Rev. **33,** 297 (1929).

Attempts to Induce Temporary Radioactivity in Matter

The experiments of Pokrowski,[1] which report the excitation of feeble radioactivity in heavy elements by irradiating them with x-rays, are of such an astonishing nature that they seem to warrant careful repetition. Gingrich[2] did not find the ionization effects, on repeating the work with detecting apparatus of higher sensitivity and with harder x-rays and irradiating the materials for longer times. This naturally casts doubt on the existence of the effect, although Pokrowski seems to have taken such careful precautions in his experiments that it is not easy to see where consistent error could have been introduced. Pokrowski found measurable ionization produced as long as 90 minutes after exposure of the specimen to x-rays, and suggested that the energy was released from nuclei by triggeraction of the photons. Even if this dubious process is admitted as possible, one might expect that the emission would only last for a very small fraction of a second after irradiation of the specimen ceased. On the other hand, if nuclei have definite eigenstates, similar to those involving extranuclear electrons, it seems reasonable to believe that the absorption of suitable gamma-radiation might cause transitions which would subsequently result in nuclear fluorescence, even from non-radioactive atoms.

I have recently completed several series of experiments in which *long-time fluorescence* was sought from various materials that had been irradiated with gamma-rays and x-rays of different wave-lengths. No such fluorescence was detected, although the intervals between irradiation and detection ranged from 7×10^{-5} sec. to an hour. A Geiger counter was used as a detector. Its approximate sensitivity was found from the increase in the counting rate due to a known amount of radium at a known distance. The "accidental" count was 110 per hour, with the shielding used, while the rate with 1 mg of radium at 4 meters was 700 per hour. From this it is deduced that the accidental counting rate would be increased 50 percent by 2.3×10^{-6} mg of radium 2 cm from the counter, or that 4.6×10^{-8} mg would give a 1 percent increase. The sensitivity, expressed as the minimum detectal le radium equivalent, depends on the distance of the material from the counter and the total number of impulses counted, hence the length of time over which the count is made.

In the first gamma-ray tests, various metals and crystals were irradiated for intervals up to an hour with gamma-rays from 1 mg of radium, at 3 mm distance, and transferred to the counter in about 30 sec. No increase in the counting rate was observed; the sensitivity of the counter was about 10^{-6} mg. The substances tried included aluminum, copper, lead, calcite, rocksalt, potassium bichromate, zinc sulphide, and quartz. The lead was a container for the radium, so had been exposed to gamma-rays for more than a year.

To test for fluorescence lasting for much shorter times, a beam of gamma-rays from 1

[1] G. I. Pokrowski, Phys. Rev. **38,** 925 (1931); also, Ann. d. Physik **9,** 505 (1931).
[2] N. S. Gingrich, Phys. Rev. **39,** 748 (1932).

mg of radium was allowed to pass through a hole in a thick lead block and strike a rotating aluminum disk. As the disk turned in the anti-clockwise direction, the irradiated spot went past a second lead tube leading to a Geiger counter, in 7×10^{-5} sec., so that fluorescence persisting that long might be detected. The corresponding time for clockwise rotation was 3.3×10^{-2} sec. Extended counts, made with the disk alternately rotating clockwise and anti-clockwise, agreed within the limits of statistical error, indicating that there was no fluorescence detectable by the means used. In addition to aluminum, beryllium (sulphate), carbon (paraffin), and lead (litharge), were successively waxed onto the disk and the experiment repeated, always with negative results. The sensitivity of the arrangement was sufficient to detect the gamma-ray equivalent of 1.2×10^{-5} mg of radium on the disk.

In another series of experiments, thick sheets of lead, molybdenum, tungsten, tantalum, and bismuth were placed 25 cm from the target of a tungsten x-ray tube, operated at 5 m.a. and 50 to 100 k.v.p., and irradiated for periods of 30 min. to an hour. After each exposure, the specimen was placed as near as possible to the counter, within 10 sec., and the subsequent counting rates were recorded at intervals of 5, 15, 30 and 60 min. There was no evident change of the counting rate with time, although the sensitivity was at least 2×10^{-6} mg. The tests were repeated under the same conditions until a sufficiently large number of impulses were recorded to make the statistical error in each interval small.

Long-time fluorescence of two x-ray tube targets was also investigated. The intense radiation incident on the targets of the tubes seemed to be a promising source of the fluorescence. A molybdenum tube was tried many times with a counter of about 44 cc volume, after running at 25 m.a. and 30 k.v.p. Lately, a tungsten tube was used with the small counter previously mentioned (volume 0.32 cc), after operation at 5 m.a., 50 to 100 k.v.p. The tubes were run for intervals of 5 sec. to an hour before each test. It was found that the counters recover their usual characteristics of response in about 0.02 sec., after being paralyzed by the intense radiation. The sensitivity of the small counter was about 5×10^{-5} mg, but no fluorescence was detected in any of the tests.

The small Geiger counter used here is a special one which also responds to ultraviolet light. A full description of its construction and operating characteristics will be published very soon. It was found that the intense discharge produced in the counter by strong x-rays temporarily sensitized it to visible light, so that it responded to the light from the x-ray tube filament, unless an opaque screen was interposed.

Clearly, the tests described here do not exclude the existence of induced gamma-ray emission, or nuclear fluorescence. But they indicate that if these effects do exist, their intensity, or duration, or both, must be below the limits of detection by the methods I have used.

GORDON L. LOCHER

Physics Department,
The Rice Institute,
May 7, 1932.

A Comparison of the Theoretical Results of Sugiura and Sommerfeld on the Production of X-rays

Recently A. Sommerfeld[1] has treated the theoretical problem of the production of x-rays by a method somewhat different from the usual quantum mechanical method used by Oppenheimer[2] and Sugiura,[3] which considerably simplifies the analytical treatment. The basic model is the same in both cases, namely an electron, whose original velocity and direction are known, is retarded and deflected by a positive nucleus, the problem being the determination of the intensity of the radiation resulting from this process. From the results of Sugiura's calculations and those of Sommerfeld, it is not immediately evident whether or not their results are in agreement, and therefore at Professor Sommerfeld's suggestion, the following comparison has been made.

The only explicit formula given by Sugiura

[1] Sommerfeld, Ann. d. Physik. **11,** 257 (1931).

[2] Oppenheimer, Zeits. f. Physik **55,** 725 (1929).

[3] Scientific Papers of the Institute of Physical and Chemical Research **17,** 99 (1931).

which is of interest in this connection is the expression for the absolute intensity of x-ray radiation at the short wave-length limit (formula 11). When terms in β_1^2 are neglected, it can be put in the following form:

$$I(\delta) = \frac{8e^2h^2a_1^4}{3R_0^2m^2c^3(e^{2\pi a_1}-1)} \left[\begin{array}{l} \sin^2\delta + (1\tfrac{1}{4}\sin^2\delta\cos\delta \\ \quad - 2\sin^3\delta)\beta_1 + (2-\sin^2\delta)a_1^2 \\ \quad + (4\cos\delta + 3\sin^3\delta \\ \quad - 2\cos\delta\sin^2\delta)\beta_1 a_1^2 \end{array}\right] \quad (I)$$

The notation of Sugiura has been retained in which δ is the angle between the initial direction of the oncoming electron and the direction of observation of the emitted radiation; $\beta_1 = v_1/c$ where v_1 is the initial velocity of the oncoming electron; $a_1 = hz/2\pi mac\beta_1$, where Z is the atomic number of the nucleus and a is the radius of the first Bohr orbit in hydrogen, and finally R_0 is the distance from the nucleus to the observer.

It is not possible to compare Sommerfeld's result with the above expression directly, but the comparison can be made by proceeding as follows: In Sommerfeld's notation the total intensity corresponding to I above is

$$A^2 = A_\theta^2 + A_z^2$$

where in turn

$$A_\theta^2 = (1/4\pi)\int A_\theta A_\theta^* \sin\alpha d\alpha d\beta$$

and

$$A_z^2 = (1/4\pi)\int A_z A_z^* \sin\alpha d\alpha d\beta \quad (1)$$

and α, β are the angles denoting the asymptotic direction of the outgoing electron. A_θ is the component of the vector potential of the emitted radiation perpendicular to the direction of observation and lying in a plane determined by this direction and that of the incident electrons for a given α and β. Correspondingly A_z is the z component. The complete expressions for A_θ and A_z for the case of the short wave-length limit are given by formulae 106a in Sommerfeld's paper apart from a multiplicative factor which contains only universal constants. These expressions were expanded according to ascending powers of n_1 and β_1 where $|n_1| = a_1$, and the integrations over α and β were performed as indicated in (1) above, and finally the expression for A^2 was obtained which contains the universal constants expressly omitted in Sommerfeld's formulae. The final expression is

$$A^2 = \frac{8e^2h^2n_1^4}{R_0^2m^2c^3(e^{2\pi|n_1|}-1)} \left[\begin{array}{l} \sin^2\theta + 4\sin^2\theta\cos\theta\cdot\beta_1 \\ \quad + \tfrac{1}{3}(7\sin^2+2)|n_1|^2 \\ \quad + \tfrac{1}{3}(28\sin^2\theta\cos\theta + 4\cos\theta)|n_1|^2\beta_1 \end{array}\right]. \quad (II)$$

A comparison of expressions I and II shows several significant differences. In the first place, there is a factor 3 in the denominator of the multiplicative factor in I, not present in II; secondly the coefficients of the terms in β, $|n_1|^2$, $|n_1|^2\beta_1$, are quite different. The intensity distribution curves therefore have a different shape, formula I yielding about one-third the intensity at $\theta = \pi/2$ given by II, while, on the other hand, the two expressions give the same result at $\theta = 0$ and $\theta = \pi$. A comparison of the intensity distribution given by I and II with the experimental result obtained by Kulenkampf[4] can not be strictly made because his results do not correspond exactly to the short wave-length limit and the theoretical intensity distribution changes very rapidly as the short wave-length limit is approached. It appears however, that II agrees with the observed intensity distribution obtained by Kulenkampf a little better than I, especially in regard to the position of maximum intensity. No attempt has been made to check all of the extremely complicated computations of Sugiura so that the source of the above mentioned discrepancies can not be pointed out.

It should be borne in mind, when applying Sommerfeld's formuale that terms in n_1^2 and β_1^2 have been neglected in most cases, as he explicitly states, both of which, however, cannot be small simultaneously, since $|n_1|^2$ and β_1^2 are connected by the reciprocal relation $|n_1|^2 = Z^2/13n^2\beta_1^2$. Thus in making comparisons with experimental results where terms in β_1^2 are negligibly small, terms containing n_1^2 should be retained. It is of little use to retain terms in β_1^2 as Sugiura has done unless the calculations are made using Dirac's wave functions. A paper giving the results of such calculations is now in the course of preparation at this institute.

LLOYD P. SMITH
National Research Fellow,
Institut für Theoretische Physik,
München, Germany.
May 10, 1932.

[4] Kulenkampf, Ann. d. Physik **57**, 597 (1928).

BOOK REVIEWS

Handbuch der Physikalischen und Technischen Mechanik. Edited by: F. AUERBACH AND W. HORT. Leipzig, Johann Ambrosius Barth. Vol. 1, 1927–1929, xviii and 780 pp., 523 figures, price 75.60 R.M. Vol. 2, 1928–1930, xiv and 673 pp., 453 figures, price 67.50 R.M.

The Handbuch der Physik of Winckelmann was the forerunner of the several handbuchs which have been appearing recently. The publishers of the original Winckelmann have decided that instead of publishing a new edition they would break it up into several specialized parts. The volumes here under discussion are the first two of the seven constituting the part which deals with mechanics. Of the editors, the first is a physicist and the second an engineer. The handbuch is intended to be a complete treatise of both pure and applied mechanics. As is natural in any work with many collaborators, the articles are of different values. Unfortunately the first two with which the handbuch starts do not belong to the best.

It is very useful that a discussion of the fundamental concepts of mechanics and their physical meaning should be given—a subject that is usually neglected. Auerbach does that in the first 95 pages. The article is very good didactically, but seems to miss the real difficulties in the definition of the fundamental concepts.

It is followed by eight articles on measurement by Bloch, extending over about 170 pages. Bloch gives a number of excellent photographs of instruments of precision. Of course the selection is personal taste, but to the reviewer it seems that the really useful discussions are missing. For example, in discussing the comparator nothing is said about how one should go about testing a comparator, and how after that the correction should be applied. Nothing is said how a screw should be improved, or what precautions are to be taken in measurements with a pycnometer.

These articles are followed by an excellent article on potential theory by A. Korn comprising about 40 pages. It omits all proofs but goes deeply into the theory, mentioning also the stricter and more recent developments. Besides he gives quite a number of actual formulas for special cases. M. Winckelmann treats in a very exact manner the principles of mechanics on about 45 pages. He has also an article on "The general principles of kinetics," that is to say essentially the differential principles in the second volume. In the first volume Winckelmann's article is followed by one on the geometry of masses by Skutsch. This contains a very useful collection of formulas for the calculation of moments of inertia of bodies of different shape.

Two chapters of R. Beyer, extending together over about 150 pages, treat the motion of mechanisms from the purely geometrical as well as from the dynamical standpoint—a subject which is of great importance for the advancement of machine design, but is not of great interest to the physicist. The same is true for four chapters by P. Stephan, respectively Hort and Stephan. The first is concerned with what is called elements of machines, the mechanics of inclined planes, screws and tooth-wheels. The third is concerned with the motion of transmitting belts and cables, while the second is still farther from the interests of the physicist, but of course of greatest importance to the engineer, and contains the mechanics of the crane.

The last is on friction under different conditions, on bearings of different types of oscillatory motions, and so on. Graphical methods in the statics of construction are discussed by H. Reissner on about 80 pages. The first volume contains in addition an excellent treatment of vibrations and waves by Auerbach. With many drawings he shows in rather an elementary manner the composition of waves, the results of Fourier analysis, giving actually a number of useful examples of Lissajous figures and the like.

In volume two he has also a discussion of about 50 pages on the pendulum from both the experimental and the theoretical standpoint. This second volume contains besides the articles mentioned an introduction into the mechanics of relativity (special as well as general) by Ph. Frank, who also deals with planetary motion and the more advanced chapters of celestial mechanics in his usual clear and precise manner. This is followed by a short description of the con-

struction of planetaria which are now to be found in several German cities. The distribution and measurement of gravity is described by Hecker and Meisser. The free fall and the motion of a projectile are discussed by O. v. Eberhard, who was one of the chief ballistic experts of Krupp. He describes in a very interesting manner the way in which the motion of projectiles are really calculated in practice. E. Bolle follows up with internal ballistics, that is to say the motion of the projectile inside the barrel as determined by the law of combustion of the powder.

The next chapter by C. Göcke on physiological mechanics contains a lot of information which it would otherwise be difficult to find, for example, on the density of the materials of the bones, on their elastic properties, strength, etc. He also describes the motions occurring in human locomotion.

After this the theory of the motion of the top is discussed by O. Martienssen, followed by the technical applications, namely the gyroscopic compass, in the construction of which the author took a prominent part, and the use of the gyroscope as a stabilizer on ships. A collection of physical demonstrations concerning the laws of mechanics, described before, and simplified discussions of some of the results are then given by Auerbach.

The volume contains finally a treatment of the graphical methods in technical dynamics, essentially in the motion of cranks, by R. Beyer.

K. F. Herzfeld
Johns Hopkins University

A Text Book of Heat. M. N. Saha and B. N. Srivastava. Pp. 771+xxv, figs. 210, Indian Press, Ltd., Allahabad, India. 1931.

Because of the rate at which research in physical phenomena has been advancing, a text presenting any modern theory may be out of date in a comparatively short time. Although there have been some very commendable treatises on heat, Saha and Srivastava's TEXT BOOK OF HEAT has been the first heat text in a number of years including much of modern theory.

It is a treatise which can be used in the physics courses given during the latter years for a B.S. degree, or in the first courses leading to an advanced degree in science. The subject matter has been well presented and somewhat condensed. Many well drawn figures have precluded considerable detailed explanation. In general there is a tendency to condense on the descriptive matter and to expand more on the theoretical. If the student wishes further information, there is a very complete list of references to original treatises and papers which will enable him to make his study as extensive as desirable.

The first twelve chapters contain the material generally included in an advance treatise on heat with some additional discussion of the subject of specific heats in the light of recent researches by Einstein, Debye and, Born and Karman. Chapters XIII and XIV are devoted to a discussion of the Quantum Theory and Statistical Mechanics, Nernst Heat Theorem and the Theory of Thermal Ionization in relation to the State of Matter at High Temperatures. The appendix presents certain special derivations and comparative data. Altogether it appears to be the best advanced heat text at the present time. In the second edition correction will probably be made of the various typographical, reference and other errors.

L. F. Miller
University of Minnesota

CURRENT LITERATURE OF PHYSICS

Extracts from the Tables of Contents of Some of our Contemporaries

NATURE

VOL. 129, NO. 3260 — APRIL 23, 1932

Letters to the Editor:

Electrochemical Periodicities. By **J. A. V. Butler and G. Armstrong** 613
Errors in Thermal Measurements. By **J. R. Partington** 615
Molecular Dissociation by Electron Impact. By **F. L. Arnot** 617
Intensity Ratio of Fluorescent X-ray lines. By **H. R. Robinson** 618
Highest Oxide of Rhenium. By **H. V. A. Briscoe, P. L. Robinson and A. J. Rudge** 618

NATURE

VOL. 129 NO. 3261 — APRIL 30, 1932

Letters to the Editor:

Disintegration of Lithium by Swift Protons. By **J. D. Cockcroft** and **E. T. S. Walton** ... 649
Isotopic Constitution of Lead from Different Sources. By **F. W. Aston** 649
Infrared Absorption Spectra of the Oxides of Chlorine. By **C. R. Bailey and A. B. D. Cassie** 652
Fluted Band at λ3900A in the Spectrum of Mercury. By **J. Okubo and E. Matuyama** ... 653
New Band System of Beryllium Oxide. By **Luise Herzberg** 653

NATURE

VOL. 129, NO. 3262 — MAY 7, 1932

Short Reviews:

Structure of Atomic Nuclei. By **C. D. Ellis** 674

Letters to the Editor:

Absolute Energies of the Lines in β-Ray Spectra. By **C. D. Ellis** 691
Passage of Neutrons through Matter: a Correction. By **H. S. W. Massey** 691

ZEITSCHRIFT FÜR PHYSIK

VOL. 75, NOS. 7 AND 8 — APRIL 20, 1932

β and γ-Radiation of Uranium *Z*. On the Branching Relation of Uranium *Z* to the Principal Branch of the Uranium Series. By **Ernst Walling** 425
Notice on the Half Value Time of UX_1. By **Ernst Walling** 432
On the Theory of Detector Action. By **Lothar Nordheim** 434
Influence of Impurities on the Cohesion Limits and Ultra-Microscopic Structure of Synthetic Rocksalt. II. Additions of Simple and Mixed Alkaline Earth Chlorides. By **Hans Schönfeld** 442
On the Theory of Fine Structure in Roentgen Absorption Spectra. By **R. de L. Kronig** ... 468
On the Equations of Motion of Accelerated Charges. By **Guido Beck** 476
Electric Conductivity of Loaded Piezoelectric Quartz. By **F. Seidl** 488
Observation of Neutral H_3 in Canal Rays. By **R. Conrad** 504
Rotation-Vibration Bands of Water Vapor between 0.9 and 6.5μ. By **P. Lueg and K. Hedfeld** 512
Measurements with the Help of Liquid Helium. XVI. Investigations on the Superconductivity of Carbides, Nitrides, Borides and Silicides. By **W. Meissner, H. Franz and H. Westerhoff** 521
On the Discontinuous Slipping of Zinc Crystals. By **E. Schmid and M. A. Valouch** 531
Light Absorption and Selective Photoeffects. By **Herbert Fröhlich** 539

On the Appearance of the Continuous Spectrum with Cathode Ray Bombardment. VI. Vapors and Gases. By **Willi M. Cohn** 544
Present Status of Ion Mobility Theories. By **Leonard B. Loeb** 555
Making Visible the Regions of Different Ferromagnetic Conditions in Solid Bodies. By **L. v. Hámos and P. A. Thiessen** 562

DIE NATURWISSENSCHAFTEN

VOL. 20, NO. 18 APRIL 29, 1932

Short Original Contributions:

On the Discharge Mechanism in Point Counters and Counter Tubes. By **Werner Schulze** 315
Method of Determining the Profile Curve of Rough Surfaces. By **Gustav Schmaltz** 315
On the Interpretation of the Red Shift of the Spiral Nebulae. By **Arthur Haas** 316
Röntgen Diagram of "Hendekamethyltriose" from Cellulose. By **C. Trogus** 317
New Method for Observing the Diffraction of Slow Electrons. By **A. Bühl** 317
Other Contributions:
Large Leiden Electromagnet. By **De H. -L.** 320

DIE NATURWISSENSCHAFTEN

VOL. 20, NO. 19 MAY 6, 1932

Short Communications:

Red Oxygen Radiation from the Night Sky. By **L. A. Sommer** 330
Comment on the Foregoing. By **W. Grotrian** 331
Change of Equilibrium through Adsorption. By **F. Hahn and R. Klockmann** 331
Raman Spectrum of Mono-, Di- and Tri-saccharides. By **Walther Kutzner** 331

PHYSIKALISCHE ZEITSCHRIFT

VOL. 33, NO. 8 APRIL 15, 1932

Mechanism of the Positive Column in Monatomic Gases. II. By **R. Seeliger** 313–327

Original Communications:

Calculation of Plane Periodic Boundary Layer Currents. By **H. Schlichting** 327–335
Investigation of the Structure of Copper Oxide Rectifiers. By **K. Scharf and O. Weinbaum** 336–341
Dipole Moment of Naphthols. By **M. Puchalik** 341–345
Capacity of the Binant Electrometer. By **G. Nadjakoff** 345–348
Relation between the Virgin and Remanent Condition of Magnetization. By **H. Kühlewein** 348–351

PHYSIKALISCHE ZEITSCHRIFT

VOL. 33, NO. 9 MAY 1, 1932

Original Communications:

Anomalous Electric Dispersion of Polar Solutions. By **R. Goldammer** 361–367
Influence of Earth Resistance on Lightning. By **F. Ollendorff** 368–376
Inhomogeneity of Highly Active Salts of Radium-Barium Chlorides. By **F. Behounek and O. Koblic** 376–378
On the Physics of the Nitrobenzene Kerr Cell. By **F. Hehlgans** 378–382
Association in Dipole Liquids. By **J. Malsch** 383–390
Dipole Moment of *n*-Propyl Ether. By **L. Meyer and A. Büchner** 390–391

PHYSICA

VOL. 12, NO. 4 APRIL 20, 1932

Address at the Inauguration of the New Electro-magnetic at the Kamerlingh Onnes Laboratory. By **W. J. de Haas** 113
On the Relation between the Hystersis Curve and the First Magnetization Curve of Ferromagnetic Materials. By **W. Elenbaas** 125

COMPTES RENDUS

VOL. 194, NO. 14 — APRIL 4, 1932

Problem of Cauchy for the Dirac Equations. By **N. Théodoresco** 1147
Acoustical Sounding by Echoes from Airplanes. By **Charles Florisson** 1149
On a Circuit with Reaction Independent of the Frequency. By **L. Brillouin and M. Lévy** . 1151
Curie Point of Ferro-Cérium. By **G. Rassat** 1153
On the Fine Structure of the α-Radiation of Thorium. By **S. Rosenblum and C. Chamie** . 1154

COMPTES RENDUS

VOL. 194, NO. 15 — APRIL 11, 1932

Investigations of the Polarization of an Electron Beam by Crystalline Reflection. By **J. Thibaud, J. -J. Trillat and Th. v. Hirsch** 1223
Influence of the Magnetic Field on Crystallization. By **Dinca Samuracas** 1225
Effect of Substitutions on the Rotation and the Magnetic Double Refraction of Napthalene Derivatives. By **Constantin Salceanu** 1227
On the Nature of Penetrating Radiation Excited in Light Nuclei by α-Particles. By **Irène Curie and M. F. Joliot** 1229
On the Fine Structure of the Magnetic Spectra of the α-Rays from Radioactinium. By **P. Curie and M. S. Rosenblum** 1232
On the Slowing Up of α-Rays of Thorium G' in Air. By **G. Mano** 1235

LE JOURNAL DE PHYSIQUE

VOL. III, SERIES VII, NO. 3 — MARCH, 1932

Application of Hughens' Principle to the Calculation of Reflectors for Ultra-Short Waves. By **R. Darbord** 105
On the Artificial Disintegration of Certain Elements with the Aid of Polonium α-Rays. By **M. C. Pawlowski** 116
Study of Speed of Condensation Pumps. By **M. Matricon** 127

PHYSIKALISCHE ZEITSCHRIFT DER SOWJET UNION

VOL. 1, NO. 2 — FEBRUARY, 1932

Detection of the Iodine Atom in the Optical Dissociation of Salt Vapors. By **N. Prileshajeva** 189
Absorption Spectrum At Low Temperatures of the Crystals of Some Compounds of the Aromatic Series. By **I. Obreimow and A. Prichotjko** 203
Skin Effect in a Ring. By **V. Fock** 215
Investigation of the Electrical Conductivity and the High Potential Polarization in Saltpeter Crystals. By **B. Hochberg and V. Joffé** 237
Capillary Electric Phenomena and the Wetting of Metals by Electrolytic Solutions. I. By **A. Frumkin, A. Gorodetzkaja, B. Kabanow and N. Nekrassow** 255
On the Theory of Stars. By **L. Landau** 285
Anomalous Dispersion of Zinc and Cadmium Vapors. By **A. Filippov** 289
Absorption Spectra of Solids. By **R. Peierls** 297
Letters:
Anomalous Dispersion of Calcium Vapor. By **A. Filippov, N. Kremenewsky** 299
Nuclear Moments of Potassium and Silver. By **S. Frisch** 303
New Sensitive Radiation Meter. By **M. Weingeroff** 304
On the Photodissociation of Atom Molecules into Ions. By **A. Terenin and B. Popow** 307

JOURNAL OF THE OPTICAL SOCIETY OF AMERICA

VOL. 22, NO. 5 — MAY, 1932

Eclipse Projector for the Franklin Institute Museum. By **James Stokley** 239
On the Concave Grating Spectrograph, Especially at Large Angles of Incidence. By **J. E. Mack, J. R. Stehn, and Bengt Edlén** 245
Determination of the Spectral Composition of X-ray Radiation from Filtration Data. By **Ludwik Silberstein** 265

Universal Spectrometer for the Infrared. By **A. H. Pfund** 281
Anomalies of Visual Acuity in Relation to Stimulus-Distance. By **Ellis Freeman** 285
New Developments in Photoelasticity—A Purely Optical Method of Stress Analysis. By **Arshag G. Solakian** 293

REVIEWS OF SCIENTIFIC INSTRUMENTS

VOL. 3, NO. 5 MAY, 1932

Construction of Thermo-Relay Amplifiers. By **C. Hawley Cartwright** 221
Method for Measuring Small Capacities. By **J. A. Van den Akker** 225
Audio Oscillator of the Dynatron Type. By **Don Hale** 230
Electrolytic Resistors of High Resistance. By **H. L. White and E. A. Van Atta** 235
Sensitive Electroscopes. By **Charles Lukens** 239
Improved Carborundum Tool for Ruling Echelette Gratings. By **Roland Schaffert** 248
Condensing Lens Support for a Large Spectrograph. By **F. W. Crawford** 251
Double Crystal X-ray Spectrometer. By **P. A. Ross** 253